Chemical approaches towards elucidating glioblastoma biology

Verena Bettina Kuchler

Submitted in accordance with the requirements for the degree of Doctor of Philosophy

The University of Leeds

School of Medicine

Faculty of Medicine and Health

June 2016

The candidate confirms that the work submitted is her own and that appropriate credit has been given where reference has been made to the work of others.

Acknowledgements

Firstly, I would like to thank my supervisor Dr Heiko Wurdak for giving me the opportunity to work on this exciting project. His guidance, encouragement and inspiration were invaluable for successful completion of this thesis. Further, I would like to thank my co-supervisors Prof Alan Melcher and Dr Fiona Errington-Mais, and also Dr Mihaela Lorger for their support and much appreciated feedback.
I am especially thankful for the contributions of Dr Euan Polson (LC3B immunostaining, sample preparation for EM, qRT-PCR, extracellular flux analysis), Dr Anjana Patel (Single cell gene expression analysis, intracranial injections of GSC cells, *in vivo* compound dosing) and Dr Tereza Andreou (intracranial injections of mouse glioma cells, *in vivo* bioluminescence imaging, FACS analysis of immune cell infiltration and macrophage polarisation). Their scientific expertise and invaluable input helped keep this project moving.
For their help throughout the last years I would also like to thank all past and present members of the Wurdak group.
I am very grateful to Dr Alastair Droop for computational analysis of gene expression data, and Edith Ross and Dr Florian Markowetz (CRUK Cambridge Institute) for computational subtype analysis and gene set enrichment analysis of single cell gene expression data. Thanks are also due to Hester Beard and Dr Robin Bon for synthesis of KHS101, Dr Helen Payne for her help running the TaqMan Fluidigm assays, and Dr David Stojdl and Charles Lefebvre (CHEO Research Institute, Ottawa) for kindly providing the CT2A cells. I would also like to acknowledge the contributions of my summer students Lucie Gack (ICAM-1 FACS analysis, live/dead cell stainings) and Adam Davies (ICAM-1 qRT-PCR screen, analysis of ICAM-1 immunohistochemistry images).
Furthermore, I thank everyone in the Leeds Institute of Cancer and Pathology, especially Nora Rippaus, Bárbara da Silva and Jennifer Williams, for their scientific and non-scientific support, for a pleasant and inspiring working atmosphere, and, most importantly, for making me feel at home in Leeds.
Lastly, I am particularly grateful to my parents and my brother for their continuous support, valuable advice, and for always finding the right words of encouragement.

Abstract

Glioblastoma multiforme (GBM) is the most aggressive, infiltrative brain cancer. Tumour recurrence is common and accounts for the poor 5-year survival rates of GBM (<10%). The ability to re-grow the tumour after surgical removal of the tumour bulk has been attributed to cells with stem cell-like phenotypes, termed glioma stem cells (GSCs). Identification of molecular GSC vulnerabilities targetable by therapeutic agents is urgently required. In this context, I examined the potential anti-GSC effect of KHS101, an experimental compound that induces differentiation in neural progenitor cells *in vitro* and *in vivo*. Interestingly, in patient-derived GSCs, KHS101 selectively reduced viability. KHS101 cytotoxicity was associated with a vacuolisation/autophagy phenotype, and loss of clonogenicity of GSCs. Consistently, KHS101 significantly reduced xenograft tumour growth and invasion and prolonged survival of mice bearing GSC-derived tumours. Analysis of the mechanism of action of KHS101 indicated the disruption of oxidative phosphorylation leading to metabolic exhaustion of GSCs.

To go beyond the possibilities of single agent treatment, I explored the potential of a combination therapy integrating oncolytic virotherapy with coxsackievirus A21 (CVA21). Targeting of tumour cells by CVA21 requires surface expression of Intercellular Adhesion Molecule-1 (ICAM-1), which is a limiting factor in GBM tumours. Notably, genetic manipulation of GSCs showed that expression of ICAM-1 is sufficient to increase susceptibility to CVA21. To identify ICAM-1 inducing compounds, I carried out a focused combination compound screen for the induction of *ICAM1* expression in GSCs. From a panel of 23 compounds, I identified combined retinoic acid (RA) and KHS101 as an efficient *ICAM1* mRNA up-regulation treatment. RA/KHS101 also significantly increased surface expression of ICAM-1 protein on GSCs. Notably, RA/KHS101-induced ICAM-1 expression rendered GSCs vulnerable to CVA21-mediated oncolysis *in vitro*. Hence, a combination of pharmacological treatment and oncolytic virotherapy could complement available chemo-/radiotherapy by eliminating the GSC population and thus preventing tumour recurrence.

Contents

List of Tables

List of Figures

1 Introduction

1.1 Glioblastoma Multiforme (GBM)

1.1.1 Glioma classification

Gliomas are tumours of the central nervous system and are thought to originate from cells of the glial lineage. Based on the morphological features the tumour shares with certain types of glial cells, gliomas can be classified into different categories including astrocytomas, ependymomas, oligodendrogliomas and oligoastrocytomas. In addition to this classification based on predominant cell types, classification of gliomas can also be done according to tumour grade. Based on pathological features of the tumour, their growth rate and potential to spread into nearby tissue, the World Health Organisation (WHO) grading system distinguishes four classes of gliomas, grade I – IV. Whereas, grades I and II are defined as low-grade gliomas, grades III and IV are rated as high-grade tumours [1] [2]. Classified as WHO grade IV, glioblastoma multiforme (GBM) poses the most common and aggressive type of primary brain tumour.

1.1.2 Incidence and prognosis of GBM

Each year approximately 2,100 new cases of GBM are diagnosed in England [3]. Incidence rates rise with increasing age peaking between 65 and 75 years of age [3]. Although they only account for ∼2% of all cancers [4], GBM tumours are among the most devastating cancers as GBM leaves patients with a median survival time of approximately 15 months from the time of diagnosis. Despite multi-modal treatment efforts, a 5-year survival rate of less than 10% has been reported [3] [5]. Moreover, GBM is associated with ∼20 life years lost, more than any other cancer [6].
The poor prognosis for GBM is mainly caused by the highly infiltrative nature of GBM concomitant with diffuse tumour edges that complicate complete surgical resection. Consequently, tumour recurrence commonly occurs near the site of the primary lesion [7]. In addition to the invasive nature, GBM tumours are char-

acterised by the presence of highly heterogeneous cell populations of molecularly different phenotypes that cause individual sensitivities and resistances of these populations to therapeutic approaches (see 1.3 'Inter- and intratumour heterogeneity of GBM'). Notably, this heterogeneity has been described at the inter- and intratumoural level, hence calling for a shift from a universal treatment regime to a combination of standard chemo-/radiotherapy and novel therapies specifically targeting distinct subpopulations of GBM tumours.

1.1.3 Treatment of GBM

The current standard of care for GBM patients includes maximal surgical resection of the main tumour mass, followed by radiotherapy and concomitant chemotherapy. In order to enhance maximal surgical resection, methods based on tumour-specific fluorescent staining using 5-aminolevulinic acid (ALA) have been developed. ALA staining facilitates differentiation between tumour and non-tumour brain tissue during surgery and therefore can help the surgeon to maximise the precision of tumour resection [8] [9]. The currently applied chemotherapeutic agent temozolomide (TMZ) is an alkylating agent that triggers apoptosis through induction of DNA methylation damage [10]. Concurrent radiotherapy and TMZ treatment has been shown to increase median survival by 2.5 months [11]. Despite multi-modal treatment efforts GBM remains mostly incurable, as tumour recurrence is inevitable [12]. Therefore, novel therapies are urgently needed. Intensive research has led to the development of new promising classes of therapeutic agents directly targeting GBM cells or modulating the tumour microenvironment. These novel therapeutic approaches include the use of monoclonal antibodies to disrupt specific ligand-receptor binding and thus prevent activation of receptor signaling. In this context, bevacizumab was developed to prevent neovascularisation through blocking vascular endothelial growth factor (VEGF) signaling. However, clinical trials have shown limited efficacy of bevacizumab in combination with standard treatment, as no significant improvement in patient survival was observed compared to standard treatment alone [13]. Monoclonal antibodies can also be used to direct a cytotoxic agent to the target cells. AMG595, for example, combines an antibody specifically targeting EGFRvIII, an epidermal growth factor receptor (EGFR) mutant frequently found in GBM, with the cytotoxic agent mertansine to facilitate specific killing of mutation-carrying tumour cells [14]. Other attempts to treat GBM are aimed at activating the patient's innate immune system to eliminate the tumour. This can be achieved through presentation of tumour lysate to the patient's own dendritic cells, thereby activating an

anti-tumour T cell response upon reintroduction of the tumour antigen-presenting dendritic cells. One such system, DCVax-L, is already being tested in a phase III clinical trial (ClinicalTrials.gov Identifier: NCT00045968; [15] [16]). Another approach relies on the *ex vivo* engineering of chimeric antigen receptor (CAR) T cells. CARs consist of a an extracellular variable antibody region enabling recognition of a tumour-specific antigen, and at least one T cell co-stimulatory domain facilitating T cell activation independent of major histocompatibility complex (MHC). The GBM-specific mutated form of EGFR (EGFRvIII) is one example of a GBM antigen that can be targeted by CAR T cells [17]. Notably, anti-EGFRvIII CAR T cell platforms are currently being evaluated in clinical trials (ClinicalTrials.gov Identifier: NCT02209376). Additionally, several studies in the field of GBM biotherapy focus on the use of oncolytic viruses and are described in 1.7 'Oncolytic virotherapy for cancer/GBM treatment'.

1.2 GBM subtype classification

A better understanding of the individual genetic and molecular alterations that drive malignant growth could be the basis for the development of personalised medicine [18]. A large number of studies focusing on revealing the genomic abnormalities and gene expression profiles associated with GBM tumourigenesis have been carried out. Mutations have been identified, for example, in retinoblastoma 1 (*RB1*), tumour protein p53 (*TP53*), phosphoinositide-3-kinase, regulatory subunit 1 (*PIK3R1*), neurofibromatosis type 1 (*NF1*), Erb-B2 receptor tyrosine kinase (*ERBB2*); gene amplification of *EGFR*, gains of chromosome 7 and loss of chromosome 10 are frequent alterations in GBM tumours [19]. In this context, work has focused on identifying clinically relevant subclasses of GBM by genomic profiling (e.g., [20]) or gene expression profiling (e.g., [21] [22] [23] [24]). Building on these studies, Verhaak et al. established a comprehensive GBM subtype classification scheme based on mutational, DNA copy number and transcriptional signatures. Applying multi-dimensional genomic data analysis, four different GBM subtypes were identified: Proneural, neural, classical and mesenchymal. The proneural subtype of GBM is mainly characterised by alterations in platelet-derived growth factor receptor α (*PDGFRA*; highest levels of *PDGFRA* amplifications/expression and sometimes *PDGFRA* mutations) or isocytrate dehydrogenase 1 (*IDH1*), together with *TP53* mutations and high expression of oligodendrocyte transcription factor 2 (*OLIG2*). Classification into the neural subtype is based on transcriptional expression of neuron markers (i.e. neurofilament, light polypeptide (*NEFL*), gamma-aminobutryc acid A receptor, α 1 (*GABRA1*), synaptotagmin 1 (*SYT1*), solute carrier family 12 member 5 (*SLC12A5*)). GBM tumours of the classical subtype are characterised by amplification of chromosome 7 and concurrent loss of chromosome 10, and amplification and mutations of *EGFR* while being *TP53* wild type. Transcriptional changes include high expression of, for example, *NES*, *NOTCH3*, smoothened, frizzled class receptor (*SMO*) and GLI family zink finger 2 (*GLI2*). Expression of mesenchymal markers such as *CHI3L1* and *MET*, together with low expression levels of *NF1* and mutations in *TP53* and phosphatase and tensin homolog (*PTEN*) define the mesenchymal subtype of GBM. The characteristic genomic profiles are suggested to be correlated with patient survival, for example a trend toward longer survival associated with the proneural subtype was observed. Furthermore, GBM subtypes are thought to be predictive for distinct responses to treatment and, therefore, are believed to have implications for future therapeutic advancements [25].

Subtype classification of other cancer types has proven advantageous for development of effective therapies [26] [27], and in the case of GBM, application of a universal treatment strategy has failed to achieve long-term remission [28] [11]. Hence, inter- and intratumoural GBM subtype classification has to be taken into account when investigating new treatment options.

1.3 Inter- and intratumour heterogeneity of GBM

An important feature of GBM tumours is their high level of heterogeneity. This heterogeneity includes mutational and transcriptional variability between tumours as well as distinct genetic, epigenetic, functional and phenotypic stages of subsets of cells or even single cells within a tumour. Early studies described differences in genetic and marker expression profiles of cells isolated from glioma specimens and glioma cell lines [29] [30]. Since then, a number of mutational events and molecular markers have been identified that contribute to heterogeneity across and within GBM tumours (e.g., [31] [32]). A well-known example of a gene heterogeneously expressed is the O^6-methylguanine-DNA methyltransferase (*MGMT*) gene, which encodes a DNA repair enzyme. Epigenetic silencing of the *MGMT* gene has been associated with a favourable response to TMZ. However, MGMT has not only been found to exhibit heterogeneous expression between different GBM specimens, but *MGMT* promoter methylation has been shown to vary between distinct tumour areas [33] [34]. Similarly, inter- and intratumour heterogeneity has also been described for expression of the *EGFR* mutant EGFRvIII, whose gene product is a constitutively active version of EGFR that drives tumourigenicity [35] [36] [37]. In a hallmark study, Sottoriva et al. investigated intratumoural heterogeneity using tumour fragments taken from different regions of the same tumour. By integration of genome-wide copy number variation and gene expression microarray profiling, the authors demonstrated that most patient tumours contained molecularly diverse subpopulations and revealed a high variability in the expression of GBM subtype classifier genes. Strikingly, identification of the clonal composition of each tumour revealed distinct patient-specific signatures of cancer evolution, thus adding a new level to GBM heterogeneity [38]. More recently, Patel et al. employed functional RNA sequencing to achieve characterisation of individual cells isolated from GBM tumours. Consistent with Sottoriva et al., they describe extensive intratumoural heterogeneity of GBM subtype classification and, in addition, in expression levels of signaling molecules relevant for GBM biology, e.g., *EGFR*, *PDGFRA*, fibroblast growth factor receptor 1 (*FGFR1*) and *NOTCH2*. This cell-to-cell variability highlights the complexity of GBM and the challenges for GBM treatment directed at specific signaling pathways [39].

Notably, given the high degree of intratumoural mutational and transcriptional heterogeneity in important factors of signaling pathways driving tumour growth, exclusive targeting of a specific pathway will not eliminate the entirety of the tumour and will promote the expansion of resistant cells. Therefore, an effective anti-GBM strategy should combine treatments aimed at different deregulated pathways, or be

targeted at vulnerabilities common to all GBM cells independent of their genetic or transcriptional background.

1.4 Cellular plasticity in GBM

Heterogeneity as described for GBM has been discussed to be a consequence of a hierarchical organisation driven by clonal evolution. In this context, the identification of cancer stem cells (CSCs) that drive cancer progression and give rise to the more differentiated cells with specific features, promoted advancement in understanding the origin of cellular heterogeneity of cancer. Similar to normal stem cells, differentiation of CSCs is thought to result in heterogeneous cell populations [40] [41]. Moreover, the influence of the tumour microenvironment on the biology of tumour cells has increasingly been investigated. In GBM, a complex network of normal brain cells, macrophages, endothelial cells and extracellular matrix provides a local environment or niches favourable for tumour growth, migration and immune escape [42]. Microenvironmental cues have been shown to play crucial roles in maintaining the glioma stem cell (GSC) pool and changes in niche factors may influence cellular plasticity resulting in altered GSC/non-GSC ratios. Accordingly, accumulating evidence indicates that tumour cell populations are dynamic with a high degree of interconversion between GSCs and non-GSCs [41]. This capacity of tumour cells to alter their phenotypic and functional state is governed by microenvironmental factors like hypoxia, transcription factors, microRNAs (miRNAs) and therapeutic pressure [41]. For example, by comparing epigenetic profiles of GSCs and their differentiated counterparts, and subsequent functional validation, Suvà et al. identified a core set of transcription factors (i.e. POU class 3 homeobox (POU3F2), SRY-box 2 (SOX2), spalt-like transcription factor 2 (SALL2) and OLIG2) that control GBM propagation. Most importantly, induction of these four neurodevelopmental transcription factors is sufficient to reprogram differentiated GBM cells into tumour-propagating GSCs [43]. Additionally, important regulatory roles in GSC biology have been attributed to miRNAs. Two examples of miRNAs that have been implicated in GSC proliferation and their tumourigenic potential *in vivo* are miRNA-34a and miR-18a* [44] [45]. Chemotherapeutic challenge of GBM cells with TMZ has also been demonstrated to affect cellular phenotypes. Auffinger et al. recently described TMZ-induced conversion of differentiated GBM cells into a stem cell-like state characterised by expression of 'stemness' markers and enhanced infiltrative behaviour *in vivo* [46]. Growing evidence highlights the importance of the bidirectional cross-talk between GSCs and their microenvironment (reviewed in [47]). In this context, hypoxia has been shown to influence the GSC pool by suppressing differentiation and promoting expression of self-renewal genes in stem and non-stem populations mainly through hypoxia inducible factor (HIF), Notch and c-Myc signaling [48] [49] [50]. Within the perivascular niche, GSC 'stemness',

metastasis and escape from therapy are promoted, for instance, by sonic hedgehog (SHH), Notch ligands (i.e. Delta-like 4 (DLL4) and Jagged-1) and the chemokine interleukin (IL)-8, secreted by endothelial cells within the niche [51] [52] [53]. Figure 1.1 depicts the signaling modes within the hypoxic and the perivascular niches that regulate GSC maintenance and contribute to cellular plasticity within GBM tumours [54]. Transition between different GSC states has recently been shown by Bhat et al. who collected evidence that GSCs are able to transition from a proneural to a more aggressive mesenchymal state via nuclear factor of κ light polypeptide gene enhancer in B-cells (NF-κB) signaling. Notably, the authors suggest an involvement of macrophages/microglia present in the tumour microenvironment [55].

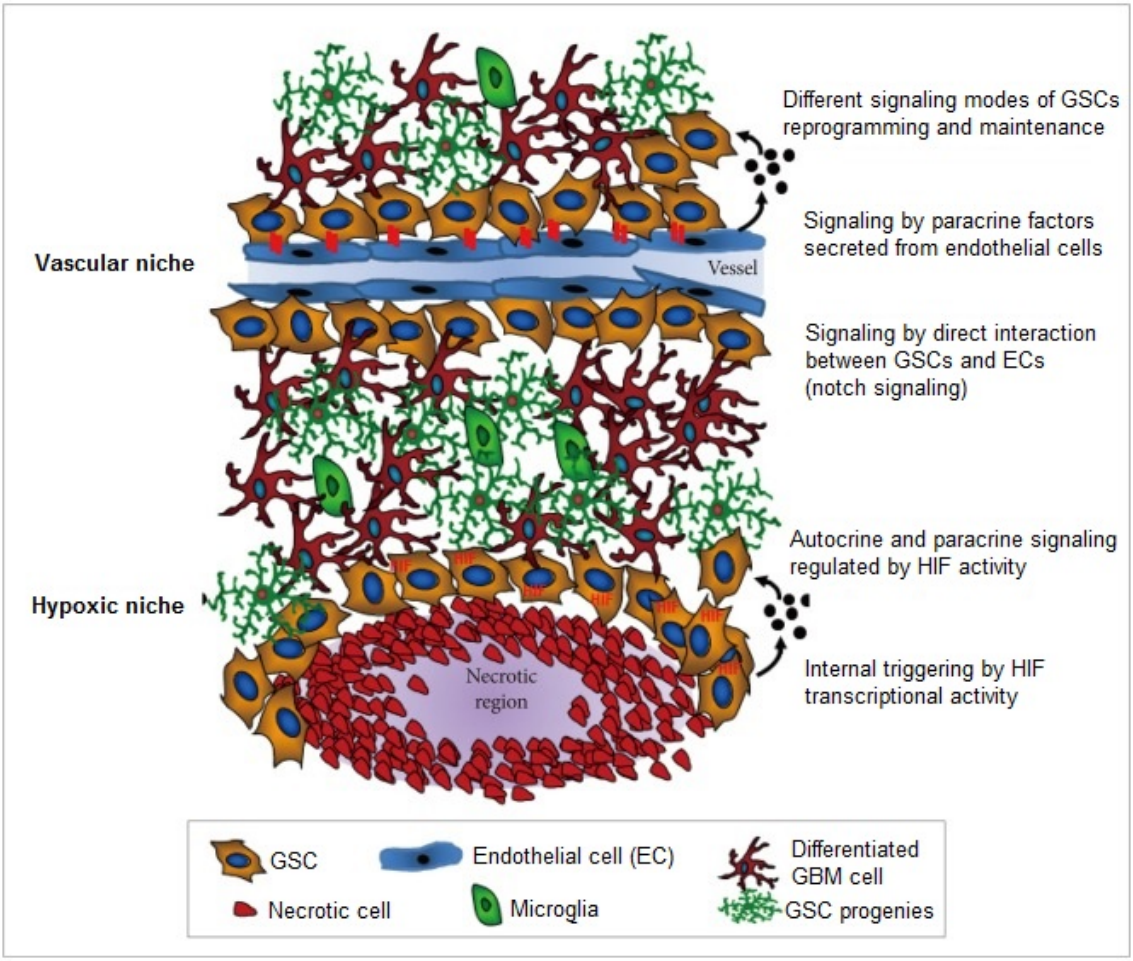

Fig. 1.1: Signaling modes within the vascular and hypoxic niches that modulate GSC maintenance (adapted from [54]).

In conclusion, adaptation of GBM cells to different microenvironmental settings providing distinct GSC-promoting cues significantly contributes to the high degree of genetic, epigenetic and functional heterogeneity observed in GBM. Moreover,

identification of key effectors that critically influence non-GSC/GSC phenotypes and trigger interconversion between different GBM cell types furthers our understanding of cellular plasticity of GBM. Insight into the molecular basis of plasticity and heterogeneity reveals potential new targets for GBM therapy. Certainly, the high degree of cellular plasticity observed for GBM tumours, necessitates comprehensive treatment strategies aiming at all cell types, including GSCs, non-GSC and their intermediate states.

1.5 Glioma Stem Cells (GSCs)

1.5.1 Characteristics of GSCs

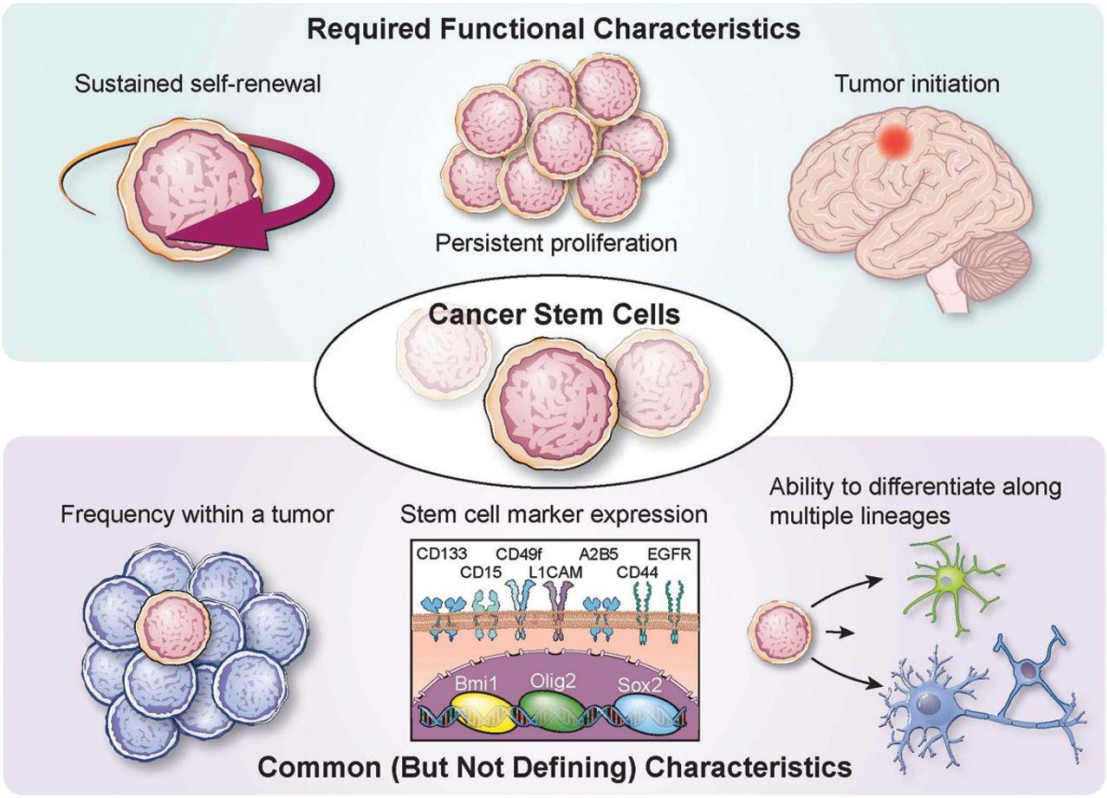

Fig. 1.2: Functional characterisation of CSCs/GSCs. GSCs are functionally defined by sustained self-renewal, proliferation and tumour initiation upon intracranial transplantation. GSCs also share characteristics with neural stem cells including their frequency within a tumour, expression of neural stem cell markers and differentiation capacity along multiple lineages [56].

The critical role of GSCs in cellular plasticity and heterogeneity of GBM necessitates a profound understanding of the nature of these cells. The main features defining GSCs are summarised in figure 1.2. By definition, GSCs are undifferentiated malignant cells that are characterised by their clonal growth ability based on their capacity to self-renew and to give rise to more differentiated cell progeny of neuronal, astroglial and oligodendroglial phenotypes. Therefore, they share several characteristics with neural stem cells (NSCs) including the expression of NSC markers (e.g., neuroectodermal stem cell marker (NESTIN), SOX2, OLIG2, CD133, CD44). *In vitro*, GSC differentiation can be induced, particularly upon exposure to bone morphogenic proteins (BMPs) or serum. Continuous propagation in the

presence of serum alters the molecular and phenotypic characteristics of GSC towards a differentiated state. Notably, the resulting GSC differentiation phenotype is associated with significantly decreased tumourigenicity. However, a recent study by Caren et al. revealed that BMP-induced astrocyte differentiation and cell cycle arrest of GSCs is heterogeneous and reversible. In fact, even after prolonged exposure (54 days) of GSCs to BMP, the cells retain the capacity for cell cycle reentry and de-differentiation, presumably due to incomplete differentiation-specific reconfiguration of DNA methylation patterns. Consistent with the described limited differentiation *in vitro*, BMP-treated GSCs as readily form orthotopic xenograft tumours as untreated GSCs [57]. The ability to initiate tumour formation upon orthotopic transplantation into immunocompetent mice is the most important method to functionally characterise GSCs. This approach allows for the assessment of the tumourigenic potential of GSCs [56] [58] [59] [60]. Strikingly, GSC-derived xenograft tumours maintain the genotypic and phenotypic features of the original patient tumour [61].
The observed interconversion between GSCs and non-GSCs (described in 1.4 'Cellular plasticity in GBM') requires an experimental therapeutic to be tested on both, GSCs and GSC-derived more differentiated cells in order to ensure a broad efficacy in a GBM tumour setting. Thus, the ability of patient-derived GSCs to give rise to differentiated progeny of diverse lineages, together with GSC-derived xenografts phenocopying the important features of the parental tumour, makes GSCs an ideal model to test the anti-GBM effects of novel treatments *in vitro* and *in vivo*.

1.5.2 Isolation of GSCs

The concept of a tumour-initiating subpopulation of cells was first validated in haematopoietic malignancies. In leukemia, surface expression levels of markers such as CD33, CD34, CD44 or chemokine (C-C motif) ligand 1 (CCL-1) are used to isolate the malignant stem cells [62] [63] [64] [65] [66] [67]. However, heterogeneity in leukemia stem cell marker signatures has been described, which complicates identification of a conclusive and universally applicable marker [68]. Similarly, enrichment of the stem cell population of brain tumours was initially based on the expression of surface markers. In 2003, Singh et al. demonstrated that the CD133-positive population isolated from human brain tumours exhibits stem cell characteristics [69]. Only the CD133+ cell population was able to grow xenograft tumours displaying histopathological resemblance with the original tumour [70]. However, other studies have shown that the informational content of CD133 as a universal GSC marker is

limited as, in some cases, CD133 negative cells can also have tumourigenic potential [71] [72]. In addition to CD133, several other GSC markers have been proposed, e.g. CD15, integrin $\alpha 6$ and CD44 [73] [74] [75]. Since cell surface markers are often involved in the cross-talk of tumour cells with their microenvironment, isolation from their tumour surroundings may lead to a reorganisation of the proteins on the cell surface. Hence, the cells' stemness marker signature is likely lost upon propagation *in vitro* [56].

Other methods of isolating and culturing of the stem cell population of brain tumours have been investigated. Enrichment of GSCs from GBM samples can also be achieved using serum-free culture conditions that select for a GSC phenotype. GSCs isolated by this method can then be grown as neurospheres or in adherent culture [69] [76]. Most notably, these GSCs and the xenograft tumours they generate closely mimic the genotype and phenotype of the parental tumour, including important features such as the highly invasive nature of GBMs. GSC-derived xenograft tumours also maintain cellular heterogeneity and populations of CD133 and CD44 expressing cells can be isolated by flow cytometry [61] [76]. The possibility of long-term maintenance of GSCs as monolayers in serum-free medium facilitates investigation into the mechanisms underlying the malignant nature of this disease and the identification of factors that can manipulate GSCs towards a less tumourigenic phenotype.

1.5.3 Differentiation therapy to target GSCs

GSCs are thought to be responsible for tumour initiation, progression and recurrence after therapeutic intervention [56]. Accordingly, resistance to radiation and DNA damaging agents, conceivably due to enhanced DNA repair mechanisms and ATP-binding cassette (ABC) transporter mediated resistance to chemotherapeutic agents have been attributed to GSCs and complicates effective targeting of these cells [77] [78] [79]. The challenge of specifically targeting GSCs has been linked to the idea of driving these cells into differentiation to deprive them of their self-renewal and tumour-initiating abilities. Upon differentiation, GSCs show a significantly decreased tumourigenicity and display increased susceptibility to conventional chemotherapy and radiotherapy [59]. Therefore, differentiation therapy could be a highly effective strategy to target GSCs, in particular, in combination with currently available DNA-damaging therapies.

Specific elimination of GSCs can be approached from different angles taking into account the increasing knowledge about proteins and networks that drive 'stemness' and the malignant nature of GSCs. Various different growth factor and cytokine

signalling pathways, such as the transforming growth factor β (TGF-β) and Notch pathways, have been implicated in the regulation of NSCs and aberrant activation of these pathways may promote tumourigenesis [80]. Several of these factors (e.g., BMP, TGF-β, Notch), and their respective downstream signaling pathways regulate GSC maintenance [58] [81] [82] [83]. Moreover, accumulating evidence suggests a role of different miRNAs, as well as genetic factors, for example the histone modifying proteins BMI1 and enhancer of zeste 2 polycomb repressive complex 2 subunit (EZH2), c-Myc, IDH1 and the transformation/transcription domain-associated protein (TRRAP) in GSC biology [84] [85] [86] [87] [88] [89] [90] [91]. Additionally, various studies indicate a differentiation effect of small chemical compounds. Among the compounds tested, retinoic acid (RA), resveratrol, curcumin, rapamycin and 2-Hydroxyoleate gave promising results leading to a more differentiated state of GSCs and/or inducing autophagy [92] [93] [94] [95]. A more detailed overview on the current concepts of induced differentiation of GSCs is given in [96].

1.6 Forward chemical genetics: Identification of small molecules for anti-GBM treatment

Unlike other types of cancer in which detection of driver mutations has led to the development of effective new drugs, the diversity of GBM genetics and the cellular plasticity associated with GBM growth and recurrence limits success of a targeted therapy against GBM [97] [98] [99]. Therefore, identification of acquired cellular properties and molecular vulnerabilities of GBM is needed and can be facilitated by investigation of patient-derived GSCs. In this context, the potential of small chemical compounds to modulate cell fate has been investigated (e.g., [100] [101] [102]). Efforts to identify small molecule disruptors of complex oncogenic mechanisms that drive GBM growth have benefited from the development of high throughput screening approaches. Unlike reverse chemical genetics, which is based on screening small molecules against a specific target, forward chemical genetics aims at identifying small molecules that cause a specific phenotypic response in a cellular system. As the choice of a molecular target is not limited in forward chemical genetics, it is a well-suited approach to tackle the complexity of GBM and support the development of therapeutic strategies that exploit GBM vulnerabilities [103] [104]. Notably, a comprehensive understanding of the mechanism underlying a compound's activity is essential to be able to explain the observed effect. Therefore, mechanism-of-action (MOA) studies are a critical addition to phenotypic screening. MOA studies mostly focus on the identification of the target the compound binds to, or the biochemical pathway the compound interferes with [105]. A commonly used method for target identification is affinity chromatography. Herein, the compound labeled with an affinity tag (e.g., biotin) is used to immobilise and separate the unknown target protein [106]. Alternatively, a biotin-labeled compound analog with a phenyl azide moiety can be used for photo-crosslinking the small molecule and the target protein. Identification of the drug target can then be achieved by SDS-PAGE or a (2D) Western Blot detecting biotin followed by mass spectrometry [106] [105]. Another frequently applied method to uncover a compound's MOA is transcriptome analysis. Here, comparing the gene expression profiles of compound-treated cells and control cells (vehicle-treated or treated with an inactive analog of the compound) reveals the gene alterations induced by the compound, thus giving an indication of the pathways affected. When investigating a toxic compound, identification of mutations in resistant cells, for example, by whole-genome sequencing can be a powerful approach to uncover the compound's MOA [105].

1.6.1 Small molecules in GBM

A growing number of studies focus on small molecule screens to discover compounds that selectively affect GBM cell fate. Tan et al., for example, screened 10,000 natural product-like compounds for their ability to inhibit the HIF-1 pathway in glioma cells. They discovered the small molecule 103D5R which strongly reduced HIF-1α protein synthesis *in vitro* and prevented the hypoxia-induced activation of *VEGF* and glucose transporter-1 (*GLUT1*), two factors critically involved in survival under anaerobic conditions [107]. Screening for GBM growth inhibitors targeted at cells carrying the EGFRvIII mutation, Trembath et al. identified the small compound NSC-154829 by using an isogenic cell-based approach; NSC-154829 selectively increases apoptosis in EGFRvIII expressing GBM cells [108]. Since stress response regulated by Heat Shock Factor 1 (HSF1) has been implicated in cancer cell survival, a phenotypic screen conducted by Santagata et al. focused on the identification of compounds able to activate the heat shock response and disrupt protein homeostasis. One candidate compound, withaferin A, was further investigated for its therapeutic potential *in vivo* and shown to increase median survival of mice bearing glioma xenograft tumours [109]. Aiming at identifying small-molecule inhibitors of the canonical Wnt signaling, the small molecule SEN461 was discovered. Notably, *in vivo* administration of SEN461 resulted in reduced growth of GBM xenograft tumour [110]. Furthermore, in order to discover novel radiosensitisers, Goglia et al. conducted a cell-based small molecule screen for inhibitors of double-strand break repair systems. Among the 20,000 compounds screened, the FDA-approved drug mibefradil dihydrochloride was found to act as a radiosensitiser *in vitro* [111]. In an attempt to identify an agent that could act synergistically with the tricyclic antidepressant, imipramine, in the induction of autophagy-associated cell death, Shchors et al. screened a number of already clinically approved drugs. The anticoagulant ticlopidine was found to improve efficacy of imipramine and combination treatment exhibited cytotoxicity in GBM cell culture and prolonged survival in a glioma mouse model [112]. Additionally, small molecule screening approaches have been applied to specifically target GSCs. For example, Visnyei et al. combined a high-throughput screen identifying compounds affecting proliferation/viability of GSCs with a subsequent target-based approach further characterising the candidate compounds for their effect on expression of mitotic genes negatively correlated with clinical outcome. Notably, the four most potent compounds demonstrated an inhibitory activity on GSC self-renewal *in vitro* and *in vivo* [113]. Similarly, in an effort to specifically target GSC proliferation without compromising growth of normal NSCs, Danovi et al. identified the compound J101 among a panel of 160 small molecule kinase

inhibitors. Their data indicate that J101 exerts its GSC-specific anti-proliferative activity through inhibition of polo-like kinase 1 [114]. More recently, a study conducted by Kitambi et al. identified a quinine derivative that displayed selective cytotoxicity in GSCs. Moreover, functional validation using an analog of the 'hit' compound, Vacquinol-1, uncovered a GSC vulnerability based on macropinocytic vacuolisation and membrane ruffling. Further investigation into the *in vivo* activity of Vacquinol-1 demonstrated attenuated tumour progression and prolonged survival in a GBM mouse model [115].
Taken together, several studies have identified and validated small molecules with anti-GBM activity through effects on cell proliferation, autophagy, cell death and transcriptional pathways known to drive GBM cell survival and therapy resistance. These studies highlight the great potential of small chemical compounds as promising new therapeutic options.

1.6.2 Candidate small molecules with potential anti-GBM properties: KHS101 and retinoic acid (RA)

1.6.2.1 The small molecule KHS101

The small chemical compound KHS101 (figure 1.3), a neuropathiazol analog, was initially identified in a phenotypic screen as a potent inducer of differentiation in the adult central nervous system. Notably, KHS101 specifically induces neuronal differentiation in neural progenitor cells (NPCs) of the adult rat hippocampus resulting in functionally active maturing neurons. The compound overrides BMP-induced astrocyte differentiation of NPCs. Additionally, microarray profiling and functional assays revealed that proliferation of NPCs is decreased in the presence of KHS101. Moreover, the differentiation and anti-proliferation effect of KHS101 on NPCs has been shown both *in vitro* and *in vivo*. Most importantly, KHS101 is able to cross the blood-brain barrier in murine models when injected intravenously or subcutaneously [116].
The MOA of KHS101 is still being investigated; however, Wurdak et al. identified the transforming acidic coiled coil containing protein 3 (TACC3) as a KHS101 target through affinity-based pulldown assays. Importantly, upon knockdown of TACC3 NPCs displayed a similar neuronal differentiation phenotype as induced by KHS101 treatment further confirming an interaction of KHS101 with TACC3. In addition, targeting TACC3 with KHS101 was shown to promote nuclear translocation of the transcription factor aryl hydrocarbon receptor nuclear translocator 2 (ARNT2), a

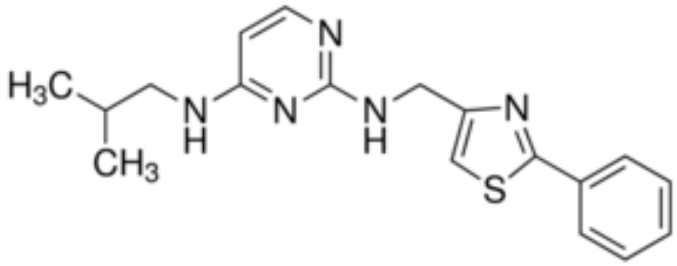

Fig. 1.3: Chemical structure of KHS101.

known interaction partner of TACC3 [116] [120]. Following up on this finding, disruption of TACC3/ARNT2 binding by KHS101 has been demonstrated to be a consequence of KHS101-mediated proteasomal degradation of TACC3. Notably, an indirect effect of KHS101 on HIF-1α protein levels under hypoxic conditions was also identified in this study, indicating KHS101 as a modulator of HIF-1α signaling [121].

As a member of the transforming acidic coiled-coil containing protein family, TACC3 is characterised by a highly conserved C-terminal coiled coil domain. The TACC3 protein co-localises with microtubules of the mitotic spindle (figure 1.4 A) and acts as a centrosomal adaptor promoting its stabilisation, thus contributing to correct chromosomal segregation [122] [118]. More precisely, phosphorylated TACC3 is able to bind to microtubules, thus enabling TACC3 to interact with clathrins and colonic and hepatic tumor overexpressed gene (ch-TOG) leading to the crosslinking between microtubules (figure 1.4 B; [118]). Consistent with its function in the assembly of the mitotic spindle, TACC3 is a proposed regulator of cellular growth and mainly expressed in highly proliferative tissue, e.g. the gastrointestinal tract or the spleen ([123]; TACC3 protein levels according to the Human Protein Atlas: www.proteinatlas.org; [124]). As a crucial factor for cell proliferation, TACC3 has been intensively investigated for its role in cancer progression. Indeed, elevated TACC3 levels were found in numerous different human cancer types including breast cancer, bladder cancer, sarcoma, lung cancer, gastric cancer, hepatocellular carcinoma, lymphoma and GBM [125]. Notably, high expression of TACC3 has been correlated with poor prognosis (figure 1.4 C; [126] [127]) and a role for TACC3 in cancer invasion, through promoting epithelial-mesenchymal transition (EMT), has been suggested [128]. Recently, an oncogenic fusion protein of FGFR3 and TACC3 has been reported in a small subset of GBM tumours. This FGFR3-TACC3 fusion protein is localised to the mitotic spindle poles (figure 1.4 D) and causes defects in chromosomal segregation leading to aneuploid cells. Strikingly, targeting FGFR3 kinase activity by a specific inhibitor results in prolonged survival of mice bearing

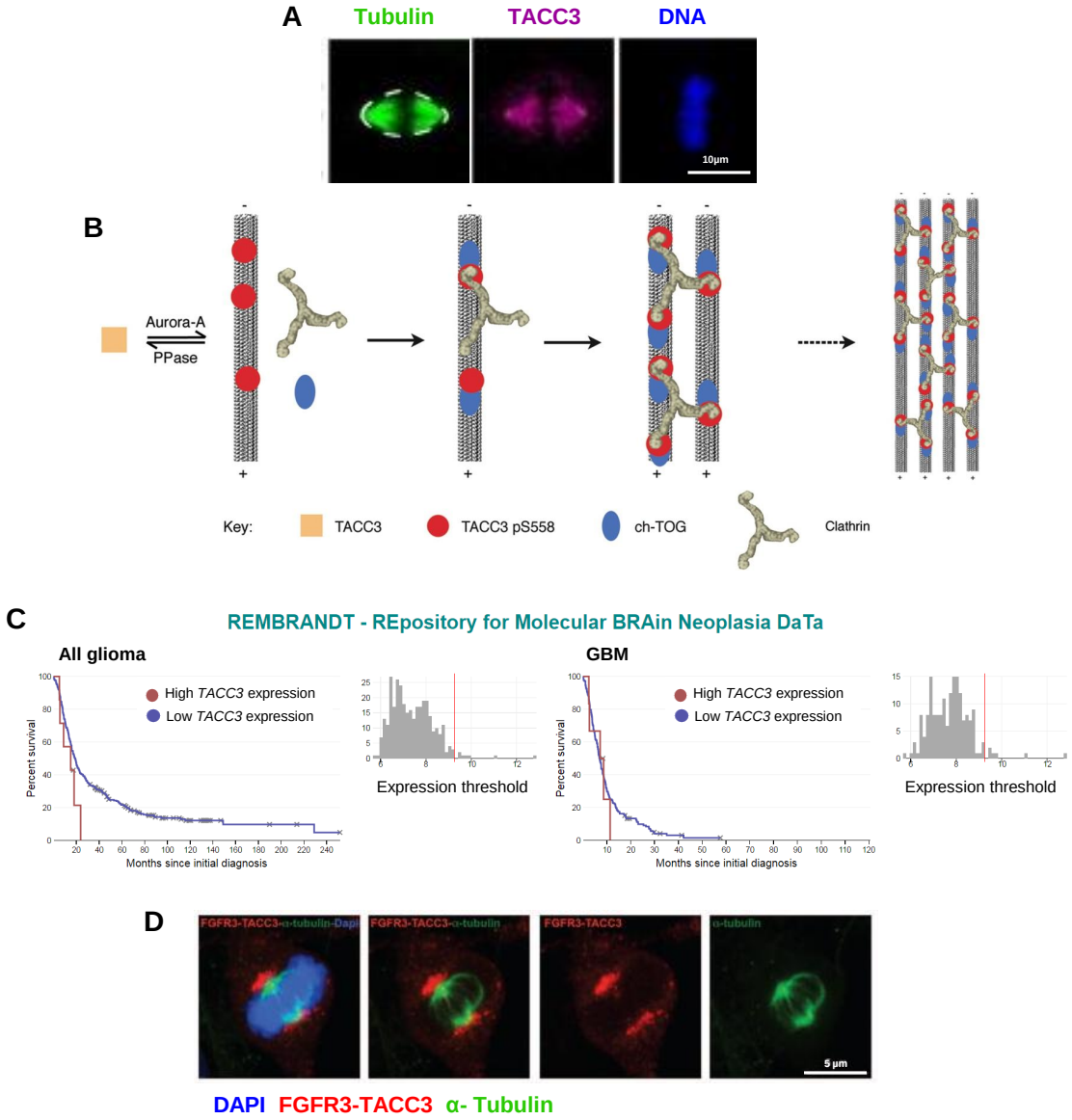

Fig. 1.4: Function of TACC3 and its role in glioma. **A)** Immunofluorescence images of HeLa cells stained for the microtubule protein tubulin and TACC3 (adapted from [117]). **B)** Scheme of proposed TACC3/ch-TOG/clathrin-mediated crosslinking of microtubules of the mitotic spindle (adapted from [118]). **C)** Kaplan-Meier survival plots of glioma (left) and GBM (right) patients with high or low *TACC3* expression levels (obtained from the REpository for Molecular BRAin Neoplasia DaTa, www.betastasis.com/glioma/rembrandt). **D)** Immunofluorescence images of cells stained for α-tubulin and FGFR3-TACC3 [119].

FGFR3-TACC3-driven glioma [119]. Similarly, FGFR3-TACC3 fusions were also detected in bladder cancer, lung cancer and cervical cancer [129] [130] [131]. Notably, disruption of TACC3 by conditional knockout in a lymphoma mouse model triggers tumour regression [132]. Moreover, targeting TACC3 protein degradation by small molecules can induce selective cancer cell death *in vitro* [133].
In conclusion, a multitude of studies implicates TACC3 in cancer progression and point to TACC3 as a potential molecular target for development of drugs against various types of highly TACC3-expressing cancer, including GBM.

1.6.2.2 The small molecule RA

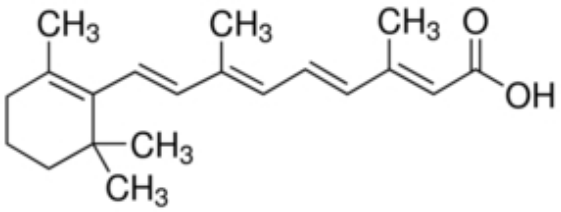

Fig. 1.5: Chemical structure of RA.

RA (figure 1.5) is a naturally occurring vitamin A metabolite that acts as an essential physiological signaling molecule regulating developmental processes in the embryo but also fulfilling crucial tasks in the adult body. Depending on the cell type, RA can induce cell growth, differentiation but also apoptosis [134]. RA elicits differentiation of NSCs, inducing an astrocytic cell fate [135]. Due to their natural occurrence, and differentiation effects on NSCs and various other cell types, retinoids have been extensively investigated for their anti-tumourigenic properties. Retinoid-based differentiation therapy alone or as part of a combination therapy, consisting of conventional chemotherapy and differentiation therapy, is particularly effective in the treatment of acute promyelocytic leukemia (APL), juvenile chronic myelogenous leukemia, Kaposi's sarcoma, breast cancer, and neuroblastoma [134] [136]. The anti-tumourigenic effect of RA has also been demonstrated in brain tumours and the RA differentiation pathway appears to be deregulated in malignant glioma as several RA signalling molecules (e.g. CRBP1, aldehyde dehydrogenase 1 family, member A1 (ALDH1A1), cytochrome P450, familiy 26, subfamily B, polypeptide 1 (CYP26B1), fatty acid binding protein 5 (FABP5)) show an aberrant expression profile [137]. Even though a differentiation effect of RA has been reported for GSCs, RA fails to bias the cells towards terminal differentiation [138]. This merely partial differentiation effect could explain the limited efficacy of RA in the treatment of malignant

glioma observed in clinical trials [139]. Nevertheless, these preclinical studies and clinical trials demonstrated the safety of RA administration and confirmed its accessibility to the brain [140]. These characteristics make RA an interesting candidate for investigation into a new application of RA in glioma therapy.

1.7 Oncolytic virotherapy for cancer/GBM treatment

The concept of using live non-pathogenic viruses that preferentially infect and destroy cancer cells, while sparing non-cancerous cells, has been known many decades [141]. These so called oncolytic viruses (OVs) have since been intensely investigated and expanding knowledge in molecular biology and virology has further expedited development of OV therapeutics. OVs can have a natural preference for cancer cells or can be manipulated to target cancer cells that express tumour-specific surface proteins or have altered signaling pathways that provide the cellular environment favourable for OV replication (e.g., [142] and [143]). Several naturally oncolytic and genetically engineered viruses have been investigated for their anti-GBM activity and safety in preclinical models and clinical trials, including reovirus, different Newcastle disease virus (NDV), adenovirus, herpes simplex virus (HSV), measles virus and vaccinia virus strains [144]. One promising naturally occurring oncolytic virus is reovirus, which has been reported to have a strong cytotoxic activity against GBM *in vitro* and *in vivo* [145]. However, genetic modifications can be introduced into OVs to enhance their oncolytic activity, and hence safety, by optimisation of selective targeting and replication in cancer/GBM cells or by expression of cytotoxic gene products in infected cancer cells. For example, increased tumour specificity of oncolytically active viruses can be achieved by retargeting OVs through manipulation of the glycoprotein composition to promote binding to tumour-associated receptors, e.g. EGFR, or more specifically, to GSCs expressing CD133 [146] [147]. The vaccinia virus strain JX594, on the other hand, exhibits improved selective replication in cancer cells through genetic deletion of thymidine kinase and has been shown to be active against GBM [148]. To improve efficiency of OV therapy by increasing the viruses' oncotoxic activity, OVs such as HSV have been engineered to carry the gene for tumour necrosis factor (TNF)-related apoptosis-inducing ligand (TRAIL) thereby prolonging survival of mice bearing intracranial tumours [149].
Notably, virus-induced lysis of tumour cells does not seem to be the sole reason for the therapeutic activity of OVs. Instead, preclinical and clinical studies indicate a role for OV-induced anti-tumour immune responses, including recruitment of natural killer (NK) cells and granulocytes. Release of cytokines and tumour-associated antigens (TAAs) by lysing tumour cells also leads to maturation of dendritic cells and presentation of TAAs on their cell surface. Consequently, cytotoxic T cells are activated and have the potential to identify and target tumour cells at distant sites (figure 1.6) [150] [151] [152] [153]. Hence, in addition to their direct oncolytic effect, therapy with oncolytic viruses stimulates an ongoing adaptive anti-tumour

immune response through activated cytotoxic T cells. Naturally occurring, unmodified oncolytic viruses known to elicit anti-tumour immunity include reovirus, HSV, coxsackievirus B3 [152] [154] [155], and in the GBM context, NDV [156].

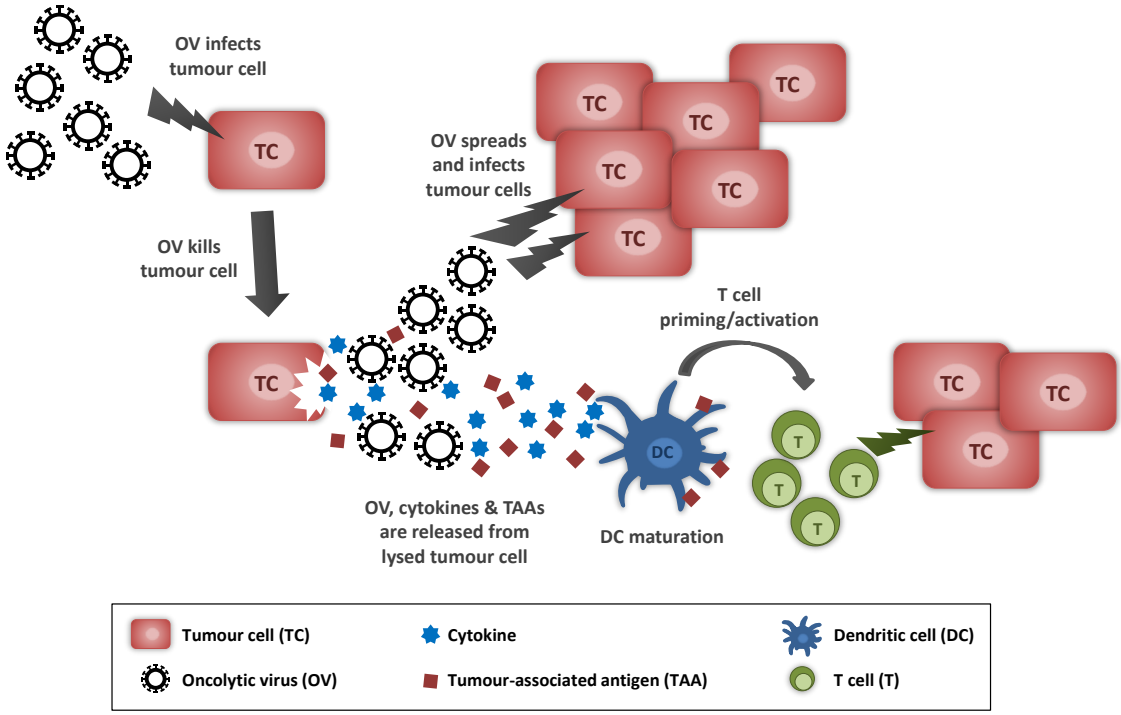

Fig. 1.6: Dual mode of action of oncolytic viruses. Upon infection of a tumour cell with an oncolytic virus, the tumour cell is lysed thereby releasing more virus particles that spread and infect more tumour cells. Also, lysis of tumour cells results in release of tumour-associated antigens and other immunogenic signals such as cytokines that trigger an anti-tumour immune response via maturation of dendritic cells and activation of T cells.

Advances in genetic manipulations offer a wide range of possibilities to improve OV selectivity, replication and lysis of cancer cells, and enhance the ability of OVs to stimulate an anti-tumour immune response. For example, OVs armed with granulocyte-macrophage colony-stimulating factor (GM-CSF), which recruits NK cells and mediates antigen presenting cell (APC)-induced T cell activation, induce anti-tumour immunity [157] [158] [159] [160] [161].

1.8 Coxsackievirus A21 (CVA21) and Intercellular Adhesion Molecule-1 (ICAM-1)

One clinical grade, naturally occurring oncolytic virus is the coxsackievirus A21 (CVA21), a human enterovirus with a positive-sense, single-stranded RNA genome [162]. CVA21 preferentially eliminates malignant cells while sparing on non-tumour cells [163]. Effective targeting and killing of tumour cells by CVA21 requires surface co-expression of Intercellular Adhesion Molecule-1 (ICAM-1) and decay-accelerating factor (DAF). While the role of DAF seems to be restricted to attachment and concentration of the viral particles, ICAM-1 is thought to facilitate both binding and internalisation of CVA21 [164]. The anti-tumour capacity of CVA21 has been demonstrated *in vitro*, for example, in multiple myeloma and prostate cancer cell lines that, in contrast to most non-malignant cells, co-express high endogenous levels of ICAM-1 and DAF [165] [166]. Treatment of subcutaneously established tumours of a prostate cancer xenograft model with CVA21 lead to tumour regression upon systemic delivery of the virus, hence demonstrating *in vivo* efficacy of CVA21 virotherapy [166]. Notably, xenograft tumours derived from ICAM-1 positive GBM cells treated with CVA21 have been shown to regress upon a single intracranial injection followed by multiple intraperitoneal CVA21 injections [167]. Thus, a number of studies demonstrate a proof-of-concept for efficient virotherapy with CVA21 in various cancers including melanoma, prostate cancer and malignant glioma. Most importantly, safety and efficiency of CVA21 therapy is already being evaluated in clinical trials for the treatment of solid tumours such as melanoma, breast cancer, lung cancer and prostate cancer (e.g., ClinicalTrials.gov identifier NCT01636882, NCT00636558, NCT02043665). However, surface expression of ICAM-1 is a prerequisite of efficient virotherapy with CVA21.

ICAM-1 (also known as CD54) is a glycosylated transmembrane protein with five extracellular immunoglobulin-like domains, a transmembrane domain and short cytoplasmic domain at the carboxyl-terminus [168]. It is constitutively expressed on the surface of various different cell types including epithelial and endothelial cells, fibroblasts and leukocytes [169]. As a ligand for $\beta 2$ integrin lymphocyte function-associated antigen (LFA)-1, ICAM-1 functions as an adhesion molecule promoting interactions between different immune cells and between immune cells and the vascular endothelium. Thus, ICAM-1 is involved in cell recognition and homing of immune cells [170] [171]. Furthermore, a role for LFA-1/ICAM-1 interaction has been suggested in the activation of T cells by facilitating cross-talk between T cells and APCs [172]. The expression of ICAM-1 is mediated by several different immune

stimuli including inflammation and viral infection as well as by certain cytokines and hormones. Inflammatory cytokines such as IL-1β, TNF-α and interferon γ (IFN-γ) represent efficient activators of ICAM-1 expression on various cell types including endothelial and epithelial cells as well as fibroblasts. In contrast, anti-inflammatory cytokines, for example TGF-β or the hormone glucocorticoid hamper the induction of *ICAM1* gene expression [173] [174]. Transcriptional activation of *ICAM1* expression is complex and, depending on the kind of stimulus and the cell type, is regulated by signaling through various different pathways such as the NF-κB, the mitogen-activated protein (MAP) kinase, the signal transducers and activators of transcription (STAT) or the protein kinase C (PKC) signaling pathways [174] [175]. The *ICAM1* promoter region contains various different transcriptional enhancer elements. These include a palindromic interferon-γ-responsive element (pIγRE), CCAAT/Enhancer binding protein (C/EBP), activator protein 1 (AP-1)-like, NF-κB, Ets and specificity protein 1 (SP1) elements, and more recently a CRE binding domain has also been identified within the *ICAM1* promoter [176] [177] [178] [179] [180] [181] [182].

A role of the small molecule RA in ICAM-1 regulation has long been investigated [183]. RA-induced gene expression is usually mediated through binding to retinoic acid receptors (RARs) and subsequent interaction with RA responsive elements (RAREs) within the promoter regions of target genes. Notably, the *ICAM1* promoter has been shown to contain a putative RARE which interacts with RARs complemented with retinoid X receptors (RXRs) [184]. In human epithelial cells, a synergistic effect of RA and TNF-α involving interplay between the RARXα and NF-κB binding sites leading to highly increased *ICAM1* promoter activity has been demonstrated [185]. Also, ICAM-1 expression has been shown to be regulated by RA in human tumour cell lines, including thyroid carcinoma cells, melanoma cells, breast cancer cells [186] [187] [188] [189]. Moreover, ICAM-1 induction through RA treatment increases susceptibility of tumour cells to immune cell-mediated lysis [188].

1.9 Aims and objectives

Despite intensive research efforts, prognosis for patients with GBM has not significantly improved due to rapid tumour recurrence after therapeutic intervention. Therefore, novel therapies to effectively target GSCs, the cell population suggested to drive tumour recurrence, are urgently needed. To achieve this, I focused on investigation of the small molecule KHS101 and oncolytic virotherapy with CVA21 as effective anti-GSC treatments and aimed to address several questions, e.g. whether single compound treatment can affect GSC viability and growth of GSC-derived tumours, whether molecularly diverse GSCs share features or vulnerabilities that can be targeted by this small molecules, or whether virotherapy with CVA21 represents a feasible treatment option for elimination of GSCs. Therefore, in this study, I sought to elucidate novel strategies to eliminate GSCs pursuing two different aims: 1) Determining the anti-tumourigenic potential of the neurogenic small molecule KHS101, and 2) assessing the efficacy of a combination therapy of small molecule treatment and oncolytic virotherapy.

1. The first aim involved the use of the small molecule KHS101 that has recently been identified as a differentiation factor in NPCs. Furthermore, KHS101 has been found to affect proliferation of NPC through degradation of the mitotic spindle protein TACC3 [116]. The functional similarities between normal NSCs and GSCs prompted investigation into KHS101 as an anti-GSC compound. To address GBM heterogeneity, a clinically and molecularly diverse panel of patient-derived GSCs was used for assessment of the effect of KHS101. For analysis of the KHS101-induced phenotype different methods determining GSC self-renewal, differentiation, proliferation, cell viability, cell death and autophagy were applied. Additionally, preliminary investigation into the MOA of KHS101 was carried out including gene expression analysis and metabolic profiling. Moreover, as KHS101 has previously been shown to access the brain, its potential as an anti-tumourigenic agent was assessed in a GSC-derived xenograft mouse model upon systemic administration.

2. For the second aim, I sought to assess the possibility of improving efficacy of virotherapy with CVA21 for GBM treatment through small molecule induced expression of ICAM-1. First, the consequences of high ICAM-1 expression in GBM on immune cell populations were determined in a syngeneic mouse model. Subsequently, a focused small molecule screen was conducted aiming at identifying a compound with the potential to synergistically stimulate *ICAM1* mRNA expression in GSCs together with the known ICAM-1 regulator RA.

Chemically induced ICAM-1 expression was further analysed *in vitro*. Finally, I investigated whether induced ICAM-1 expression is sufficient to increase susceptibility of GSCs to CVA21-mediated cell lysis.

2 KHS101 abrogates the tumourigenic potential of GSCs through induction of a cellular self-destruction phenotype

2.1 Results

2.1.1 KHS101 induces vacuolisation, autophagy and apoptotic cell death in a panel of molecularly different GSCs

2.1.1.1 Characterisation of patient-derived GSCs

The small molecule KHS101 has been previously described as an agent with differentiating effects on rat NPCs of the rat dentate gyrus [116]. Given the molecular and phenotypic characteristics shared between NPCs and glioma stem cells (e.g., [59] [56]), I aimed to analyse the effect of KHS101 on GSCs. For investigation of the potential anti-tumourigenic effects of KHS101, I used patient-derived GSC models that were propagated under adherent and serum-free cell culture conditions. These conditions have been shown to maintain stem cell-like characteristics including self-renewal/clonal growth and BMP/serum-induced differentiation capabilities [76]. Moreover, GSCs give raise to xenograft tumours that mirror the invasive nature of GBM [61]. These qualities make patient-derived GSCs a well suited *in vitro* and pre-clinical *in vivo* model for investigating the anti-tumourigenic activity of small molecules.

I used six different GSC lines derived from primary GBM (GSC1, 4, 13), recurrent GBM (GSC14, 20) and gliosarcoma (GSC11; table 2.1). In contrast to GSC1, 4, 11 and 13, GSC14 and GSC20 cells were derived from recurrent GBM with a treatment history of radiation and chemotherapy (TMZ). Notably, glioma cells cultured under GSC conditions have been shown to maintain their overall phenotype, genotype and gene expression profile upon propagation *in vitro* for at least 11-13 passages [61]. Validation of these findings in my GSC models was beyond the scope of this thesis. However, in order to ensure reproducibility of my results, I only used GSCs that have been passaged for less than 12 passages.

All patient tumours and GSC lines were tested for methylation status of the *MGMT* promoter. MGMT is an enzyme involved in DNA repair mechanisms, for example in response to DNA damage caused by alkylating agents such as TMZ. Upon methylation of the *MGMT* promoter, the *MGMT* gene is silenced and TMZ can more efficiently exert its genotoxic effect [190]. Therefore, *MGMT* promoter methylation has been described as predictive of a survival benefit for GBM patients treated with TMZ. Among our set of GSCs, *MGMT* hypermethylation was only detected in GSC lines GSC1, GSC11 and GSC14. The respective GSC1 and GSC11 patient tumours were also tested positive for *MGMT* methylation. However, the GSC14 patient tumour only showed moderate levels of methylation at the *MGMT* locus. As

Cell line	Patient		Type	Treatment	*MGMT* hyper-methylation	
	Age	Gender		history	Patient	GSC line
GSC1	58	F	Primary GBM	None	Yes	67%
GSC4	Unknown	Unknown	Primary GBM	None	Low	19%
GSC11	75	F	Gliosarcoma	None	Yes	60%
GSC13	79	F	Primary GBM	None	No	2%
GSC14	58	M	Recurrent Giant Cell GBM	Radiotherapy, TMZ	Moderate	91%
GSC20	50	M	Recurrent GBM	Radiotherapy, TMZ, IMA950	No	2%
GBMX	50	F	Giant Cell GBM	None	No	N/A

Cell line	Karyotype	Cytogenetics	GSC Subtype
	Patient	GSC line	GSC line
GSC1	Unknown	Ch7 Amp	**Classical, Proneural**
GSC4	Unknown	Ch7 Amp	**Mesenchymal**, Classical, Proneural
GSC11	45,XX,+7.-10.der (11:13) (q10:q10) [4]/46, idem, +8 [2]	Ch7 Amp, Ch10 Amp	**Mesenchymal**
GSC13	Unknown	Ch7 Amp (& centromere imbalance)	**Proneural**
GSC14	45.X.-Y[20]/46,XY [10]	Ch7 Amp	**Proneural**, Mesenchymal
GSC20	Unknown	Ch7 Amp, Ch10 monosomy	**Proneural, Mesenchymal**
GBMX	Unknown	N/A	N/A

Table 2.1: Clinical information, cytogenetic data and molecular subtype classification of the patient-derived cell lines (TMZ: temozolomide; MGMT: O^6-methylguanine-DNA methyltransferase). The predominant GBM subtypes are shown in bold.

mentioned in 1.3 'Inter- and intratumour heterogeneity of GBM', *MGMT* promoter methylation can be heterogeneous within a tumour [34]; therefore, in the GSC14 model, selection of the GSC subpopulation or the cell culture conditions might have

led to an enrichment of cells with a hypermethylated *MGMT* locus, as observed in the GSC14 cell line.

Additional cytogenetic analysis was carried out to identify chromosomal aberrations in the different GSC lines revealing gains of chromosome 7 in all GSC lines. Chromosome 7 polysomy with or without amplification of *EGFR* is a frequently observed alteration in GBM tumours [191]. In GSC20, a chromosome 10 monosomy was detected. Loss of heterozygosity on chromosome 10 includes the deletion of the tumour suppressor gene *PTEN* and is associated with decreased survival of patients [191]. Moreover, mutational analysis for the presence of a *FGFR3-TACC3* fusion and immunoblot assays showed that none of our GSC lines are harbouring the fusion mutation/protein, but all have elevated TACC3 protein levels compared to non-malignant neural progenitor cells (E. Polson, unpublished data).

In 2010 Verhaak et al. postulated a molecular subtype classification for GBM by multi-dimensional genomic data analysis. Based on mutational, gene expression and DNA copy number data, they established four different subtype signatures classifying GBM tumours into proneural, neural, classical and mesenchymal subtypes [25]. Notably, application of this GBM classification at the single cell level revealed a high level of intratumour heterogeneity of GBM subtypes [39]. Thus, to determine the molecular subtypes of our GSC models and concomitantly address heterogeneity, we performed single cell qRT-PCR quantifying the expression of 88 selected stemness, proliferation and 'Verhaak et al.' GBM classifier genes. This methodology provides the opportunity to determine the relevant gene expression signatures in individual cells of a cell population and, thus, indicates subtype heterogeneity within and across the GSC models. In order to integrate the Verhaak data and our single cell data, the expression values of both data sets were discretised using a 3-level data discretisation approach (Edith Ross, personal communication). Finally, after cell cycle normalisation, the discretised Verhaak data set provided the basis for subtype prediction of individual GSCs. This analysis revealed that GSC models contain cell populations of up to two different subtypes. GSC11 and GSC13 showed predominantly mesenchymal, and proneural signatures, respectively. GSC1, GSC14 and GSC20 contained two subpopulations of cells with different subtype features (GSC1: Classical and proneural; GSC14/GSC20: Proneural and mesenchymal). Our GSC4 model harboured three different subtype compartments: the predominant subtype in GSC4 cells was mesenchymal that mixed with smaller proneural and classical subtype compartments (table 2.1).

Taken together, the clinical, cytogenetic and GBM subtype classification data of our patient-derived GSC lines indicate that our panel of GSC models cover a con-

siderable spectrum of clinical and molecular GBM subtypes. We reasoned that the various GBM types (primary, recurrent GBM, gliosarcoma), the genetic differences and the GBM transcriptional and subtype heterogeneity across and within the GSC lines provide the molecular variety needed for comprehensively investigating KHS101-induced anti-GBM responses.

2.1.1.2 KHS101 reduces proliferation of GSCs

KHS101 has been shown to bind TACC3 protein leading to its proteasome degradation [116] [121], TACC3 is critically involved in the stabilisation of the mitotic spindle during cell division [122] [118]. Work in our lab has shown that TACC3 protein levels are significantly reduced in GSCs upon treatment with KHS101 (E. Polson, unpublished data). As KHS101 targets a protein crucial for cell division, my hypothesis was that KHS101 treatment affects the proliferative capacity of GSCs.
To this end, I examined cell proliferation using immunofluorescence staining for the nuclear protein KI67, which is only expressed in cycling cells, and therefore a commonly used marker for proliferation [192]. To address the effect of KHS101 on proliferation in different GBM subtype contexts, I used the proneural/classical GSC1, the mesenchymal/proneural/classical GSC4, the mesenchymal GSC11, and the proneural/mesenchymal GSC20 models. Additionally, the normal adult NPC line NP1, which has been derived from tissue samples taken from patients during epilepsy surgery [89], was used as a non-cancerous control cell line. As an inactive derivative of KHS101, such as KHS92, was not available at the time of this study and previous studies indicated that KHS92 and the vehicle, dimethyl sulfoxide (DMSO), gave similar results regarding gene expression changes in rat NPCs [116], DMSO was used as the control treatment. Images of KI67 stainings of GSC1, GSC4, GSC11, GSC20 and NP1 cells treated with vehicle reveal a highly proliferative phenotype with the majority of nuclei (DAPI-stained) being KI67-positive. Upon treatment with 1 µM or 7.5 µM KHS101 the number of DAPI/KI67 co-stained nuclei decreased (expectedly) in both GSCs and NP1 cells (figure 2.1A).
The lowest KHS101 concentration tested (1 µM) reduced the percentage of proliferative GSCs from ∼60% to 18-25% (∼3-fold; GSC1 and GSC4), from 75% to 40% (1.9-fold; GSC11) or from ∼70% to 10% (7-fold; GSC20). Treatment with 7.5 µM KHS101 further diminished these percentages to ∼15% (4-fold; GSC1), ∼8% (7.5-fold; GSC4), ∼25% (3-fold; GSC11) or ∼1% (70-fold; GSC20). Interestingly, a similar trend was visible for NP1 cells with 7.5 µM KHS101 leading to a decrease from ∼50% to ∼12% (4-fold) in proliferative cells compared to the vehicle-treated

cells. However, while a KHS101 concentration of 2.5 µM was sufficient to induce a significant reduction in KI67 positive GSCs ($p<0.05$), statistical significance in NP1 cells was only achieved by the higher concentration of 7.5 µM KHS101 (figure 2.1B).

2.1.1.3 KHS101 induces a lethal vacuolisation phenotype in GSCs

Expression of the proliferation marker KI67 in CSCs has been associated with maintenance of the cells' stem cell properties [193]. Accordingly, studies suggest that GSC differentiation is associated with a reduction in GSC proliferation [58]. Furthermore, forced differentiation of GSCs is accompanied by marked morphological changes [58]. Thus, to be able to study GSC behaviour including possible alterations in cell morphology I used live cell imaging monitoring GSCs upon treatment with vehicle (0.1% DMSO) or KHS101 (7.5 µM). Surprisingly, time lapse movies of GSC1 cells treated with KHS101 over 72 hours revealed a different GSC fate. Compared to the vehicle control (0.1% DMSO) treated GSC1 cells, KHS101 (7.5 µM) treated cells displayed a distinct phenotype characterised by reduced cell growth and the emergence of large vacuoles. This phenotype was followed by cell fragmentation associated with cell rounding and death. In contrast, NP1 cells did not exhibit vacuolisation or cell fragmentation upon KHS101 (7.5 µM) treatment (figure 2.2A).
The observed macro-vacuolisation phenotype has not been previously attributed to KHS101, and we therefore sought to investigate this finding further. First, we tested whether the KHS101-related vacuolisation phenotype can be exclusively observed in GSC1 cells or also in different patient-derived GSC lines. Phase contrast images of GSC11 and GSC20 cells taken after 12 hours of KHS101 (7.5 µM) treatment showed the presence of vacuoles (as observed in KHS101-treated GSC1 cells). Interestingly, KHS101 treatment did not induce vacuolisation in NP1 cells and no obvious morphological changes were observed in KHS101-treated NP1 cells when compared to vehicle (0.1% DMSO)-treated NP1 cells (figure 2.2B).
In order to quantify the KHS101-induced vacuolisation phenotype, randomly selected phase contrast images of GSC1, GSC11, GSC20 and NP1 cells treated with vehicle (0.1% DMSO) or KHS101 (1, 2.5 and 7.5 µM) for 12 hours were analysed using ImageJ software. To this end, the vacuolated cellular area was highlighted by colour thresholding (see image panels in figure 2.2C) and quantified as percentage of the total cellular area. The bar graph in figure 2.2C depicts the dose-dependent increase in the percentage of vacuolated area in the tested GSC lines upon treatment with 1, 2.5 and 7.5 µM KHS101. The lowest tested concentration of KHS101 (1 µM) significantly increased vacuolisation in GSCs by ∼4- to 8-fold compared

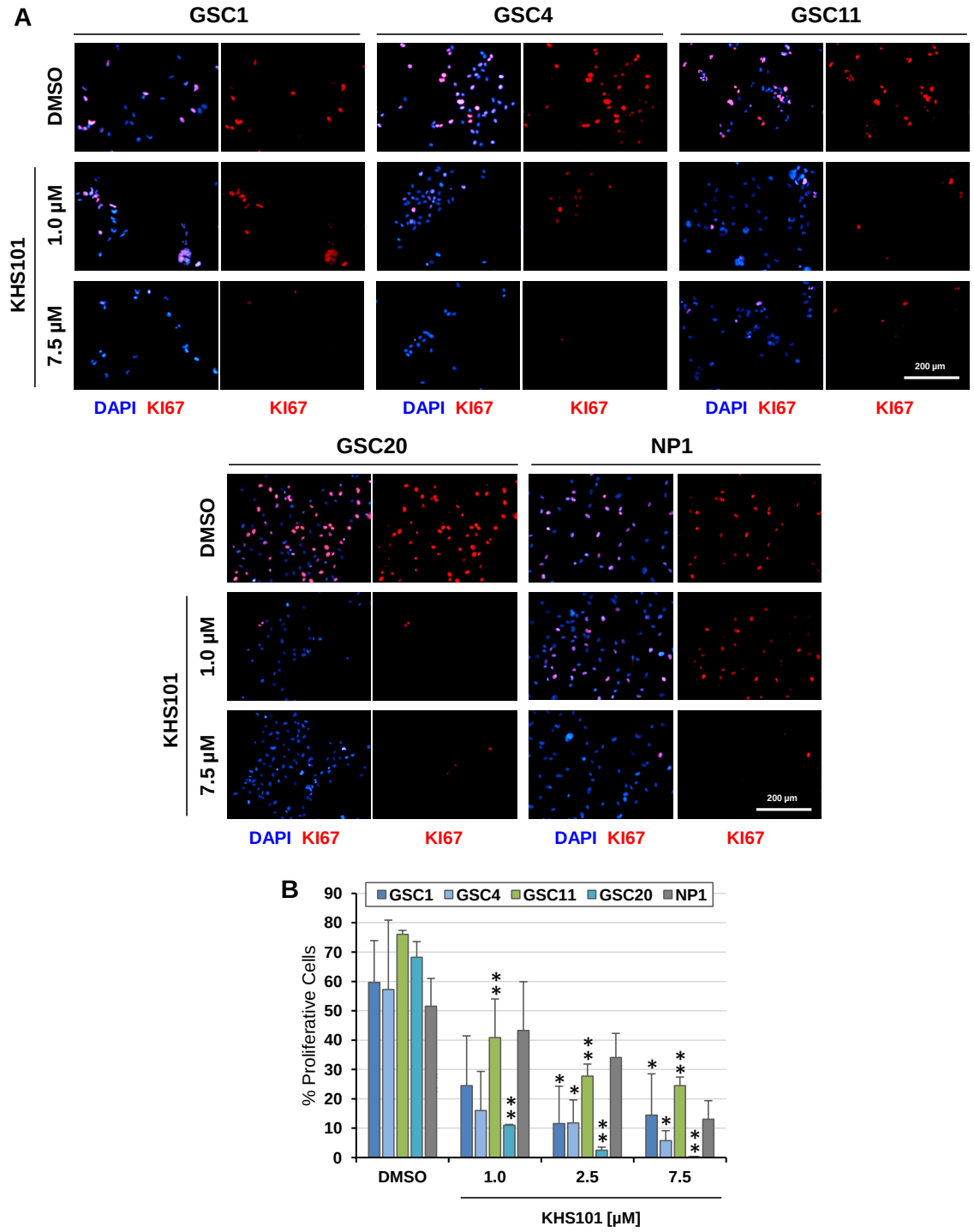

Fig. 2.1: KHS101 reduces proliferation of GSCs. **A)** Example images of KI67 immunofluorescence staining in GSC1, GSC4, GSC11, GSC20 and NP1 cells treated with vehicle or KHS101 (1 µM or 7.5 µM) for 48 hours. Nuclei were stained with DAPI. **B)** Quantification of the concentration-dependent reduction in the percentage of proliferative (KI67 positive) cells 48 hours after KHS101 treatment of GSC1, GSC4, GSC11, GSC20 and NP1 cells (data shown as mean ± SD; n=3; *, $P<0.05$; **, $P<0.01$; Student t test).

to their vehicle-treated counterparts. Treatment with 7.5 µM KHS101 increased the percentage of vacuolated cellular area by ∼16-fold (GSC1), ∼33-fold (GSC20) and ∼40-fold (GSC11) compared to the vehicle-treated control cells. In contrast, quantification of vacuolisation in NP cells demonstrated that there is no significant change in the percentage of vacuolated area in NP1 cells upon KHS101 treatment. Notably, comparing KHS101-induced vacuolisation in GSC and NP1 cells revealed a statistically significant difference in vacuolated GSC cellular area ($P<0.01$), hence confirming the initial observation of a selectively induced vacuolisation phenotype in GSCs (figure 2.2C).

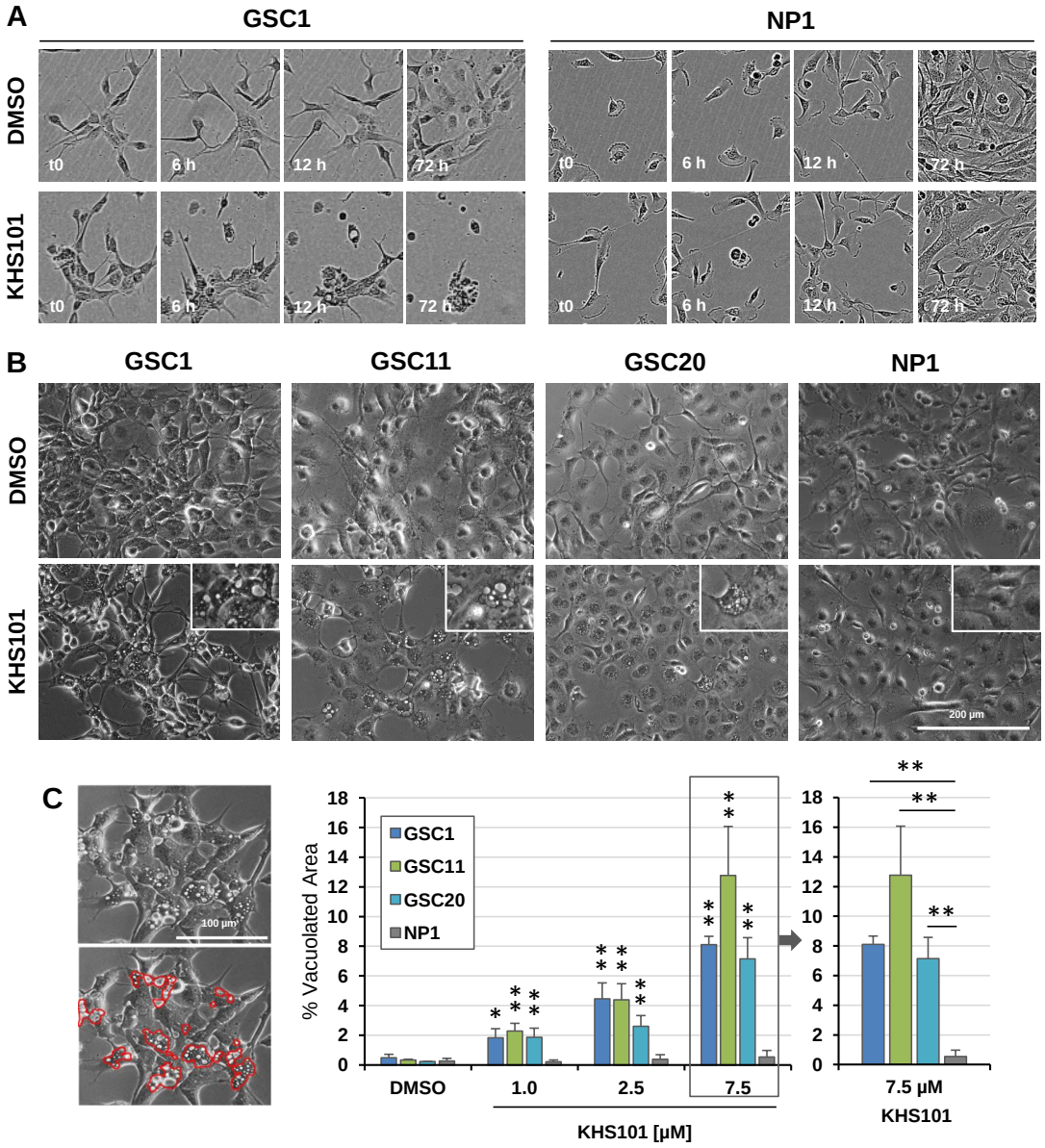

Fig. 2.2: KHS101 induces a lethal vacuolisation phenotype in GSC models. **A)** Representative still images of live cell imaging of GSC1 and NP1 cells treated with vehicle (0.1% DMSO) or 7.5 µM KHS101 indicating vacuolisation and cell death only in GSC1. **B)** Example phase contrast images of GSC1, GSC11, GSC20 and the normal NPC line NP1 treated with vehicle or 7.5 µM KHS101 for 12 hours. Magnified images in top right corner highlight macro-vacuolisation in KHS101-treated GSCs compared with NP cells. **C)** Left: phase contrast images of GSC1 cells treated with 7.5 µM KHS101 for 12 hours. Red outlines mark the vacuolated cytoplasmic area. Right: quantification of the concentration-dependent KHS101-induced vacuolisation in GSC1, GSC11, GSC20 and NP1 cells after 12 hours of KHS101 treatment. Statistical significance was either determined for KHS101 treatment versus vehicle treatment (middle graph) or KHS101-treated GSCs versus KHS101-treated NP1 cells (right graph; data shown as mean ± SD; n=3; *, $P<0.05$; **, $P<0.01$; Student t test).

2.1.1.4 KHS101 affects autophagic activity in GSCs

Recently, a vacuolisation phenotype has been described in GSCs in response to the small molecule Vacquinol-1 [115]. Kitambi et al. conclude that the observed catastrophic vacuolisation induced by Vacquinol-1 is not associated with accumulation of autophagic vacuoles but appears as a result of membrane ruffling and macropinocytosis. Given the similarity of the Vacquinol-1 and KHS101-induced phenotypes, I tested whether pinocytosis is the underlying mechanism of vacuolisation and self-destruction in KHS101-treated GSCs. To this end, I treated GSC11 cells with KHS101 in the presence of the extracellular-phase fluid tracer Lucifer Yellow (LY), whose endocytic uptake into the cells is indicative of the pinocytotic process. However, KHS101 treatment did not increase intercellular incorporation of LY and, therefore, does not seem to affect GSC pinocytosis (figure 2.3A).
In addition to pinocytosis, cellular vacuolisation has been linked to cell starvation and autophagy [194]. To test this possibility, I used the CytoID® assay, which allows for selective staining of autophagic compartments in live cells and quantification of CytoID®-positive/autophagic cells based on fluorescence images, as a first line investigation method. Indeed, CytoID® positive staining was obtained for all tested GSC lines (GSC1, GSC4, GSC11, GSC20) upon treatment with KHS101 (7.5 µM; figure 2.3B). For assessment of a KHS101 dose dependent autophagy induction, the different GSCs were treated with increasing concentrations of KHS101 for 48 hours. The graph in figure 2.3C depicts the obtained dose response data for GSC1, GSC4, GSC11 and GSC20 cells. Significant ($P<0.01$) induction of autophagy was triggered by KHS101 (2.5 µM and 7.5 µM concentrations were tested) in all cell lines resulting in 75-98% of autophagic cells. In contrast, only 1-7% autophagic cells were detected in vehicle-treated cells. Observation of GSCs over time revealed a steady increase of CytoID® positive cells over a 12-hour KHS101 treatment peaking at 48 hours with ∼90% of CytoID® positive cells (figure 2.3D). Importantly, CytoID® positive staining was significantly elevated after treatment with KHS101 for 48 hours in the four different GSC models (GSC1, GSC4, GSC11, GSC20) as compared with vehicle (DMSO 0.1%) treated cells. The strongest effect was observed in the gliosarcoma model GSC11 and co-staining of the autophagosomal CytoID® dye with the lysosomal LysoID® dye revealed their partial co-localisation (figure 2.3E). This suggested fusion of autophagosomes with lysosomes upon KHS101 treatment. However, autophagy is a complex process, thus requiring a more detailed insight into the nature of KHS101-induced autophagy. To test this, I additionally carried out immunofluorescence staining for microtubule-associated protein 1 light chain 3 β (LC3B), a protein that is ubiquitously distributed in the cytoplasm and is recruited

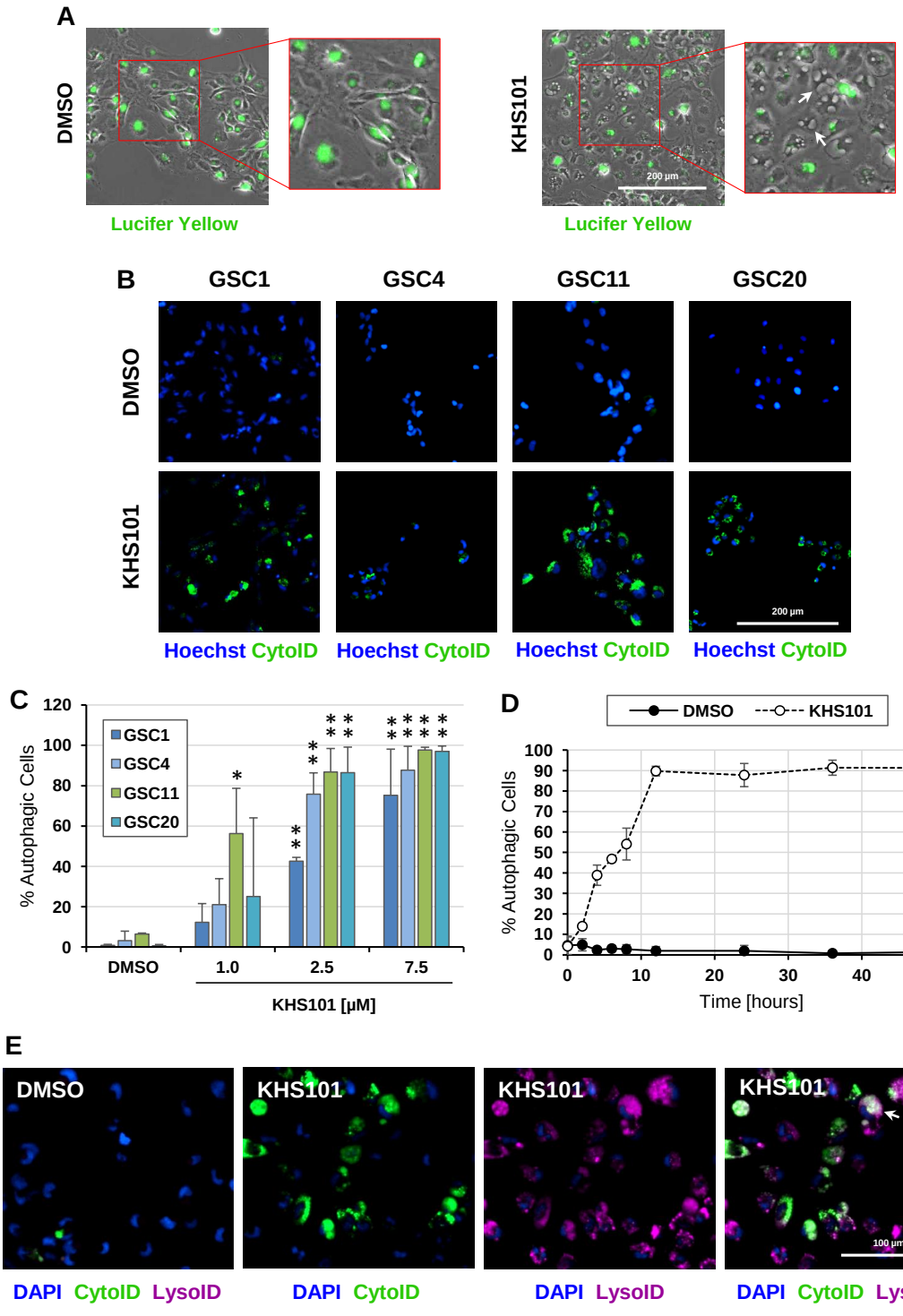
A
DMSO
KHS101
Lucifer Yellow
Lucifer Yellow
B
GSC1
GSC4
GSC11
GSC20
DMSO
KHS101
Hoechst CytoID
Hoechst CytoID
Hoechst CytoID
Hoechst CytoID
C
% Autophagic Cells
GSC1
GSC4
GSC11
GSC20
DMSO
1.0
2.5
7.5
KHS101 [μM]
D
DMSO
KHS101
% Autophagic Cells
Time [hours]
E
DMSO
KHS101
KHS101
KHS101
DAPI CytoID LysoID
DAPI CytoID
DAPI LysoID
DAPI CytoID LysoID

to form autophagosomes, e.g. during starvation [195] [196] [197]. High resolution confocal LC3B immunofluorescence images of vehicle- and KHS101-treated GSC11 cells at the 12-hour time point showed a clear difference in staining patterns. In contrast to the diffuse signal in the control cells, the KHS101-treated cells displayed a punctate LC3B staining pattern as characteristic for LC3B protein associated with autophagosomes (figure 2.4A; [195]).

As expected, the other tested GSC lines (GSC1 and 20) also presented altered LC3B staining upon KHS101 treatment as shown by phase contrast/LC3B overlay images in figure 2.4B. Based on those images, we determined the LC3B positive area as a percentage of the total cellular area using the ImageJ software. The images in figure 2.4C show the selection of the LC3B positive area by the software and the graph depicts the results of the LC3B measurements for GSC1, 11, 20 and NP1 cells. In all tested GSC lines, a significant increase in LC3B positive area, ranging between 9-fold (in GSC1) and 23-fold (in GSC11) was obtained by treatment with 7.5 µM KHS101. The apparent discrepancy between CytoID® data and LC3B stainings at lower (1 µM, 2.5 µM) KHS101 concentrations can be explained by the different time points and different read-outs chosen for the analysis. While the quantification of the LC3B staining, based on the determination of the percentage of LC3B positive area, represents the autophagic stage after 12 hours of KHS101 treatment, the CytoID® stainings, analysed by determination of the percentage of positive cells, were done at the 48-hour time point. Therefore, at an earlier time point (12 hours), only a KHS101 concentration of 7.5 µM leads to a significant increase in autophagic vesicles in all tested GSC models. However, upon a prolonged exposure (48 hours), a KHS101 concentration of 2.5 µM significantly induces the number of autophagic

Fig. 2.3 ***(preceding page)***: KHS101 induces a CytoID positive phenotype in GSC models. **A)** Example images of LY uptake into GSC11 cells treated with vehicle (0.1% DMSO) or 7.5 µM KHS101 for 16 hours indicating that KHS101-induced vacuolisation is not a result of increased endocytotic activity (white arrows highlight vacuoles not containing LY). **B)** Example images of CytoID/LysoID co-staining in GSC11 cells treated with vehicle or 7.5 µM KHS101 for 48 hours. Nuclei were stained with Hoechst 33342. White arrows highlight examples of CytoID/LysoID staining overlap. **C)** Example images of CytoID staining in GSC1, GSC4, GSC11, GSC20 and NP1 cells treated with vehicle or 7.5 µM KHS101 for 48 hours. Nuclei were counterstained with Hoechst 33342. **D)** Graph showing the increase in the percentage of autophagic (CytoID-positive) GSC11 cells over time peaking at 12 hours of KHS101 (7.5 µM) treatment. **E)** Graph summarising the percentage of autophagic (CytoID positive) cells after treatment with vehicle or increasing concentrations of KHS101 in GSC1, GSC4, GSC11, GSC20 and NP1 cells at the 48 hour time point (data shown as mean ± SD; n=3; *, $P<0.05$; **, $P<0.01$; Student t test).

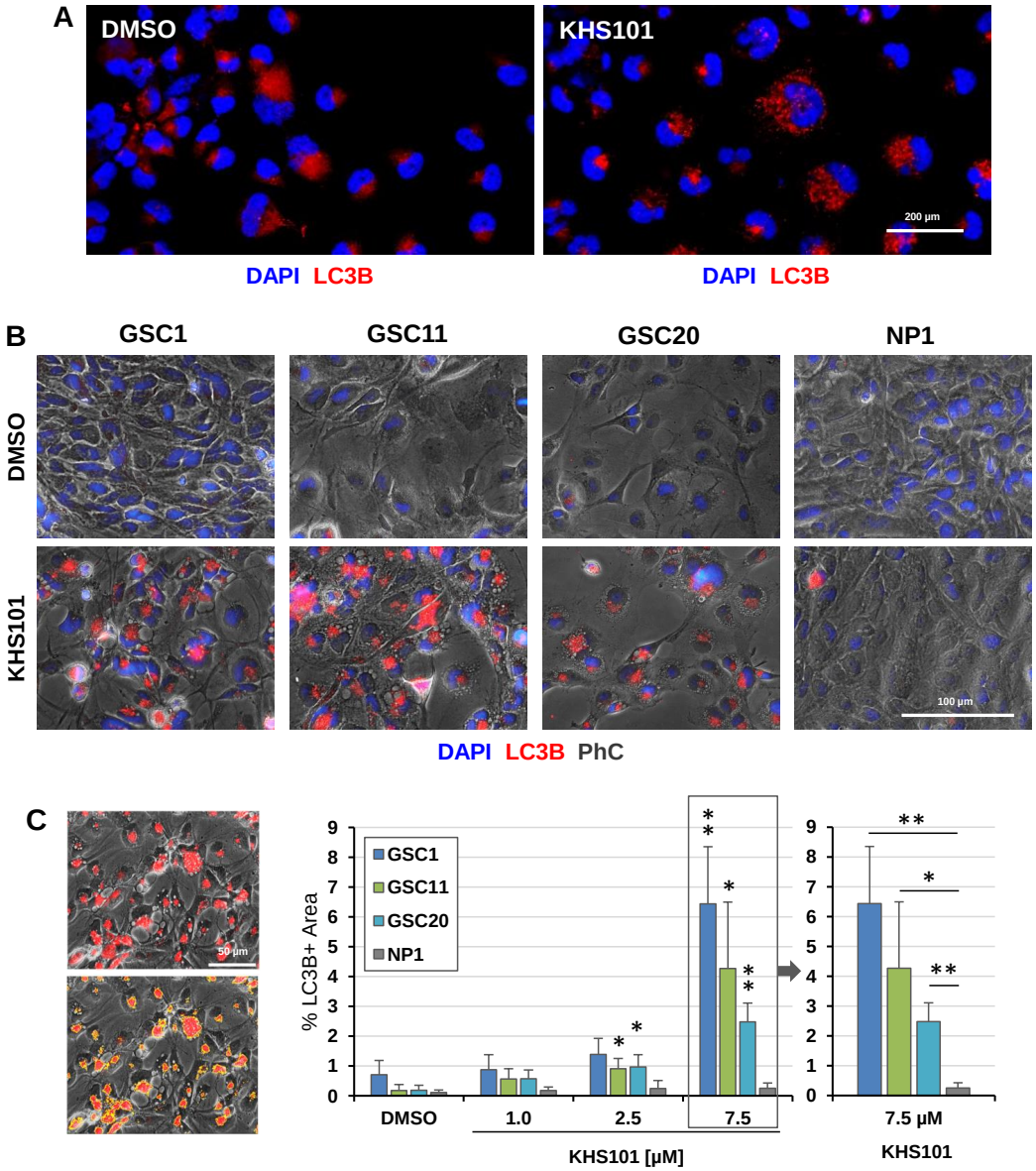

Fig. 2.4: KHS101 induces LC3B-positive early autophagosome formation in GSCs. **A)** Example images of LC3B immunofluorescence staining in GSC11 cells treated with vehicle (0.1% DMSO) or 5 µM KHS101 for 12 hours. Nuclei were counterstained with DAPI. **B)** Representative images of LC3B immunofluorescence staining in GSC1, GSC11, GSC20 and NP1 cells treated with vehicle or 7.5 µM KHS101 for 12 hours. Nuclei were counterstained with DAPI. **C)** Left: LC3B immunofluorescence images of GSC1 cells treated with 7.5 µM KHS101 for 12 hours. Yellow outlines mark the LC3B positive area. Right: Quantification of the concentration-dependent KHS101-induced LC3B-positive staining in GSC1, GSC11, GSC20 and NP1 cells. Statistical significance was either determined for KHS101 treatment versus vehicle treatment (middle graph) or KHS101-treated GSCs versus KHS101-treated NP1 cells (right graph; data shown as mean ± SD; n=3; *, $P<0.05$; **, $P<0.01$; Student t test).

cells. Notably, in contrast to GSCs, NP1 cells did not exhibit a significant change in LC3B staining upon KHS101 (7.5 µM; 12 hours) treatment.

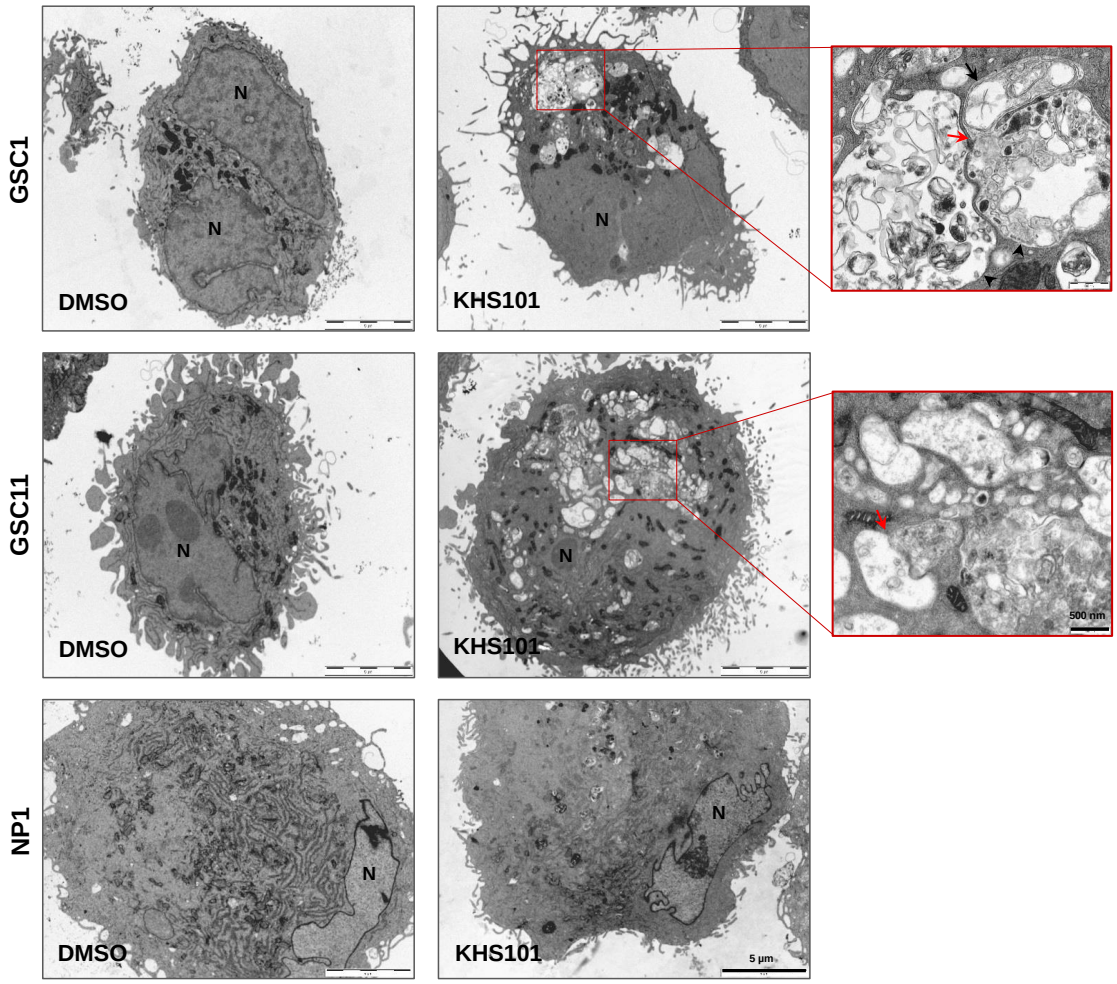

Fig. 2.5: Representative EM images of GSC1, GSC11 and NP1 cells treated with vehicle (0.1% DMSO) or 7.5 µM KHS101 for 12 hours. Scale bar: 5 µm. Magnified images on the right show electron-dense vacuoles in KHS101-treated GSC1 and GSC11 cells. Scale bar: 500 nm. N: nucleus; black arrow highlights vacuole with double membrane; black arrowheads highlight vacuoles with single membrane; red arrows highlight fusing vacuoles.

In addition to CytoID® and LC3B detection methods, a third line investigation of KHS101-induced autophagy was based on electron microscopy (EM). We conducted EM analysis of two representative GSC models (GSC1, GSC11) and NP1 cells treated with 7.5 µM KHS101 for 12 hours. The EM images of KHS101-treated GSC1 and GSC11 cells shown in figure 2.5 display the presence of macro-vacuoles (>1 µm in diameter). Higher magnification of the vacuoles in KHS101-treated GSCs revealed double-membraned vacuoles filled with electron-dense material (indicative of autophagosomes) and single-membraned vacuoles (indicative of lysosomes). Par-

tial fusion of these vacuoles could also be seen in the high magnification images (figure 2.5). In contrast to GSC1 and GSC11 cells, no vacuoles were formed in KHS101-treated NP1 cells. This was consistent with live cell imaging of NP1 cells and the observation that KHS101 treatment did not alter the vacuolated and LC3B-positive cellular area measured in NP1 cells in contrast to vehicle-treated cells, thus further supporting the notion of a selective and combined KHS101-induced vacuolisation and autophagic phenotype in molecularly different GSC lines.
Together, these observations indicate the recycling of various cytoplasmic components through an autophagic route, suggesting a self-degradation process triggered by KHS101. However, autophagy is a dynamic process and an increase in autophagic and lysosomal vesicles, as observed in KHS101-treated GSCs, could also be indicative of a block in autophagic flux. Hence, further investigation into the effect of KHS101 on autophagic flux would be a future task and could be achieved by assessing LC3 turnover by immunoblot analysis or by detection of autophagosomal/lysosomal degradation of labeled proteins (see also 2.2 'Discussion').

2.1.1.5 KHS101 reduces viability of molecularly different GSCs and induces apoptosis in GSCs but not NPs

As a cellular degradation process, autophagy has been associated with cell death programs, e.g., apoptosis and necroptosis [198]. Notably, recent studies link increased cellular autophagy with reduced cell viability and apoptosis of glioma cell lines [112] [199] [200]. Therefore, I sought to assess whether KHS101-induced autophagy is associated with reduced GSC viability and onset of apoptosis. To test the effect of KHS101 on cell viability, we conducted luminescence-based cell viability assays (CellTiter-Glo®, Promega) using our panel of six molecularly diverse GSCs (GSC1, GSC4, GSC11, GSC13, GSC14 and GSC20), thus enabling us to ascertain whether diverse GSC lines show differential responses to KHS101. Additionally, two different NPC lines (NP1 and NP2) were tested serving as non-cancerous controls. Figure 2.6 shows the cell viability dose response curves and respective IC50 values for GSCs and NPs treated with KHS101 (0-20 µM) for 2 days and for 5 days. Consistent with previous observations from live cell imaging, KHS101 did not significantly affect cell viability of NP cells. Even after 5 days of treatment with up to 20 µM KHS101, both tested NP cell lines, NP1 and NP2, displayed only a small reduction in cell viability (IC50 $>$ 18 µM). In contrast, GSC lines exhibited a significant concentration-dependent decrease in viability after 2 and 5 days of KHS101 treatment. For example, treatment of GSC1 with 5 µM KHS101 for 2 days reduced

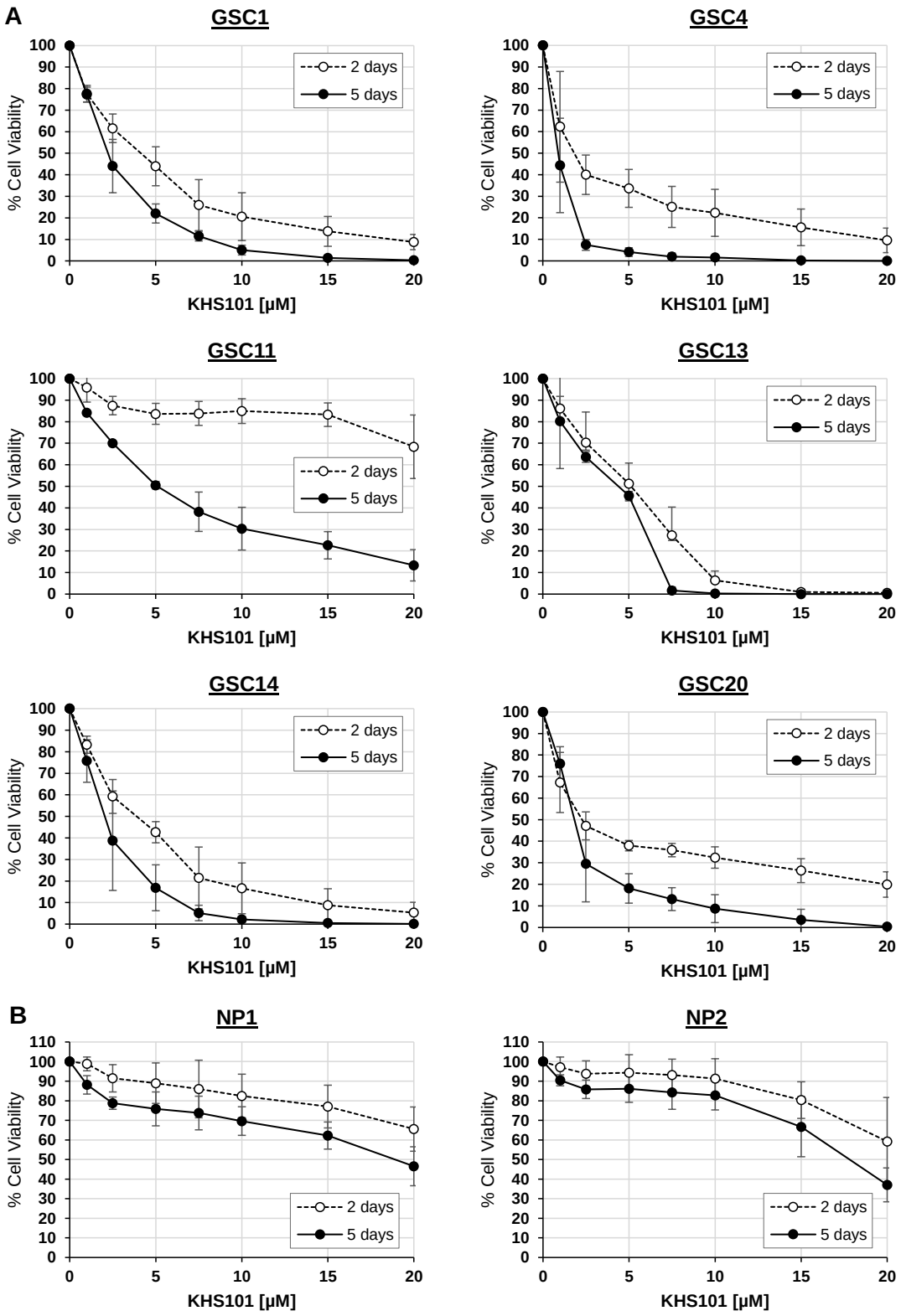

Fig. 2.6: KHS101 exhibits differential cytotoxicity in GSCs and adult neural progenitor cells. **A** and **B)** Differential cell viability dose response curves of the patient-derived GSC lines GSC1, GSC4, GSC11, GSC13, GSC14 and GSC20 (A), and the patient-derived normal NPC lines NP1 and NP2 (B) are shown (data shown as mean ± SD; n=3).

the percentage of cell viability by ∼56%. Treatment with 20 µM KHS101 for 2 days decreased cell viability by >90%. Longer exposure (5 days) of GSC1 cells to KHS101 led to a decrease in cell viability by 78% (5 µM) and 100% (20 µM; figure 2.6A). In summary, irrespective of their subtype classification, clinical background or cytogenetic profile, all tested GSCs were susceptible to KHS101-induced cytotoxicity with 5-day-IC50 values ranging between ∼1 µM in GSC4 and ∼5 µM in GSC11 (table 2.2).

Cell line	IC50	
	2 days	**5 days**
GSC1	3.62 (3.10;4.23)	2.23 (2.02;2.47)
GSC4	2.37 (1.73;3.25)	0.97 (0.90; 1.04)
GSC11	> 18	5.05 (4.51;5.64)
GSC13	4.25 (3.65;4.95)	3.28 (2.77;3.89)
GSC14	3.46 (2.98;4.02)	1.98 (1.67;2.33)
GSC20	3.39 (2.63;4.36)	1.87 (1.58;2.21)
NP1	> 18	> 18
NP2	> 18	> 18

Table 2.2: IC50 values [µM] for GSCs and NPs treated with KHS101 for 2 days or 5 days (data shown with 95% confidence interval).

To investigate whether KHS101-induced autophagy in GSCs, and the observed reduction in GSC viability, is associated with cell death via the apoptotic pathway, I assessed the activity of executioner caspases of the apoptosis pathway in KHS101-treated GSCs. To this end, caspase 3/7 activity was measured using a luminescence assay (Caspase-Glo® 3/7 Assay). First, I analysed the induction of apoptosis over time to determine the optimal time point for further analysis of caspase 3/7 activity. To this end, the combined activity of caspase-3 and -7 was determined in GSC1 cells at t0 and after 6, 12, 24 and 48 hours of treatment with 7.5 µM KHS101. Caspase 3/7 activity steadily increased upon KHS101 treatment from 2-fold at 12 hours over 4.5-fold at 24 hours to 7-fold at 48 hours (compared to t0). In comparison to vehicle-treated cells, a significant 3.5-fold higher fold change value was obtained for KHS101-treated GSC1 cells at the 48 hour time point (figure 2.7A). Next, I tested whether caspase 3/7 activity was also induced by KHS101 in other GSC lines. Due to the KHS101-induced caspase 3/7 activation peak at 48 hours, I measured apoptosis activation in KHS101-treated GSC1, GSC11 and GSC20 cells at this time point. Treatment with KHS101 (7.5 µM) significantly induced activation of

caspase-3 and -7 resulting in a 4-fold (GSC11), 8-fold (GSC1) and 15-fold (GSC20) increase compared to the vehicle controls (figure 2.7B). The presence of the caspase inhibitor Z-VAD-FMK efficiently abolished KHS101-induced caspase activity in all tested cell lines reducing the signal to baseline levels measured in vehicle-treated cells. Notably, KHS101 treatment induced caspase3/7 activity comparable to treatment with 1 µM of the known apoptosis inducer staurosporine [201], which was used as a positive control. Staurosporine also activated the apoptotic pathway in NP1 cells (>5-fold); however, treatment of NP1 cells with KHS101 did not significantly alter caspase-3/7 activity. Statistical comparison of the obtained data for GSCs and NP1 cells showed a significant difference in apoptosis activation by KHS101 between the GSC models and the non-tumour NP cells.

Taken together, the data presented in section 2.1.1 indicate that in a glioma stem cell-like context, KHS101 dose-dependently induces a distinct phenotype characterised by reduced cell proliferation, the formation of large vacuoles, and the onset of autophagy. Notably, this KHS101-induced vacuolisation/autophagy GSC phenotype is associated with reduced cell viability and onset of caspase-dependent apoptosis in molecularly different GSC models. This lethal phenotype is selectively induced in GSCs, but not NP cells indicating differential cellular responses to KHS101 in malignant glioma versus non-cancerous cells. Interestingly, TACC3 knockdown studies indicate a TACC3-independent MOA of KHS101-induced cytotoxic vacuolisation/autophagy in GSCs (E. Polson, unpublished data).

2.1.2 KHS101 attenuates the GSC phenotype

Assessment of the effect of KHS101 on cell viability (figure 2.6) revealed that the cytotoxic effect of KHS101 is dose dependent leaving 44-84% and up to 38% viable cells after 5 days of KHS101 treatment with 1 µM and 7.5 µM, respectively. Therefore, I was interested in determining the cell fate of these 'surviving' cells. Literature evidence indicates that autophagy plays a critical role in development and differentiation [202] and increased autophagy has been shown to be correlated with reduced 'stemness' properties of GSCs [93]. Thus, I sought to analyse the 'stemness' characteristics of KHS101-treated GSCs. To this end I assessed the expression of GSC 'stemness' markers NESTIN and SOX2 [203] [204] [205] and determined the clonal growth capacity of GSCs.
NESTIN and SOX2 immunofluorescence stainings of GSC1 and GSC20 cells treated with a low (1 µM) and a high (7.5 µM) concentration of KHS101 for 5 days sug-

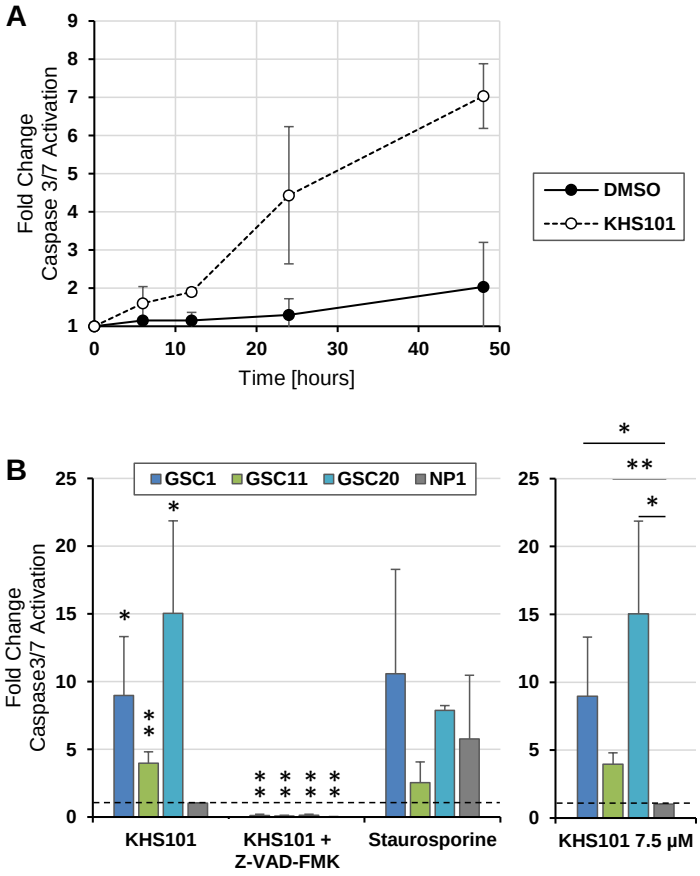

Fig. 2.7: KHS101 selectively induces apoptotic cell death in GSCs. **A)** Time course of KHS101-induced caspase 3/7 activation in GSC1 cells indicating an increase over time. Data normalised to t0 (data shown as mean ± SD; n=3). **B)** Fold changes of caspase 3/7 activation in GSC1, GSC11, GSC20 and NP1 cells induced by 7.5 µM KHS101 (K) or 7.5 µM KHS101 + 2 µM Z-VAD-FMK (Z; caspase inhibitor) for 2 days, or 1 µM staurosporine (S; apoptosis inducer) for 6 hours. Data normalised to vehicle control (0.1% DMSO). Statistical significance was either determined for compound treatment versus vehicle treatment (left graph) or KHS101-treated GSCs versus KHS101-treated NP1 cells (right graph; data shown as mean ± SD; n=3; *, $P<0.05$; **, P$P<0.01$; Student t test).

gested a reduced expression of both 'stemness' markers compared to vehicle (0.1% DMSO)-treated cells (figure 2.8A). Quantification of NESTIN stainings was done by allocating stained cells into three different groups based on the intensity of the immunofluorescence signal. The three groups were defined by measuring the mean fluorescence intensity (MFI) of single cells using ImageJ software. The cells were then classified as NESTIN^{high} (MFI > 25), NESTIN^{low} (MFI = 5-25) or non-expressing (MFI < 5) cells. The resulting percentages of NESTIN^{high}, NESTIN^{low} or NESTIN-negative GSC1 and GSC20 cells are depicted in figure 2.8B. In GSC1 cells, KHS101 treatment decreased the percentage of NESTIN^{high} cells from ∼50% to ∼28% (1 µM) and ∼10% (7.5 µM). Similarly, the percentage of NESTIN^{high} GSC20 cells was reduced upon KHS101 treatment from 21.6% to 16.4% (1µM) and 0.8% (7.5 µM). Quantification of SOX2 stainings by allocating cells into SOX2^{high}, SOX2^{low} and SOX2-negative cells revealed a similar trend as observed for NESTIN. In GSC1, the percentage of SOX2^{high} cells was decreased from 56% to 32% (1 µM) and 11% (7.5 µM). A comparable pattern was obtained for GSC20 cells with KHS101 causing a decrease in the percentage of SOX2^{high} cells from 49% to 38% (1 µM) and 2.5% (7.5 µM; figure 2.8B). Notably, the observed reduction in the expression of 'stemness' markers was not accompanied by a concurrent increase in the expression of proteins associated with a more differentiated phenotype, i.e. glial fibrillary acidic protein (GFAP; [206]), an astroglial lineage marker, and neuron-specific class III β-tubulin (TUJ1; [207]), a neuronal lineage marker (data not shown).

In order to assess the effect of KHS101 on the clonal growth ability of GSCs, the cells were seeded at clonal density, treated with KHS101 and the single cells were counted the following day. As soon as colonies consisted of a minimum of six cells (after 7-10 days), the number of colonies was determined and the percentage of colony forming cells was calculated (see left part of scheme in figure 2.9A). All five tested GSC lines (GSC1, GSC4, GSC11, GSC13, GSC20) completely lost their ability to form colonies upon treatment with KHS101 (1 µM and 7.5 µM; figure 2.9B).

In the light of reports indicating that differentiated GSCs are able to regain GSC features after removal of the differentiation stimulus, e.g. BMP [57], I tested whether cells recover from KHS101-induced impairment of GSCs' clonal growth capacity after removal of the compound. To address this, a second approach for assessment of the colony formation efficiency was adopted. GSCs were treated with KHS101 (1 µM; 7.5 µM) for 2 days, the compound removed and the colony formation efficiency was determined 7-10 days later (pre-treatment; see right part of scheme in figure 2.9A). Notably, 1 µM KHS101 did not have a significant effect on the colony formation capability of GSC1 and GSC20 cells. However, compared to vehicle (0.1%

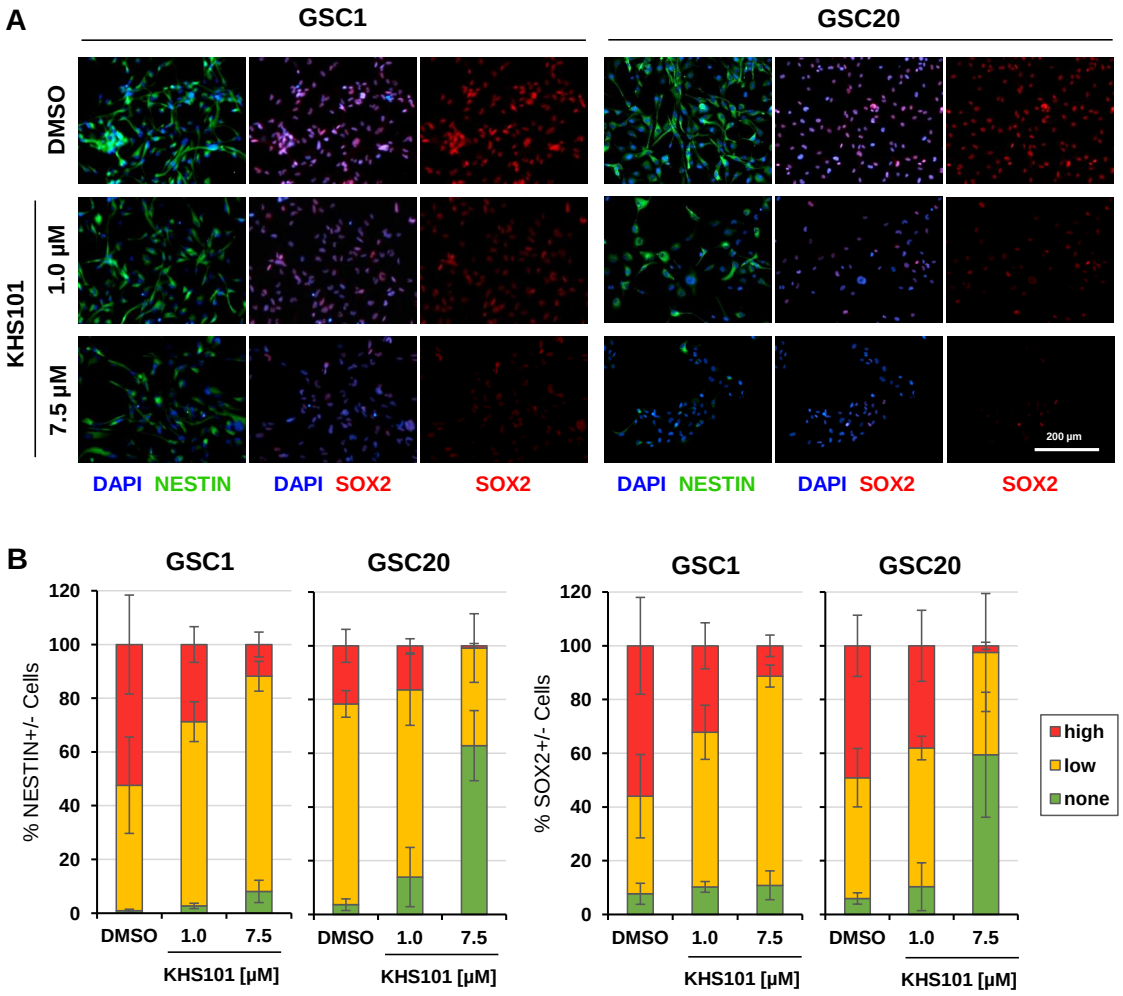

Fig. 2.8: KHS101 reduces expression of the stem cell markers NESTIN and SOX2. **A)** Example images of NESTIN and SOX2 immunofluorescence staining in GSC1 and GSC20 cells treated with vehicle (0.1% DMSO) or KHS101 (1 µM or 7.5 µM) for 5 days. Nuclei were stained with DAPI. **B)** Quantification of the concentration-dependent reduction in highly NESTIN- or SOX2-expressing GSC1 and GSC20 cells after 5 days of KHS101 treatment. NESTIN/SOX2^{negative}: MFI<5; NESTIN/SOX2^{low}: MFI 5-25; NESTIN/SOX2^{high}: MFI>25 (MFI: Mean Fluorescence Intensity; data shown as mean ± SD; n=3).

DMSO) treatment, pre-treatment with 7.5 µM KHS101 reduced the colony formation efficiency of all three tested GSCs by 5.7-fold (GSC1), 8-fold (GSC11) and ~3-fold (GSC20; figure 2.9C). Hence, even after removal of KHS101, GSCs exhibit a diminished ability to form colonies from single cells.

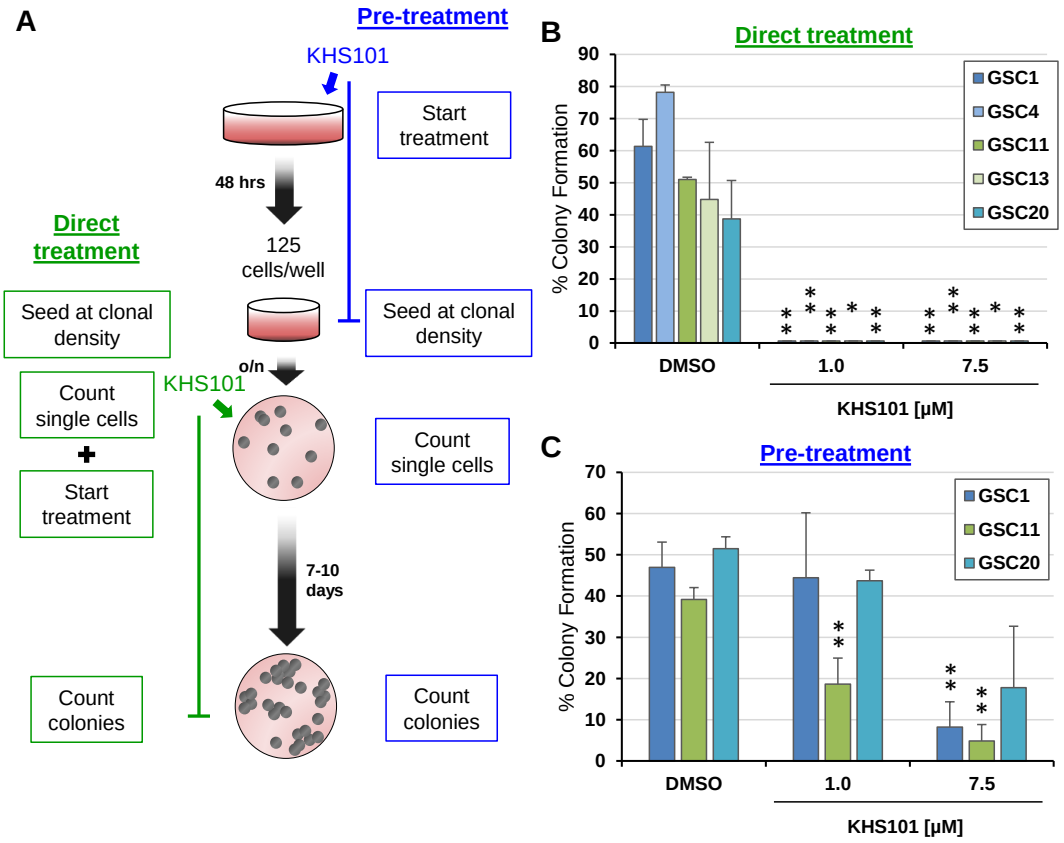

Fig. 2.9: KHS101 reduces/abrogates the clonal growth capability of GSCs. **A)** Scheme depicting the experimental protocol for assessment of the clonal growth capability of GSCs upon direct treatment with KHS101 (green) or after 48 hours of treatment with KHS101 (blue). **B)** KHS101 treatment leads to complete abrogation of clonal growth capacity of GSC1, GSC4, GSC11, GSC13 and GSC20 (as determined according to the workflow depicted in green in A). **C)** Reduction of clonal growth capability of KHS101 pre-treated GSC1, GSC11 and GSC20 cells compared to vehicle-treated cells (as determined according to the workflow depicted in blue in A). Data shown as mean ± SD; n=3; *, $P<0.05$; **, $P<0.01$; Student t test.

In conclusion, parallel investigation into the fate of KHS101-treated GSCs was conducted addressing their 'stemness' characteristics by applying marker as well as functional assays. Strikingly, the GSC population that survives 5 days of KHS101 treatment displayed reduced levels of 'stemness' markers NESTIN and SOX2. More-

over, a significant reduction in the clonal growth capacity was observed in KHS101-treated GSCs. In summary, KHS101 targets GSCs by mitigating essential stem cell characteristics.

2.1.3 KHS101 elicits anti-tumourigenic effects in vivo

2.1.3.1 Systemic administration of KHS101 leads to reduced proliferation of GSCs in established xenograft tumours

To investigate the effect of KHS101 *in vivo*, I used a pre-clinical mouse model based on intracranial injection of GSC1 cells into immunocompromised mice [89]. After xenograft tumours had established (six weeks), KHS101 was systemically administered according to a dosing regimen adapted from published work [116]. In their study, Wurdak et al. describe quick brain distribution of KHS101 upon intravenous injection of 3 mg/kg reaching >30 µM and significant neurogenic effects of KHS101 after 14 days when injected subcutaneously (s.c.) at 6 mg/kg. However, the pharmacokinetic profile of KHS101 was obtained for rats and in the context of a neurogenesis readout. Also, the half-life of KHS101 in the brain was demonstrated to be <1 hour. Together with my finding that KHS101 function (e.g., on cell viability and clonal growth capability) is stronger upon prolonged exposure, the short *in vivo* half life of KHS101 prompted adaptation of the dosing regimen applied by Wurdak et al. to ensure extended exposure of tumours to KHS101. Therefore, a 10-week treatment strategy of two daily s.c. injections of KHS101 (6 mg/kg) was applied. However, to reduce skin irritation caused by continuous s.c. injections, dosing was limited to 5 and 3 treatment days per week with bi-weekly alteration.

To confirm *in vitro* data on the effect of KHS101 on proliferation, immunological analysis for the expression of the proliferation marker KI67 in the xenograft tumours was performed. The immunofluorescence images shown in figure 2.10A demonstrate a strong nuclear KI67 staining in the control tumours and a reduced positivity for KI67 in KHS101-treated tumours. Identification of the nuclear KI67 immunopositive area in vehicle- and KHS101-treated tumours revealed a significant decrease in the percentage of KI67-positive tumour area upon KHS101 treatment by 2-fold (12% to 6%; graph in figure 2.10A).

Furthermore, histological analysis of KHS101-treated tumours revealed morphological features associated with necrosis including small nuclear fragments and overall decreased nuclear density (figure 2.10B).

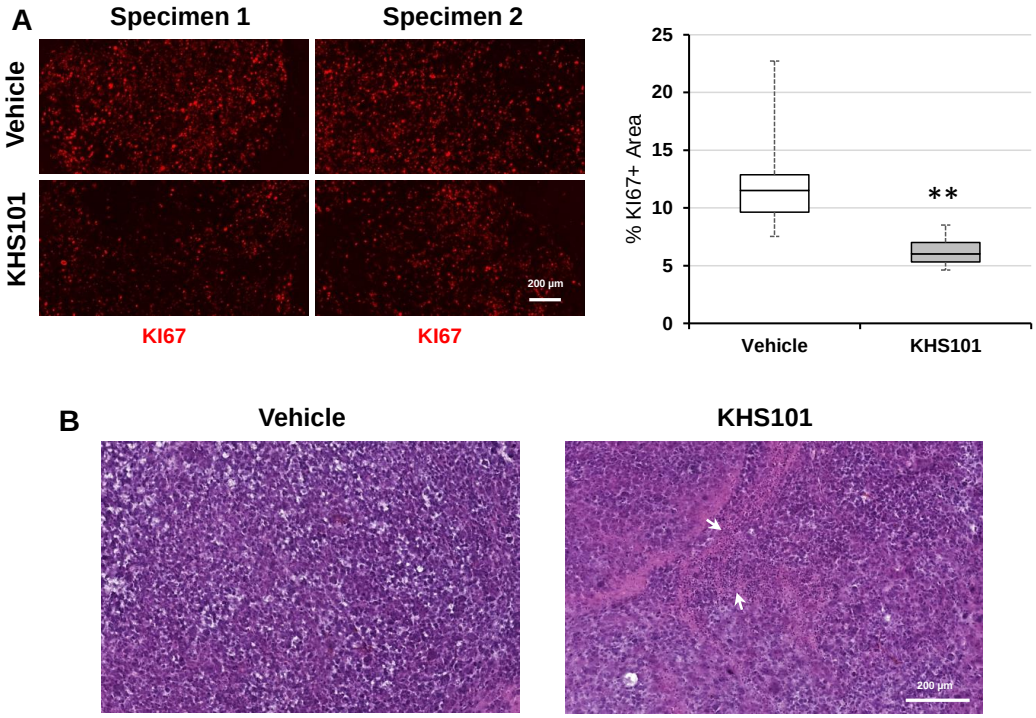

Fig. 2.10: KHS101 reduces proliferation of GSCs in xenograft tumours and leads to changes in tumour morphology. **A)** Left: Representative images of HK2-stained GSC1-derived tumour sections (examples of two different specimen per group are shown). Right: Quantification of the HK2-positve tumour area indicating an increased HK2 expression in KHS101- versus vehicle-treated tumours (n=5; **, $P<0.01$; Mann Whitney U-test). **B)** Example images of H&E stained sections of GSC1-derived xenograft tumours treated with vehicle of KHS101 showing changes in tumour morphology upon KHS101 treatment including highly necrotic areas (marked with white arrows). Scale bar: 200 µm.

2.1.3.2 KHS101 reduces GSC invasion and tumour burden

The highly invasive nature of GBM tumours complicates treatment and targeting this feature of GBM tumours constitutes a much needed addition to current therapies to control GBM tumours [208]. Since a defining feature of GSCs is their highly infiltrative growth behaviour *in vivo*, GSC-derived xenograft model, which have been shown to be characterised by infiltrative behaviour [61], are well suited for investigating the effect of KHS101 on tumour cell invasion. After engraftment of GSC1 cells into the striatum (2.5 mm from the midline, 2.5 mm anterior from the bregma), GSC1 xenograft tumours expand caudally, but cells also migrate along the corpus callosum (CC) into the brain hemisphere contralateral to the injection site. Notably, infiltration of tumour cells into the hemisphere contralateral to the original tumour site is a pathological measure to define advanced GBM tumours in patients (personal correspondence with neurosurgeon R. Mathew; [209]). Therefore, to analyse the effect of KHS101 on GSC invasion, I measured both, caudal tumour expansion and GSC migration into the other brain hemisphere.

To assess caudal tumour expansion, I determined the tumour area in different parts of the mouse brains based on hematoxilin and eosin (H&E) stainings. To this end, four distinct brain areas (rostral to caudal) were defined. The mouse brain sketch and H&E-stained sections in figure 2.11A illustrate the location and histological features of the selected brain areas 1-4. Area 1 covers the most rostral brain part and includes the GSC injection site, thus representing the original tumour site. Area 4, on the other hand, is defined by the emergence of the ventricles and constitutes the most caudal brain part used for this analysis. Figure 2.11B depicts images of H&E sections of vehicle- or KHS101-treated brains with example sections shown for the four analysed areas. Based on the H&E-stained sections, the tumour area was calculated as a percentage of the total area of the brain section and results are shown in figure 2.11C. As expected tumour burden was most pronounced in proximity to the injection site (area 1; ∼19% tumour area in control group) and gradually attenuates reaching the lowest level in area 4 (∼8% tumour area in control group). Compared to treatment with vehicle, treatment with KHS101 significantly reduced tumour mass in areas 2-4 indicating a reduction in caudal tumour expansion.

Further assessment of invasiveness was achieved by determining cell migration across the CC into the contralateral hemisphere. To this end, I stained the brain sections obtained from the GSC xenograft model for human VIMENTIN (VIM) to visualise VIM-positive GSC cells engrafted in the brain. CC-infiltration by GSCs was quantified by fluorescence threshold-based measurement of VIM-positive area in the CC of the hemisphere contralateral to the injection site. Notably, only 8% of CC area

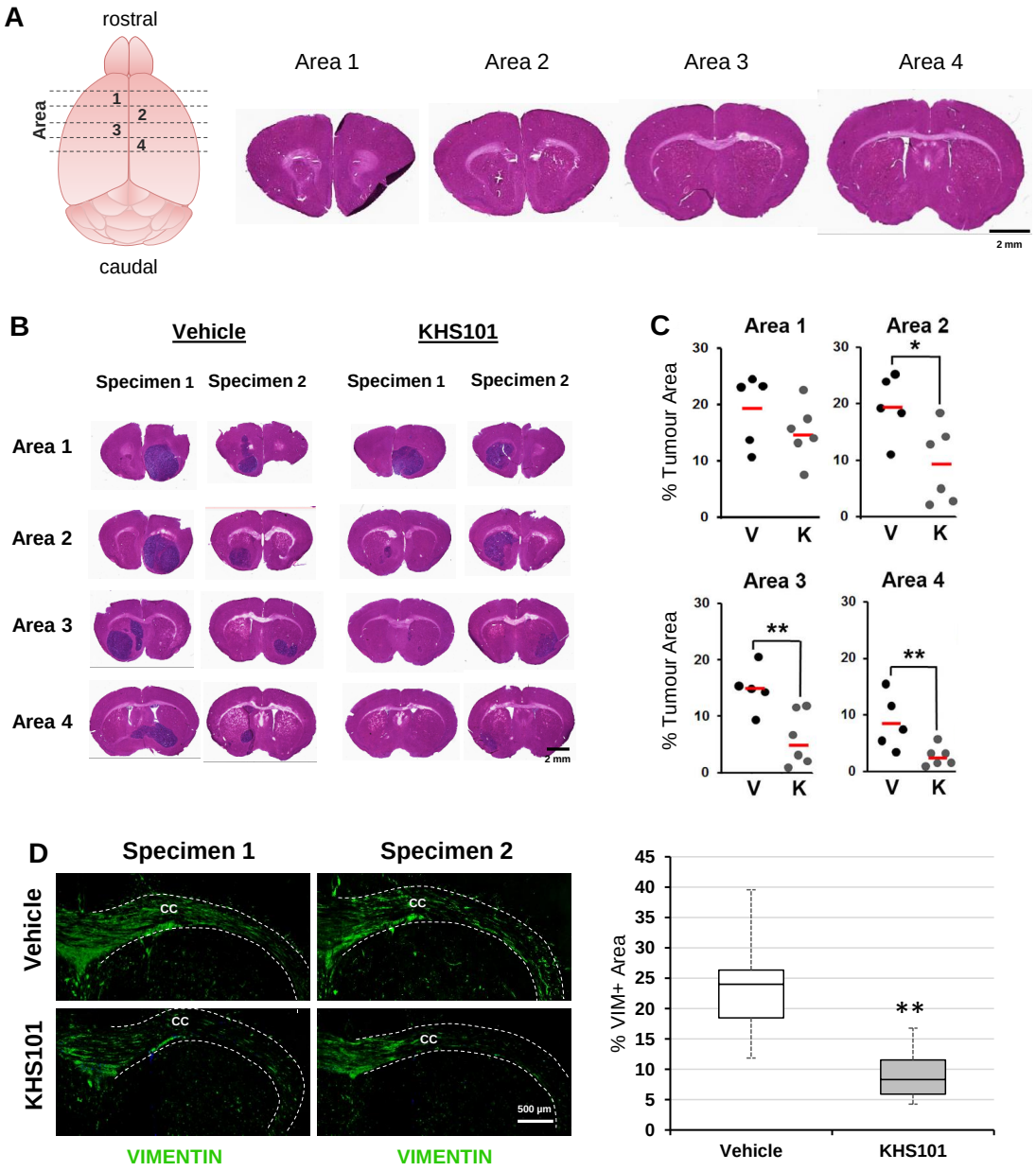

Fig. 2.11: KHS101 reduces tumour burden and invastion in GSC1 xenograft models after 10 weeks of systemic administration. **A)** Left: Sketch of mouse brain illustrating the approximate location of the four brain areas chosen for analysis. Right: H&E stained sections of a mouse brain showing the morphological features of areas 1, 2, 3 and 4. Scale bar: 2 mm. **B)** Example images of H&E stained sections of GBM1-derived xenograft tumours treated with vehicle or KHS101. Scale bar: 2 mm. **C)** Quantification of GSC1 tumour size in different areas of the brain indicating reduced caudal tumour expansion in KHS101 (K) versus vehicle (V) treated animals (n=5 (V) or 6 (K); *, $P<0.05$; **, $P<0.01$; Mann Whitney U-test). **D)** Left: Representative images of VIMENTIN-stained GSC1-derived tumour sections with the area of the corpus callosum (CC) highlighted (examples of two different specimen per group are shown). Right: Quantification of VIMENTIN-positive area in the corpus callosum of the hemisphere contralateral to the injection site indicating reduced GSC invasion in KHS101- versus vehicle-treated brains (n=4; **, $P<0.01$; Mann Whitney U-test).

of KHS101-treated brains contained VIM-positive cells (GSCs) compared to 24% in vehicle-treated brains suggesting an inhibitory effect of KHS101 on GSC invasion across the CC (figure 2.11D).
The observation of reduced tumour burden associated with reduced GSC proliferation and invasiveness upon treatment with KHS101 further supports the notion that KHS101 significantly suppresses the tumourigenic potential of GSCs.

2.1.3.3 KHS101 prolongs survival in the GBMX xenograft model

Encouraged by the promising results obtained for GSC1-based xenografts (reduced tumour burden and tumour cell invasion), I further investigated whether KHS101 treatment also affects survival of mice bearing intracranial GBM xenograft tumours. To this end, I used a different patient-derived GBM xenograft model based on the exclusively *in vivo* propagated GBMX cells. The predictable time frame of morbidity in the GBMX model (11-13 weeks) facilitates survival analysis upon KHS101 treatment. Determination of the experimental endpoint for the survival readout was based on early removal criteria (e.g., significant weight loss or neurological signs).
For a first survival analysis, established GBMX tumours (6 weeks after intracranial injection) were treated with systemically administered KHS101 (according to the dosing regimen described above) until the experimental endpoint. The brains harvested at the end of the experiment were subjected to histological analysis. The obtained H&E-stained brain sections of two different specimens per group are shown in figure 2.12A and were used to calculate the percentage of tumour area per section. In line with the results of the tumour burden assessment in the GSC1 model, the analysis of tumour burden in the GBMX survival model indicated a significantly reduced tumour mass in the KHS101-treated group compared to the vehicle-treated group (>2-fold; figure 2.12B). Consistent with a reduced tumour burden in the treatment group, KHS101 treatment significantly prolonged survival of GBMX-bearing animals compared to the control group (P=0.0062; left graph in figure 2.12C).
To test whether the effect of KHS101 on survival is sustained after termination of KHS101 administration, I performed a second survival analysis. To this end, treatment with KHS101 started two weeks after intracranial injection of GBMX cells and was maintained for 70 days following the treatment regime described above. Whereas the survival endpoint of the vehicle control group was reached shortly after the end of treatment with a median survival time of 90 days, KHS101 treatment significantly prolonged survival resulting in a median survival time of 130 days (P=0.0279; right graph in figure 2.12C).

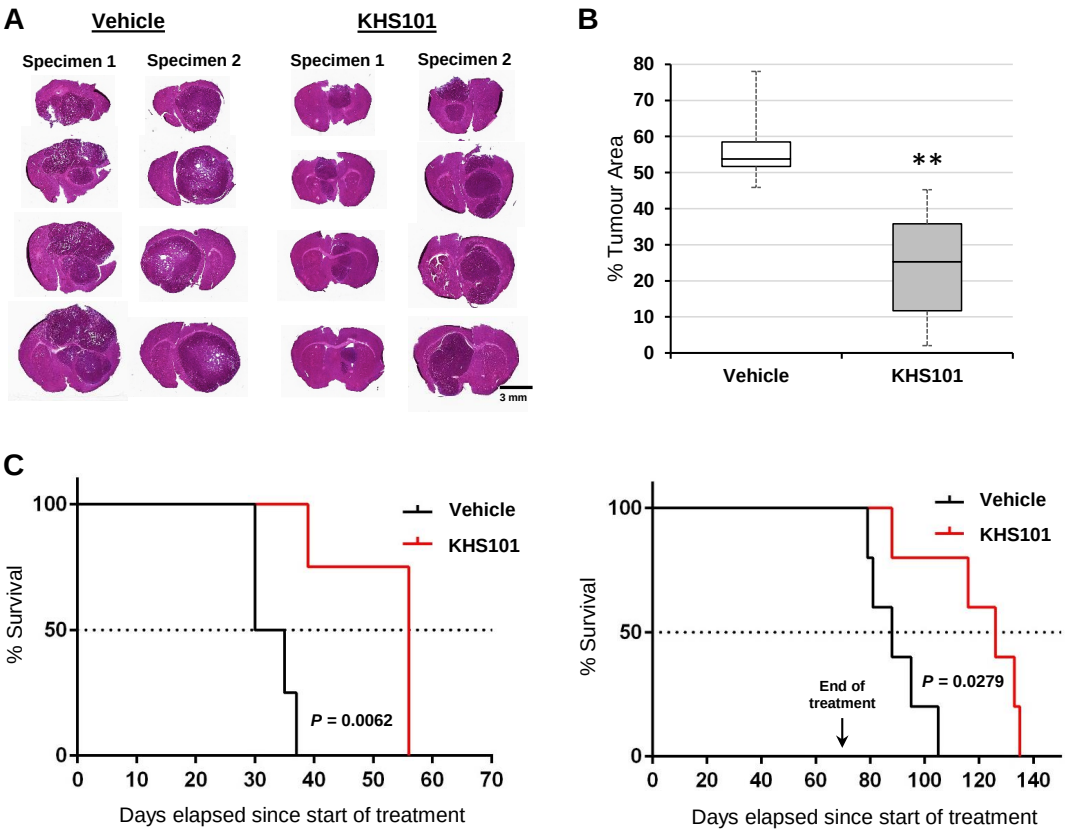

Fig. 2.12: KHS101 reduces tumour burden and prolongs survival in GBMX xenograft models after 10 weeks of systemic administration. **A)** Images of H&E stained sections of GBMX-derived xenograft tumours treated with vehicle or KHS101. Brains were harvested at the experimental endpoint as defined by survival. Scale bar: 3 mm. **B)** Quantification of GBMX tumour size indicating decreased tumour burden in KHS101- versus vehicle-treated mice (n=4; **, $P<0.01$; Mann Whitney U-test). **C)** Kaplan-Meier survival curves of GBMX tumour-carrying animals showing prolonged survival in the KHS101 versus vehicle treatment group with dosing start after 6 weeks of tumour establishment and continued treatment (left; n=4; $P=0.0062$; log-rank test) or after 2 weeks of tumour establishment and 10 week of treatment (right; n=5; $P=0.0279$; log-rank test).

In summary, *in vivo* findings indicate KHS101 as an anti-GSC compound that significantly reduces tumour cell proliferation and tumour burden, and also hinders GSC invasion into caudal brain regions and the brain hemisphere opposite the initial engraftment site. Accordingly, KHS101 has a beneficial effect on the survival of GBMX-bearing mice upon continued systemic administration, and this effect persists even after treatment termination. Importantly, the KHS101 treatment regimen applied in this study did not cause any obvious side effects or signs of intolerance in the two different mouse models tested. Also, H&E-stained liver sections of mice treated with vehicle or KHS101 for 10 weeks did not show any noticeable differences

in the morphological features of the livers (figure 2.13, suggesting that KHS101 administration for 10 weeks does not have any acute toxic effects in the tested mouse models.

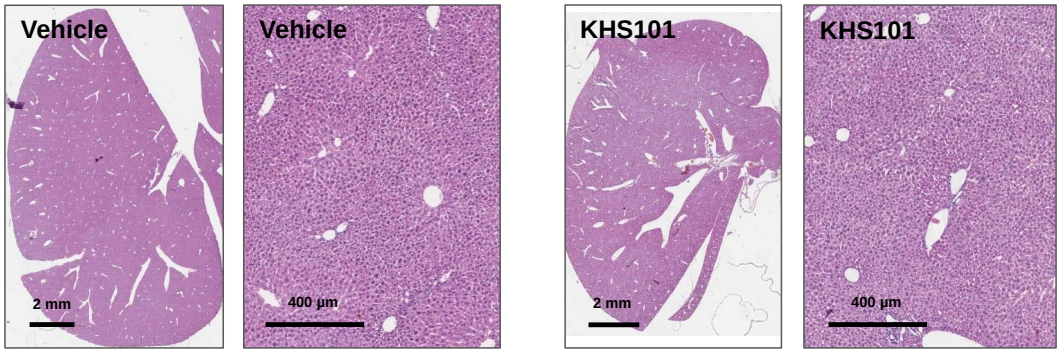

Fig. 2.13: Liver sections show intact tissue morphology after 10 weeks of treatment with KHS101. Representative images of H&E stained liver sections of GSC1 tumour bearing animals treated with KHS101 for 10 weeks show no indication of toxicity compared with the vehicle-treated controls.

2.1.4 Gene expression and metabolic flux analysis suggest an energy metabolism-obstructing mechanism of action of KHS101

2.1.4.1 KHS101 alters expression of 'stemness', metabolism and glioma proliferation genes

The mitotic spindle protein TACC3 has been identified as a KHS101 target in rat NPCs and HEK293T cells [116] [121] and TACC3 immunoplot analysis shows a reduction in TACC3 levels in GSCs upon treatment with KHS101 (E. Polson, unpublished data). Notably, lentivirally-induced knockdown of TACC3 results in reduced proliferation, as measured by KI67 immunofluorescence stainings, comparable to KHS101 treatment. However, knockdown of TACC3 in GSCs does not induce the vacuolisation/autophagy phenotype characteristic for KHS101-treated GSCs (E. Polson, unpublished data), pointing to other mechanisms that play a role in the phenotype induced by KHS101. Therefore, unknown KHS101 targets must be responsible for the observed phenotype, hence requiring further MOA studies. A commonly applied method of MOA investigation is transcriptome analysis, which allows for the identification of direct or indirect consequences of compound treatment on gene expression. By following a comprehensive gene expression analysis approach, I an-

ticipated to better understand the molecular basis of KHS101-induced phenotypic changes characterised by vacuolisation, autophagy and cell death, and to identify potential pathways affected by KHS101. To achieve this, we performed a gene expression analysis using the Illumina HumanHT-12 v4 beadchip (Cambridge genomic services). For this analysis, total mRNA isolated from GSC1 cells after 24 hours of treatment with vehicle or KHS101 (7.5 µM) was used.

Differentially expressed genes were defined by fold changes (FC) $\leq$ -2 or $\geq$ 2, a *P*-value $\leq$ 0.001 and a false discovery rate (FDR) $\leq$ 0.075, yielding a total of 828 significantly altered genes. Gene set enrichment analysis (GSEA) of vehicle (0.1% DMSO) versus KHS101-treated GSC1 cells indicated a number of pathways affected by KHS101. Consistent with known effects of KHS101 in rat NPCs, several cell cycle pathways were identified to be altered in KHS101-treated cells. Notably, GSEA also revealed changes in metabolic pathways such as oxidative phorphorylation and the tricarboxylic acid (TCA) cycle (figure 2.14A). A number of factors critically involved in oxidative phosphorylation (e.g., heme oxygenase (*HMOX2*) and thioredoxin reductase 1 (*TXNRD1*); [210] [211]) and glycolysis (e.g. hekokinase 2 (*HK2*), *SLC2A3* and phosphoglycerate kinase 1 (*PGK1*); [212] [213]) were upregulated upon KHS101 treatment. Additionally, genes implicated in 'stemness' (e.g., nitric oxide synthase 2 (*NOS2*) and S-phase kinase-associated protein 2 (*SKP2*); [214] [215]) and tumour growth (e.g., v-akt murine thymoma viral oncogene homolog 1 (*AKT1*); [216]) were downregulated, whereas tumour suppressors (e.g., tribbles pseudokinase (*TRIB3*) and n-myc downstream regulated 1 (*NDRG1*); [217] [218]) and autophagy/apoptosis activators (e.g., harakiri (*HRK*), gamma-aminobutyric acid A receptor-associated protein-like 1 (*GABARAPL1*) and BCL2/adenovirus E1B 19 kDa interacting protein (*BNIP3*); [219] [220] [221]) were upregulated. Based on their cellular function, we allocated 25 of those factors to five different groups: 'tumour suppression/growth', 'glycolysis', 'mitochondrial stress', 'autophagy/death' and 'stemness'. Displaying the gene expression alterations of those 25 genes in a radar chart layout yielded a distinctive pattern of gene expression changes caused by KHS101 (see red line in figure 2.14B), which were confirmed by qRT-PCR (see blue line in figure 2.14B).

Since GSEA pointed to KHS101-induced metabolic changes *in vitro*, I sought to test this finding *in vivo* by determining expression of HK2, a key factor in glucose metabolism whose expression was found to be significantly altered upon KHS101 treatment. Consistent with up-regulation of *HK2* mRNA in cultured GSCs, HK2 immunostainings of GSC1-derived xenograft tumours showed elevated levels of HK2 upon treatment with KHS101 compared to vehicle-treated tumours (immunofluorescence images in figure 2.14C). Quantification of the HK2-positive area by colour

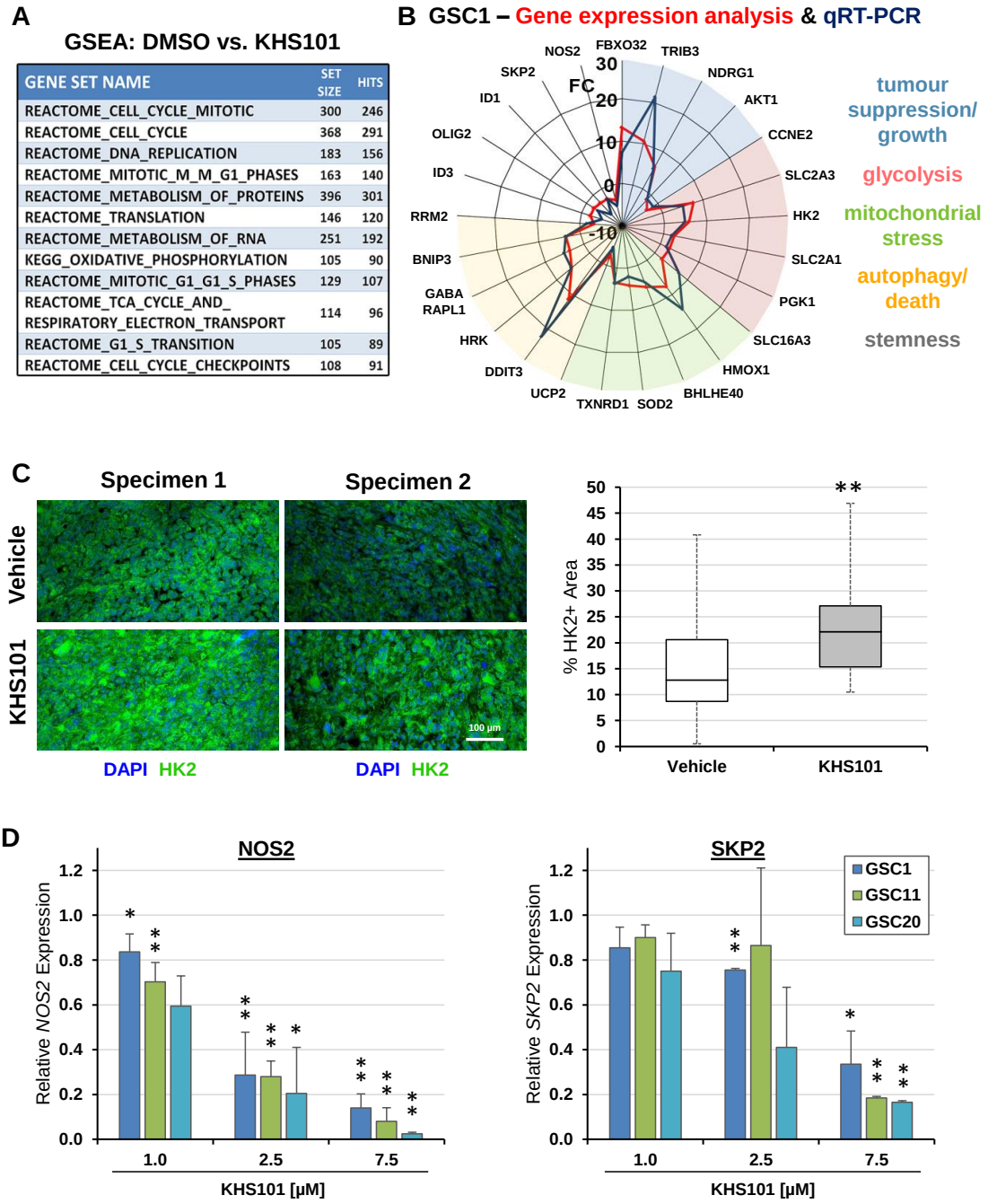

Fig. 2.14: KHS101 affects expression of 'stemness', metabolism and glioma proliferation genes. **A)** Results of gene set enrichment analysis. **B)** Radar charts depicting gene expression changes from microarray gene expression analysis (red line) and targeted qRT-PCR (blue line) in GSC1 24 hours after with 7.5 µM KHS101 showing comparable results. **C)** Left: Representative images of HK2-stained GSC1-derived tumour sections (examples of two different specimen per group are shown). Right: Quantification of the HK2-positve tumour area indicating an increased HK2 expression in KHS101- versus vehicle-treated tumours (n=5; **, $P<0.01$; Mann Whitney U-test). **D)** Concentration dependent reduction of mRNA expression of glioma 'stemness' markers *NOS2* (left) and *SKP2* (right) in KHS101-treated GSC1, GSC11 and GSC20 cells after 24 hours (data normalised to vehicle control and shown as mean of fold changes ± SD; n=2/3; *, $P<0.05$; **, $P<0.01$; Student t test).

thresholding confirmed the qualitative observation by revealing a significant increase of approximately 2-fold (comparing the data means) in the percentage of HK2-positive area in KHS101-treated tumours compared to control tumours (graph in figure 2.14C).
Two of the 'stemness' factors whose expression were decreased in KHS101-treated GSC1 cells, *SKP2* and *NOS2*, have previously been demonstrated to promote GSC features and tumour growth [214] [215]. To further corroborate the finding of the gene expression analysis, I assessed the effect of KHS101 on *NOS2* and *SKP2* gene expression in three different GSC models. To this end, GSC1, GSC11 and GSC20 cells were treated with vehicle or 1 µM, 2.5 µM and 7.5 µM KHS101 for 24 hours and the relative *NOS2* and *SKP2* expression was determined by qRT-PCR. As expected, KHS101 treatment of GSCs reduced expression of *NOS2* mRNA in a concentration-dependent manner reaching a reduction of up to ∼86% (GSC1), 92% (GSC11) and 97% (GSC20) after treatment with 7.5 µM KHS101 for 24 hours (left graph in figure 2.14D). Similarly, KHS101 decreased *SKP2* expression in all three GSC lines resulting in up to 66% (GSC1), 81% (GSC11) and 83% (GSC20) (right graph in figure 2.14D).

2.1.4.2 KHS101 induces metabolic exhaustion in GSCs

Gene expression analysis and GSEA indicated KHS101-induced transcriptional alterations in components of metabolic pathways (i.e. glycolysis and oxidative phosphorylation). Therefore, we investigated the effect of KHS101 on the metabolic phenotype of GSCs. We used an extracellular flux analyser to determine the extracellular acidification rate (ECAR), a measure of the glycolytic activity of the cells, and the oxygen consumption rate (OCR) to assess mitochondrial respiration in live cells [222].
The direct consequence of KHS101 on the mitochondrial function was determined measuring the OCR levels of GSCs and NPs upon addition of vehicle (0.1% DMSO) or 7.5 µM KHS101. OCR measurements were taken every 10 minutes for the duration of 140 minutes. Three measurements after addition of KHS101, compounds that specifically target different components of the electron transport chain were injected to allow for the identification of the effect of KHS101 on key parameters of mitochondrial respiration. First, the adenosine triphosphate (ATP) synthase inhibitor oligomycin was injected which obstructs ATP production in the mitochondria leading to a decrease in OCR below basal respiration levels. Addition of carbonyl cyanide-4 (trifluoromethoxy) phenylhydrazone (FCCP) then uncouples

oxygen consumption from ATP generation leading to disruption of the proton gradient across the mitochondrial membrane which results in maximum oxygen consumption. Consequently, OCR levels were elevated to maximal respiration. Lastly, the complex I inhibitor rotenone and the complex III inhibitor antimycin A were simultaneously injected to fully disable mitochondrial respiration and reduce OCR levels to non-mitochondrial respiration levels. Control GSC1 cells (vehicle-treated) showed reduced OCR levels upon oligomycin injection, followed by an increase above basal levels upon addition of FCCP, and a drop in OCR to a minimum after rotenone/antimycin A injection. In contrast, KHS101 treatment of GSC1 cells immediately decreased OCR from ∼124 pmol/min (basal respiration) to ∼80 pmol/min indicating an immediate effect of KHS101 on respiration. Addition of oligomycin did not reduce OCR any further and the KHS101-treated cells were not able to reach their maximum respiration capacity upon FCCP injection. Similarly, injection of KHS101 limited oxygen consumption of NP1 cells depriving the cells of their capacity to generate ATP by mitochondrial respiration. However, the basal respiration levels of NP1 cells were approximately 2.5-fold lower compared to GSC1 cells, indicating a lower energy demand and, thus, reduced dependency on constantly high rates of mitochondrial respiration. In conclusion, KHS101 immediately affected mitochondrial respiration in GSC and NP cells by obstructing oxidative phosphorylation (figure 2.15A).

The direct consequence of KHS101 on glycolysis was assessed by measuring the ECAR levels. First, the baseline acidification caused by non-glycolytic proton extrusion was determined by ECAR measurements in glucose-starved cells. Then, vehicle (0.1% DMSO) or 7.5 µM KHS101 was added. After three more ECAR measurements, glucose was added to activate the glycolytic pathway. Catabolism of glucose by the cells leads to production of ATP and an accumulation of protons in the media which results in an increase in ECAR. This proton accumulation allows for the assessment of the basal glycolytic activity of the cells [222]. Addition of the ATP synthase inhibitor oligomycin then disables ATP production by the mitochondria, thus further promoting the glycolytic pathway as the alternative route of energy production. The resulting increase of ECAR revealed the cells' maximum glycolytic capacity. Finally, glycolysis was inhibited by addition of the glucose analog 2-Deoxyglucose (2-DG) causing a drop in ECAR to baseline level. The resulting 'glycolytic stress test' profiles for GSC1 and NP1 cells are shown in figure 2.15B. Compared to vehicle-treated cells, GSC1 cells treated with KHS101 (7.5 µM; acute injection) elevated glycolytic energy production in the presence of glucose but lost their ability to reach their glycolytic maximum since injection of oligomycin had no

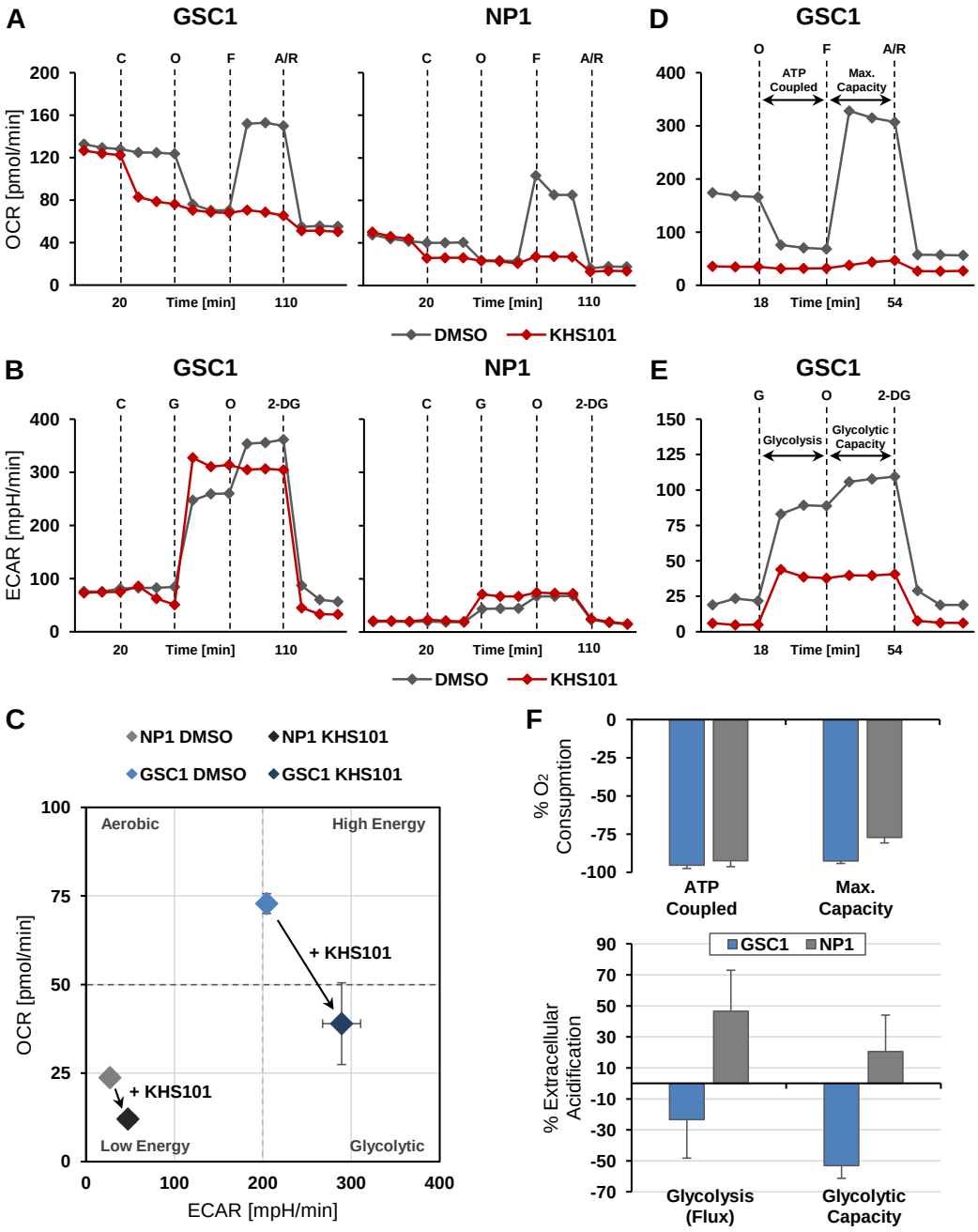

Fig. 2.15: KHS101 induces metabolic exhaustion in GSCs. **A)** Representative mitochondrial bioenergetic flux curves (measured as oxygen consumption rate; OCR) in GSC1 (left) and NP1 (right) cells upon addition of vehicle or 7.5 µM KHS101. **B)** Representative glycolytic flux curves (measured as extracellular acidification rate; ECAR) in GSC1 (left) and NP1 (right) cells upon addition of vehicle (0.1% DMSO) or 7.5 µM KHS101. **C)** Extracellular flux phenogram of basal ECAR and OCR in GSC1 and NP1 cells. Arrows indicate changes induced by treatment with 7.5 µM KHS101 (data shown as mean ± SD; n=3). **D** and **E)** Representative OCR (D) and ECAR (E) curves in GSC1 cells after 24 hours of treatment with vehicle or 7.5 µM KHS101. **F)** Quantification of mitochondrial and glycolytic bioenergetic flux and capacity in GSC1 and NP1 cells 24 hours after treatment with 7.5 µM KHS101 (data normalised to vehicle control and shown as mean ± SD; n=3). (C: Compound; O: Oligomycin; F: FCCP; A: Antimycin A; R: Rotenone; G: Glucose; 2-DG: 2-Deoxy-D-Glucose)

additional effect on ECAR levels. The immediate effect of KHS101 on glycolysis in NP1 cells was similar to GSC1 cells. However, NP1 cells treated with KHS101 still had the capacity to attain their maximum glycolytic potential and had a significantly lower ECAR rate consistent with the lower energy demand of non-tumour cells compared to the highly energetic malignant cells.

The diagram in figure 2.15C summarises the findings of the metabolic profiling of GSC1 and NP1 cells as a direct consequence of KHS101 treatment. The non-malignant NP1 cells only showed a minimal immediate response to KHS101 treatment. Upon exposure to KHS101, NP1 cells switched from a low aerobic/very low glycolytic state to a very low aerobic/low glycolytic phenotype; however, remaining in an overall low energy state. In contrast, GSC1 cells exhibited a more drastic direct response to KHS101 and switched from a high aerobic/medium glycolytic to a low aerobic/high glycolytic metabolism.

Critical gene expression changes in components of glycolytic and oxidative phosphorylation pathways were identified after 24 hours of KHS101 treatment. Therefore, we sought to assess the metabolic state of KHS101-treated GSC1 and NP1 cells at the 24 hour time point. In contrast to vehicle-treated cells, GSC1 cells treated with 7.5 µM KHS101 for 24 hours exhibited an oxygen consumption rate at the level of non-mitochondrial respiration indicating a 'shutdown' of oxidative phosphorylation (figure 2.15D). In contrast to the direct effect of KHS101 on glycolysis, GSC1 cells treated with KHS101 for 24 hours displayed both, a reduced glycolytic activity and a reduced maximal glycolytic capacity compared to vehicle-treated control cells (figure 2.15E). The graphs in figure 2.15F outline the findings of KHS101-induced changes in mitochondrial respiration and glycolysis in GSC1 and NP1 cells after 24 hours of treatment. GSC1 cells displayed almost 95% reduction in O_2 consumption compared to vehicle-treated cells (top graph in figure 2.15F) with a concomitant reduction in glycolysis by 25% and in glycolytic capacity by >50% (bottom graph in figure 2.15F). In NP1 cells, treatment with KHS101 had the same effect on O_2 consumption leading to a decrease in ATP coupled respiration by 90% and, in maximum capacity of mitochondrial respiration, by almost 80% (top graph in figure 2.15F). However, in contrast to GSC1 cells, NP1 cells responded to KHS101 treatment with up-regulation of the glycolytic pathway. After 24 hours of treatment with KSH101, the extracellular acidification upon glucose addition was raised by almost 50% and the cells' maximum glycolytic capacity was 20% higher compared to vehicle-treated NP1 cells (bottom graph in figure 2.15F).

In conclusion GSEA of transcriptome data indicated a thus far unobserved effect of KHS101 on metabolism pathways (i.e. glycolysis and oxidative phosphorylation). Accordingly, preliminary data investigating mitochondrial respiration and glycolysis by extracellular flux analysis revealed that KHS101-treated GSCs decrease mitochondrial respiration and show a reduced glycolytic capacity compared to vehicle-treated control cells. This KHS101-induced obstruction of the cells energy metabolism ultimately leads to metabolic exhaustion in GSCs, but not NPs.

2.2 Discussion

GBM is among the most devastating cancers and despite intensive research, treatment options are limited and patient prognosis remains grim [3] [5]. Therefore, new treatment approaches aiming at exploiting GBM vulnerabilities are urgently needed. Identification of a tumour-driving stem-cell like subpopulation in GBM has fueled research into GSCs and targeting this cancer cell population is thought to constitute a promising therapeutic approach in order to prevent brain tumour recurrence [56]. Recently, a number of studies have demonstrated the anti-GBM potential of small molecules, for example, through disruption of mitotic pathways [114], cell death programs [108], pinocytotic activity [115] or autophagy regulation [112]. The small molecule KHS101 has previously been identified as an anti-proliferation, neuronal differentiation compound in NPCs that acts through targeting the mitotic spindle protein TACC3. Moreover, KHS101 is able to cross the blood brain barrier [116]. Based on these properties, I sought to investigate the potential anti-GSC activity of KHS101 by identifying molecular vulnerabilities intrinsic to GSCs.

One major challenge for GBM therapy is the molecularly and phenotypically heterogeneous nature of GBM tumours [223]. In order to address this diversity, I used a panel of patient-derived GSC lines from various clinical backgrounds including primary and recurrent GBM, the latter with treatment history of radiation and TMZ, and different *MGMT* methylation status. Moreover, single cell qRT-PCR analysis revealed highly diverse transcriptional profiles among and within the different GSC lines. Further computational analysis applying a recently published GBM subtype classification scheme [25] indicated the presence of classical, proneural and mesenchymal subtype compartments in the GSC lines. Thus, our patient-derived GSC lines constitute a considerable set of clinically and molecularly heterogeneous cell populations representative of various GBM phenotypes, hence, providing an adequate basis for investigation into the possible anti-GBM activity of KHS101 (table 2.1).

Consistent with previous findings on KHS101 as an anti-proliferative agent in NPCs [116], KHS101 treatment also significantly decreased the proliferative potential of GSCs (figure 2.1). This KHS101 effect on GSCs can be attributed to its known target TACC3, a protein essentially involved in mitotic spindle assembly, and thus cell proliferation. In accordance to TACC3's role in mitotic spindle architecture, depletion of TACC3 has been linked to chromosomal instability and cell death. However, these effects have only been reported for prolonged depletion of TACC3 (e.g., [224]). In the case of KHS101, it is unlikely that genomic instability caused by KHS101-induced reduction in TACC3 protein levels will have significant consequences as

KHS101 exhibits strong cytotoxic effects through TACC3-independent mechanisms (see below).

As a link between reduced proliferation and GSC differentiation has been described (e.g., [225] [85]), I proceeded by monitoring KHS101-treated GSCs for morphological changes indicative of a differentiation phenotype. However, live cell imaging of GSCs revealed massive cellular vacuolisation resulting in cell death (figure 2.2). A similar catastrophic vacuolisation phenotype has recently been described for the small molecule Vacquinol-1 by Kitambi et al. and found to be a consequence of excessive pinocytotic activity. *In vitro* and preclinical validation of this phenotype confirmed selective targeting of GSCs through compound-induced vacuolisation [115]. To test whether KHS101 exerts its effects exclusively through hyper-vacuolization, I initially assessed both the cells' endocytotic activity (using a low permeability endocytosis marker; [115] [226]), and autophagy. In contrast to the excessive pinocytosis described for Vaquinol-1, treatment with KHS101 did not alter the level of extracellular fluid uptake by GSCs. However, using different autophagy detection methods, I gathered convincing evidence (increased dye-based staining and LC3B immunostaining of autophagosomal vacuoles as well as EM imaging showing the presence of electron-dense autophagic/lysosomal vacuoles) that indicates a markedly increased number of autophagosomes and lysosomes in KHS101-treated GSCs (figures 2.3, 2.4 and 2.5). Increased numbers of autophagic vacuoles can be indicative of a hyperactive autophagic flux or can be the mere accumulation of autophagosomes due to an interrupted flux, for example caused by impaired fusion with lysosomes [227]. Staining of KHS101-treated GSCs with an autophagosomal and lysosomal dye showed a partial co-localisation of the two dyes indicating an active autophagic flux (figure 2.3). Consistently, examination of the EM images revealed the presence of both, double and single membraned electron-dense vacuoles, representing autophagosomes and lysosomes, respectively. Moreover, membrane fusion of presumptive autophagosomes and lysosomes was observed, further corroborating the notion of a KHS101-induced autophagic activity rather than a KHS101-induced perturbation of the cells' baseline autophagic flux (figure 2.5). This notion could be further strengthened by applying methodologies specifically detecting autophagic flux, such as measuring LC3 protein turnover by Western Blot in the presence or absence of late-phase autophagy inhibitors (e.g. bafilomycin A1, chloroquine) and the determination of the difference in the amount of the lipidated form of LC3 (LC3-II). Additional methods to assess autophagic flux are based on using mRFP-GFP-LC3 constructs and monitoring their cellular location and the colour change occurring upon lysosomal degradation, or measuring isotopes released by degradation of long-

lived isotope-labeled proteins [228].

As a 'recycling' process for degradation of cellular components, autophagy has been described to be activated in response to damaged organelles or as an energy source upon starvation. Hereby, autophagy serves as a survival mechanism of the cell, for example to altered environmental stimuli or chemical compounds [229] [230]. However, formation of autophagic vesicles has also been found to be indicative of a cell death program distinct from apoptotic cell death. In this autophagic cell death, the autophagic activity is thought to be the cause of death rather than an attempt to prevent it [231]. Shchors et al., for example, identified chemical compounds that exhibit GBM cell cytotoxicity through induction of this so called autophagy associated cell death, a cell death program that is independent of apoptosis [112]. My data on caspase 3/7 activity, however, suggest apoptosis as the cell death mechanism induced by KHS101 (figure 2.7). Future experiments focusing on using autophagy inhibitors (e.g., wortmannin, 3-methyladenine) or silencing critical components of the autophagic machinery (e.g., Beclin 1, autophagy related 5 (ATG5), unc-51 like autophagy activating kinase 1 (ULK1)) by shRNA knockdown could give further insight into the role of autophagy in KHS101 cytotoxicity and its link to KHS101-induced vacuolisation.

Strikingly, by conducting comprehensive cell viability studies using a diverse set of GSC models, I demonstrated that the cytotoxic effect of KHS101 is independent of GBM subtype, parental tumour origin, treatment history and *MGMT* methylation status (figure 2.6 and table 2.2). Thus, KHS101 may target a common vulnerability of GSCs irrespective of their clinical and molecular background. Notably, GSC11, derived from a gliosarcoma, exhibited a slightly delayed response to KHS101 compared to the other five GSC lines tested. Interestingly, GSC11 also displayed the most pronounced vacuolisation/autophagy phenotype in the phase contrast and EM images. Hence, a more efficient recycling of cellular components through autophagy could be one explanation of the longer survival of GSC11 cells upon KHS101 treatment. However, other resistance or coping mechanism could play a part in a delayed response to KHS101. Most importantly, assessment of cell viability upon KHS101 treatment demonstrated a marked differential cytotoxicity of KHS101 in GSCs and NPs. With 5-day-IC50 values of >18 µM, KHS101 exhibits only minimal cytotoxic effects on NP cells suggesting a selective cytotoxic activity of KHS101. This is consistent with the observed selective induction of the vacuolisation/autophagy phenotype in GSCs but not in NPs. Overall, these results indicate that KHS101 targets a molecular vulnerability intrinsic to the malignant GSCs without affecting viability of normal NP cells. The role of the KHS101 target TACC3 in KHS101 cytotoxicity

has still to be elucidated. In this context, it would also be interesting to investigate whether glioma cells with a FGFR3-TACC3 fusion protein, as it has been identified in several different cancer types including glioma [119][129] [130] [131], display an increased susceptibility to KHS101 compared to our TACC3 wild-type GSC models. Notably, targeting the FGFR3-TACC3 fusion protein by inhibiting the FGFR3 kinase activity in a glioma mouse model has been shown to have a beneficial effect on survival [119]. However, FGFR3-TACC3 fusions are only detected in a small subset of GBM specimen [232], hence limiting the possibility to obtain a GSC line harbouring this mutation. An alternative approach could be the establishment of FGFR3-TACC3 expressing NP cells by lentiviral transduction. Comparing the cytotoxic effect of KHS101 on TACC3 wild-type GSCs, FGFR3-TACC3 NP cells and wild-type NP cells could then give an indication of the efficacy of KHS101 treatment in the FGFR3-TACC3 context.

Viability assays also showed a residual viable cell population upon treatment with lower concentrations of KHS101, which prompted the question whether GSCs that survive KHS101 treatment still exhibit stem cell properties. This could have implications for the *in vivo*/pharmacological use of KHS101 (e.g., upon systemic administration in mice), when cells are not continuously and equally exposed to lethal KHS101 concentrations. Notably, surviving GSCs are characterised by markedly reduced levels of stemness markers (NESTIN and SOX2) and an attenuated clonal growth capacity (figures 2.8 and 2.9). Thus, GSC populations that are exposed to sublethal concentrations of KHS101 (<2 µM) exhibit a reduction in GSC features (i.e. undifferentiated state, self-renewal) potentially making them less tumourigenic (e.g., [58] [59]). However, consistent with the incomplete terminal differentiation and reversible cell cycle exit reported for BMP-treated GSCs and GSC-derived oligodendrocyte-like cells [57], KHS101 only abrogates the colony formation capability of GSCs upon prolonged exposure (figure 2.9B). When KHS101 is removed, some cells are able to re-enter the cell cycle and grow colonies (figure 2.9C), indicating that a 2-day-KHS101 treatment is not sufficient to induce a sustained differentiated state in GSCs. Therefore, further investigation into the effect of long-term KHS101 treatment on GSC features and proliferation are required.

Consistent with the herein described anti-proliferative, anti-stemness, and cytotoxic effects of KHS101 in GSC cultures, GSC-derived mouse xenograft models displayed decreased KI67 immunostaining, increased necrotic areas and a significant reduction in tumour burden (figures 2.10 and 2.11). Notably, the difference in tumour burden is most pronounced in areas distant from the initial tumour site indicating that KHS101 inhibits caudal expansion of established GSC-derived xenograft tumours.

Moreover, KHS101 also inhibited contralateral tumour cell invasion as shown by VIM staining (figure 2.11). This experimental readout has clinical relevance, as GBM tumour spread into the other hemisphere constitutes a pathological sign for advanced GBM in patients (R. Mathew, personal correspondence; [209]). Finally, consistent with *in vivo* tumour growth inhibiting properties in GSC-derived xenograft, KHS101 also significantly prolonged survival of mice bearing GBM xenograft tumours (figure 2.12). Notably this survival effect was shown for a xenograft model based on *in vivo*-propagated patient-derived GBM cells indicating an anti-tumourigenic function of KHS101 beyond cell culture-propagated GSCs. Importantly, after 10 weeks of systemic administration of KHS101, H&E-stained liver sections showed intact tissue architecture and no obvious side effects of KHS101 were observed in treated animals (figure 2.13). This is consistent with previously reported safety of KHS101 administration in rats [116]. Together, my *in vivo* data indicate a potential therapeutic window of KHS101 treatment. Moreover, upon systemic administration KHS101 significantly reduces tumour burden, GSC invasion and prolongs survival of mice bearing GBM xenograft tumours. Future *in vivo* work may include validation of these findings using additional GSC-derived xenograft models as well as genetic and/or syngeneic mouse models of GBM.

A commonly applied first line investigation method for small molecule MOA studies is gene expression analysis which allows for the identification of critical gene expression alterations induced by a compound [105]. Furthermore, transcriptome data can be used to reveal functional connections between compounds of unknown MOA and compounds with known targets through identification of common gene expression alterations [233]. Hence, in order to establish a possible explanation of the mechanism that underlies KHS101-induced cytotoxicity, we performed transcriptome analysis followed by GSEA. Consistent with previously identified KHS101 effects in rat NPCs [116], cell cycle and 'stemness' genes (e.g., *NOS2*, *SKP2*) were significantly affected in GSCs. In addition to already known KHS101 effects, GSEA of the gene expression data revealed altered expression levels of genes involved in diverse metabolic pathways including oxidative phosphorylation and glycolysis (figure 2.14). Notably, an altered energy metabolism has been recognized as a hallmark and potential molecular vulnerability of cancer cells [234]. Cancer cells have adjusted their energy metabolism in order to be able to meet their high energy demands and fuel their rapid growth. It has long been known, that cancer cells can reprogram their glucose metabolism to produce energy through glycolysis even in the presence of oxygen [234]. This metabolic switch highlights the functional difference in energy production of cancer and normal cells and makes the metabolic state of malignant

cells a cancer-specific, 'targetable' feature. To uncover the metabolic state of our GSC lines, we performed extracellular flux measurements. This analysis revealed that GSCs have a massively increased bioenergetic demand (with both high oxidative phosphorylation and high glycolysis rates) compared with the non-malignant NP cells. KHS101 treatment alters the highly energetic metabolic phenotype of GSCs by disrupting mitochondrial respiration and thereby inducing compensatory glycolytic flux (figure 2.15). Consistent with the observed induction of glycolysis by KHS101 determined by ECAR measurements, lactate accumulates in the media of KHS101-treated GSCs (E. Polson and S. Allison, unpublished data). Lactate is produced by glycolytic cells through lactic acid fermentation, thereby re-oxidising NADH to NAD^+, in order to provide the NAD^+ needed for the glycolytic pathway. Therefore, raised levels of lactate released by the cells is an additional indication of an increased glycolytic activity. Other standard ways of identifying changes in glycolytic activity include the measurement of glucose uptake by the cells, tracing of ^{13}C-labeled glucose and activity assays of rate-limiting glycolytic enzymes [235], and could be part of future experiments on the effect of KHS101 on the glycolytic pathway. In addition to evidence of elevated glycolysis derived from extracellular flux measurements, increased expression of HK2, which catalyses the first step in the glycolytic pathway and therefore critically defines the rate of glucose metabolism, is detected *in vitro* and *in vivo* (figure 2.14). In its role as a critical rate-limiting glycolytic enzyme, HK2 acts together with glucose transporters (e.g., SLC2A1 and SLC2A3) to allow cancer cells to metabolise glucose at an elevated rate to fuel cell proliferation [236]. This induction of HK2 and glucose transporters is consistent with the observation that KHS101 treatment markedly increased HIF1α in the nucleus of GSCs (E. Polson & C. Abbosh, unpublished data). HIF1α-dependent transcriptional changes include the upregulation of various glycolytic enzymes and glucose transporters [237]. Therefore, HIF1α signaling might play a role in up-regulation of glycolytic enzymes upon KHS101 treatment. However, although GSCs initially manage to compensate 'shutdown' of mitochondrial respiration by elevating their glycolytic rate, they exhaust their energy resources. An explanation for progressive glycolytic exhaustion could be the functional dependence of HK2 on ATP provided by active mitochondria [238]. In contrast to GSCs, the less energy dependent NP cells are able to adjust their metabolic phenotype upon KHS101-induced obstruction of oxidative phosphorylation. These results indicate that selectivity of KHS101-induced cell death could be due to distinct bioenergetic demands of malignant and non-malignant cells. Together, this data suggest an energy metabolism-obstructing MOA of KHS101. Various studies have demonstrated the interrelationship of metabolism

and autophagy (e.g., reviewed in [239]). This includes systems to detect changes in metabolic states and availability of nutrients that regulate autophagic pathways. The herein observed KHS101-induced changes in GSC metabolism together with increase in autophagic components are consistent with interactions described in the literature. Especially, a decrease in cellular ATP levels, as detected by CellTiter-Glo® assays (figure 2.6), accompanied by a massive rise in AMP levels, as revealed by metabolomics analysis (data not shown), is known to stimulate autophagy through activation of AMP-activated protein kinase (AMPK) [240]. Consistently, immunoblot analysis revealed the presence of phosphorylated (activated) AMPK in KHS101-treated GSCs (data not shown). Upon phosphorylation, AMPK activates the tuberous sclerosis complex2 (TSC2), a suppressor of mammalian target of rapamycin complex 1 (mTORC1), thereby stimulating autophagy [241]. Additionally, inhibition of mTORC1 can be mediated through HK2 [242]. Notably, KHS101 treatment also induced *HK2* gene expression in GSCs (figure 2.14), further strengthening the link between KHS101-induced metabolic changes and the observed increased autophagic activity. As mentioned above, an accumulation of nuclear HIF1α is also detected in KHS101-treated GSCs (data not shown), as well as transcriptional activation of HIF1α target genes, including *BNIP3* (figure 2.14). Notably, BNIP3 is an autophagy regulator that stimulates the clearance of dysfunctional mitochondria, a selective form of autophagy termed mitophagy [243]. Taken together, the accumulation of autophagic vesicles observed in GSCs upon KHS101 treatment can be linked to our proposed metabolism-targeting MOA of KHS101. Strikingly, TACC3 knockdown studies showed that this MOA is independent of the KHS101 target TACC3 (E. Polson, unpublished data) and points to additional target proteins involved in cellular energy production. Subsequent identification of the direct binding partners of KHS101 required the use of a benzophenone-KHS101 (BP-KHS101) probe, which I had demonstrated to exhibit similar cytotoxic activity as unconjugated KHS101 (data not shown). Upon exposure to UV light BP-KHS101 forms a covalent bond with its target, thus facilitating isolation of the target proteins. In order to identify additional KHS101 targets affinity-based pull-down studies followed by mass spectrometry analysis have been carried out and results are currently being validated.

In summary, this study suggests an anti-tumourigenic activity of the small molecule KHS101 through selective induction of a lethal vacuolisation phenotype. Most importantly, this destructive GSC cell state was triggered in a clinically and molecularly heterogeneous panel of GSCs. Notably, selective KHS101 cytotoxicity in GSCs was associated with decreased proliferation, activation of autophagy and reduction

of 'stemness' features. Moreover, preliminary data indicate the perturbation of metabolic processes by KHS101 resulting in glycolytic exhaustion of GSCs. Preclinical validation corroborated the notion of KHS101 as an anti-GBM agent, since systemic administration of KHS101 significantly reduced tumour burden and prolonged survival of mice bearing GBM tumours.

3 CVA21 oncolytic glioma therapy through chemically-induced ICAM-1 expression

3.1 Results

A number of OVs has been investigated for their oncolytic activity in GBM and been demonstrated to have significant therapeutic effects *in vitro*, in preclinical models and clinical trials [144]. One OV that has been shown to exhibit selective toxicity in ICAM-1 positive GBM models, leading to tumour regression upon intracranial injection, is CVA21 [167]. CVA21 is also an effective anti-cancer agent for the treatment of other ICAM-1 positive tumours (e.g., multiple myeloma, prostate cancer; [165] [166]) and is currently being evaluated for its safety and efficacy in clinical trials (e.g., ClinicalTrials.gov identifier NCT01636882, NCT00636558, NCT02043665). Together, these promising results prompted me to further investigate the potential of CVA21 as an anti-GBM therapy.

3.1.1 ICAM-1 expression in GBM is highly variable

Given the dependence of efficient infection with CVA21 on ICAM-1, establishment of a virotherapy with CVA21 for treatment of GBM requires ICAM-1 to be present at the cell surface. Therefore, we sought to assess the presence of ICAM-1 in patient-derived high-grade glioma specimens. To this end, we analysed immunohistochemistry (IHC) images from the Human Protein Atlas database [124] for ICAM-1 immunopositivity using the ImageJ software. The percentage of ICAM-1 positive area was determined by colour thresholding for ICAM-1 positive staining (see example images in figure 3.1A). A total of 69 or 61 images from 12 or 11 patients were analysed for two different ICAM-specific antibodies (HPA002126 or HPA004877), respectively. The graph in figure 3.1B depicts the results of this analysis. Notably, a high variability was observed between specimens with values ranging from 0-35% for HPA002126 and from 0-24% for HPA004877. This is consistent with previously reported minimal to moderate ICAM-1 expression in GBM cells with variable levels between different tumours and cell lines [244] [245]. Consistently, a high degree of variability in the percentage of ICAM-1 positive cells is found in our panel of GSC lines, as determined by FACS analysis (figure 3.1C). Here, values range between ∼3% (GSC20) to ∼80% (GSC11) of ICAM-1 positive cells. The high variability in ICAM-1 levels of GBM tumours and GSCs potentially limits efficacy of CVA21 virotherapy. Therefore, the objective was to identify a method that upregulates ICAM-1 expression in tumour cells, and thus increase CVA21 efficacy in GBM.

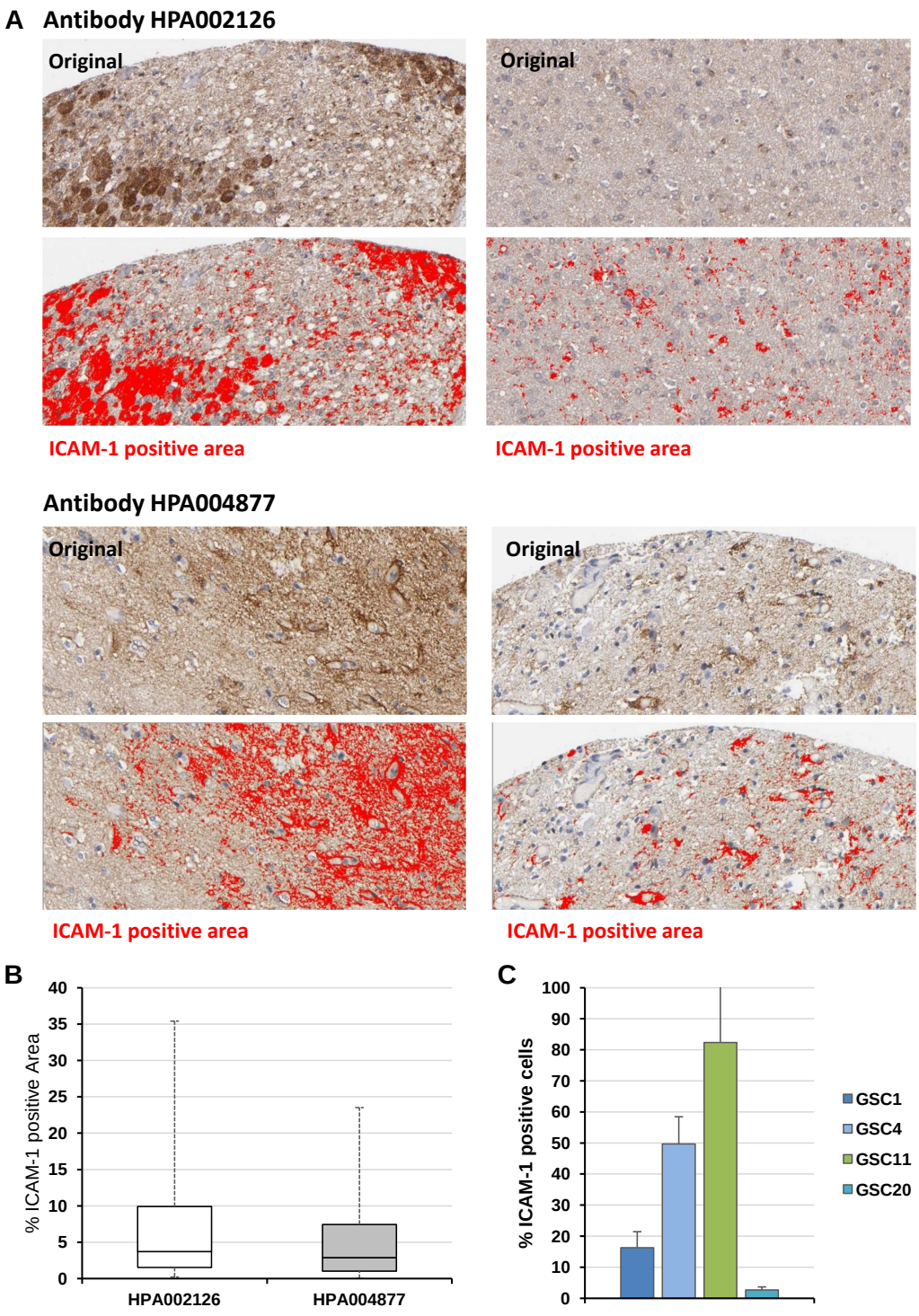

Fig. 3.1: ICAM-1 expression is highly variable in malignant glioma and GSCs. **A)** Representative images of human glioma specimens stained for ICAM-1 using two different antibodies (source: www.proteinatlas.org). Using colour thresholding ICAM-1 positive areas are highlighted in red. **B)** Quantification of the ICAM-1 positve tumour area in human glioma specimen (n=11/12). **C)** ICAM-1 surface expression in GSC1, GSC4, GSC11 and GSC20 cells. The percentage of ICAM-1 positive cells as determined by flow cytometry is shown (data shown as mean ± SD; n=3).

3.1.2 Mouse ICAM-1 expression in a syngeneic mouse model affects macrophage polarisation but not tumour growth

Increased ICAM-1 expression in tumours is expected to facilitate CVA21 entry and efficiency. However, ICAM-1 expression in solid tumours has been implicated in malignancy through cross-talk between cancer cells and immune cells including ICAM-1-mediated macrophage adhesion, and promoting migration of cancer cells (e.g., [246] [247] [248]). Hence, the potential pro-tumourigenic effect of ICAM-1 expression in tumours has to be taken into account. Therefore, I sought to assess the consequences of ICAM-1 expression on possible pro- or anti-tumour immune responses in an immunocompetent (syngeneic) mouse model based on CT2A mouse glioma cells. The CT2A cell line was initially established by Seyfried et al. through chemical induction with a highly carcinogenic polycyclic aromatic hydrocarbon and forms poorly differentiated highly malignant anaplastic astrocytomas [249]. Moreover, the CT2A model has been found to represent important GBM features including intra-tumoural heterogeneity and migration [250]. These characteristics make it a suitable model for studying GBM biology in an immunocompetent environment. The CT2A cells were lentivirally transduced with a mouse (m)ICAM-1 overexpression vector or the respective empty vector. Additionally, control and mICAM1-transduced CT2A (mICAM1↑) cells were lentivirally transduced to stably express firefly luciferase (F-luc) in order to enable *in vivo* monitoring of tumour growth by non-invasive bioluminescence (IVIS) imaging. To test the efficiency of mICAM-1 overexpression in the transduced CT2A cells, I carried out fluorescence-activated cell sorting (FACS) analysis detecting mICAM-1 on the cell surface. Approximately 90% of mICAM1↑ CT2A cells were ICAM-1 positive compared to only ∼4% of control CT2A cells transduced with the empty vector (figure 3.2A). After intracranial implantation of control and mICAM1↑ CT2A cells into immunocompetent C57BL/6 mice, tumour size was determined weekly until a bioluminescence signal of $1x10^8$-$1x10^9$ photons/second was reached (an empirically determined maximum tolerable signal intensity indicating an imminent onset of neurological signs). The graph in figure 3.2B displays the growth curves obtained for control and mICAM1↑ CT2A tumours. Notably, the mICAM-1 positive CT2A cells expanded *in vivo* at a rate that was similar to mICAM-1 negative control cells. Hence, mICAM-1 overexpression in CT2A did not accelerate tumour growth in this syngeneic GBM mouse model experiment.

Immune cell infiltration was investigated at the experimental endpoint (23 days). To this end, the presence of different populations of immune cells (i.e. macrophages, T cells, NK cells, granulocytic myeloid-derived suppressor cells [MDSC], monocytic

MDSCs) in the CT2A tumours was determined by FACS analysis detecting the respective immune cell markers. Cells of the myeloid lineage were identified by their expression of the surface marker CD11b. Among those CD11b positive cells, macrophages were distinguished by concomitant expression of F4/80 and high expression of CD45, while lacking expression of myeloid differentiation antigen GR1. GR1 positivity, however, marks MDSCs, and expression of lymphocyte antigen 6 complex (Ly6)G and Ly6C allows differentiation between granulocytic and monocytic MDSCs, respectively. Within the CD11b negative population, those cells that were double positive for CD45 and CD3 were classified as T cells. Lastly, NK cells were defined as CD45 positive, CD3e negative and natural killer cell p46-related protein (NKp46) positive. Notably, infiltration of CT2A tumours by any of the tested immune cell types was not significantly altered upon overexpression of mICAM-1 compared to control tumours and the number of immune cells present within the tumour were generally low: macrophages constituted 1.4-1.9%, T cells ∼0.1%, NK cells 0.2-0.4%, granulocytic MDSCs ∼0.05% and monocytic MDSCs 6.1-12.3% of all detected cells (figure 3.2C).

In addition to immune cell infiltration, we tested the polarisation status of the infiltrating macrophages and MDSCs, a measure that has been used to indicate their tumour-promoting or anti-tumourigenic potential. Whereas macrophages/MDSCs with a predominantly M2 phenotype have been described as immunosuppressive, tumour growth- and invasion-promoting, M1-polarised macrophages/MDSCs have been proposed to activate an anti-cancer immune response [251] [252]. The hallmarks that are applied to define the M1 subset of macrophages/MDSCs in murine models are expression of nitric oxide synthase 2 (iNOS) and MHC class II molecule, whose presence is critical to trigger an immune response [253] [254]. Markers for the M2 subset are arginase-1 (Arg1) and mannose receptor C type 1 (Mrc1 or CD206; [253]). Therefore, we assessed the expression of Arg1, iNOS, CD206 and MHCII on macrophage/MDSC populations present within mICAM1↑ and control CT2A tumours. Within the MDSC (GR1 positive) population, expression of Arg1 and CD206 was significantly decreased in mICAM1↑ CT2A tumours compared to control tumours. This is overall an indication of a shift of MDSCs away from a M2 tumour-promoting phenotype state. Expression of iNOS was significantly reduced and expression of MHCII, remained unchanged in MDSCs from mICAM1↑ CT2A tumours. Similar to MDSC phenotype within the macrophage (GR1 negative) population, Arg1 and CD206 protein levels were significantly lower upon expression of mICAM-1 compared to control tumours. Notably, ICAM-1 positivity did not alter expression of iNOS in this subset of cells and MHCII was undetectable in

both, macrophages isolated from control and from mICAM1↑ tumours (figure 3.2D). Taken together, overexpression of mICAM-1 in CT2A intracranial tumours in immunocompetent mice did not significantly alter the rate of tumour growth and had no significant effect on immune cell infiltration into the tumour. The activation state of tumour-infiltrating MDSCs and macrophages, however, was altered by ICAM-1 positivity leading to a switch away from a pro-tumourigenic phenotype.

3.1.3 Increased ICAM-1 expression renders GSCs susceptible to CVA21-mediated cell death

ICAM-1 on the surface of human cancer cells is thought to be a prerequisite to successful CVA21 virotherapy through rendering cells susceptible to CVA21-mediated cell death [164]. To investigate whether ICAM-1 positivity increases susceptibility of GSCs to CVA21 virotherapy, I generated human ICAM-1 overexpressing (hICAM-1↑) GSCs by lentiviral transduction and tested their vulnerability to CVA21-mediated oncolysis. The proneural/classical GSC1 and the mesenchymal GSC4 line were used to assess susceptibility of GSCs of different subtypes. FACS analysis confirmed the presence of ICAM-1 on hICAM-1↑ GSC1 and GSC4 cells. Consistent with the observation of ICAM-1 expression on mesenchymal stem cells [255], ∼35% of control vector-harbouring GSC4 cells were ICAM-1 positive. Lentivirally induced ICAM-1 overexpression resulted in a GSC4 population with 90% ICAM-1 positive cells. Similarly, 96% of GSC1 cells were ICAM-1 positive upon transduction with the ICAM-1 overexpression vector, wich equals a >10-fold increase compared to GSC1 cells transduced with the empty control vector (figure 3.3A).
Next, to test the susceptibility of GSC1 and GSC4 control and hICAM-1↑ cells to CVA21-mediated cell death, the cells were infected with CVA21 at increasing multiplicities of infection (MOI) of 0, 0.01, 0.1 and 1, and the percentage of dead cells was determined 7 days post infection with CVA21 by FACS analysis using the LIVE/DEAD® Fixable Red Dead Cell Stain (Invitrogen). Consistent with their ICAM-1 expression levels, control GSC1 and GSC4 cells showed a cell death rate of 20-50% upon CVA21 infection. However, lentivirally-induced ICAM-1 overexpression doubled those numbers reaching up to 95% cell death upon treatment with CVA21, thereby strengthening the notion of an ICAM-1 dependence of efficient killing by CVA21. Interestingly, addition of CVA21 at a MOI of 0.1 was sufficient to induce cell death in 90% of hICAM-1↑ GSC1 cells, and 86% of hICAM-1↑ GSC4 cells (figure 3.3B).

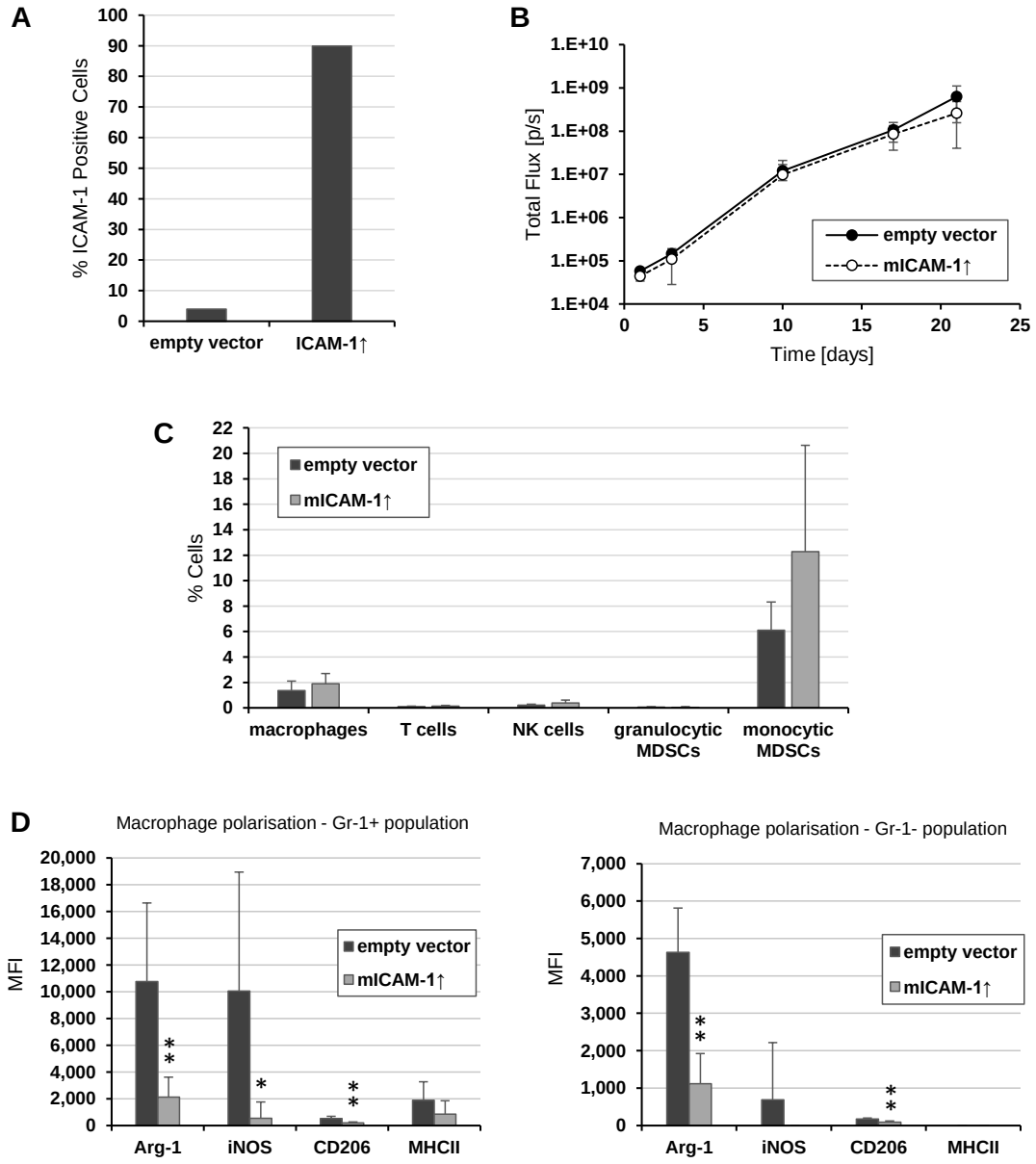

Fig. 3.2: Mouse ICAM-1 (mICAM-1) expression in a syngeneic glioma model affects macrophage polarisation but not tumour growth. **A)** ICAM-1 surface expression is increased in mICAM-1 overexpressing mouse glioma cells (CT2A). The percentage of ICAM-1 positive cells as determined by flow cytometry is shown. **B)** Monitoring CT2A (firelfy luciferase labelled) tumour growth by bioluminescence imaging reveals a comparable rate of tumour growth over time in CT2A cells transduced with an mICAM-1 overexpression vector (mICAM-1↑) and CT2A cells transduced with an empty vector (data shown as mean ± SD; n=5). **C)** FACS analysis showing no significant difference in infiltration of immune cells (macrophages, T-cells, NK cells, granulocytic MDSCs, monocytic MDSCs) into CT2A tumours four weeks after intracranial injection of CT2A mICAM-1 overexpressing cells (mICAM-1↑) or CT2A control cells (empty vector; data shown as mean ± SD; n=5). **D)** Flow cytometric analysis detecting macrophage polarisation markers in mICAM-1 overexpressing CT2A tumours compared with control tumours (data shown as mean ± SD; n=5; *, $P<0.05$; **, $P<0.01$; Mann Whitney U-test).

In order to assess an alternative to lentiviral transduction-mediated overexpression, I sought to determine whether induction of *ICAM1* gene expression could be achieved by treatment with known modulators of ICAM-1 expression. A potent inducer of *ICAM1* mRNA expression is the cytokine TNF-α, an immune cell regulator involved in inflammation [173]. Thus, I tested TNF-α-induced *ICAM1* mRNA expression in GSCs by qRT-PCR. Treatment of GSC4 cells with TNF-α for 6 hours led to a marked increase of *ICAM1* mRNA levels compared to vehicle-treated cells (left graph in figure 3.4). This induction of *ICAM1* at the gene expression level was followed by an increase in ICAM-1 on the cell surface after 24 hours of treatment with TNF-α as shown by FACS analysis (right graph in figure 3.4). Similar to lentivirally induced ICAM-1 expression in GSC4 cells, TNF-α treatment of GSC4 cells led to a 3-fold increase (from 32% in control cells to 91% in TNF-α-treated cells) in the percentage of ICAM-1 positive cells.

In conclusion, ICAM-1 expression can be induced in GSC cells through genetic manipulation or by treatment with TNF-α. Notably, overexpression of ICAM-1 markedly increases susceptibility of GSCs to CVA21-mediated cell death suggesting a potential applicability of CVA21 treatment for effective elimination of ICAM-1 positive GSCs. However, TNF-α, which is currently only used as a locally delivered anti-cancer treatment of sarcomas and melanomas [256], cannot be administered systemically due to its severe side effects when given in therapeutically-active doses [257]. In contrast, small molecules can offer a better balance between therapeutic activity and adverse effects. Therefore, I sought to identify small molecules that could selectively induce ICAM-1 in GSCs.

3.1.4 Combination of RA and KHS101 induces ICAM-1 expression in GSCs

3.1.4.1 A focused qRT-PCR screen identifies the combination of RA and KHS101 as inducers of ICAM1 expression in GSCs

One small molecule that is known for its role as an inducer of ICAM-1 expression in various different cell types is RA [183] [186] [187] [188] [189]. RA acts through signalling via RAR and RXR [184]. Furthermore, RA has been shown to exhibit differentiation-inducing activity in a cancer stem cell background and has been investigated in a preclinical and clinical setting as an anti-tumourigenic agent [134] [139]. Most importantly, *in vivo* studies have demonstrated brain accessibility of RA

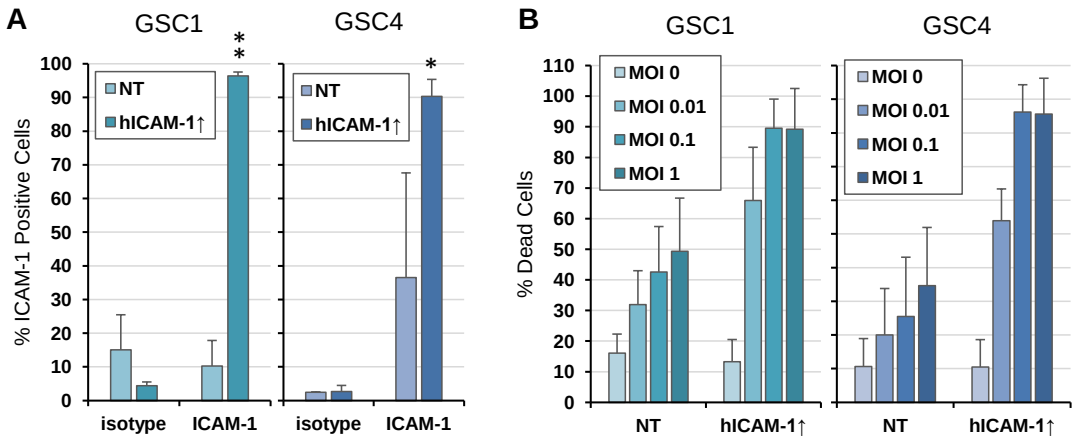

Fig. 3.3: Induced overexpression of human ICAM-1 (hICAM-1) increases susceptibility of GSCs to CVA21-mediated cell death. **A)** ICAM-1 surface expression is increased in hICAM-1 overexpressing GSC1 and GSC4 cells. The percentage of ICAM-1 positive cells as determined by flow cytometry is shown (data shown as mean ± SD; n=3; *, $P<0.05$; **, $P<0.01$; Student t test). **B)** Increased cell death of hICAM-1 overexpressing GSC1 and GSC4 cells infected with CVA21 at multiplicity of infection (MOI) of 0, 0.01, 0.1 and 1 for 7 days. The percentage of dead cells as determined by flow cytometry using a LIVE/DEAD® fixable dead cell stain is shown (data shown as mean ± SD; n=1).

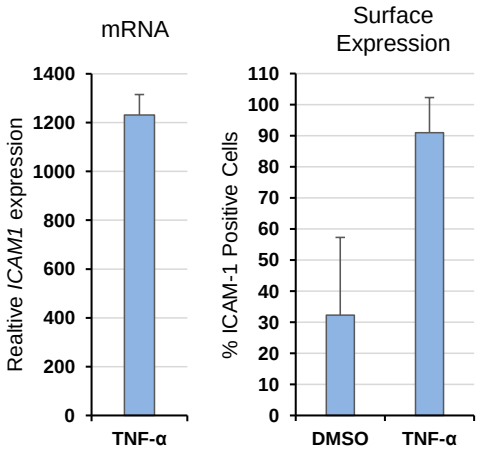

Fig. 3.4: ICAM-1 expression can be chemically induced in GSCs by TNF-α. Left: *ICAM1* mRNA is induced in GSC4 cells after 6 hours of treatment with TNF-α (10 ng/ml; data normalised to vehicle control and shown as mean of fold changes ± SD of technical triplicates; n=1). Right: ICAM-1 surface expression is increased in GSC4 cells after 24 hours of treatment with TNF-α (10 ng/ml). The percentage of ICAM-1 positive cells as determined by flow cytometry is shown (data shown as mean ± SD; n=2).

[140], a feature that makes RA a promising candidate for modulating GSC biology. Notably, assessment of the effect of the compound in our GSC models revealed no obvious differentiation, anti-proliferative vacuolisation and cytotoxic activity of RA as shown by immunostainings for the astroglial differentiation marker GFAP, the GSC 'stemness' markers NESTIN and SOX2, the proliferation marker KI67, and by cell viability assays (figure 3.5). Moreover, treatment of GSCs with RA only moderately increased *ICAM1* mRNA levels compared to TNF-α, which is 24-fold more potent than RA in inducing *ICAM1* gene expression (figures 3.4 and 3.6). Therefore, my aim was to identify a compound that could either induce *ICAM1* expression greater than RA, or potentiate the effect of RA on *ICAM1* expression in GSCs. To this end, I conducted a focused qRT-PCR screen testing 23 small molecules for their potential to induce *ICAM1* expression as single agents or in combination with RA. Two groups of compounds were tested: 1) Compounds that are known to be involved in modulation of *ICAM1* transcriptional regulations (ICAM-1 relevant compounds), and 2) brain-penetrable compounds without reported connection(s) to the regulation of *ICAM1* expression. The full list of chemical compounds is shown in table 3.1 and includes the PKC signaling modulators phorbol-12-myristat-13-acetat (PMA) and (-)-indolactam-V, the RAR agonist AM580, the RXR agonists Bexarotene and 9-cis-RA, the mitogen-activated protein kinase kinase (MEK) inhibitor PD98059, the p38 inhibitor SB202190, the Wnt antagonist sulindac, the TGF inhibitor Losartan, the SRC-family kinase inhibitor CGP76030, the omega-6 fatty acid linoleic acid, the rho-associated protein kinase (ROCK) inhibitor Y27632, the HAT inhibitor curcumin and the peroxisome proliferator-activated receptor (PPAR) α/γ ligand troglitazone, as well as the anti-GBM chemotherapeutic TMZ and KHS101.

For the ICAM-1 screen, GSC1 cells were treated with RA or the test compound alone, or with a combination of RA and the given compound. The relative gene expression levels of *ICAM1* were determined by qRT-PCR after 24 hours of treatment. In contrast to single treatment with RA, none of the compounds tested had an effect on *ICAM1* mRNA levels upon single treatment. Also, most of the double treatments only induced *ICAM1* expression to the same extent as RA alone, hence indicating no additive effect of the combination treatment. However, two of the 'ICAM-1 relevant' compounds, i.e. CGP76030 and (-)-indolactam-V, enhanced the effect of RA single treatment on *ICAM1* mRNA levels by >4-fold and 2.5-fold, respectively. Strikingly, the two top hits of the screen were the compounds KHS101 and Vacquinol-1, which share the common feature of causing (lethal) hyper-vacuolisation selectively in glioma cells (see also section 2.1.1 'KHS101 induces vacuolisation, autophagy and apoptotic cell death in a panel of molecularly different GSCs'; [115]). Com-

pared to treatment with RA alone, a highly significant >7-fold increase in relative *ICAM1* mRNA expression was obtained upon treatment with RA in combination with KHS101. Combining RA with Vacquinol-1 had a comparable effect on *ICAM1* expression (figure 3.6).

Since I comprehensively investigated the effect of the small molecule KHS101 on GSCs in the first part of this thesis, I here focused on further investigating RA/KHS101-induced ICAM-1 upregulation in GSCs with a focus on the question as to whether chemical upregulation of ICAM-1 can be exploited for CVA21 virotherapy in GSCs.

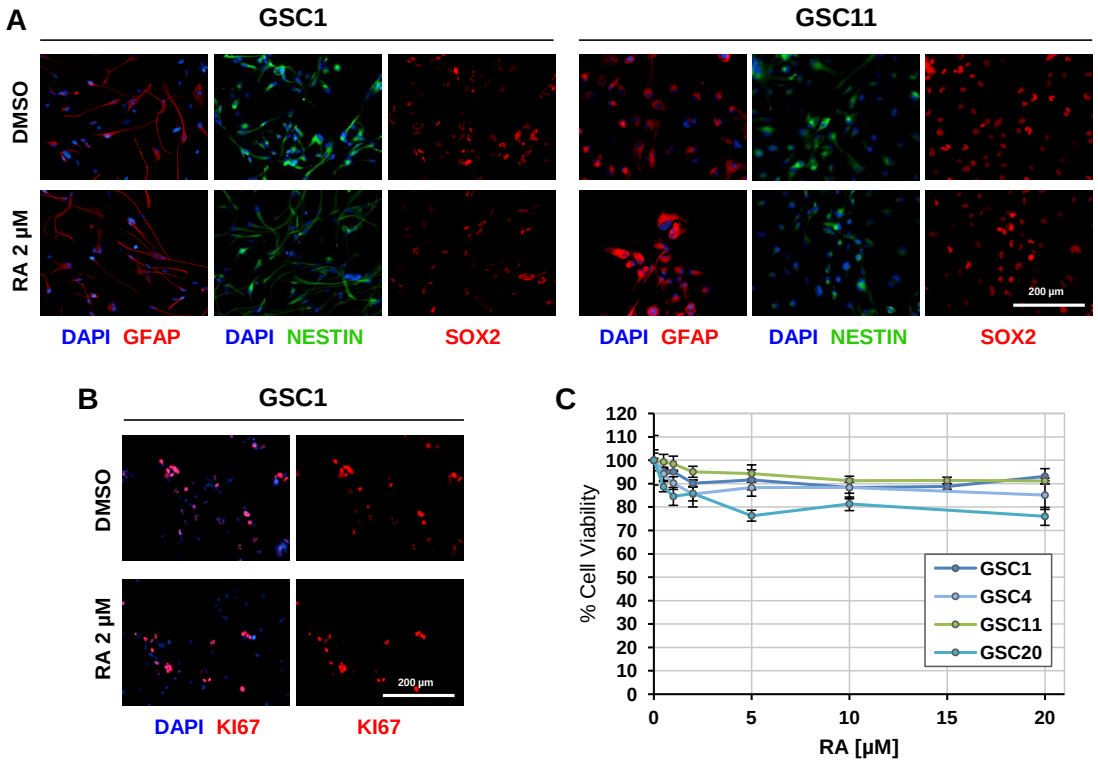

Fig. 3.5: The small molecule RA has only minimal effect on GSC differentiation, proliferation and cell viability of GSCs. **A)** Example images of GFAP, NESTIN and SOX2 immunofluorescence staining in GSC1 and GSC11 cells treated with vehicle (0.1% DMSO) or RA (2 µM) for 5 days. Nuclei were stained with DAPI. **B)** Example images of KI67 immunofluorescence staining in GSC1 cells treated with vehicle (0.1% DMSO) or RA (2 µM) for 2 days. Nuclei were stained with DAPI. **C)** Cell viability curves of GSC1, GSC4, GSC11 and GSC20 treated with RA for 2 days (data shown as mean ± SD; n=2/3).

Compound	Function	Conc.	References
PD98059	MEK inhibitor	30 µM	[258] [259]
SB202190	p38 inhibitor	5 µM	[260]
Sulindac	Wnt antagonist	50 µM	[261] [262]
PMA	PKC inhibitor	1 µM	[263] [264]
Losartan	TGF inhibitor	5 µM	[265] [266] [267]
CGP76030	SRC-family kinase inhibitor	10 µM	[268] [269]
Linoleic acid	Omega-6 fatty acid	10 µM	[270] [271]
9-cis retinoic acid	RXR Agonist	1 µM	[185]
Y27632	ROCK inhibitor	20 µM	[270] [272]
(-)-indolactam-V	PKC activator	10 µM	[273] [274]
Curcumin	HAT inhibitor	2 µM	[95]
Troglitazone	PPAR alpha and gamma ligand	20 µM	[275]
AM580	RAR agonist	50 nM	[276]
Bexarotene	RXR agonist	1 µM	[277]
SU5416	VEGF inhibitor	20 µM	[278]
Alsterpaullone	Inhibitor of GSK-3β and CDK5/p25; potent inhibitor of CDK1/cyclin B	1 µM	[279] [280]
Mianserin	Serotonin receptor antagonist	1 µM	[281] [282]
Lapatinib	RTK inhibitor of HER2 / EGFR	2 µM	[283] [284]
Niacin	Vitamin B3	10 µM	[285] [286]
Yohimbine	A2 antagonist adrenergic	10 µM	[287] [288]
Temozolomide	Alkylating agent for treatment of GBM	200 µM	[289]
KHS101	Inducer of neural differentiation in rat neural progenitor cells	7.5 µM	[116]
Vacquinol-1	Inducer of catastrophic vacuolisation in GBM cells	2.5 µM	[115]

Table 3.1: List of the 14 ICAM-1 relevant compounds (top) and 9 blood brain barrier penetrable compounds (bottom) selected for the *ICAM1* qRT-PCR screen.

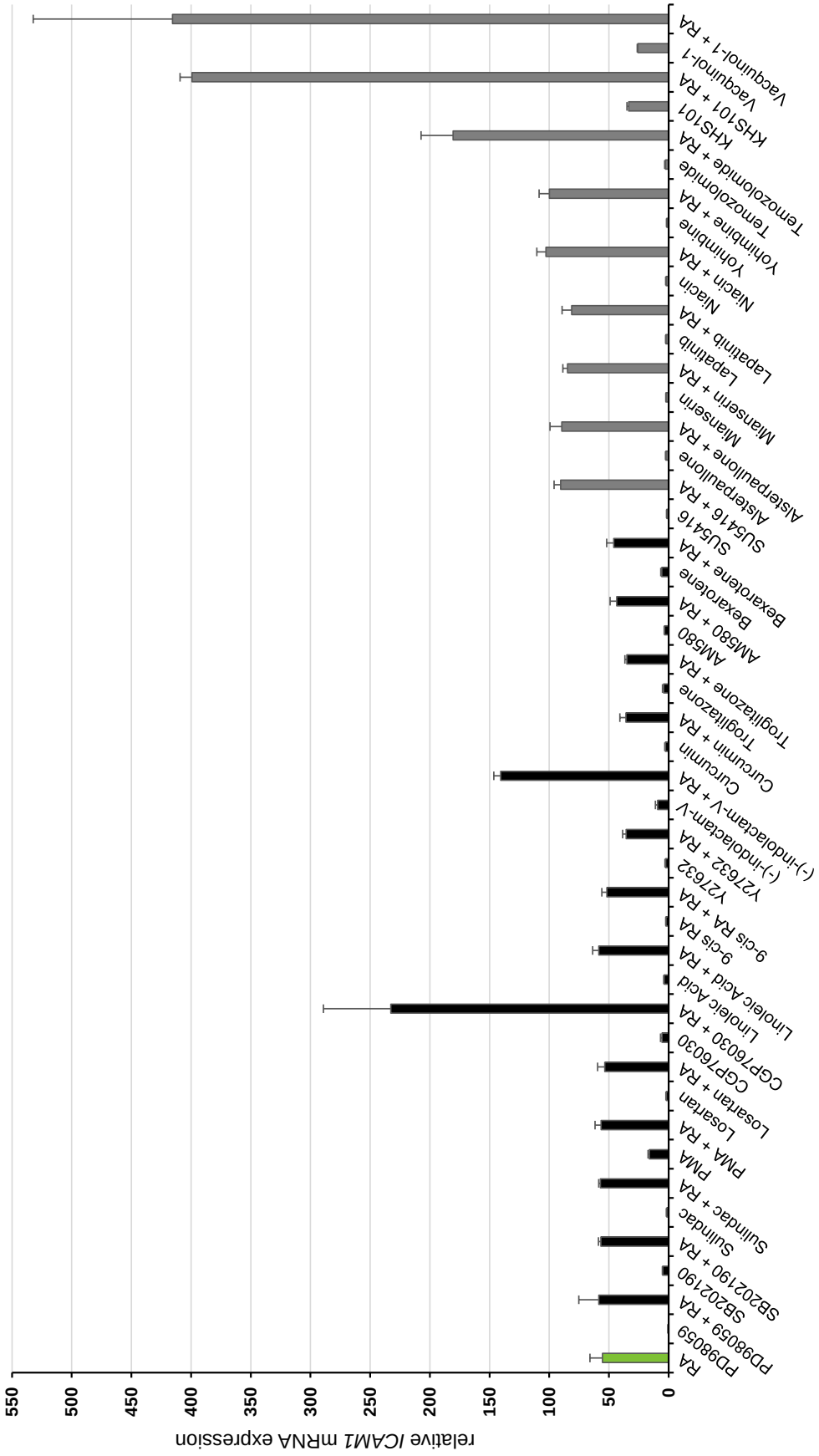

Fig. 3.6: A focused qRT-PCR screen identifies the combination of RA and KHS101 as inducers of *ICAM1* expression in GSCs. *ICAM1* mRNA expression in GSC1 cells treated with 2 µM RA ± compound or compound alone for 24 hours (data normalised to vehicle control and shown as mean of fold changes ± SD; n=3).

3.1.4.2 Double treatment with RA and KHS101 affects viability, proliferation and clonal growth of GSCs

Results on KHS101 as a single agent (see chapter 2 'KHS101 abrogates the tumourigenic potential of GSCs through induction of a cellular self-destruction phenotype') have demonstrated that the compound has anti-GSC activity. Therefore, I sought to assess whether combining KHS101 with RA changes KHS101 effects in GSCs. To this end, I determined the effect of RA/KHS101 compared to KHS101 alone on key features that define KHS101 activity in GSCs, i.e. vacuolisation, cell viability, proliferation and clonal growth capacity. Notably, addition of RA does not significantly affect the KHS101-induced vacuolisation phenotype (data not shown). For cell viability assays, GSCs were treated with vehicle (0.1% DMSO) or RA (2 µM; non-toxic dose, see figure 3.5) and increasing concentrations of KHS101 (up to 20 µM), and the percentage of viable cells was measured after 2 and 5 days of treatment. All tested GSC lines showed a marked decrease in cell viability upon treatment with RA/KHS101. However, compared to cell viability dose response curves obtained for KHS101 single treatment (figure 2.6A), the 2-day-IC50 values of RA/KHS101 were elevated (2.7-fold for GSC1, 2.6-fold for GSC4, 4.7-fold for GSC20). In GSC11, 2-day-IC50 values for RA/KHS101 and KHS101 were both >18 µM indicating minimal effects on cell viability. Notably, prolonged treatment diminished the differences between RA/KHS101 and KHS101 treatment in GSC model responses (figures 3.7A and 2.6A). Five-day-IC50 values of RA/KHS101 were only slightly elevated (1.5-fold for GSC1, 2.3-fold for GSC4, 1.3-fold for GSC11, 1.4-fold for GSC20) compared with the 5-day-IC50 values of KHS101 (figure 3.7A and table 3.2).

In order to ascertain the effect of RA/KHS101 on GSC proliferation, GSCs were stained for the proliferation marker KI67 after 48 hours of treatment and the percentage of KI67-positive cells was determined. Consistent with the results from the dose-dependent effect of KHS101 single treatment on GSC proliferation (figure 2.1), treatment with RA/KHS101 markedly reduced the percentage of KI67-positive cells by 5-fold (GSC1), 8.3-fold (GSC4), 8.5-fold (GSC11), and 14.8-fold (GSC20). Notably, this abrogation of GSC proliferation could mainly be attributed to KHS101, as comparable values were obtained for treatment with KHS101 alone (figure 3.7B). Additionally, I tested whether RA/KHS101 affects the colony formation efficiency of GSCs compared to KHS101 single treatments. To this end, GSC colony formation efficiency was determined following the pre-treatment protocol depicted in figure 2.9A. As expected, the colony formation efficiency of GSCs was reduced upon treatment with RA/KHS101 leading to a reduction of ≤6-fold (GSC1), ≤4.2-fold (GSC11) and ≤3.9-fold (GSC20) compared to control cells. Similar values were ob-

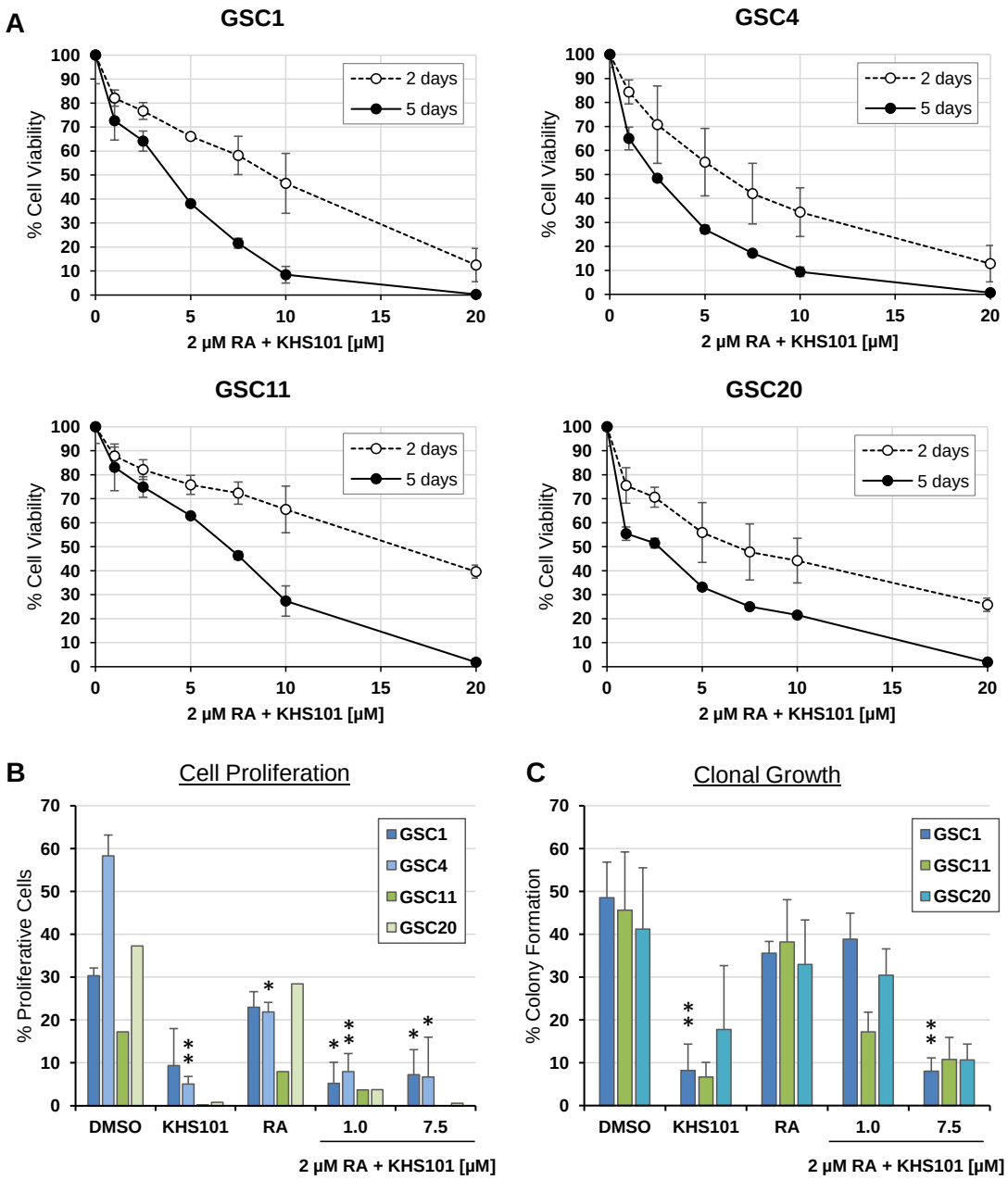

Fig. 3.7: RA/KHS101 double treatment affects viability, proliferation and clonal growth capability of GSCs. **A)** Differential cell viability dose response curves of the patient-derived GSC lines GSC1, GSC4, GSC11 and GSC20 after 2 days and after 5 days of treatment with RA (2 µM) and KHS101 (1 – 20 µM) are shown (data normalised to vehicle control and shown as mean ± SD; n=3 [2 days] or n=1 [5 days]). **B)** Quantification of the percentage of proliferative (KI67 positive) cells 48 hours after treatment or GSC1, GSC4, GSC11 and GSC20 cells with vehicle (0.1% DMSO), KHS101 (7.5 µM), RA (2 µM) or RA (2 µM) and KHS101 (1 or 7.5 µM; data shown as mean ± SD; n=2 [GSC1, GSC4] or n=1 [GSC11, GSC20] ; *, $P<0.05$; **, $P<0.01$; Student t test). **C)** Quantification of the clonal growth capability of GSC1, GSC11 and GSC20 cells pre-treated with vehicle (0.1% DMSO), KHS101 (7.5 µM), RA (2 µM) or RA (2 µM) and KHS101 (1 or 7.5 µM; data shown as mean ± SD; n=2; **, $P<0.01$; Student t test.

tained for KHS101 single treatment, indicating minimal influence of RA in the effect of RA/KHS101 on GSC clonal growth capacity (figure 3.7C).
In summary, the combination of KHS101 and RA treatment does not have an additive effect on cell viability, proliferation and clonal growth of GSCs as compared to KHS101 single treatment. However, neither does addition of RA significantly hamper the anti-GSC activity of KHS101.

Cell line	2 days		5 days	
	KHS101	RA/KHS101	KHS101	RA/KHS101
GSC1	**3.62** (3.10;4.23)	**9.65** (6.48;14.36)	**2.23** (2.02;2.47)	**3.40** (2.17;5.22)
GSC4	**2.37** (1.73;3.25)	**6.21** (4.27;9.04)	**0.97** (0.90; 1.04)	**2.19** (1.66;2.88)
GSC11	> **18**	> **18**	**5.05** (4.51;5.64)	**6.46** (4.12;10.11)
GSC20	**3.39** (2.63;4.36)	**15.9** (4.20;60.42)	**1.87** (1.58;2.21)	**2.61** (0.95;7.19)

Table 3.2: IC50 values [µM] for GSCs treated with KHS101 or RA/KHS101 for 2 days or 5 days (data shown with 95% confidence interval).

3.1.4.3 Combination of RA and KHS101 induces ICAM-1 mRNA and protein expression in different GSC models

RA/KHS101 treatment induced *ICAM1* mRNA levels in GSC1 cells at the 24-hour-time point (figure 3.6). To assess whether the RA/KHS101-induced *ICAM1* mRNA expression was transient, I determined *ICAM1* mRNA levels by qRT-PCR in GSC1 cells treated with vehicle (0.1% DMSO) or RA (2 µM) and KHS101 (7.5 µM) at different time points (0, 6, 24, 48 hours, 3 and 7 days). Activation of *ICAM1* gene expression reached a maximum after 24 hours of treatment with RA/KHS101 and levels dropped thereafter reaching nearly baseline levels after 7 days (figure 3.8A). Next, I tested whether shorter exposure of GSCs to RA/KHS101 followed by a 'wash out' of compounds causes an increase of *ICAM1* mRNA at the 24-hour-time point. I treated GSC1 cells with RA (2 µM) and KHS101 (7.5 µM). The compounds were removed (through media replacement) after 1, 2, 3, 4 or 7 hours of exposure and *ICAM1* mRNA levels were determined after 24 hours. All tested shorter treatment times only reached up to ∼25% of *ICAM1* mRNA levels compared to those induced by 24 hours of treatment (figure 3.8B).
Based on these findings, the dose-dependence of *ICAM1* mRNA expression in GSC lines of proneural (GSC1), mesenchymal (GSC4, GSC11) and proneural/mesenchymal (GSC20) subtypes was determined at the 24-hour-time point. GSC1, GSC4, GSC11

and GSC20 cells were treated with vehicle (0.1% DMSO), KHS101 (7.5 µM), RA (2 µM) or RA (2 µM) and KHS101 (1, 2.5, 7.5 µM) and *ICAM1* mRNA levels were assessed by qRT-PCR. In all tested GSC lines, *ICAM1* expression was significantly up-regulated upon RA (>35-fold in GSC1, >20-fold in GSC4, >6-fold in GSC11, >14-fold in GSC20) and RA/KHS101 (7.5 µM; >130-fold in GSC1, >22-fold in GSC4, >25-fold in GSC11, >78-fold in GSC20) treatments. Notably, with the exception of GSC4, RA/KHS101 treatment markedly potentiated the effect of RA treatment by >3.5-fold (GSC1), >4-fold (GSC11) and >5.5-fold (GSC20; figure 3.8C).

Since ICAM-1 can only serve as an entry site for CVA21 when present at the cell surface, I investigated whether the RA/KHS101-induced *ICAM1* mRNA expression leads to ICAM-1 protein incorporated into the cell membrane of GSCs. To this end, I performed immunofluorescence staining for ICAM-1 on GSC1 cells treated with vehicle (0.1% DMSO) or RA (2 µM) and KHS101 (7.5 µM) for 48 hours. Vehicle-treated control cells showed a predominantly negative ICAM-1 immunostaining. Upon treatment with RA/KHS101, a large population of GSC1 cells became positive for ICAM-1 showing a ICAM-1 immunofluorescence signal at the cell edges indicative of a cell membrane location of ICAM-1 protein (see middle image and right image in figure 3.9A).

To further confirm the presence of ICAM-1 on the cell surface and to determine the number of ICAM-1 positive cells, FACS analysis was performed. GSC1 cells were treated with vehicle (0.1% DMSO), KHS101 (7.5 µM), RA (2 µM) or RA (2 µM) and KHS101 (1, 2.5, 7.5 µM) for 48 hours, stained for ICAM-1 and the percentage of ICAM-1 positive cells was determined. Figure 3.9B shows example histograms obtained for GSC1 cells and highlights the gating strategy used to define ICAM-1 positive cell populations based on the background fluorescence signal of the isotype control. The isotpye signal was unchanged irrespective of treatment. Compared to control cells, RA/KHS101 treatment significantly increased the number of ICAM-1 positive GSC1 and GSC4 cells reaching >80% (GSC1) and >90% (GSC4). Interestingly, single treatment with RA also led to a significantly increased number of ICAM-1 positive cells (>65% for GSC1, ∼95% for GSC4), indicating that at the protein level, KHS101 does not have an additive effect over RA. In contrast to GSC1 and GSC4 cells, RA or RA/KHS101 treatment did not significantly alter the number of ICAM-1 positive GSC11 and GSC20 cells compared to control cells. Notably, >80% of vehicle-treated GSC11 cells were ICAM-1 positive and RA/KHS101 only slightly increased this number to ∼94%. Vehicle-treated GSC20 cells, however, were mostly ICAM-1 negative and RA/KHS101 treatment only led to ∼30% of ICAM-1

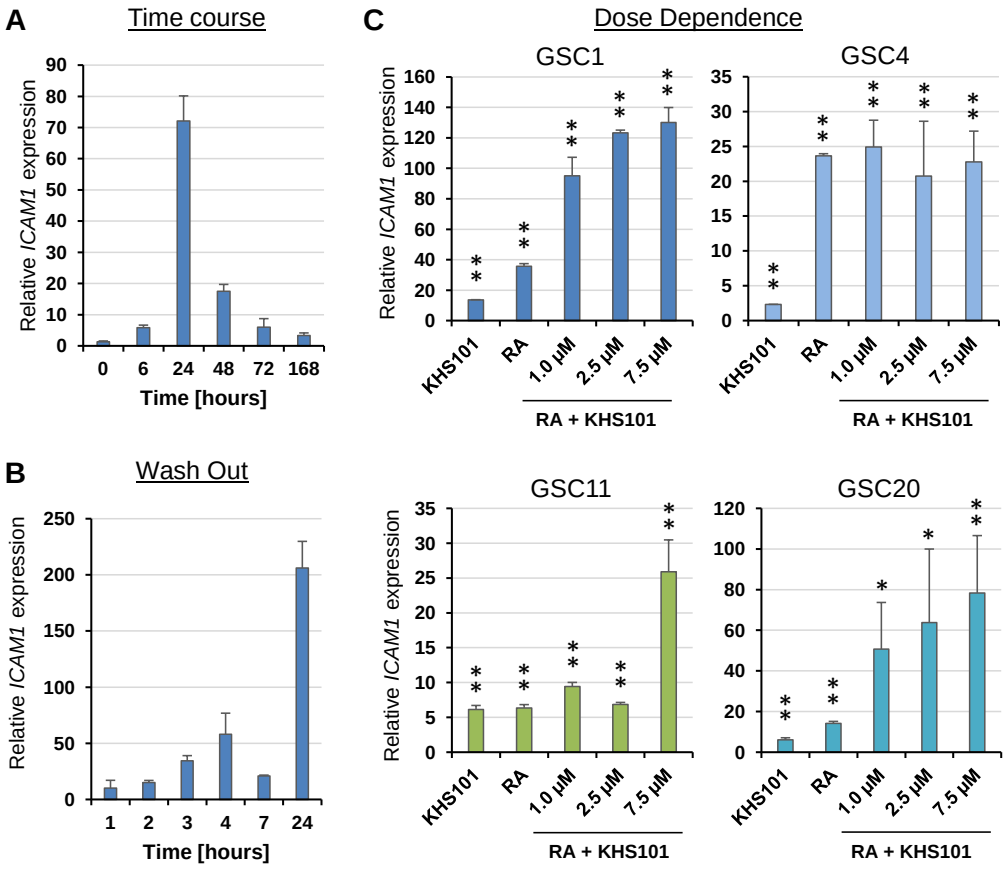

Fig. 3.8: RA/KHS101 double treatment induces *ICAM1* mRNA expression in different GSC models. **A)** Time course of *ICAM1* mRNA induction in GSC1 cells treated with 2 µM RA and 7.5 µM KHS101 for 0, 6, 24, 48 h, 3 and 7 days showing that *ICAM1* mRNA levels are highest after 24 hours of treatment (data normalised to vehicle control and shown as mean of fold changes ± SD of technical triplicates; n=1). **B)** *ICAM1* mRNA expression in GSC1 cells treated with 2 µM RA and 7.5 µM KHS101. Compounds were 'washed out' after 1, 2, 3, 4, 7, 24 hours and cells harvested after 24 hours (data normalised to vehicle control and shown as mean of fold changes ± SD of technical triplicates; n=1). **C)** Dose dependent *ICAM1* mRNA up-regulation in GSC1, GSC4, GSC11 and GSC20 cells treated with 2 µM RA in combination with increasing concentrations of KHS101 or with 2 µM RA or 7.5 µM KHS101 alone for 24 hours (data normalised to vehicle control and shown as mean of fold changes ± SD; n=3; *, $P<0.05$; **, $P<0.01$; Student t test.

positive cells (figure 3.9C and D).

In conclusion, RA/KHS101 double treatment more potently increases *ICAM1* mRNA levels in GSCs compared to RA single treatment. Only GSC4 cells show a comparable *ICAM1* mRNA expression upon RA and RA/KHS101 treatment. The evidence from ICAM-1 immunofluorescence staining and ICAM-1 FACS analysis jointly demonstrates that RA/KHS101, but also RA alone leads to elevated ICAM-1 protein levels and significantly increased numbers of ICAM-1 positive GSC1 and GSC4 cells. Therefore, RA single treatment could be sufficient to induce ICAM-1 surface protein required for CVA21 entry. Compared to GSC1 and GSC4 cells, GSC11 and GSC20 cells showed a differential response to RA/KHS101 treatment. Although *ICAM1* mRNA expression was significantly increased upon RA/KHS101 treatment in GSC11 and GSC20 cells, RA/KHS101 treatment did not significantly alter the numbers of GSC11 and GSC20 cells positive for ICAM-1 on the cell surface. Based on my initial focus to investigate the feasibility of compound-induced ICAM-1 expression to increase susceptibility of GSCs to CVA21 virotherapy, the subsequent validation of a combination therapy consisting of compound treatment and CVA21 infection was carried out using the two responsive cell lines GSC1 and GSC4 cells.

3.1.5 Chemically-induced ICAM-1 expression increases susceptibility of GSCs to CVA21-mediated oncolysis

Induced overexpression of ICAM-1 has been demonstrated to increase efficiency of CVA21-mediated cell killing (figure 3.3B). Therefore, I sought to assess whether RA/KHS101 treatment could also lead to increased infection and cell death of GSCs upon CVA21 treatment. To determine whether compound-induced ICAM-1 expression facilitates infection with CVA21 and to determine virus load in the cells, I used single cell qRT-PCR detecting CVA21 mRNA. This technology allows for assessment of gene expression in individual cells. This single cell resolution enables detection of a possible heterogeneous infection pattern and identification of diverse responders to compound treatment. I treated GSC1 cells with vehicle (0.1% DMSO) or RA (2 µM) and KHS101 (1 µM) for 48 hours followed by infection with CVA21 (MOI 1). The presence of CVA21 in the cells was determined 48 hours post infection in individual cells using primers specific for the 5' untranslated region (UTR) of the CVA21 mRNA. CVA21 expression was calculated for each cell with relative expression values ranging between 0 (no expression) and 30 (maximum expression).

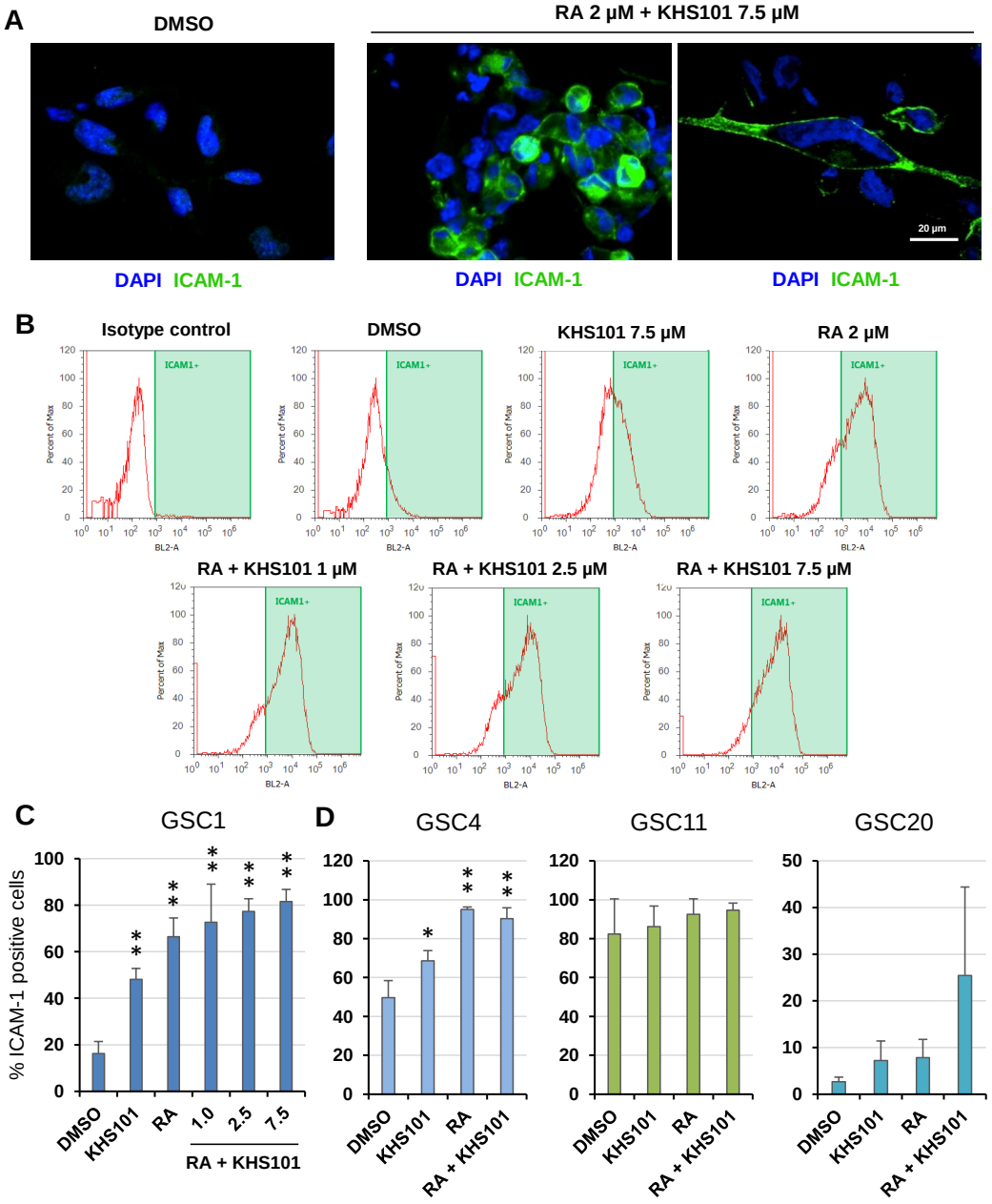

Fig. 3.9: RA/KHS101 double treatment induces ICAM-1 protein expression in different GSC models. **A)** Example images of ICAM-1 immunofluorescence staining in GSC1 cells treated with vehicle (0.1% DMSO) or RA (2 µM) and KHS101 (7.5 µM) for 48 hours showing ICAM-1 positivity in the RA and KHS101 treated cells. The high-resolution image on the right highlights the localisation of ICAM-1 to the cell membrane. **B)** Representative FACS histograms of isotype control or ICAM-1 stained GSC1 cells after 48 hours of treatment with vehicle (0.1% DMSO), KHS101 (7.5 µM), RA (2 µM), or RA (2 µM) and KHS101 (1, 2.5, 7.5 µM). A gating strategy based on forward and side scatter was applied to exlude debris and dead cells from the analysis. **C** and **D)** Compound-induced ICAM-1 surface expression as determined by FACS. The percentage of ICAM-1 positive cells is depicted for GSC1 cells treated with vehicle (0.1 % DMSO), RA (2 µM), KHS101 (7.5 µM) or RA (2 µM) and KHS101 (1, 2.5, 7.5 µM; C) and for GSC4, GSC11 and GSC20 treated with vehicle (0.1% DMSO), KHS101 (7.5 µM), RA (2 µM) or RA (2µM) and KHS101 (1 µM; D) for 48 hours (data shown as mean ± SD; n=3; *, $P<0.05$; **, $P<0.01$; Student t test).

The data is shown as bean plots in figure 3.10A. Due to the sequence similarity of the 5' UTR of CVA21 and other enteroviruses, the primers used here possibly detect not only CVA21 but other enterovirus species as well. Furthermore, since it is highly unlikely that the person our GSC1 cells are derived from was never exposed to any enteroviruses, it is expected that the primers will detect virus mRNA even in CVA21-uninfected cells. Accordingly, a low to moderate relative virus expression was measured in vehicle-treated and RA/KHS101-treated GSC1 cells that were not infected with CVA21. Upon infection with CVA21, the virus mRNA was detected at levels that were markedly higher than the background signal in both, vehicle- and RA/KHS101-treated GSC1 cells. Notably, the expression pattern obtained for vehicle-treated cells infected with CVA21 indicates the presence of a single population of medium/high expressers (relative expression values: 17-20). In contrast, RA/KHS101-treated cells displayed a bimodal expression pattern of elevated CVA21 expression (relative expression values: 19-27) suggesting increased efficiency of CVA21 infection of RA/KHS101-treated GSCs (figure 3.10A).

As CVA21 is an oncolytic virus that lyses and kills cancer cells upon infection, I next investigated the effect of RA/KHS101 treatment on susceptibility of GSCs to CVA21-mediated cell death. In order to be able to determine cell death caused by the oncolytic activity of CVA21, the cytotoxic effect of KHS101 was to be kept minimal. Therefore, a KHS101 concentration of 1 µM, which was shown to leave >75% of viable GSC1 and ∼45% of viable GSC4 cells after 5 days of treatment (figure 2.6A), was used. Most importantly, FACS analysis showed that RA/KHS101 treatment with 1 µM KHS101 leads to comparable percentages of ICAM-1 positive GSC1 cells as RA/KHS101 treatment with 7.5 µM KHS101 (figure 3.9C). Thus, GSC1 and GSC4 cells were treated with vehicle (0.1% DMSO), KHS101 (1 µM), RA (2 µM) or RA (2 µM) and KHS101 (1 µM) for 48 hours. Then the cells were infected with CVA21 at increasing MOIs (0, 0.01, 0.1, 1) and the percentage of dead cells was determined by FACS after 7 days. Notably, KHS101 and RA/KHS101 treatment (no CVA21) only caused low levels of cell death (<10%) similar to vehicle treatment indicating that the observed cell death in CVA21-treated cells is a consequence of the virus' oncolytic function rather than KHS101-induced cytotoxicity. In the presence of CVA21, however, cell death was significantly elevated in RA/KHS101-treated GSCs reaching ∼69% in GSC1 and even ∼96% in GSC4 cells, which equals a >5-fold increase compared to their respective CVA21-treated control cells. Similar to RA/KHS101 double treatment, single treatment with RA significantly increased CVA21-mediated cell death in GSC1 and GSC4 cells leading to 74.3% and 93.9% of dead cells, respectively (figure 3.10B).

In summary, RA/KHS101 double treatment as well as single treatment with RA rendered GSC1 and GSC4 cells vulnerable to CVA21-mediated cell death. Moreover, a positive correlation between the number of ICAM-1 positive cells as detected by FACS analysis and susceptibility of GSCs to CVA21-mediated oncolysis could be observed.

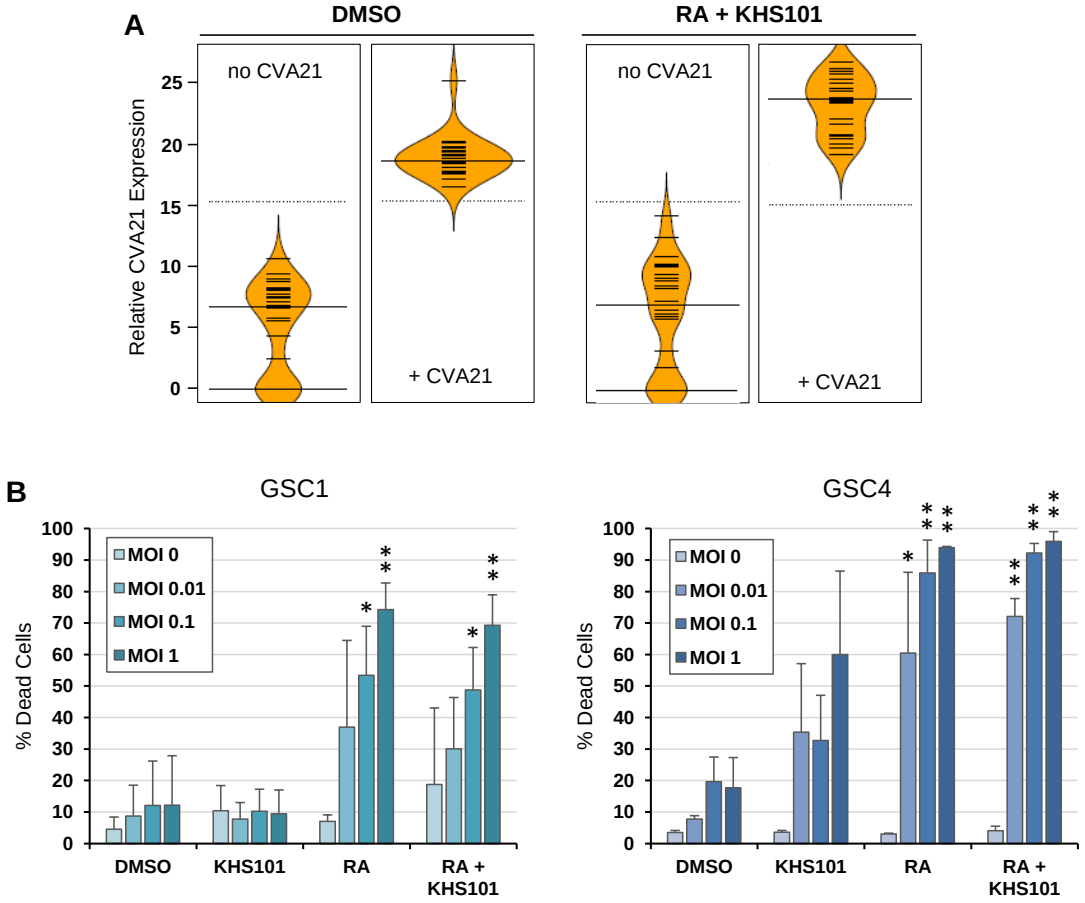

Fig. 3.10: RA/KHS101-induced expression of ICAM-1 increases susceptibility of GSCs to CVA21-mediated cell death. **A)** Bean plots of single cell gene expression analysis detecting CVA21 mRNA in GSC1 cells treated with vehicle (0.1% DMSO) or RA (2 µM) and KHS101 (1 µM) for 48 hours followed by infection with CVA21 (MOI 1) for 48 hours. **B)** Increased cell death of GSC1 (left) and GSC4 (right) cells treated with vehicle (0.1% DMSO), RA (2 µM), KHS101 (1 µM) or RA (2 µM) and KHS101 (7.5 µM) for 48 hours followed by infection with CVA21 at MOI of 0, 0.01, 0.1 and 1. The percentage of dead cells was determined by FACS using a LIVE/DEAD® fixable dead cell stain 7 days post infection (data shown as mean ± SD; n=3; *, $P<0.05$; **, $P<0.01$; Student t test).

3.2 Discussion

Oncolytic virotherapy is a promising field in GBM therapy. Numerous studies have investigated the potential of different oncolytically active viruses including reovirus, vaccinia virus, NDV, HSV and CVA21 [145] [144] [167]. The oncolytic activity of several OVs has been demonstrated in human glioma cell culture and preclinical models, and some strains have already been evaluated for their safety in phase I and II clinical trials [144].The naturally occurring CVA21 is currently being tested in the clinic for treatment of different solid tumours (e.g., ClinicalTrials.gov identifier NCT01636882, NCT00636558, NCT02043665) and its efficacy has been demonstrated in intracranial xenograft models of malignant glioma [167]. In their study, Chan et al. show tumour regression of xenograft tumours derived from ICAM-1 positive GBM cells corroborating the requirement of ICAM-1 protein on the surface of tumour cells for CVA21 infection and oncolysis. However, ICAM-1 expression in GBM is heterogeneous and generally low (figure 3.1; [244] [245]), hence hindering effective CVA21 virotherapy. Consistently, analysis of ICAM-1 expression on two different patient-derived GSC lines, GSC1 and GSC4, that exhibit distinct molecular features (hyper- and hypomethylation of *MGMT* gene, classical/proneural and mesenchymal subtype, respectively) also revealed minimal to moderate ICAM-1 levels, and accordingly, these cells showed limited vulnerability to CVA21. When ICAM-1 overexpression was induced through genetic manipulation by lentiviral transduction or through treatment with TNF-α, a significant increase in ICAM-1 positive GSCs was detected by FACS and CVA21-mediated cell death of GSCs significantly elevated supporting an ICAM-1 dependent susceptibility to CVA21 in the GSC context (figure 3.3).

The role of ICAM-1 in cancer has been controversially discussed (e.g., [290] [291] [189] [292] [293] [294] [247] [248]). Studies focusing on ovarian, breast and gastric cancer have linked upregulated ICAM-1 mRNA and protein expression to reduced tumour growth and metastasis [290] [189] [292]. However, a correlation between high ICAM-1 expression and cancer cell migration as well as poor patient prognosis has been suggested for breast cancer, hepatocellular carcinoma and esophageal squamous cell carcinoma [248] [294] [295] [247]. In this context, ICAM-1 has been implicated in modulating immune responses through facilitating macrophage infiltration [246]. These observations raised the question whether ICAM-1 overexpression in GBM would affect the composition and functional profile of infiltrating immune cells. To this end, the tumour-infiltrating immune cell population and the macrophage/MDSC polarisation state was analysed using a syngeneic mouse model based on intracranial transplantation of ICAM-1 overexpressing mouse glioma cells.

Non-invasive bioluminescence imaging revealed comparable growth rates of ICAM-1 overexpressing and empty vector-expressing tumours. Furthermore, no increase in the number of infiltrating immune cells was observed. The role of tumour-infiltrating macrophages/MDSCs has been found to depend on their functional state. While a M2 polarisation state of tumour macrophages has been found to be favoured in an immunosuppressed microenvironment and further supports an immunosuppressive network and tumour growth, M1-polarised macrophages correlate with an anti-tumourigenic activity. Notably, in GBM tumours, macrophages are mostly of the M2-polarised, tumour supportive subtype [296]. In our ICAM-1 overexpressing syngeneic mouse model, the number of infiltrating macrophages was not significantly changed compared to control tumours. However, macrophage profiles were altered with reduced expression of M2 defining markers (Arg-1, CD206) in ICAM-1 positive tumours. As the markers for M1-polarised macrophages do not simultaneously increase, the macrophages might be in an intermediate activation state with the potential to transition to M1-polarised macrophages. Still, this data indicates a shift away from the pro-tumourigenic M2 polarisation state (figure 3.2). This finding is consistent with a recently published role for ICAM-1 in suppressing M2 polarisation of macrophages leading to reduced metastatic tumour progression [297]. Hence, induction of ICAM-1 expression in GBM could potentially trigger a shift from a tumour-promoting to an anti-tumourigenic immune response in infiltrating macrophages. However, since M1/M2 polarised macrophages represent functionally diverse groups that are strongly influenced by various different extracellular stimuli, including chemokines and cytokines secreted by the tumour, macrophage polarisation phenotypes are not as well defined *in vivo* as they are *in vitro* [253]. Therefore, additional studies are required to further clarify macrophage polarisation states in ICAM-1 expressing tumours, for example, by combining detection of M1/M2 markers, pro-inflammatory cytokines and transcription factors that regulate macrophage polarisation [298] [253].

In my study, the aim was to identify compounds with the ability to selectively induce ICAM-1 expression in GSCs and thus increasing homogeneity of ICAM-1 expression in GBM in order to enhance efficiency of CVA21-mediated oncolysis. One known modulator of ICAM-1 expression acting through signaling via RAR/RXR is RA [184]. As a differentiation-inducing agent, RA has been investigated in CSCs and its anti-tumourigenic activity has been demonstrated *in vivo* and in the clinic for treatment of APL [134]. Consistent with previous reports demonstrating that RA fails to induce terminal differentiation of GSCs [138], no marked effect of RA on GSC 'stemness' and differentiation was observed (figure 3.5). Although tran-

scriptional expression of *ICAM1* was induced upon RA treatment, this increase was minimal compared to TNF-α, a potent ICAM-1-inducing cytokine (figures 3.4 and 3.6). Therefore, to identify compounds that strongly induce ICAM-1 or potentiate ICAM-1 induction by RA in GSCs, I carried out a focused small molecule qRT-PCR screen. Among the 23 compounds tested, 14 compounds known to modulate *ICAM1* transcription and 9 brain-penetrable compounds that had not yet been implicated in the regulation of *ICAM1* expression were tested (table 3.1). Notably, I identified two small molecules that synergistically upregulated *ICAM1* mRNA expression together with RA: Vacquinol-1 and KHS101 (figure 3.6). Interestingly, both compounds have been demonstrated to selectively induce hyper-vacuolisation in GSCs (see section 2.1.1.3 'KHS101 induces a lethal vacuolisation phenotype in GSCs'; [115]). Although eliciting a cell vacuolisation comparable to KHS101, Vacquinol-1 induced cell death has been described as being independent of autophagy and apoptosis activation, but being characterised by macropinocytosis. However, similar to my findings on KHS101-induced ATP (energy) depletion, Kitambi et al. also detect a reduction in cellular ATP levels upon treatment with Vacquinol-1. The authors link this depletion of ATP to energy consumption by membrane ruffling and vacuole acidification [115]. Whether metabolic processes such as glycolysis or oxidative phosphorylation are also affected by Vacquinol-1 as a cause of low ATP levels, was not further investigated. Given the similar vacuolisation phenotype and the similar effect of KHS101 and Vacquinol-1 on RA-induced upregulation of *ICAM1* expression, it would be interesting to investigate if Vacquinol-1 shares an MOA with KHS101 in our GSC models. However, testing the effect of Vacquinol-1 on autophagy, proliferation, 'stemness' and metabolism in GSCs side by side with KHS101 would have been beyond the scope of this thesis. Thus, based on the study by Kitambi et al., the MOA described for Vacquinol-1 differs from my data on the MOA of KHS101. Vacquinol-1 treatment leads to massive macropinocytosis through activating the MAP kinase MKK4 [115] and the MAP kinase pathway has been shown to be a critical signaling pathway regulating *ICAM1* transcription [174]. This could explain the effect of RA/Vacquinol-1 on *ICAM1* mRNA levels. However, activated MKK4 has been found to phosphorylate the retinoic acid receptor RXR resulting in suppression of RA-induced transcription [299]. I found no evidence that KHS101 acts in a Vacquinol-1-like manner. Instead, our data suggests that KHS101 downregulates the critical cell cycle/mitotic spindle regulator protein TACC3 (E.Polson, unpublished data; [116]), and interferes with (yet to be validated) cellular components that are required for mitochondrial respiration (see section 2.1.4.2 'KHS101 induces metabolic exhaustion in GSCs'). A possible explanation why KHS101 acts as an

ICAM1 inducer in combination with RA could be provided by an interesting observation regarding HIF-1α: KHS101-induced metabolic changes are accompanied by HIF-1α accumulation in the nucleus of GSCs under hypoxic as well as normoxic conditions leading to HIF-1α target gene expression (E. Polson & C. Abbosh, unpulished data). Notably, hypoxia/HIFs have been found to be able to activate the *ICAM1* promoter *in vitro* [300] [301]. Consistently, stronger ICAM-1 immunopositivity has been detected in hypoxic tumour areas [301]. Hence, KHS101-induced HIF nuclear translocation and subsequent interaction with the *ICAM1* promoter might lead to improved accessibility of the promoter for RA-induced binding of RAR/RXR to RA responsive elements within the promoter, thus resulting in *ICAM1* upregulation. This hypothesis could be tested by chromatin immunoprecipitation experiments detecting RAR/RXR or RA (e.g., biotin-labeled) binding to the *ICAM1* promoter upon RA, KHS101, RA/KHS101 and RA/hypoxia treatment. To this end, specific RAR/RXR or biotin antibodies could be used for pulldown of crosslinked protein/DNA complexes and unlinked/purified DNA fragments could be analysed by PCR using primers specific for the *ICAM1* promoter sequence.

Because I had comprehensively studied the effect of KHS101 as a single agent in GSCs, I focused on RA/KHS101 for further investigation of chemical compound-induced ICAM-1 expression. Notably, RA/KHS101 significantly induced *ICAM1* mRNA upregulation in all four tested GSC lines (figure 3.8). However, FACS analysis revealed that, in contrast to the additive effect of KHS101 on RA-induced *ICAM1* mRNA expression, RA/KHS101 double treatment does not lead to an increase in ICAM-1 protein over RA single treatment. Furthermore, only GSC1 and GSC4 cells showed a significant increase in the percentage of ICAM-1 positive cells (figure 3.9). Interestingly, the GSC11 model, which is mainly classified as the mesenchymal subtype, already comprised of >80% ICAM-1 positive cells, respectively. This is consistent with high levels of ICAM-1 expression reported for mesenchymal stem cells [255]. In contrast, GSC20 cells, which are derived from a recurrent GBM and harbour proneural and mesenchymal subtype signatures, are mostly ICAM-1 negative and no significant increase in the number of ICAM-1 positive cells was induced by RA/KHS101 treatment. This was unexpected, as significant upregulation of *ICAM1* mRNA levels was observed for GSC20 cells. This discrepancy between RA/KHS101-induced *ICAM1* mRNA expression and ICAM-1 protein on the cell surface could be due to failed translation of mRNA into protein, deficient direction to the endoplasmatic reticulum, immediate degradation of newly synthesised ICAM-1, impaired transport of ICAM-1 protein through the Golgi apparatus and vesicles to the plasma membrane, defective or incomplete internalisation of ICAM-1 into the

plasma membrane or release of ICAM-1 protein into the medium/extracellular space. The latter seems to be the most likely explanation, as a soluble form of ICAM-1 (sICAM-1) exists, which has been found to be modulated by the same stimuli as membrane-bound ICAM-1 and which is produced through proteolytic cleavage [302]. Future work should therefore include assays for detection of the amount of ICAM-1 protein released by GSCs (e.g., enzyme-linked immunosorbent assay). Notably, similar to membrane-bound ICAM-1, its soluble form also has immunomodulatory activity [302] and *in vivo* accumulation of sICAM-1 in the extracellular space induced by RA/KHS101 could have an effect on immune cells.

To address the question whether RA/KHS101-induced ICAM-1 expression is able to enhance infection of GSCs with CVA21, single cell qRT-PCR for CVA21 mRNA was performed, a method allowing identification of heterogeneous responses to compound/virus treatment that potentially could not be detected by bulk qRT-PCR analysis. Indeed, a bimodal expression pattern indicating two subpopulations with distinct responses to CVA21 infection was identified in RA/KHS101-treated GSCs. However, both populations showed increased levels of CVA21 mRNA compared to vehicle-treated cells indicating improved accessibility and replication of CVA21 in RA/KHS101-treated GSCs. Accordingly, increased CVA21-mediated cell death was observed in RA/KHS101-treated GSCs compared to vehicle-treated GSCs (figure 3.10). Consistent with the FACS data on RA-induced ICAM-1 protein expression, RA single treatment also led to significantly enhanced susceptibility of GSCs to CVA21.

In a pilot experiment, I further tested whether systemically administered RA/KHS101 could increase ICAM-1 protein levels in GSC1-derived xenograft tumours upon a 2-week dosing using an immunofluorescence readout. However, validation of RA/KHS101-induced ICAM-1 expression has proven difficult in this setting as no significant increase in ICAM-1 immunopositivity was detected (data not shown). Notably, a high variability in ICAM-1 immunopositivity in both, control and treatment group, was observed. This heterogeneity could be explained by the existence of hypoxic areas in GBM tumours [303] and the correlation of hypoxia and ICAM-1 expression [301] [300]. There are several other factors that might have influenced this result and complicated its interpretation. For example, reliability of antibody binding and accessibility of the antigen for the antibody could have been an issue. Also, the brain bioavailability of RA and KHS101 could have been insufficient to induce ICAM-1 expression. Furthermore, *in vitro* RA/KHS101-induced *ICAM1* mRNA upregulation has been found to be transient (figure 3.8). Thus, timing is critical in detection of ICAM-1 induction and the *in vivo* dosing regimen has to be adjusted

accordingly. Therefore, pharmacokinetic studies of combined RA/KHS101 linked to ICAM1 expression as a biomarker could provide valuable clues for pharmacological upregulation of ICAM1 in brain tumours. Suitable dosing regimens could then be tested to identify the correct timing for RA/KHS101-induced ICAM-1 expression *in vivo*. Moreover FACS analysis could provide a more reliable readout to assess the *in vivo* applicability of compound-induced ICAM-1 protein expression. Investigating ICAM-1 expression by FACS would allow for detection of ICAM-1 protein on the cell surface and could be combined with detection of proposed 'stemness' markers (such as CD133 and CD44), thus defining whether ICAM-1 expression is associated with 'stemness' profiles (in contrast to bulk tumour cells).

Interestingly, my *in vitro* data showed that RA single treatment leads to an increase in GSC vulnerability to CVA21-induced oncolysis to the same extent as RA/KHS101 treatment (figure 3.10). Hence, the synergistic/additive effects of RA/KHS101 on *ICAM1* expression observed at mRNA level, are negligible at protein level and regarding susceptibility to CVA21, indicating that RA could be sufficient to render GSCs susceptible to CVA21 virotherapy. How this finding may be translated into a clinical setting would be worth investigating in the future, as RA is a brain-penetrable agent and already approved for clinical use [140] [134].

Future pre-clinical *in vivo* work regarding CVA21 virotherapy would focus on determining tolerable doses for CVA21 injected intratumourally according to protocols published for intracranial injection of OVs (e.g., [304]). Most importantly, future work would also include proof-of-principle experiments determining whether ICAM-1 expression could enhance efficacy of CVA21 virotherapy. For these studies RA or RA/KHS101 pre-treated or ICAM-1 overexpressing GSCs could be used and CVA21 injected intratumourally. Monitoring tumour growth and animal survival as well as determining tumour burden at the experimental endpoint would give valuable insight into the feasibility of this combination treatment approach.

A major obstacle for clinical use of CVA21 therapy is a possible anti-viral immune response of the patient. As a naturally occurring virus, neutralising antibodies against CVA21 might be present in patient serum which would counteract efficient virotherapy. However, strategies to overcome an anti-viral immune response such as combined virotherapy and immunosuppressive treatment, e.g., using cyclophosphamide, have proven effective for other OVs [305]. Another option could be the use of carrier cells such as mesenchymal stem cells or NSCs which have been successfully applied for delivery of adenovirus to the tumour site in orthotopic mouse glioma models [306] [307]. Both strategies, concomitant immunosuppressive therapy and the use of carrier cells, might therefore constitute a feasible option for CVA21

therapy to overcome the possible inhibitory effect of the immune system by suppressing an innate immune response or hiding the virus from detection by immune cells.

4 Conclusion

Despite multi-modal treatment efforts and intensive investigation into novel therapeutic approaches such as the use of monoclonal antibodies, immune therapy, oncolytic virotherapy and new promising chemical compounds, GBM remains an unmet clinical need as tumour recurrence remains inevitable [13] [15] [16] [144] [12]. The ability to re-grow the tumour after therapeutic intervention has been attributed to GBM cells with stem-cell characteristics, herein called GSCs. In this study, I focused on investigating anti-GSC potential using small molecules combined with cell phenotype-based discovery to 1) identify GSC molecular vulnerabilities, and 2) chemically induce an ICAM-1 positive cell surface phenotype in GSCs required for CVA21 oncolytic virotherapy.

In order to identify 'targetable' acquired properties intrinsic to cancer cells, a number of studies have focused on the potential of small molecules (e.g., [114] [108] [115] [112]). In this context, I investigated the potential anti-tumourigenic activity of the small molecule KHS101, which has been identified as a differentiation-inducing agent in rat NPCs. My data indicate that KHS101 exhibits anti-GSC properties by inducing a GSC fate characterised by lethal vacuolisation. Catastrophic vacuolisation has recently been identified as a selective vulnerability of GBM cells that can be efficiently targeted by small molecules (i.e. Vacquinol-1; [115]). In contrast to the study by Kitambi et al., the vacuolisation induced by KHS101 was accompanied by a pronounced autophagy phenotype, and significantly reduced GSC 'stemness' features upon treatment with sublethal KHS101 doses. Furthermore, gene expression analysis and extracellular flux assessment revealed that KHS101 exploits pivotal GSC dependencies by disruption of cell proliferation (through TACC3), GSC 'stemness' (e.g., through significant downregulation of GSC-promoting factors *NOS2* and *OLIG2*), and the critical metabolic process of mitochondrial respiration. By disrupting oxidative phosphorylation, KHS101 initially triggers compensatory glycolytic energy production in the highly metabolically-active GSCs, but ultimately causes glycolytic exhaustion. Together this data confirms that KHS101-induced hyper-vacuolisation and autophagy is critically linked to decreased tumourigenicity of GSC. Future work will focus on the identification of the additional direct target of KHS101. We expect that these MOA studies (such as affinity chromatog-

raphy approaches) will reveal novel metabolic targets responsible for the energy metabolism-obstruction caused by KHS101. Thereby, it will be possible to further clarify the specificity of KHS101 cytotoxicity for malignant cells as determined in this study for GSCs in contrast to NP cells. Since an altered energy metabolism is a common hallmark of cancer, specific targeting of the cells' metabolic state by KHS101 could potentially be an efficient treatment strategy for other types of cancer. Therefore, it would be interesting to test KHS101 treatment on malignant cells isolated from various different cancer types. Of course, further in *vitro* and *in vivo* examination into the potential therapeutic window of KHS101 treatment would be equally important to be able to establish tolerable doses of the compound and to predict possible side effects. However, despite its favourable properties, such as blood brain barrier penetration, the pharmakokinetics of KHS101, especially its half-life, would need to be improved via medicinal chemistry. Here, it is important to achieve a longer half-life and more potent cancer cell cytotoxicity, while keeping side effects and normal tissue toxicity to a minimum. This approach would increase the prospect of a translation of KHS101 or KHS101-like drugs into the clinical trial phase.

Acquired resistance to cytotoxic drugs is a major issue in cancer treatment [308]. These limitations of single drug treatment could be overcome by combination therapy, for example combining pharmacological and biotherapy approaches. Here, I carried out a focused small molecule screen and identified RA/KHS101 as a potent *ICAM1* mRNA-inducing combination treatment. I further investigated RA/KHS101 treatment followed by oncolytic virotherapy as an anti-GSC treatment strategy. My findings on this novel combination treatment demonstrate that RA/KHS101-induced ICAM-1 expression in GSCs results in increased efficiency of infection with CVA21 and CVA21-mediated cell death. For the advancement of this study, it would be essential to further elaborate and optimise compound-induced ICAM-1 expression *in vivo* using different xenograft mouse models. Here, it is worth including the already clinically approved agent RA as a single treatment, since my *in vitro* data suggests that RA single treatment is sufficient in increasing susceptibility to CVA21 through ICAM-1 induction. If RA proves to be efficient enough to enhance CVA21-mediated cell death in preclinical models, this combination treatment could more readily become applicable for clinical development, because RA and CVA21 are already approved for use in human trials.

In conclusion, my thesis describes a cellular phenotyping profiling approach to identify targetable vulnerabilities in GSCs and high-grade brain tumours using chemical and viral treatment approaches. My pre-clinical data on single compound (KHS101) and compound (KHS101/RA)/oncolytic virus combination treatment may provide the basis for development of a novel anti-GBM therapy. Importantly, if these two treatment approaches prove safe and efficient for use in patients, they could be applied to complement currently available therapies to treat GBM. For instance, after surgical removal of the main tumour mass and radio-/chemotherapy, combined KHS101-based therapy could be applied to target the remaining GBM cell population and impeding re-growth of the tumour. This treatment strategy could then even be followed by another line of treatment consisting of RA/KHS101 or RA administration and virotherapy with CVA21 to even further increase the chance of extinguish all tumour cells.
Elimination of a highly invasive and heterogeneous cancer like GBM requires a multimodal treatment strategy targeting a variety of GBM cell features. Ultimately, KHS101-like drugs and compound/virotherapy could be part of a anti-GBM therapy and benefit patients with incurable brain tumours.

5 Materials and methods

5.1 Cell culture

GSC lines were derived from surgically resected tumour tissues of consented patients under the governance of the ethically-approved Leeds multi-disciplinary research tissue bank. The obtained cells were cultured as monolayers in Neurobasal medium (Gibco; 21103-049) supplemented with basic fibroblast growth factor (bFGF; 40 ng/mL; Gibco; PHG0024), recombinant human epidermal growth factor (rhEGF; 40 ng/mL; R&D; 236-EG) and 0.5x B-27 (Gibco; 17504-044) and 0.5x N-2 (Gibco; 17502-048) at 37°C with 5% CO_2 on poly-L-ornithin (5 µg/mL; Sigma; P3655)/laminin-coated (5 µg/mL; Invitrogen; 23017-015) cell culture flasks/dishes.
Human NP cells were derived from non-tumour brain surgical specimens obtained during epilepsy surgery at Stanford University Medical Center and cultured in DMEM/F-12 medium (Gibco; 2133-020) supplemented with bFGF (40 ng/mL), rhEGF (40 ng/mL), 0.5x B-27, 0.5x N-2, 1x GlutaMAX (Gibco; 35050-038) and 5% (v/v) fetal bovine serum (FBS) at 37°C with 5% CO_2 [89] [309].
Mouse glioma cell line CT2A was cultured in Dulbecco's Modified Eagle (DMEM) medium (Sigma; D6046) containing 10% (v/v) FBS at 37°C with 5% CO_2.

5.2 Single cell gene expression analysis - GBM subtyping

Individual GBM cells were captured from cell suspensions using the microfluidic Fluidigm C1 single-cell auto prep system (Fluidigm). Reverse transcription and pre-amplification were carried out within a 96-well microfluidic C1 chip according to the manufacturer's instructions using DELTAgene assays (Fluidigm).
Pre-amplified complementary DNA (cDNA) samples from single cells were analysed by qRT-PCR using 96.96 Dynamic Array™ IFCs and the BioMark™ HD System (Fluidigm). Each analysis comprised up to 96 cDNA samples from individual cells and DELTAgene assays (listed below). Amplified cDNA (3.3 µL) was mixed with 2x Ssofast EvaGreen Supermix (2.5 µL), Low ROX buffer (2.5 µL; Bio-Rad, PN 172-

5211), and 'sample loading agent' (0.25 µL; Fluidigm, PN 100-3738). DELTAgene forward and reverse primers were mixed with Fluidigm Assay Loading Reagent (2.5 µL). Samples and assays were loaded onto Fluidigm M96 chips using the HX IFC Controller (Fluidigm) and then transferred to the BioMark™ HD real-time PCR reader following the manufacturer's instructions. PCR was performed using the (GE Fast 96 x 96 PCR + Melt v2.pcl) thermal protocol:

Step	Temperature	Time
Thermal Mix	70°C	40 minutes
	60°C	30 seconds
Hot Start	95°C	1 minute
Cycle x30	96°C	5 seconds
	60°C	20 seconds
Melting	60°C	
	at 1°C/3 seconds	

Data were analysed using the Fluidigm Real-Time PCR Analysis software and Ct and melting-curve data were exported to Excel and R for further analysis. Results were assessed using the Fluidigm Real-Time PCR Analysis software (heat map view). Melting curve analyses was carried out to identify non-specific amplicons, which were removed from the final data set. For calculation of relative expression values (ΔCt = LoD Ct - Ct), the limit of detection (LoD) was set to a Ct value of 30 (Ct values of '999' were allocated artificial values $\geq$30 to allow for the visualisation of 'non-expressors' in bean plots). Box plots were created using BoxPlotR [310].

Gene	Assay ID	Assay Name	Forward Primer	Reverse Primer
ID3	GEA0001 6231	ID3_16231_i1	AAAAGGAGC TTTTGCCAC TGAC	TTCCGGCAG GAGAGGTTC C
CRYAB	GEA0001 6958	CRYAB_16958_i0	CACCCAGCT GGTTTGACA C	TGCTTCACA TCCAGGTTG ACA
PDGFRA	GEP0005 6732	PDGFRA_56732_i6	GAGATCACC ACTGATGTG GAA	CTTCTTCCT TAGCACGGA TCA
RRM2	GEA0002 6114	RRM2_26114_i3	GCAGCAAGC GATGGCATA	GAAACAGCG GGCTTCTGT AA

Gene	Assay ID	Assay Name	Forward Primer	Reverse Primer
SLC2A1	GEP00056173	SLC2A1_56173_i8	ATTGTGGGCATGTGCTTCC	AGAACCAGGAGCACAGTGAA
ARID5B	GEP00062252	ARID5B_62252_i5	GAAAGGAAAACGCCGATAGAA	GAGCAGCTTGAAACATAGTCC
NDRG1	GEP00056378	NDRG1_56378_i5	ATGTACCCCTCCATGGATCA	CTCCTGTTCCCATGCCAATA
ATF4	GEP00059442	ATF4_59442_i0	TTGGTCAGTCCCTCCAACAA	ATACCCAACAGGGCATCCAA
MET	GEP00055841	MET_55841_i11	TCCCCAATGACCTGCTGAAA	CTTTTCCAAGGACGGTTGAAGAA
THY1	GEA00013840	THY1_13840_i1	TCAGCATCGCTCTCCTGCTA	TCCACTAGGCAGGCCGTTA
CSPG4	GEA00026608	CSPG4_26608_i0	CCTTGGCTTTGACCCTGACTA	CACCTCCAGGTGGTTCTCAC
TIMP2	GEA00020949	TIMP2_20949_i3	GAAGAGCCTGAACCACAGGTA	GGAGATGTAGCACGGGATCA
FLCN	GEA00028538	FLCN_28538_i5	ATCAACTCCTGGCCCTTCC	ATCCAAACTGCTCTGCCTCA
SERPINE1	GEP00056400	SERPINE1_56400_i3	TGGCTCAGACCAACAAGTTCA	GCAGTTCCAGGATGTCGTAGTA
CCNE2	GEP00060570	CCNE2_60570_i6	ACCTCATTATTCATTGCTTCCAAAC	CAAGCACCATCAGTGACGTA
KLF4	GEA00013688	KLF4_13688_i3	CTGCGGCAAAACCTACACAA	CGTCCCAGTCACAGTGGTAA
SERPINI1	GEP00062253	SERPINI1_62253_i2	AATGTAGCCGTGGCCAACTA	GCATCAAAATCCCTTGGGGATAC

Gene	Assay ID	Assay Name	Forward Primer	Reverse Primer
G0S2	GEA00015255	G0S2_15255_i0	CAACGGACGCGCTGAC	AGCTCCTGGACCGTTTCC
HRK	GEA00015757	HRK_15757_i0	GCAGGCGGAACTTGTAGGAA	TCCAAGGACACAGGGTTTTCAC
MYOF	GEA00031577	MYOF_31577_i19	CCTGTAAGCCTTTGGCATCAA	TGGGCCCAAGGCAAGTAATA
SLC7A1	GEP00056173	SLC2A1_56173_i8	ATTGTGGGCATGTGCTTCC	AGAACCAGGAGCACAGTGAA
TGFBR2	GEA00012318	TGFBR2_12318_i6	GAGGGCGACCAGAAATTCCC	GGTCCCAGCACTCAGTCAAC
PROM1	GEA00013765	PROM1_13765_i17	AATTCACCAGCAACGAGTCC	CATTCCCTGTGCGTTGAAGTA
MKI67	GEA00012539	MKI67_12539_i4	GGAAGGAAGTCAACTGAATTTCCAA	CAGAAGAGAAGCTAGATCTTGAGACA
TWIST1	GEA00015474	TWIST1_15474_i0	CATGTCCGCGTCCCACTA	AGTCTCTAGACTGTCCATTTTCTCC
NF1	GEA00012355	NF1_12355_i4	GGATTGTGCAAAATTAAAACGACTCC	AACTGCTAACTGCGCAACC
PTEN	GEA00011899	PTEN_11899_i0	CCAGACATGACAGCCATCA	TGCAGGAAATCCCATAGCAA
ACTB	GEA00003909	ACTB_3909_i2	CCAACCGCGAGAAGATGAC	TAGCACAGCCTGGATAGCAA
FOS	GEA00012925	FOS_12925_e3	ACTTCCTGTTCCCAGCATCAT	AGGACCCAGATAGGTCCATGT
SQSTM1	GEA00025348	SQSTM1_25348_i7	AGGAAGCTGCCTTGTACCC	TCTGGGAGAGGGACTCAATCA

Gene	Assay ID	Assay Name	Forward Primer	Reverse Primer
GFAP	GEA0001 1930	GFAP_11930_i4	GCCAGTTGC AGTCCTTGA C	GCGCATCTG CCTCTCCA
RB1	GEA0000 5822	RB1_5822_i22	AATTTCAGA AGGTCTGCC AACAC	CCCGAATGA TTCACCAAT TGATACTAA
HIF1A	GEA0001 2495	HIF1A_12495_i5	CAGTCGACA CAGCCTGGA TA	TTCTTCTGG CTCATATCC CATCAA
MYC	GEA0005 1751	MYC_51751_i1	CCTGGTGCT CCATGAGGA	CCTGCCTCT TTTCCACAG AAA
CCNE1	GEA0000 4353	CCNE1_4353_i3	TGGCCAAAA TCGACAGGA C	GGTCTGCAC AGACTGCAT TA
CD44	GEA0000 7844	CD44_7844_i0	CCGGACACC ATGGACAAG TT	CCTGCAAAG CGGCAGGT
CDKN2A	GEA0001 2387	CDKN2A_12387_e2	CCGGAAGCT GTCGACTTC A	GCCATTTGC TAGCAGTGT GAC
VEGFA	GEA0001 2311	VEGFA_12311_i1	GAGGAGGGC AGAATCATC AC	GTCTCGATT GGATGGCAG TA
BMI1	GEA0002 6432	BMI1_26432_i1	ACTTCATTG ATGCCACAA CCA	TGGTCTCCA GGTAACGAA CA
CEBPB	GEA0001 2385	CEBPB_12385_e0	TTCCTCTCC GACCTCTTC TCC	CAGGCTCAC GTAGCCGTA C
C1orf61	GEA0001 2387	C1orf61_24068_i3	CCGGAAGCT GTCGACTTC A	GCCATTTGC TAGCAGTGT GAC
ATF3	GEA0001 2311	ATF3_51995_e3	GAGGAGGGC AGAATCATC AC	GTCTCGATT GGATGGCAG TA
NES	GEA0001 1931	NES_11931_i0	GCTGCGGGC TACTGAAAA	CTGAGCGAT CTGGCTCTG TA

Gene	Assay ID	Assay Name	Forward Primer	Reverse Primer
TRRAP	GEA0003 1155	TRRAP_31155_i27	CCTTCCGTC ACTCGTACC TTTA	TCCCTGGAC TGAGGAAGG TAA
CDKN1A	GEA0000 6173	CDKN1A_6173_i1	TGGAGACTC TCAGGGTCG AAAA	CGGCGTTTG GAGTGGTAG AA
TACC3	GEA0002 9705	TACC3_29705_i12	AAAGAGGTG ATCGAGGGC TA	GTGATCCTT GCCAGGTAA TCC
PDGFA	GEA0002 3786	PDGFA_23786_i2	GCCCATTCG GAGGAAGAG AA	CTGACTCCG AGGAATCTC GTAAA
TOX3	GEA0002 3365	TOX3_23365_i3	CTTCACCTC CAGCAAGCA AA	GAGCAGCTC TTTTCTCTC CAA
WEE1	GEA0002 7199	WEE1_27199_i1	AGGACAGTG TCGTCGTAG AA	AAGCTCATA ATCACTGGC TTCC
OLIG2	GEA0001 1949	OLIG2_11949_i0	CGGAGCGAG CTCCTCAAA	ATGGCCCCA GGGGAAGAT A
NOS2	GEA0001 2347	NOS2_12347_i17	CTCACAGCC TTTGGACCT CA	GAGATTTGA GCCTCATGG TGAAC
BECN1	GEA0002 8024	BECN1_28024_i10	GGTTGAGAA AGGCGAGAC AC	ACTGCCTCC TGTGTCTTC AA
STAT3	GEA0001 2324	STAT3_12324_i22	GGAAATAAT GGTGAAGGT GCTGAAC	CCGAGGTCA ACTCCATGT CAAA
AURKA	GEA0001 3527	AURKA_13527_i6	GGTGGTCAG TACATGCTC CA	GCATCCGAC CTTCAATCA TTTCA
TP53	GEA0001 2790	TP53_12790_i9	TGAATGAGG CCTTGGAAC TCA	TCAGGCCCT TCTGTCTTG AA
S0X2	GEA0001 3148	SOX2_13148_e0	CATGAAGGA GCACCCGGA TTA	CGGGCAGCG TGTACTTAT CC

Gene	Assay ID	Assay Name	Forward Primer	Reverse Primer
GAPDH	GEA0000 7833	GAPDH_7833_i1	ACACCATGG GGAAGGTGA AG	GTGACCAGG CGCCCAATA
VCAM1	GEP0005 6408	VCAM1_56408_i5	CAGGCTGGA AGAAGCAGA AA	CACTCTCAG AAGGAAAAG CTGTA
TUBB3	GEA0000 5739	TUBB3_5739_i1	GAGCGGATC AGCGTCTAC TA	GGTTCCAGG TCCACCAGA A
BAX	GEA0001 2405	BAX_12405_i3	GGGTTGTCG CCCTTTTCT AC	TCTTGGATC CAGCCCAAC A
PIK3R4	GEA0003 0626	PIK3R4_30626_i17	AGTCCTGCA GATGGAAAT CC	TTTCTGGGT AAGCCAAGT CC
S100B	GEP0005 6445	S100B_56445_i1	GGAGACAAG CACAAGCTG AA	CCATGACTT TGTCCACAA CC
ATF2	GEP0005 6453	ATF2_56453_i0	CGGGTGACC GAAAGGATC A	AGCAGTCCT TTCTCAAGT TTCCA
BCL2	GEP0005 3782	BCL2_53782_e1	ATGTGTGTG GAGAGCGTC AA	GTGCCGGTT CAGGTACTC A
CDKN2B	GEP0005 6456	CDKN2B_56456_i0	GGATCCCAA CGGAGTCAA C	GCGCTGCCC ATCATCA
EPHA2	GEA0002 9979	EPHA2_29979_i5	AGTGTGGAA GTACGAGGT CAC	TCCAGGGTC ACGGAGAAA C
NEUROD1	GEP0005 5465	NEUROD1_55465_i0	GGCCCCAGG GTTATGAGA CTA	ATCAGCCCA CTCTCGCTG TA
ATG10	GEP0005 6449	ATG10_56450_i2	CCCAGACCA AGAAGTTGG AAC	ACGCCTGAG ACTTGCAGT AA
CCND2	GEA0000 4282	CCND2_4282_i0	GCAGAAGGA CATCCAACC CTA	TCTTCGCAC TTCTGTTCC TCA

Gene	Assay ID	Assay Name	Forward Primer	Reverse Primer
EPHA3	GEA0002 3953	EPHA3_23953_i1	GAGCTGGGC TGGATCTCT TA	GGTAAGTCC TGATGGGTG TGTA
ID1	GEP0005 6360	ID1_56360_i0	CCCTCAACG GCGAGATCA	GCGCTTCAG CGACACAA
ATG12	GEA0000 4282	ATG12_56449_i2	GCAGAAGGA CATCCAACC CTA	TCTTCGCAC TTCTGTTCC TCA
CCND3	GEP0005 6455	CCND3_56455_i1	CGACAGGCC TTGGTCAAA A	ATCATGGAT GGCGGGTAC A
ID2	GEP0005 6444	ID2_56444_i0	CTCAACACG GATATCAGC ATCC	CACACAGTG CTTTGCTGT CA
IRF1	GEA0001 3682	IRF1_13682_i2	AACAAGGAT GCCTGTTTG TTCC	TGGGATCTG GCTCCTTTT CC
ATG4A	GEA0002 7806	ATG4A_27806_i2	AAGTGCTCG TCTATGGTT TACA	CCCAACCAG CATCTGATG AA
IGFBP3	GEA0001 3118	IGFBP3_13118_i1	CGAGTCCAA GCGGGAGAC	GGGACTCAG CACATTGAG GAA
JUN	GEA0001 2227	JUN_12227_e0	AAGAACTCG GACCTCCTC AC	TGGATTATC AGGCGCTCC A
ATG5	GEP0005 6447	ATG5_56447_i2	TGGTTTGAA TATGAAGGC ACAC	GAGCTGAAC TTGATGCAA GAA
HK2	GEP0005 6433	HK2_56433_i12	CTGCTGAAG GAAGCGATC CA	TAGTTCCGA CTGTGTCGT TCAC
ATG7	GEA0003 0493	ATG7_30493_i9	GCACCTTGG GTTGCAATG TA	GAGATCTTG GCATTGTCC ACAAA
AXIN1	GEA0000 4125	AXIN1_4125_i8	CAAGGAGCT GCTGACCAA AA	CACCACCCC ACAGTCAAA C

Gene	Assay ID	Assay Name	Forward Primer	Reverse Primer
CDKN1B	GEP00056333	CDKN1B_56333_i0	GCAATGCGCAGGAATAAGGAA	TTGGGGAACCGTCTGAAACA
PIK3C3	GEA00013756	PIK3C3_13756_i7	ACCTTCTGACCACGATCTGAAA	GCTTGGTTGGTGGATAACTCAC
PPIA	GEA00007842	PPIA_7842_e4	TCTGGTTCCTTCTGCGTGAA	CACCCAGGGAATACGTAACCA
CD24	GEA00014498	CD24_14498_e0	CCAACTAATGCCACCACCAA	CGAAGAGACTGGCTGTTGAC
CD34	GEP00055189	CD34_55189_i3	GCATCTGCCTGGAGCAAAA	CCTCTCCCCTGTCCTTCTTAAA
VIM	GEP00055720	VIM_55720_i2	TGCAGGAGGAGATGCTTCA	CCAGAGACGCATTGTCAACA
CVA21	GEP00062260	CVA21_62260	CCCTGAATGCGGCTAATCCT	ACGGACACCCAAAGTAGTCG

Table 5.1: List of DELTAgene assays.

5.3 Computational single cell gene expression analysis

After transformation of Ct to expression values, missing values (e.g., resulting from unspecific amplicons removed after melting curve analysis) were imputed using k-nearest neighbor imputation [311]. Single-cell expression levels were adjusted for cell cycle-dependent heterogeneity as described in Buettner et al. using 20 known cell cycle markers [312]. Gene expression levels of tumour samples with subtype annotation were obtained from Verhaak et al. and integrated with our single cell qPCR data set. To this end, both data sets were separately discretised to three levels on a per gene basis using mixture models. Subsequently, a Random Forest classifier was trained on the data set reported by Verhaak and colleagues [25], and used to predict the subtypes of the single cells. Variability of gene expression was analysed by (i) calculating the fraction of cells expressing a certain gene among all cells with a non-missing measurement, and (ii) calculating the coefficient of variation

among all cells with a non-zero expression value.

5.4 Cell viability assay

Cells were seeded at densities of 20,000 cells/well (2 day treatment), or 10,000 cells/well (5 day treatment) in white 96-well plates (Greiner bio-one; 655083) and allowed to adhere overnight. The following day, cells were treated with DMSO (0.1% v/v; Sigma; 34869) or increasing concentrations of KHS101 in 100 µL volume of media. Cell viability was determined using the CellTiter-Glo® assay (Promega; G7572) after 2 or 5 days. Briefly, after both reagent and cells had equilibrated to room temperature (RT), 100 µL CellTiter-Glo® reagent were added to each well, mixed by agitation, and then incubated for 10 minutes in the dark. The luminescence signal was measured using the Mithras LB 940 plate reader.

5.5 Caspase3/7 activity assay

Cells were seeded at a density of 2,500 cells/well in a white 96-well plate and allowed to adhere overnight. The following day, cells were treated with DMSO (0.1% v/v), 7.5 µM KHS101 with or without the caspase inhibitor Z-VAD-FMK (2 µM; Enzo Life Sciences; ALX-260-020), or staurosporine (1 µM; Sigma; S5921) in 100 µl media. Caspase3/7 activity was assessed using the Caspase-Glo® 3/7 Assay kit (Promega; G8090). Reagent and cells were allowed to equilibrate to RT before 100 µL of the Caspase-Glo® 3/7 reagent was added, mixed by agitation and incubated for 1 hour at RT. The luminescence signal was measured using the Mithras LB 940 plate reader.

5.6 Live cell imaging

For live cell imaging, cells were plated at a density of 30,000 cells per well in 48-well plates and allowed to adhere. Cells were treated with DMSO (0.1% v/v) or KHS101 (7.5 µM) and monitored using the IncuCyte ZOOM® live cell imaging system (Essen Bioscience).

5.7 Lucifer Yellow assay

For measurement of endocytotic activity, GBM cells were treated with DMSO or KHS101 together with 2 mM Lucifer Yellow (Thermo Fisher Scientific; L1177) for 16 hours. Then, the cells were washed with phosphate buffered saline (PBS) and

fixed with 4% (w/v) paraformaldehyde (PFA) for 10 minutes at RT. Images were obtained using an EVOS digital inverted fluorescence microscope.

5.8 CytoID/LysoID staining

Autophagic and lysosomal compartments were stained using the CytoID® (Enzo Life Sciences; ENZ-51031) and the LyosID® (Enzo Life Sciences; ENZ-51005) detection kit respectively according to the manufacturer's instructions. Briefly, adherently-grown cells were treated with DMSO (0.1% v/v) or KHS101 (1-7.5 µM) for the indicated times. Cells were then washed twice with PBS and subsequently incubated with CytoID® Green (1:500), LysoID® Red (1:500) and Hoechst 33342 nuclear stain (1:1,000) in PBS for 20 minutes in the cell culture incubator (37°C, 21% O_2, 5% CO_2). After two PBS washes, live cells were imaged immediately using an EVOS digital inverted fluorescence microscope.

5.9 Immunocytochemistry

Adherently-grown cells were fixed with 4% (w/v) PFA (Sigma; P6148) at RT for 10 minutes. For LC3B staining, cells were then permeabilised with ice-cold methanol at -20°C for 10 minutes. For Ki67, SOX2 and NESTIN staining, cells were permeabilised with PBS containing 0.2% (v/v) Triton X-100 (Sigma; X100) at RT for 10 minutes. Non-specific antibody binding was reduced in PBS 'blocking buffer' containing 10% (v/v) FBS and 0.03% (v/v) Triton X-100 at RT for 1 hour. Subsequently, cells were incubated with primary antibodies in PBS containing 10% (v/v) FBS and 0.03% (v/v) Triton X-100 at 4°C overnight. The following primary antibodies were used: anti-KI67 (abcam; ab16667; 1:200), anti-LC3B (Cell Signaling; 2775S; 1:200), anti-NESTIN (Millpore; MAB5326; 1:200), anti-SOX2 (Cell Signaling; 3579S; 1:200), anti-GFAP (DAKO; Z0334; 1:200) and anti-ICAM-1 (Millipore; MAB2146; 1:200). After three PBS washing steps of 5 minutes each, the cells were incubated with secondary antibody in PBS containing 10% (v/v) FBS and 0.03% (v/v) Triton X-100 at RT for 1 hour. Secondary antibodies used were AlexaFluor488 (Molecular Probes; A11029; 1:200) or Cy3 (Jackson ImmunoResearch; 711-165-152; 1:400) conjugated. Following incubation with 4',6-diamidino-2-phenylindole (DAPI; 1 µg/ml; Sigma) in PBS for 5 minutes at RT and two PBS washes (5 minutes each), images were acquired using an EVOS digital inverted fluorescence microscope (life technologies) or a Nikon A1R confocal microscope.

5.10 Electron microscopy

TEM was performed within the imaging and cytometry department in the bioscience technology facility at the University of York.
Cell pellets were fixed in 4% formaldehyde/glutaraldehyde solution in 100 mM phosphate buffer at RT for 30 minutes, and subsequently washed (2 x 10 minutes) and stored at 4°C in 100 mM phosphate buffer. Cells were then post-fixed with 1% buffered osmium tetroxide on ice for 45 minutes, washed in 100 mM phosphate buffer (2 x 10 minutes), then treated with buffered 1% tannic acid solution (10 minutes) and washed again (100 mM phosphate buffer; 2 x 10 minutes). Cell samples were stained with 2% uranyl acetate and dehydrated in increasing concentrations of ethanol/acetone before embedding. These samples were then polymerised overnight at 70°C. Processed cell pellets were sectioned to 1 µm on a Leica EM UC7 microtome and stained with toluidine blue. Further thin sections were then taken (70 nm) and placed on 300 mesh uncoated copper grids; these were stained with saturated uranyl acetate in 50% ethanol followed by Reynolds lead citrate for 10 minutes each. The sections were imaged using a FEI Tecnai 12 transmission electron microscope at an accelerating voltage of 120 kV.

5.11 Clonal growth assays

Cells were seeded at a density of 125 cells/well in 24-well plates and allowed to adhere. The following day, the single cells per well were counted and triplicate wells were treated with DMSO (0.1% v/v) or KHS101. Clonal colonies consisting of >6 cells were counted 7-10 days later and the percentage of cells that were able to form a colony was determined.
To assess the colony formation capability of GBM cells after treatment with KHS101, cells that had been treated with DMSO (0.1% v/v) or KHS101 for 48 hours, were harvested and re-seeded in triplicates at a density of 125 cells/well in 24-well plates. Cells were allowed to adhere overnight and single cells per well were counted. Clonal colonies consisting of >6 cells were counted 7-10 days later and the percentage of cells that were able to form a colony was determined.

5.12 Illumina gene expression analysis

Cells were grown under adherent conditions and RNA was isolated after 24 hours of treatment with DMSO (0.1% v/v) or KHS101 (7.5 µM) using the RNeasy Mini Kit

(Qiagen; 74106) following the manufacturer's instructions for purification of total RNA from animal cells. Homogenisation of the samples was achieved by passing the samples through QIAshredder spin columns (Qiagen; 79656). Gene expression profiling was performed by Cambridge genomic services, University of Cambridge, using the Illumina HumanHT-12 v4 beadchip. Analysis of raw data was performed by Alastair Droop (University of Leeds). Raw data were pre-processed with a quantile normalisation method using Bioconductor. Differential analysis log fold changes were calculated for all probes and those with a false discovery rate (FDR) ≤ 0.075 were selected.

5.13 Quantitative RT-PCR of bulk cells

Cells were grown under adherent conditions and RNA was isolated after 24 hours of treatment using the RNeasy Mini Kit following the manufacturer's protocol for purification of total RNA from animal cells. Homogenisation of the samples was achieved by passing the samples through QIAshredder spin columns. Synthesis of cDNA was performed using SuperScript II Reverse Transcriptase (Invitrogen; 18064-014) according to the manufacturer's instructions for cDNA synthesis using Oligo(dT) primer (Invitrogen; 18418012).
For the qPCR using TaqMan Gene Expression Assays (Applied Biosystems) the following 15 µL reaction mixtures were prepared in triplicates:

Component	Volume for 1 reaction
20x TaqMan Gene Expression Assay	0.75 µL
2x TaqMan Universal PCR Master Mix II, no UNG	7.5 µL
cDNA	0.375 µL
Nuclease-free H_2O	6.375 µL
Total reaction volume	**15 µL**

The qPCR reaction was performed using the following PCR conditions:

Step	Temperature	Time
Hold	95°C	10 minutes
Cycle x40	95°C	15 seconds
	60°C	1 minute

The qPCR data was analysed using the $2^{-\Delta\Delta Ct}$ method with the obtained ΔCt values being normalised against the ΔCt values of the DMSO-treated control. GAPDH or β-actin were used as housekeeping genes.

Gene	Assay ID
ACTB	Hs01060665_g1
AKT1	Hs00178289_m1
BHLHE40	Hs01041212_m1
BNIP3	Hs00969291_m1
CCNE2	Hs00180319_m1
DDIT3	Hs00358796_g1
FBXO32	Hs01041408_m1
GABARAPL1	Hs00740588_mH
GAPDH	Hs02758991_g1
HK2	Hs00606086_m1
HMOX1	Hs01110250_m1
HRK	Hs02621354_s1
ICAM1	Hs00164932_m1
ID1	Hs03676575_s1
ID3	Hs00954037_g1
NDRG1	Hs00608387_m1
NOS2	Hs01075529_m1
OLIG2	Hs00300164_s1
PGK1	Hs00943178_g1
RRM2	Hs00357247_g1
SKP2	Hs01021864_m1
SLC16A3	Hs00358829_m1
SLC2A1	Hs00892681_m1
SLC2A3	Hs00359840_m1
SOD2	Hs00167309_m1
TRIB3	Hs01082394_m1
TXNRD1	Hs00917067_m1
UCP2	Hs01075227_m1

Table 5.2: List of TaqMan probes used for (bulk cell) qRT-PCR.

5.14 Extracellular flux analysis - metabolic phenotyping

Assessment of the metabolic phenotypes of GBM and NP cells was performed using the Seahorse XF extracellular flux analyser. For acute compound injections, cells were seeded into the provided microplates at a density of 30,000 cells per well and allowed to adhere overnight. Prior to analysis, the culture medium was replaced with XF base media (Seahorse Bioscience; 102353-100) and transferred to a 37°C non-CO_2 humidified incubator. For the 'Mito Stress Test' in GBM cells, XF base media was supplemented with glucose (25 mM; Sigma; G8769) and sodium pyruvate (0.5 mM; Sigma; S8636). L-glutamine (2 mM; Gibco; 35050-061) was added for both 'Mito and Glycolysis Stress Tests' with NP cells. Supplemented culture media were adjusted to pH 7.4 and filtered through a 0.2 µm filter, and maintained at 37°C throughout the experiments. After the baseline readings of metabolic flux were established (∼18 minutes), DMSO (0.1% v/v) or KHS101 (7.5 µM) were injected. Oligomycin (1 µM), FCCP (0.5 µM), antimycin and rotenone (0.5 µM) were injected according to the 'Mito Stress Test' (Seahorse Bioscience; 101848-400) protocol. Glucose (10 mM), oligomycin (1 µM) and 2-deoxy-glucose (100 mM) were injected according to 'Glycolysis Stress Test' (Seahorse Bioscience; 103020-400) protocols. To assess the bioenergetic phenotype after 24 hours of compound treatment, treated cells were seeded into poly-ornithine/laminin coated microplates by centrifugation (300 x g for 2 minutes, no brake) at a density of 30,000 live cells per well in the required XF base medium. 'Mito Stress Tests' and 'Glycolysis Stress Tests' were performed according to the manufacturer's protocols.

5.15 Animal experiments

Animal experiments were approved by the University of Leeds Animal Welfare & Ethical Review Committee (AWERC) and carried out under UK Home Office project license approval in line with the Animal (Scientific Procedures) Act 1986 and in accordance with the UK National Cancer Research Institute Guidelines for the welfare of animals. Animals were maintained under standard conditions on a 12 hour day/night cycle with food and water ad libitum.

For intracranial xenograft tumour assays 6 to 10-week-old mice were stereotactically injected with 2 µL of GSC/GBM cells (see table below for cell numbers; containing 30% Matrigel™ BD Biosciences) into the right striatum (2.5 mm from the midline, 2.5 mm anterior from bregma, 3 mm deep). Surgery was performed under general

anaesthesia using aseptic techniques. Mice were monitored daily for signs of sickness, pain or weight loss. Six weeks after intracranial injection, 6 mg/kg KHS101 or vehicle control (5% (v/v) ethanol, 15% (w/v) (2-Hydroxypropyl)-β-cyclo-dextrin [Sigma; H107]) was administered subcutaneously (s.c.) twice daily. KHS101 dosing was maintained for 10 weeks with bi-weekly alteration of 5 and 3 treatment days per week. Endpoints were 16 weeks after intracranial injections for the GSC1 model. The mice were sacrificed and tissue was fixed by intracardiac perfusion with PBS followed by 4% (w/v) PFA. The brains and livers were removed and transferred into 4% (w/v) PFA. Tissue was subjected to immunohistological analysis (see 5.16 'Histology and immunohistochemistry').

Early removal criteria (significant weight loss, hunched position, rough hair coat, neurological signs or any condition interfering with daily activities e.g. eating and drinking) were applied for determining survival of mice carrying GBMX-derived xenograft tumours.

For analysis of immune cell infiltration in a syngeneic mouse model of glioma, C57BL/6J mice with GFP-expressing hematopoietic cells were used. To generate this mouse model, bone marrow was isolated from the femur and tibia of UBC-GFP mice (bred at St. James's Biological Services unit) and GFP+ hematopoietic stem cells (Sca-1+) were isolated by MACS using Sca-1 MicroBead Kit (Miltenyi; 130-092-529). The obtained GFP+ hematopoietic stem cells were transplanted into lethally irradiated (8.45 Gy) female C56BL/6J mice (Charles River Laboratories, UK) by intravenous (i.v.) injection (1 x 10^6 cells/mouse). Flow cytometric analysis was performed six weeks post-transplantation to confirm successful bone marrow reconstitution. The ICAM-1 and Firefly luciferase expressing CT2A cells were intracranially injected into these mice as described above for GBM1 and GBMX xenograft models. Tumour growth was monitored by bioluminescence imaging using an IVIS 200 system (PerkinElmer) after subcutaneous injection of luciferin (Regis Technologies; 1-360223-200). Four weeks post-surgery, mice were sacrificed and brain tissue was harvested after terminal perfusion with a saline/heparin solution. Tissue was further processed for flow cytometry (see 5.19 'Immune cell infiltration and macrophage polarisation')

Cell line	Number of cells injected	Mouse model	Dosing	Analysis
GSC1	2 x 10^5 (in 30% Matrigel^{TM})	NSG	KHS101 for 10 weeks	Phenotypic analysis
GBMX	8 x 10^4 (in 30% Matrigel^{TM})	BALB/c Nude	KHS101 for 10 weeks	Survival
CT2A-mICAM1-Fluc	5 x 10^4	C57BL/6J	N/A	Immune cell infiltration & Macrophage polarisation

Table 5.3: *In vivo* studies.

5.16 Histology and immunohistochemistry (IHC)

The harvested brains were fixed in (4% (w/v) PFA at 4°C for two days and subsequently placed in a tube containing sucrose solution (25% sucrose [Sigma; S7903] in 0.5 M NaH_2PO_4, 0.5 M Na_2HPO_4). After the brains had sunken to the bottom of the tube, they were snap frozen using dry ice and cut on a cryostat to obtain 30 µm thick frozen sections. The sections were stored at -20°C in Walter's antifreeze solution (13 mM NaH_2PO_4, 55 mM Na_2HPO_4, 30% (v/v) ethyleneglycol, 30% (v/v) glycerol) until they were needed for analysis. Prior to staining, the brain sections were equilibrated in PBS at RT for 10 minutes. Staining with Hematoxylin and Eosin was then performed following standard protocols.
For IHC, the sections were equilibrated in PBS and subsequently permeabilised with PBS containing 0.2% (v/v) Triton X-100 for 10 minutes, followed by blocking with PBS containing 10% (v/v) FBS and 0.03% (v/v) Triton X-100 at RT for 1 hour. Primary antibodies were diluted in PBS containing 10% (v/v) FBS and 0.03% (v/v) Triton X-100 and the sections incubated in the antibody solution at 4°C overnight. Following antibodies were used: anti-KI67 (abcam; ab16667; 1:200), anti-HK2 (biorbyt; orb69302; 1:150), and anti-Vimentin (DAKO; M0725; 1:200). After three PBS washing steps of 5 minutes each, the sections were incubated with secondary antibody in PBS containing 10% (v/v) FBS and 0.03% (v/v) Triton X-100 at RT for 1 hour. Secondary antibodies used were AlexaFluor488 (Molecular Probes; A11029; 1:200) or Cy3 (Jackson ImmunoResearch; 711-165-152; 1:400) conjugated. Following incubation with DAPI (1 µg/ml; Sigma) in PBS for 5 minutes at RT and two PBS washes, whole sections were analysed using the EVOS digital inverted fluorescence microscope or Nikon A1R confocal microscope and selected slides were scanned using the Leica Ariol system at a magnification of x20 with a resolution of ∼0.35 microns per pixel.

5.17 Flow cytometry

For staining of cultured cells, the adherently-grown cells were harvested by trypsinisation after 48 hours of treatment with DMSO (0.1% v/v) or RA (2 µM) ± KHS101 (1-7.5 µM). Pelleted cells were resuspended in PBS and 10 µL FcR blocking reagent (Miltenyi; 130-059-901) was added to block Fc receptors on the cell surface and prevent unspecific binding of the antibody. After 10 minutes incubation at 4°C, cells were pelleted and washed with PBS. Then, cells were pelleted and resuspended in 100 µL antibody solution (CD54-PE [BD Biosciences; 347977], diluted 1:10 in PBS). To determine the background signal of non-specific binding, the cells were stained with appropriate isotype controls (PE mouse IgG1,κ [BioLegend; 400112]) alongside the CD54 antibody. After incubation with the antibody/isotype control (20-30 minutes at 4°C) the cells were washed with PBS, fixed with 500 µL 1% (w/v) PFA and analysed using the Attune Acoustic Focusing cytometer (Applied Biosystems). For the live/dead cell staining all cells (detached cells in the supernatant, trypsinised cells) were harvested and pelleted cells were resuspended in 1 mL PBS containing 1 µL red fluorescent reactive dye (LIVE/DEAD® Fixable Red Dead Cell Stain Kit; Invitrogen; L23102) and incubated for 20 minutes at RT. The cells were analysed using the Attune Acoustic Focusing cytometer (Applied Biosystems).

5.18 Lentiviral transduction

Production of lentivirus stocks for firefly luciferase labeling of cells, HEK293 cells were used. First, cells were seeded in poly-L-lysine coated 10-cm plates at a density of 2x10^6 cells per plate. The following day, a transfection mixture of 0.1x TE (10 mM Tris, pH 8.0, 1 mM ethylenediaminetetraacetic acid [EDTA]) containing Gag-pol plasmid (6.5 µg), VSV-G plasmid (3.5 µg), Prsv-rev plasmid (2.5 µg) and the Fluc plasmid (10 µg) in a total volume of 450 µL per plate was prepared. While this mixture was being vortexed, 500 µL 2x HBS (100 mM HEPES, 281 mM NaCl, 1.5 mM Na_2HPO_4) was added. This final transfection mixture was then added to the HEK293 cells drop-wise. The following day, the medium was replaced by fresh medium. The virus was collected after 24 hours, fresh medium added and a second batch of virus was harvested another 24 hours later. Prior to storage at -80°C, the harvested virus was filtered using 0.45 µm filters.
For luciferase labeling, CT2A cells were seeded in 12-well plates and lentiviral particles containing firefly luciferase expression vector were added immediately afterwards. The medium was replaced by fresh medium the following day. The labeled

cells were used for intracranial injection into mice within two weeks of lentiviral transduction.

For generation of ICAM-1 overexpressing cells, the cells were seeded in 12-well plates at a density of approximately 50,000 cells/well. Human ICAM-1 (hICAM-1), mouse ICAM-1 (mICAM-1) overexpression or their respective empty vector containing lentiviral particles were added before cells had attached. The following day, the medium was replaced with fresh medium containing 5 µg/mL puromycin (Millipore; 540411) selection marker. Three days later, the puromycin concentration was reduced and maintained at 1 µg/mL throughout the course of the experiments.

Construct	Accession Number	Vector backbone	Markers	Supplier
hICAM-1	NM_000201.2	pLenti-TetCMV-Insert-Rsv(GFP-Puro)	GFP/Puromycin	GenTarget
Null	N/A			
mICAM-1	NM_010493	pLenti-GIII-CMV	Puromycin	abm
Blank	N/A			

Table 5.4: Lentiviral vector information.

5.19 Immune cell infiltration and macrophage polarisation

The anterior right half of the brain was mechanically disrupted, followed by dissociation with collagenase A (3 mg/mL; Roche; 10103578001)/hyaluronidase (250 U/mL; Sigma; H3506-500MG) solution containing DNaseI (100 µg/mL; Roche) at 37°C for 20 minutes. Myelin was removed using Myelin removal beads (Miltenyi; 130-096-733) according to the manufacturer's instructions. The obtained cells were blocked with 10% rat serum (AbD Serotec; 135B2) and subsequently stained for different heamatopoietic markers (table 5.7). For intracellular staining, cells were fixed and permeabilised using the Intracellular Fixation & Permeabilisation buffer kit (eBiosciences; 88-8824-00) according to the manufacturer's instructions. The cells were then analysed on the LSRII flow cytometer (BD Bioscience).

Panel 1 - Immune cell infiltration:

Antibody	Supplier	Catalog Number	Volume [µL]*
F4/80-AlexaFluor700	BioRad	MCA497A700T	1.2
CD45-PeCy7	BioLegend	103114	1.2
NKp46-PE	Miltenyi	130-102-395	2.4
CD11b-V450	BD Biosciences	560455	2.4
CD3e-APC-Vio770	Miltenyi	130-098-142	1.2
Gr1-PerCP	BioLegend	108426	1.2
Ly6G-APC	BioLegend	127613	1.2
Ly6C-Viogreen	Miltenyi	130-102-207	2.4

Panel 2- Macrophage polarisation:

Antibody	Supplier	Catalog Number	Volume [µL]*
F4/80-AlexaFluor700	BioRad	MCA497A700T	1.2
CD45-APC Vio770	Miltenyi	130-105-463	2.4
CD11b-APC	BioLegend	101212	1.2
Gr1-PerCP clone RB6-8C5	BioLegend	108426	1.2
MHCII-Vioblue	Miltenyi	130-102-145	2.4
Arg1-PE †	R&D	IC5868P	1.2
iNOS-PE Cy7 †	eBioscience	25-5920-82	1.2
CD206-BrillViol605 †	BioLegend	141721	1.2

Isotype controls:

Antibody	Supplier	Catalog Number	Volume [µL]*
PeCy7 rat IgG2b,κ	BioLegend	400617	1.2
Rat IgG2a-PE	Miltenyi	130-102-654	2.4
Rat (IgG2b)-AF700	AbD Serotec	MCA1125A700	1.2
V450 rat IgG2b,κ	eBioscience	48-4031-80	1.2
Rat (IgG2b,κ)-APC-Vio770	Miltenyi	130-102-657	2.4
PerCP rat IgG2b,κ	BioLegend	400629	1.2

Antibody	Supplier	Catalog Number	Volume [µL]*
APC rat IgG2a,κ	eBioscience	17-4321-81	1.2
Viogreen rat IgG2a	Miltenyi	130-102-650	2.4
Rat (IgG2b,κ)-APC clone RTK4530	BioLegend	400612	1.2
Rat (IgG2b,κ)-PerCP clone RTK4530	BioLegend	400629	1.2
Rat IgG2b Vioblue	Miltenyi	130-102-661	2.4
Rat (IgGa,κ)-PECy7 clone eBR2a	eBioscience	25-4321-82	1.2
Iso-BV605	BioLegend	400539	1.2

Table 5.7: List of FACS antibodies for analysis of immune cell infiltration and macrophage polarisation. *for max. 1 x 10^6 cells; †intracellular stains.

5.20 ICAM1 qRT-PCR screen

GBM1 cells were seeded in 12-well plates at a density of 75,000 cells/well and treated with RA (2 µM), the compounds or a combination of RA and the compounds (see table 3.1 for a full list of compounds tested). Cells were harvested after 24 hours and RNA isolation, sample homogenization, cDNA synthesis and qRT-PCR performed as described in 5.13 'Quantitative RT-PCR of bulk cells'.

5.21 Infection with CVA21

ICAM-1 overexpressing cells or GBM cells pre-treated with DMSO (0.1% v/v), RA (2 µM) or KHS101 (1-7.5 µM) for 48 hours were seeded at a density of 50,000 cells/well in 12-well plates. The same day, coxsackievirus A21 (CVA21; CAVATAK™; provided by Viralytics Ltd, AU) was added to the cells at multiplicities of infection (MOI) of 0, 0.01, 0.1 or 1 and cell death was assessed 7 days post-infection by flow cytometry using the LIVE/DEAD® Fixable Red Dead Cell Stain Kit (see 5.17 'Flow cytometry').

5.22 Image analysis

Immunocytochemistry: Regions of interest (ROIs such as vacuolated area or LC3B positive area) were manually defined or by colour thresholding using ImageJ (default settings, color space: HSB), and their percentage of the total cellular area was calculated. The number of KI67 or CytoID® positive cells was determined in randomly selected images totaling ≥500 cells per single experiment.
Immunohistochemistry: ROIs (KI67, HK2, VIMENTIN, ICAM1 stained areas or eosin-dense regions) were isolated from immunofluorescence/phase contrast or immunohistological images using ImageJ software and color thresholding with default settings (color space: HSB). Selected ROIs were measured and percentage of the total area of interest was determined. Five different tumour sections per specimen (KI67-positive ROI) or 15 randomly selected images per specimen (HK2-positve ROI) were analysed for quantification of immunofluorescence staining. For determination of GBM cell invasion in xenograft tumours, three or four VIMENTIN-stained sections per specimen were analysed. For determination of ICAM-1 expression in GBM, ROIs were defined in IHC images from the Human Protein Atlas database [124] by colour thresholding using ImageJ software. A total of 69 or 61 images from 12 or 11 patients were analysed for antibodies HPA002126 or HPA004877, respectively (images available from v13.proteinatlas.org).

5.23 Statistical analysis

In vitro data is shown as mean ± SD or mean of fold changes ± SD and was analysed using the student's t-test (two-tailed). For analysis of xenograft tumour data, the Mann-Whitney U-test was used (http://www.socscistatistics.com/tests/mannwhitney/; one-tailed). For Kaplan-Meier analysis, the significance was calculated using the log-rank test. P values of ≤ 0.05 were considered significant (*) and P values of ≤ 0.01 were considered highly significant (**).

List of abbreviations

µL	microlitre
µM	micromolar
µm	micrometer
2-DG	2-Deoxy-D-Glucose
A	Antimycin A
ABC	ATP-binding cassette
AKT1	V-akt Murine Thymoma Viral Oncogene Homolog 1
ALA	5-aminolevulinic acid
ALDH1A1	Aldehyde Dehydrogenase 1 Family, Member A1
AMP	Adenosine monophosphate
AP-1	Activator protein 1
APC	Antigen presenting cell
APL	Acute promyelocytic leukemia
Arg1	Arginase-1
ARNT2	Aryl hadrocarbon receptor nuclear translocator 2
ATG5	Autophagy related 5
ATP	Adenosine triphosphate
bFGF	Basic fibroblast growth factor
BHLHE40	Basic Helix-Loop-Helix Familiy Member E40
BMI1	BMI1 Proto-Oncogene, Polycomb Ring Finger
BMP	Bone Morphogenic Protein
BNIP3	BCL2/adenovirus E1B 19 kDa Interacting Protein
C	Compound
C/EBP	CCAAT/Enhancer Binding Protein
CC	Corpus callosum
CCL-1	Chemokine (C-C Motif) Ligand 1
CCNE2	Cyclin E2
CD	Cluster of differentiation
CDK	Cyclin-dependent Kinase
cDNA	complementary DNA
CHI3L1	Chitinase 3-Like 1 (Cartilage Glycoprotein-39)
ch-TOG	colonic and hepatic tumor overexpressed gene
cm	Centimeter

CNS	Central Nervous System
CRBP1	Cellular retinol binding protein 1
CSC	Cancer stem cell
CVA21	Coxsackievirus A21
CYP26B1	Cytochrome P450, Family 26, Subfamily B, Polypeptide 1
DAF	Decay-accelerating factor
DAPI	4',6-diamidino-2-phenylindole
DDIT3	DNA-Damage-Inducible Transcript 3
DLL4	Delta-like 4
DMEM	Dulbecco's Modified Eagle Medium
DMSO	Dimethylsulfoxide
DNA	Deoxyribonucleic acid
e.g.	exempli gratia
ECAR	Extracellular acidification rate
EDTA	Ethylenediaminetetraacetic acid
EGF	Epidermal Growth Factor
EGFR	Epidermal Growth Factor Receptor
EM	Electron microscopy
EMT	Epithelial-mesenchymal transition
ERBB2	Erb-B2 Receptor Tyrosine Kinase 2
EZH2	Enhancer Of Zeste 2 Polycomb Repressive Complex 2 Subunit
F	FCCP
FABP5	Fatty Acid Binding Protein 5
FACS	Fluorescence-activated Cell Sorting
FBS	Fetal Bovine Serum
FBXO32	F-box Protein 32
FC	Fold Change
FCCP	Carbonyl cyanide-4 (trifluoromethoxy) phenylhydrazone
FcR	Fc receptor
FDA	U.S. Food and Drug Administration
FDR	False Discovery Rate
FGF	Fibroblast growth factor
FGFR	Fibroblast growth factor receptor
F-luc	Firefly luciferase
G	Glucose
GABARAPL1	Gamma-aminobutyric Acid A Receptor-associated Protein-like 1
GABRA1	Gamma-Aminobutyric Acid (GABA) A Receptor, Alpha 1
GBM	Glioblastoma Multiforme
GFAP	Glial fibrillary acidic protein
GFP	Green fluorescent protein
GLI2	GLI family zink finger 2

GM-CSF	granulocyte-macrophage colony-stimulating factor
GSC	Glioma Stem Cell
GSEA	Gene set enrichment analysis
GSK	Glycogen Synthase Kinase
H&E	Hematoxilin & Eosin
HAT	Histone Acetyltransferase
HER	Human Epidermal Growth Factor Receptor
HIF	Hypoxia inducible factor
HK2	Hexokinase 2
HMOX	Heme oxygenase
HMT	Histone Methyltransferase
HRK	Harakiri
HSF	Heat shock factor
HSV	Herpes simplex virus
HT	Hydroxytryptamine
i.e.	id est
i.p.	intraperitoneal
i.v.	intravenous
IC50	Inhibitory concentration 50
ICAM-1	Intercellular Adhesion Molecule-1
ID	Inhibitor of DNA Binding
IDH1	Isocitrate dehydrogenase 1
IHC	Immunohistochemistry
IL	Interleukin
kg	Kilogram
LC3	Microtubule-associated Protein 1 Light Chain 3
LFA	Lymphocyte function-associated antigen
LY	Lucifer Yellow
Ly6	Lymphocyte antigen 6 complex
MAP	Mitogen-activated protein
MDSC	Myeloid-derived suppressor cells
MEK	Mitogen-activated protein kinase kinase
MFI	Mean Fluorescence Intensity
mg	Milligram
MGMT	O^6-methylguanine-DNA methyltransferase
MHCII	Major histocompatibility complex class II
miRNA	microRNA
MKK4	Mitogen-activated protein kinase kinase 4
mm	Millimeter
MOA	Mechanism-of-action
MOI	Multiplicity of Infection

Mrc1	Mannose receptor C type 1 (synonym: CD206)
mRNA	messenger RNA
mTORC1	mammalian target of rapamycin complex 1
N/A	not applicable
NDRG1	N-myc Downstream Regulated 1
NDV	Newcastle disease virus
NEFL	Neurofilament, Light Polypeptide
NESTIN	Neuroectodermal Stem Cell Marker
NF1	Neurofibromatosis type 1
NF-κB	Nuclear Factor Of Kappa Light Polypeptide Gene Enhancer In B-Cells
NK cell	Natural killer cell
NKp46	Natural Killer Cell P46-Related Protein
nm	nanometer
nM	nanomolar
NOS2	Nitric oxide synthase 2 (synonym: iNOS)
NPC	Neural progenitor cell
NSC	Neural stem cell
NSG	NOD scid gamma
O	Oligomycin
OCR	Oxygen consumption rate
OLIG2	Oligodendrocyte Transcription Factor 2
OV	Oncolytic virus
PBS	Phosphate buffered saline
PDGFRA	Platelet-derived growth factor receptor α
PE	Phycoerythrin
PFA	Paraformaldehyde
PGK1	Phosphoglycerate Kinase 1
PIK3R1	Phosphoinositide-3-Kinase, Regulatory Subunit 1
PKC	Protein kinase C
plγRE	Interferon-γ-responsive element
PMA	Phorbol 12-myristate 13-acetate
POU3F2	POU Class 3 Homeobox 2
PPAR	Peroxisome Proliferator-Activated Receptor
PTEN	Phosphatase and Tensin homolog
qRT-PCR	Quantitative Reverse Transcription-Polymerase Chain Reaction
R	Rotenone
RA	Retinoid Acid
RAR	Retinoic acid nuclear receptor
RARE	RA responsive elements
RB1	Retinoblastoma 1
RFP	Red fluorescent protein

rhEGF	Recombinant human epidermal growth factor
RNA	Ribonucleic acid
ROCK	Rho-associated protein kinase
ROI	Region of Interest
RRM2	Ribonucleoside-diphosphate Reductase Regulatory Subunit M2
RT	Room temperature
RTK	Receptor Tyrosine Kinase
RXR	Retinoid X Receptor
s.c.	subcutaneously
SALL2	Spalt-Like Transcription Factor 2
SD	Standard deviation
SDS-PAGE	Sodium dodecyl sulfate polyacrylamide gel electrophoresis
SHH	Sonic hedgehog
SKP2	S-phase Kinase-Associated Protein 2
SLC	Solute Carrier Familiy
SMO	Smoothened, Frizzled Class Receptor
SOD2	Superoxide Dismutase 2
SOX2	SRY-box 2
SP1	Specificity Protein 1
STAT	Signal transducers and activators of transcription
SYT1	Synaptotagmin 1
TAA	Tumour-associated antigen
TACC3	Transforming Acidic coiled-coil containing protein 3
TCA	Tricaboxylic acid
TGF-β	Transforming growth factor β
TMZ	Temozolomide
TNF-α	Tumour necrosis factor α
TP53	Tumour protein p53
TRAIL	TNF-related apoptosis-inducing ligand
TRIB3	Tribbles Pseudokinase 3
TRRAP	Transformation/transcription domain-associated protein
TSC2	Tuberous sclerosis complex 2
TXNRD1	Thioredoxin Reductase 1
UCP1	Uncoupling Protein 1
ULK1	Unc-51 like autophagy activating kinase 1
UTR	Untranslated region
VEGF	Vascular Endothelial Growth Factor
VIM	VIMENTIN
WHO	World Health Organisation

References

[1] P. Kleihues, P. C. Burger, and B. W. Scheithauer, "The new who classification of brain tumours," *Brain Pathol*, vol. 3, no. 3, pp. 255–68, 1993.

[2] P. Kleihues, D. N. Louis, B. W. Scheithauer, L. B. Rorke, G. Reifenberger, P. C. Burger, and W. K. Cavenee, "The who classification of tumors of the nervous system," *J Neuropathol Exp Neurol*, vol. 61, no. 3, pp. 215–25; discussion 226–9, 2002.

[3] A. Brodbelt, D. Greenberg, T. Winters, M. Williams, S. Vernon, V. P. Collins, and G. National Cancer Information Network Brain Tumour, "Glioblastoma in england: 2007-2011," *Eur J Cancer*, vol. 51, no. 4, pp. 533–42, 2015.

[4] T. E. Taylor, F. B. Furnari, and W. K. Cavenee, "Targeting egfr for treatment of glioblastoma: molecular basis to overcome resistance," *Curr Cancer Drug Targets*, vol. 12, no. 3, pp. 197–209, 2012.

[5] S. A. Grossman and J. F. Batara, "Current management of glioblastoma multiforme," *Semin Oncol*, vol. 31, no. 5, pp. 635–44, 2004.

[6] N. G. Burnet, S. J. Jefferies, R. J. Benson, D. P. Hunt, and F. P. Treasure, "Years of life lost (yll) from cancer is an important measure of population burden–and should be considered when allocating research funds," *Br J Cancer*, vol. 92, no. 2, pp. 241–5, 2005.

[7] T. Hide, K. Makino, H. Nakamura, S. Yano, S. Anai, T. Takezaki, J. Kuroda, N. Shinojima, Y. Ueda, and J. Kuratsu, "New treatment strategies to eradicate cancer stem cells and niches in glioblastoma," *Neurol Med Chir (Tokyo)*, vol. 53, no. 11, pp. 764–72, 2013.

[8] W. Stummer, A. Novotny, H. Stepp, C. Goetz, K. Bise, and H. J. Reulen, "Fluorescence-guided resection of glioblastoma multiforme by using 5-aminolevulinic acid-induced porphyrins: a prospective study in 52 consecutive patients," *J Neurosurg*, vol. 93, no. 6, pp. 1003–13, 2000.

[9] W. Stummer, U. Pichlmeier, T. Meinel, O. D. Wiestler, F. Zanella, H. J. Reulen, and A. L.-G. S. Group, "Fluorescence-guided surgery with 5-aminolevulinic acid for resection of malignant glioma: a randomised controlled multicentre phase iii trial," *Lancet Oncol*, vol. 7, no. 5, pp. 392–401, 2006.

[10] S. K. Carlsson, S. P. Brothers, and C. Wahlestedt, "Emerging treatment strategies for glioblastoma multiforme," *EMBO Mol Med*, vol. 6, no. 11, pp. 1359–70, 2014.

[11] R. Stupp, W. P. Mason, M. J. van den Bent, M. Weller, B. Fisher, M. J. Taphoorn, K. Belanger, A. A. Brandes, C. Marosi, U. Bogdahn, J. Curschmann, R. C. Janzer, S. K. Ludwin, T. Gorlia, A. Allgeier, D. Lacombe, J. G. Cairncross, E. Eisenhauer, R. O. Mirimanoff, R. European Organisation for, T. Treatment of Cancer Brain, G. Radiotherapy, and G. National Cancer Institute of Canada Clinical Trials, "Radiotherapy plus concomitant and adjuvant temozolomide for glioblastoma," *N Engl J Med*, vol. 352, no. 10, pp. 987–96, 2005.

[12] S. Roy, D. Lahiri, T. Maji, and J. Biswas, "Recurrent glioblastoma: Where we stand," *South Asian J Cancer*, vol. 4, no. 4, pp. 163–73, 2015.

[13] M. R. Gilbert, J. J. Dignam, T. S. Armstrong, J. S. Wefel, D. T. Blumenthal, M. A. Vogelbaum, H. Colman, A. Chakravarti, S. Pugh, M. Won, R. Jeraj, P. D. Brown, K. A. Jaeckle, D. Schiff, V. W. Stieber, D. G. Brachman, M. Werner-Wasik, I. W. Tremont-Lukats, E. P. Sulman, K. D. Aldape, J. Curran, W. J., and M. P. Mehta, "A randomized trial of bevacizumab for newly diagnosed glioblastoma," *N Engl J Med*, vol. 370, no. 8, pp. 699–708, 2014.

[14] K. J. Hamblett, C. J. Kozlosky, S. Siu, W. S. Chang, H. Liu, I. N. Foltz, E. S. Trueblood, D. Meininger, T. Arora, B. Twomey, S. L. Vonderfecht, Q. Chen, J. S. Hill, and W. C. Fanslow, "Amg 595, an anti-egfrviii antibody-drug conjugate, induces potent antitumor activity against egfrviii-expressing glioblastoma," *Mol Cancer Ther*, vol. 14, no. 7, pp. 1614–24, 2015.

[15] J. S. Yu, G. Liu, H. Ying, W. H. Yong, K. L. Black, and C. J. Wheeler, "Vaccination with tumor lysate-pulsed dendritic cells elicits antigen-specific, cytotoxic t-cells in patients with malignant glioma," *Cancer Res*, vol. 64, no. 14, pp. 4973–9, 2004.

[16] R. M. Prins, H. Soto, V. Konkankit, S. K. Odesa, A. Eskin, W. H. Yong, S. F. Nelson, and L. M. Liau, "Gene expression profile correlates with t-cell infiltration and relative survival in glioblastoma patients vaccinated with dendritic cell immunotherapy," *Clin Cancer Res*, vol. 17, no. 6, pp. 1603–15, 2011.

[17] S. Krebs, T. G. Rodriguez-Cruz, C. Derenzo, and S. Gottschalk, "Genetically modified t cells to target glioblastoma," *Front Oncol*, vol. 3, p. 322, 2013.

[18] J. Baselga, "Bringing precision medicine to the clinic: from genomic profiling to the power of clinical observation," *Ann Oncol*, vol. 24, no. 8, pp. 1956–7, 2013.

[19] N. Cancer Genome Atlas Research, "Comprehensive genomic characterization defines human glioblastoma genes and core pathways," *Nature*, vol. 455, no. 7216, pp. 1061–8, 2008.

[20] C. Brennan, H. Momota, D. Hambardzumyan, T. Ozawa, A. Tandon, A. Pedraza, and E. Holland, "Glioblastoma subclasses can be defined by activity among signal transduction pathways and associated genomic alterations," *PLoS One*, vol. 4, no. 11, p. e7752, 2009.

[21] P. S. Mischel, R. Shai, T. Shi, S. Horvath, K. V. Lu, G. Choe, D. Seligson, T. J. Kremen, A. Palotie, L. M. Liau, T. F. Cloughesy, and S. F. Nelson, "Identification of molecular subtypes of glioblastoma by gene expression profiling," *Oncogene*, vol. 22, no. 15, pp. 2361–73, 2003.

[22] R. Shai, T. Shi, T. J. Kremen, S. Horvath, L. M. Liau, T. F. Cloughesy, P. S. Mischel, and S. F. Nelson, "Gene expression profiling identifies molecular subtypes of gliomas," *Oncogene*, vol. 22, no. 31, pp. 4918–23, 2003.

[23] Y. Liang, M. Diehn, N. Watson, A. W. Bollen, K. D. Aldape, M. K. Nicholas, K. R. Lamborn, M. S. Berger, D. Botstein, P. O. Brown, and M. A. Israel, "Gene expression profiling reveals molecularly and clinically distinct subtypes of glioblastoma multiforme," *Proc Natl Acad Sci U S A*, vol. 102, no. 16, pp. 5814–9, 2005.

[24] H. S. Phillips, S. Kharbanda, R. Chen, W. F. Forrest, R. H. Soriano, T. D. Wu, A. Misra, J. M. Nigro, H. Colman, L. Soroceanu, P. M. Williams, Z. Modrusan, B. G. Feuerstein, and K. Aldape, "Molecular subclasses of high-grade glioma predict prognosis, delineate a pattern of disease progression, and resemble stages in neurogenesis," *Cancer Cell*, vol. 9, no. 3, pp. 157–73, 2006.

[25] R. G. Verhaak, K. A. Hoadley, E. Purdom, V. Wang, Y. Qi, M. D. Wilkerson, C. R. Miller, L. Ding, T. Golub, J. P. Mesirov, G. Alexe, M. Lawrence, M. O'Kelly, P. Tamayo, B. A. Weir, S. Gabriel, W. Winckler, S. Gupta, L. Jakkula, H. S. Feiler, J. G. Hodgson, C. D. James, J. N. Sarkaria, C. Brennan, A. Kahn, P. T. Spellman, R. K. Wilson, T. P. Speed, J. W. Gray, M. Meyerson, G. Getz, C. M. Perou, D. N. Hayes, and N. Cancer Genome Atlas Research, "Integrated genomic analysis identifies clinically relevant subtypes of glioblastoma characterized by abnormalities in pdgfra, idh1, egfr, and nf1," *Cancer Cell*, vol. 17, no. 1, pp. 98–110, 2010.

[26] D. J. Toft and V. L. Cryns, "Minireview: Basal-like breast cancer: from molecular profiles to targeted therapies," *Mol Endocrinol*, vol. 25, no. 2, pp. 199–211, 2011.

[27] J. F. Linnekamp, X. Wang, J. P. Medema, and L. Vermeulen, "Colorectal cancer heterogeneity and targeted therapy: a case for molecular disease subtypes," *Cancer Res*, vol. 75, no. 2, pp. 245–9, 2015.

[28] C. Alifieris and D. T. Trafalis, "Glioblastoma multiforme: Pathogenesis and treatment," *Pharmacol Ther*, vol. 152, pp. 63–82, 2015.

[29] J. R. Shapiro, W. K. Yung, and W. R. Shapiro, "Isolation, karyotype, and clonal growth of heterogeneous subpopulations of human malignant gliomas," *Cancer Res*, vol. 41, no. 6, pp. 2349–59, 1981.

[30] C. J. Wikstrand, S. H. Bigner, and D. D. Bigner, "Demonstration of complex antigenic heterogeneity in a human glioma cell line and eight derived clones by specific monoclonal antibodies," *Cancer Res*, vol. 43, no. 7, pp. 3327–34, 1983.

[31] K. Harada, T. Nishizaki, S. Ozaki, H. Kubota, H. Ito, and K. Sasaki, "Intratumoral cytogenetic heterogeneity detected by comparative genomic hybridization and laser scanning cytometry in human gliomas," *Cancer Res*, vol. 58, no. 20, pp. 4694–700, 1998.

[32] V. Jung, B. F. Romeike, W. Henn, W. Feiden, J. R. Moringlane, K. D. Zang, and S. Urbschat, "Evidence of focal genetic microheterogeneity in glioblastoma multiforme by area-specific cgh on microdissected tumor cells," *J Neuropathol Exp Neurol*, vol. 58, no. 9, pp. 993–9, 1999.

[33] L. Juillerat-Jeanneret, C. C. Bernasconi, C. Bricod, S. Gros, S. Trepey, J. Benhattar, and R. C. Janzer, "Heterogeneity of human glioblastoma: glutathione-s-transferase and methylguanine-methyltransferase," *Cancer Invest*, vol. 26, no. 6, pp. 597–609, 2008.

[34] N. R. Parker, A. L. Hudson, P. Khong, J. F. Parkinson, T. Dwight, R. J. Ikin, Y. Zhu, Z. J. Cheng, F. Vafaee, J. Chen, H. R. Wheeler, and V. M. Howell, "Intratumoral heterogeneity identified at the epigenetic, genetic and transcriptional level in glioblastoma," *Sci Rep*, vol. 6, p. 22477, 2016.

[35] R. Nishikawa, T. Sugiyama, Y. Narita, F. Furnari, W. K. Cavenee, and M. Matsutani, "Immunohistochemical analysis of the mutant epidermal growth factor, deltaegfr, in glioblastoma," *Brain Tumor Pathol*, vol. 21, no. 2, pp. 53–6, 2004.

[36] K. D. Aldape, K. Ballman, A. Furth, J. C. Buckner, C. Giannini, P. C. Burger, B. W. Scheithauer, R. B. Jenkins, and C. D. James, "Immunohistochemical detection of egfrviii in high malignancy grade astrocytomas and evaluation of prognostic significance," *J Neuropathol Exp Neurol*, vol. 63, no. 7, pp. 700–7, 2004.

[37] H. S. Huang, M. Nagane, C. K. Klingbeil, H. Lin, R. Nishikawa, X. D. Ji, C. M. Huang, G. N. Gill, H. S. Wiley, and W. K. Cavenee, "The enhanced tumorigenic

activity of a mutant epidermal growth factor receptor common in human cancers is mediated by threshold levels of constitutive tyrosine phosphorylation and unattenuated signaling," *J Biol Chem*, vol. 272, no. 5, pp. 2927–35, 1997.

[38] A. Sottoriva, I. Spiteri, S. G. Piccirillo, A. Touloumis, V. P. Collins, J. C. Marioni, C. Curtis, C. Watts, and S. Tavare, "Intratumor heterogeneity in human glioblastoma reflects cancer evolutionary dynamics," *Proc Natl Acad Sci U S A*, vol. 110, no. 10, pp. 4009–14, 2013.

[39] A. P. Patel, I. Tirosh, J. J. Trombetta, A. K. Shalek, S. M. Gillespie, H. Wakimoto, D. P. Cahill, B. V. Nahed, W. T. Curry, R. L. Martuza, D. N. Louis, O. Rozenblatt-Rosen, M. L. Suva, A. Regev, and B. E. Bernstein, "Single-cell rna-seq highlights intratumoral heterogeneity in primary glioblastoma," *Science*, vol. 344, no. 6190, pp. 1396–401, 2014.

[40] A. Kreso and J. E. Dick, "Evolution of the cancer stem cell model," *Cell Stem Cell*, vol. 14, no. 3, pp. 275–91, 2014.

[41] A. R. Safa, M. R. Saadatzadeh, A. A. Cohen-Gadol, K. E. Pollok, and K. Bijangi-Vishehsaraei, "Glioblastoma stem cells (gscs) epigenetic plasticity and interconversion between differentiated non-gscs and gscs," *Genes Dis*, vol. 2, no. 2, pp. 152–163, 2015.

[42] R. Bonavia, M. M. Inda, W. K. Cavenee, and F. B. Furnari, "Heterogeneity maintenance in glioblastoma: a social network," *Cancer Res*, vol. 71, no. 12, pp. 4055–60, 2011.

[43] M. L. Suva, E. Rheinbay, S. M. Gillespie, A. P. Patel, H. Wakimoto, S. D. Rabkin, N. Riggi, A. S. Chi, D. P. Cahill, B. V. Nahed, W. T. Curry, R. L. Martuza, M. N. Rivera, N. Rossetti, S. Kasif, S. Beik, S. Kadri, I. Tirosh, I. Wortman, A. K. Shalek, O. Rozenblatt-Rosen, A. Regev, D. N. Louis, and B. E. Bernstein, "Reconstructing and reprogramming the tumor-propagating potential of glioblastoma stem-like cells," *Cell*, vol. 157, no. 3, pp. 580–94, 2014.

[44] S. S. Rathod, S. B. Rani, M. Khan, D. Muzumdar, and A. Shiras, "Tumor suppressive mirna-34a suppresses cell proliferation and tumor growth of glioma stem cells by targeting akt and wnt signaling pathways," *FEBS Open Bio*, vol. 4, pp. 485–95, 2014.

[45] L. Turchi, D. N. Debruyne, F. Almairac, V. Virolle, M. Fareh, Y. Neirijnck, F. Burel-Vandenbos, P. Paquis, M. P. Junier, E. Van Obberghen-Schilling, H. Chneiweiss, and T. Virolle, "Tumorigenic potential of mir-18a* in glioma initiating cells requires notch-1 signaling," *Stem Cells*, vol. 31, no. 7, pp. 1252–65, 2013.

[46] B. Auffinger, A. L. Tobias, Y. Han, G. Lee, D. Guo, M. Dey, M. S. Lesniak, and A. U. Ahmed, "Conversion of differentiated cancer cells into cancer stem-like cells in a glioblastoma model after primary chemotherapy," *Cell Death Differ*, vol. 21, no. 7, pp. 1119–31, 2014.

[47] E. Codrici, A. M. Enciu, I. D. Popescu, S. Mihai, and C. Tanase, "Glioma stem cells and their microenvironments: Providers of challenging therapeutic targets," *Stem Cells Int*, vol. 2016, p. 5728438, 2016.

[48] A. Soeda, M. Park, D. Lee, A. Mintz, A. Androutsellis-Theotokis, R. D. McKay, J. Engh, T. Iwama, T. Kunisada, A. B. Kassam, I. F. Pollack, and D. M. Park, "Hypoxia promotes expansion of the cd133-positive glioma stem cells through activation of hif-1alpha," *Oncogene*, vol. 28, no. 45, pp. 3949–59, 2009.

[49] L. Qiang, T. Wu, H. W. Zhang, N. Lu, R. Hu, Y. J. Wang, L. Zhao, F. H. Chen, X. T. Wang, Q. D. You, and Q. L. Guo, "Hif-1alpha is critical for hypoxia-mediated maintenance of glioblastoma stem cells by activating notch signaling pathway," *Cell Death Differ*, vol. 19, no. 2, pp. 284–94, 2012.

[50] J. M. Heddleston, Z. Li, R. E. McLendon, A. B. Hjelmeland, and J. N. Rich, "The hypoxic microenvironment maintains glioblastoma stem cells and promotes reprogramming towards a cancer stem cell phenotype," *Cell Cycle*, vol. 8, no. 20, pp. 3274–84, 2009.

[51] G. N. Yan, L. Yang, Y. F. Lv, Y. Shi, L. L. Shen, X. H. Yao, Q. N. Guo, P. Zhang, Y. H. Cui, X. Zhang, X. W. Bian, and D. Y. Guo, "Endothelial cells promote stem-like phenotype of glioma cells through activating the hedgehog pathway," *J Pathol*, vol. 234, no. 1, pp. 11–22, 2014.

[52] T. S. Zhu, M. A. Costello, C. E. Talsma, C. G. Flack, J. G. Crowley, L. L. Hamm, X. He, S. L. Hervey-Jumper, J. A. Heth, K. M. Muraszko, F. DiMeco, A. L. Vescovi, and X. Fan, "Endothelial cells create a stem cell niche in glioblastoma by providing notch ligands that nurture self-renewal of cancer stem-like cells," *Cancer Res*, vol. 71, no. 18, pp. 6061–72, 2011.

[53] D. W. Infanger, Y. Cho, B. S. Lopez, S. Mohanan, S. C. Liu, D. Gursel, J. A. Boockvar, and C. Fischbach, "Glioblastoma stem cells are regulated by interleukin-8 signaling in a tumoral perivascular niche," *Cancer Res*, vol. 73, no. 23, pp. 7079–89, 2013.

[54] S. Y. Oh and H. Kim, "Molecular culprits generating brain tumor stem cells," *Brain Tumor Res Treat*, vol. 1, no. 1, pp. 9–15, 2013.

[55] K. P. Bhat, V. Balasubramaniyan, B. Vaillant, R. Ezhilarasan, K. Hummelink, F. Hollingsworth, K. Wani, L. Heathcock, J. D. James, L. D. Goodman, S. Conroy, L. Long, N. Lelic, S. Wang, J. Gumin, D. Raj, Y. Kodama, A. Raghunathan, A. Olar, K. Joshi, C. E. Pelloski, A. Heimberger, S. H. Kim, D. P. Cahill, G. Rao, W. F. Den Dunnen, H. W. Boddeke, H. S. Phillips, I. Nakano, F. F. Lang, H. Colman, E. P. Sulman, and K. Aldape, "Mesenchymal differentiation mediated by nf-kappab promotes radiation resistance in glioblastoma," *Cancer Cell*, vol. 24, no. 3, pp. 331–46, 2013.

[56] J. D. Lathia, S. C. Mack, E. E. Mulkearns-Hubert, C. L. Valentim, and J. N. Rich, "Cancer stem cells in glioblastoma," *Genes Dev*, vol. 29, no. 12, pp. 1203–17, 2015.

[57] H. Caren, S. H. Stricker, H. Bulstrode, S. Gagrica, E. Johnstone, T. E. Bartlett, A. Feber, G. Wilson, A. E. Teschendorff, P. Bertone, S. Beck, and S. M. Pollard, "Glioblastoma stem cells respond to differentiation cues but fail to undergo commitment and terminal cell-cycle arrest," *Stem Cell Reports*, vol. 5, no. 5, pp. 829–42, 2015.

[58] S. G. Piccirillo, B. A. Reynolds, N. Zanetti, G. Lamorte, E. Binda, G. Broggi, H. Brem, A. Olivi, F. Dimeco, and A. L. Vescovi, "Bone morphogenetic proteins inhibit the tumorigenic potential of human brain tumour-initiating cells," *Nature*, vol. 444, no. 7120, pp. 761–5, 2006.

[59] P. B. Dirks, "Brain tumor stem cells: the cancer stem cell hypothesis writ large," *Mol Oncol*, vol. 4, no. 5, pp. 420–30, 2010.

[60] M. Venere, H. A. Fine, P. B. Dirks, and J. N. Rich, "Cancer stem cells in gliomas: identifying and understanding the apex cell in cancer's hierarchy," *Glia*, vol. 59, no. 8, pp. 1148–54, 2011.

[61] J. Lee, S. Kotliarova, Y. Kotliarov, A. Li, Q. Su, N. M. Donin, S. Pastorino, B. W. Purow, N. Christopher, W. Zhang, J. K. Park, and H. A. Fine, "Tumor stem cells derived from glioblastomas cultured in bfgf and egf more closely mirror the phenotype and genotype of primary tumors than do serum-cultured cell lines," *Cancer Cell*, vol. 9, no. 5, pp. 391–403, 2006.

[62] S. J. Horton and B. J. Huntly, "Recent advances in acute myeloid leukemia stem cell biology," *Haematologica*, vol. 97, no. 7, pp. 966–74, 2012.

[63] T. Lapidot, C. Sirard, J. Vormoor, B. Murdoch, T. Hoang, J. Caceres-Cortes, M. Minden, B. Paterson, M. A. Caligiuri, and J. E. Dick, "A cell initiating human acute myeloid leukaemia after transplantation into scid mice," *Nature*, vol. 367, no. 6464, pp. 645–8, 1994.

[64] D. Bonnet and J. E. Dick, "Human acute myeloid leukemia is organized as a hierarchy that originates from a primitive hematopoietic cell," *Nat Med*, vol. 3, no. 7, pp. 730–7, 1997.

[65] L. Jin, K. J. Hope, Q. Zhai, F. Smadja-Joffe, and J. E. Dick, "Targeting of cd44 eradicates human acute myeloid leukemic stem cells," *Nat Med*, vol. 12, no. 10, pp. 1167–74, 2006.

[66] D. C. Taussig, D. J. Pearce, C. Simpson, A. Z. Rohatiner, T. A. Lister, G. Kelly, J. L. Luongo, G. A. Danet-Desnoyers, and D. Bonnet, "Hematopoietic stem cells express multiple myeloid markers: implications for the origin and targeted therapy of acute myeloid leukemia," *Blood*, vol. 106, no. 13, pp. 4086–92, 2005.

[67] A. van Rhenen, G. A. van Dongen, A. Kelder, E. J. Rombouts, N. Feller, B. Moshaver, M. Stigter-van Walsum, S. Zweegman, G. J. Ossenkoppele, and G. Jan Schuurhuis, "The novel aml stem cell associated antigen cll-1 aids in discrimination between normal and leukemic stem cells," *Blood*, vol. 110, no. 7, pp. 2659–66, 2007.

[68] K. Eppert, K. Takenaka, E. R. Lechman, L. Waldron, B. Nilsson, P. van Galen, K. H. Metzeler, A. Poeppl, V. Ling, J. Beyene, A. J. Canty, J. S. Danska, S. K. Bohlander, C. Buske, M. D. Minden, T. R. Golub, I. Jurisica, B. L. Ebert, and J. E. Dick, "Stem cell gene expression programs influence clinical outcome in human leukemia," *Nat Med*, vol. 17, no. 9, pp. 1086–93, 2011.

[69] S. K. Singh, I. D. Clarke, M. Terasaki, V. E. Bonn, C. Hawkins, J. Squire, and P. B. Dirks, "Identification of a cancer stem cell in human brain tumors," *Cancer Res*, vol. 63, no. 18, pp. 5821–8, 2003.

[70] S. K. Singh, I. D. Clarke, T. Hide, and P. B. Dirks, "Cancer stem cells in nervous system tumors," *Oncogene*, vol. 23, no. 43, pp. 7267–73, 2004.

[71] D. Beier, P. Hau, M. Proescholdt, A. Lohmeier, J. Wischhusen, P. J. Oefner, L. Aigner, A. Brawanski, U. Bogdahn, and C. P. Beier, "Cd133(+) and cd133(-) glioblastoma-derived cancer stem cells show differential growth characteristics and molecular profiles," *Cancer Res*, vol. 67, no. 9, pp. 4010–5, 2007.

[72] J. Wang, P. O. Sakariassen, O. Tsinkalovsky, H. Immervoll, S. O. Boe, A. Svendsen, L. Prestegarden, G. Rosland, F. Thorsen, L. Stuhr, A. Molven, R. Bjerkvig, and P. O. Enger, "Cd133 negative glioma cells form tumors in nude rats and give rise to cd133 positive cells," *Int J Cancer*, vol. 122, no. 4, pp. 761–8, 2008.

[73] M. J. Son, K. Woolard, D. H. Nam, J. Lee, and H. A. Fine, "Ssea-1 is an enrichment marker for tumor-initiating cells in human glioblastoma," *Cell Stem Cell*, vol. 4, no. 5, pp. 440–52, 2009.

[74] J. D. Lathia, J. Gallagher, J. M. Heddleston, J. Wang, C. E. Eyler, J. Macswords, Q. Wu, A. Vasanji, R. E. McLendon, A. B. Hjelmeland, and J. N. Rich, "Integrin alpha 6 regulates glioblastoma stem cells," *Cell Stem Cell*, vol. 6, no. 5, pp. 421–32, 2010.

[75] G. Liu, X. Yuan, Z. Zeng, P. Tunici, H. Ng, I. R. Abdulkadir, L. Lu, D. Irvin, K. L. Black, and J. S. Yu, "Analysis of gene expression and chemoresistance of cd133+ cancer stem cells in glioblastoma," *Mol Cancer*, vol. 5, p. 67, 2006.

[76] S. M. Pollard, K. Yoshikawa, I. D. Clarke, D. Danovi, S. Stricker, R. Russell, J. Bayani, R. Head, M. Lee, M. Bernstein, J. A. Squire, A. Smith, and P. Dirks, "Glioma stem cell lines expanded in adherent culture have tumor-specific phenotypes and are suitable for chemical and genetic screens," *Cell Stem Cell*, vol. 4, no. 6, pp. 568–80, 2009.

[77] S. Spiegl-Kreinecker, J. Buchroithner, L. Elbling, E. Steiner, G. Wurm, A. Bodenteich, J. Fischer, M. Micksche, and W. Berger, "Expression and functional activity of the abc-transporter proteins p-glycoprotein and multidrug-resistance protein 1 in human brain tumor cells and astrocytes," *J Neurooncol*, vol. 57, no. 1, pp. 27–36, 2002.

[78] M. Dean, T. Fojo, and S. Bates, "Tumour stem cells and drug resistance," *Nat Rev Cancer*, vol. 5, no. 4, pp. 275–84, 2005.

[79] S. Bao, Q. Wu, R. E. McLendon, Y. Hao, Q. Shi, A. B. Hjelmeland, M. W. Dewhirst, D. D. Bigner, and J. N. Rich, "Glioma stem cells promote radioresistance by preferential activation of the dna damage response," *Nature*, vol. 444, no. 7120, pp. 756–60, 2006.

[80] R. Faigle and H. Song, "Signaling mechanisms regulating adult neural stem cells and neurogenesis," *Biochim Biophys Acta*, vol. 1830, no. 2, pp. 2435–48, 2013.

[81] H. Ikushima, T. Todo, Y. Ino, M. Takahashi, K. Miyazawa, and K. Miyazono, "Autocrine tgf-beta signaling maintains tumorigenicity of glioma-initiating cells through sry-related hmg-box factors," *Cell Stem Cell*, vol. 5, no. 5, pp. 504–14, 2009.

[82] S. Penuelas, J. Anido, R. M. Prieto-Sanchez, G. Folch, I. Barba, I. Cuartas, D. Garcia-Dorado, M. A. Poca, J. Sahuquillo, J. Baselga, and J. Seoane, "Tgf-beta increases glioma-initiating cell self-renewal through the induction of lif in human glioblastoma," *Cancer Cell*, vol. 15, no. 4, pp. 315–27, 2009.

[83] Z. Wang, Y. Li, S. Banerjee, and F. H. Sarkar, "Emerging role of notch in stem cells and cancer," *Cancer Lett*, vol. 279, no. 1, pp. 8–12, 2009.

[84] M. E. Valk-Lingbeek, S. W. Bruggeman, and M. van Lohuizen, "Stem cells and cancer; the polycomb connection," *Cell*, vol. 118, no. 4, pp. 409–18, 2004.

[85] J. Silber, D. A. Lim, C. Petritsch, A. I. Persson, A. K. Maunakea, M. Yu, S. R. Vandenberg, D. G. Ginzinger, C. D. James, J. F. Costello, G. Bergers, W. A. Weiss, A. Alvarez-Buylla, and J. G. Hodgson, "mir-124 and mir-137 inhibit proliferation of glioblastoma multiforme cells and induce differentiation of brain tumor stem cells," *BMC Med*, vol. 6, p. 14, 2008.

[86] J. Wang, H. Wang, Z. Li, Q. Wu, J. D. Lathia, R. E. McLendon, A. B. Hjelmeland, and J. N. Rich, "c-myc is required for maintenance of glioma cancer stem cells," *PLoS One*, vol. 3, no. 11, p. e3769, 2008.

[87] M. Christensen and G. M. Schratt, "microrna involvement in developmental and functional aspects of the nervous system and in neurological diseases," *Neurosci Lett*, vol. 466, no. 2, pp. 55–62, 2009.

[88] F. Guessous, Y. Zhang, A. Kofman, A. Catania, Y. Li, D. Schiff, B. Purow, and R. Abounader, "microrna-34a is tumor suppressive in brain tumors and glioma stem cells," *Cell Cycle*, vol. 9, no. 6, pp. 1031–6, 2010.

[89] H. Wurdak, S. Zhu, A. Romero, M. Lorger, J. Watson, C. Y. Chiang, J. Zhang, V. S. Natu, L. L. Lairson, J. R. Walker, C. M. Trussell, G. R. Harsh, H. Vogel, B. Felding-Habermann, A. P. Orth, L. J. Miraglia, D. R. Rines, S. L. Skirboll, and P. G. Schultz, "An rnai screen identifies trrap as a regulator of brain tumor-initiating cell differentiation," *Cell Stem Cell*, vol. 6, no. 1, pp. 37–47, 2010.

[90] D. Schraivogel, L. Weinmann, D. Beier, G. Tabatabai, A. Eichner, J. Y. Zhu, M. Anton, M. Sixt, M. Weller, C. P. Beier, and G. Meister, "Camta1 is a novel tumour suppressor regulated by mir-9/9* in glioblastoma stem cells," *EMBO J*, vol. 30, no. 20, pp. 4309–22, 2011.

[91] C. Lu, P. S. Ward, G. S. Kapoor, D. Rohle, S. Turcan, O. Abdel-Wahab, C. R. Edwards, R. Khanin, M. E. Figueroa, A. Melnick, K. E. Wellen, D. M. O'Rourke, S. L. Berger, T. A. Chan, R. L. Levine, I. K. Mellinghoff, and C. B. Thompson, "Idh mutation impairs histone demethylation and results in a block to cell differentiation," *Nature*, vol. 483, no. 7390, pp. 474–8, 2012.

[92] R. Castino, A. Pucer, R. Veneroni, F. Morani, C. Peracchio, T. T. Lah, and C. Isidoro, "Resveratrol reduces the invasive growth and promotes the acquisition of a long-lasting differentiated phenotype in human glioblastoma cells," *J Agric Food Chem*, vol. 59, no. 8, pp. 4264–72, 2011.

[93] W. Z. Zhuang, L. M. Long, W. J. Ji, and Z. Q. Liang, "Rapamycin induces differentiation of glioma stem/progenitor cells by activating autophagy," *Chin J Cancer*, vol. 30, no. 10, pp. 712–20, 2011.

[94] S. Teres, V. Llado, M. Higuera, G. Barcelo-Coblijn, M. L. Martin, M. A. Noguera-Salva, A. Marcilla-Etxenike, J. M. Garcia-Verdugo, M. Soriano-Navarro, C. Saus, U. Gomez-Pinedo, X. Busquets, and P. V. Escriba, "2-hydroxyoleate, a nontoxic membrane binding anticancer drug, induces glioma cell differentiation and autophagy," *Proc Natl Acad Sci U S A*, vol. 109, no. 22, pp. 8489–94, 2012.

[95] W. Zhuang, L. Long, B. Zheng, W. Ji, N. Yang, Q. Zhang, and Z. Liang, "Curcumin promotes differentiation of glioma-initiating cells by inducing autophagy," *Cancer Sci*, vol. 103, no. 4, pp. 684–90, 2012.

[96] V. Kuchler, E. S. Polson, A. Patel, and H. Wurdak, *Induced Differentiation of Brain Tumour Stem Cells*, pp. 149–158. Dordrecht: Springer Netherlands, 2014.

[97] R. Y. Bai, V. Staedtke, and G. J. Riggins, "Molecular targeting of glioblastoma: Drug discovery and therapies," *Trends Mol Med*, vol. 17, no. 6, pp. 301–12, 2011.

[98] J. Polivka, J., J. Polivka, V. Rohan, O. Topolcan, and J. Ferda, "New molecularly targeted therapies for glioblastoma multiforme," *Anticancer Res*, vol. 32, no. 7, pp. 2935–46, 2012.

[99] M. Huang, A. Shen, J. Ding, and M. Geng, "Molecularly targeted cancer therapy: some lessons from the past decade," *Trends Pharmacol Sci*, vol. 35, no. 1, pp. 41–50, 2014.

[100] C. A. Lyssiotis, L. L. Lairson, A. E. Boitano, H. Wurdak, S. Zhu, and P. G. Schultz, "Chemical control of stem cell fate and developmental potential," *Angew Chem Int Ed Engl*, vol. 50, no. 1, pp. 200–42, 2011.

[101] P. Diamandis, J. Wildenhain, I. D. Clarke, A. G. Sacher, J. Graham, D. S. Bellows, E. K. Ling, R. J. Ward, L. G. Jamieson, M. Tyers, and P. B. Dirks, "Chemical genetics reveals a complex functional ground state of neural stem cells," *Nat Chem Biol*, vol. 3, no. 5, pp. 268–73, 2007.

[102] A. J. Firestone and J. K. Chen, "Controlling destiny through chemistry: small-molecule regulators of cell fate," *ACS Chem Biol*, vol. 5, no. 1, pp. 15–34, 2010.

[103] D. S. Thorpe, "Forward and reverse chemical genetics using spos-based combinatorial chemistry," *Comb Chem High Throughput Screen*, vol. 6, no. 7, pp. 623–47, 2003.

[104] M. McMillan and M. Kahn, "Investigating wnt signaling: a chemogenomic safari," *Drug Discov Today*, vol. 10, no. 21, pp. 1467–74, 2005.

[105] B. K. Wagner and S. L. Schreiber, "The power of sophisticated phenotypic screening and modern mechanism-of-action methods," *Cell Chem Biol*, vol. 23, no. 1, pp. 3–9, 2016.

[106] B. Lomenick, R. W. Olsen, and J. Huang, "Identification of direct protein targets of small molecules," *ACS Chem Biol*, vol. 6, no. 1, pp. 34–46, 2011.

[107] C. Tan, R. G. de Noronha, A. J. Roecker, B. Pyrzynska, F. Khwaja, Z. Zhang, H. Zhang, Q. Teng, A. C. Nicholson, P. Giannakakou, W. Zhou, J. J. Olson, M. M. Pereira, K. C. Nicolaou, and E. G. Van Meir, "Identification of a novel small-molecule inhibitor of the hypoxia-inducible factor 1 pathway," *Cancer Res*, vol. 65, no. 2, pp. 605–12, 2005.

[108] D. G. Trembath, A. Lal, D. J. Kroll, N. H. Oberlies, and G. J. Riggins, "A novel small molecule that selectively inhibits glioblastoma cells expressing egfrviii," *Mol Cancer*, vol. 6, p. 30, 2007.

[109] S. Santagata, Y. M. Xu, E. M. Wijeratne, R. Kontnik, C. Rooney, C. C. Perley, H. Kwon, J. Clardy, S. Kesari, L. Whitesell, S. Lindquist, and A. A. Gunatilaka, "Using the heat-shock response to discover anticancer compounds that target protein homeostasis," *ACS Chem Biol*, vol. 7, no. 2, pp. 340–9, 2012.

[110] A. De Robertis, S. Valensin, M. Rossi, P. Tunici, M. Verani, A. De Rosa, C. Giordano, M. Varrone, A. Nencini, C. Pratelli, T. Benicchi, A. Bakker, J. Hill, K. Sangthongpitag, V. Pendharkar, B. Liu, F. M. Ng, S. W. Then, S. Jing Tai, S. M. Cheong, X. He, A. Caricasole, and M. Salerno, "Identification and characterization of a small-molecule inhibitor of wnt signaling in glioblastoma cells," *Mol Cancer Ther*, vol. 12, no. 7, pp. 1180–9, 2013.

[111] A. G. Goglia, R. Delsite, A. N. Luz, D. Shahbazian, A. F. Salem, R. K. Sundaram, J. Chiaravalli, P. J. Hendrikx, J. A. Wilshire, M. Jasin, H. M. Kluger, J. F. Glickman, S. N. Powell, and R. S. Bindra, "Identification of novel radiosensitizers in a high-throughput, cell-based screen for dsb repair inhibitors," *Mol Cancer Ther*, vol. 14, no. 2, pp. 326–42, 2015.

[112] K. Shchors, A. Massaras, and D. Hanahan, "Dual targeting of the autophagic regulatory circuitry in gliomas with repurposed drugs elicits cell-lethal autophagy and therapeutic benefit," *Cancer Cell*, vol. 28, no. 4, pp. 456–71, 2015.

[113] K. Visnyei, H. Onodera, R. Damoiseaux, K. Saigusa, S. Petrosyan, D. De Vries, D. Ferrari, J. Saxe, E. H. Panosyan, M. Masterman-Smith, J. Mottahedeh, K. A. Bradley, J. Huang, C. Sabatti, I. Nakano, and H. I. Kornblum, "A molecular screening approach to identify and characterize inhibitors of glioblastoma stem cells," *Mol Cancer Ther*, vol. 10, no. 10, pp. 1818–28, 2011.

[114] D. Danovi, A. Folarin, S. Gogolok, C. Ender, A. M. Elbatsh, P. G. Engstrom, S. H. Stricker, S. Gagrica, A. Georgian, D. Yu, K. P. U, K. J. Harvey, P. Ferretti, P. J. Paddison, J. E. Preston, N. J. Abbott, P. Bertone, A. Smith, and S. M. Pollard, "A high-content small molecule screen identifies sensitivity of glioblastoma stem cells to inhibition of polo-like kinase 1," *PLoS One*, vol. 8, no. 10, p. e77053, 2013.

[115] S. S. Kitambi, E. M. Toledo, D. Usoskin, S. Wee, A. Harisankar, R. Svensson, K. Sigmundsson, C. Kalderen, M. Niklasson, S. Kundu, S. Aranda, B. Westermark, L. Uhrbom, M. Andang, P. Damberg, S. Nelander, E. Arenas, P. Artursson, J. Walfridsson, K. Forsberg Nilsson, L. G. Hammarstrom, and P. Ernfors, "Vulnerability of glioblastoma cells to catastrophic vacuolization and death induced by a small molecule," *Cell*, vol. 157, no. 2, pp. 313–28, 2014.

[116] H. Wurdak, S. Zhu, K. H. Min, L. Aimone, L. L. Lairson, J. Watson, G. Chopiuk, J. Demas, B. Charette, R. Halder, E. Weerapana, B. F. Cravatt, H. T. Cline, E. C. Peters, J. Zhang, J. R. Walker, C. Wu, J. Chang, T. Tuntland, C. Y. Cho, and P. G. Schultz, "A small molecule accelerates neuronal differentiation in the adult rat," *Proc Natl Acad Sci U S A*, vol. 107, no. 38, pp. 16542–7, 2010.

[117] W. Fu, H. Chen, G. Wang, J. Luo, Z. Deng, G. Xin, N. Xu, X. Guo, J. Lei, Q. Jiang, and C. Zhang, "Self-assembly and sorting of acentrosomal microtubules by tacc3 facilitate kinetochore capture during the mitotic spindle assembly," *Proc Natl Acad Sci U S A*, vol. 110, no. 38, pp. 15295–300, 2013.

[118] F. E. Hood and S. J. Royle, "Pulling it together: The mitotic function of tacc3," *Bioarchitecture*, vol. 1, no. 3, pp. 105–109, 2011.

[119] D. Singh, J. M. Chan, P. Zoppoli, F. Niola, R. Sullivan, A. Castano, E. M. Liu, J. Reichel, P. Porrati, S. Pellegatta, K. Qiu, Z. Gao, M. Ceccarelli, R. Riccardi, D. J. Brat, A. Guha, K. Aldape, J. G. Golfinos, D. Zagzag, T. Mikkelsen, G. Finocchiaro, A. Lasorella, R. Rabadan, and A. Iavarone, "Transforming fusions of fgfr and tacc genes in human glioblastoma," *Science*, vol. 337, no. 6099, pp. 1231–5, 2012.

[120] C. L. Partch and K. H. Gardner, "Coactivators necessary for transcriptional output of the hypoxia inducible factor, hif, are directly recruited by arnt pas-b," *Proc Natl Acad Sci U S A*, vol. 108, no. 19, pp. 7739–44, 2011.

[121] Y. Guo, C. L. Partch, J. Key, P. B. Card, V. Pashkov, A. Patel, R. K. Bruick, H. Wurdak, and K. H. Gardner, "Regulating the arnt/tacc3 axis: multiple approaches to manipulating protein/protein interactions with small molecules," *ACS Chem Biol*, vol. 8, no. 3, pp. 626–35, 2013.

[122] F. Gergely, C. Karlsson, I. Still, J. Cowell, J. Kilmartin, and J. W. Raff, "The tacc domain identifies a family of centrosomal proteins that can interact with microtubules," *Proc Natl Acad Sci U S A*, vol. 97, no. 26, pp. 14352–7, 2000.

[123] C. M. Sadek, M. Pelto-Huikko, M. Tujague, K. R. Steffensen, M. Wennerholm, and J. A. Gustafsson, "Tacc3 expression is tightly regulated during early differentiation," *Gene Expr Patterns*, vol. 3, no. 2, pp. 203–11, 2003.

[124] M. Uhlen, L. Fagerberg, B. M. Hallstrom, C. Lindskog, P. Oksvold, A. Mardinoglu, A. Sivertsson, C. Kampf, E. Sjostedt, A. Asplund, I. Olsson, K. Edlund, E. Lundberg, S. Navani, C. A. Szigyarto, J. Odeberg, D. Djureinovic, J. O. Takanen, S. Hober, T. Alm, P. H. Edqvist, H. Berling, H. Tegel, J. Mulder, J. Rockberg, P. Nilsson, J. M. Schwenk, M. Hamsten, K. von Feilitzen, M. Forsberg, L. Persson, F. Johansson, M. Zwahlen, G. von Heijne, J. Nielsen, and F. Ponten, "Proteomics. tissue-based map of the human proteome," *Science*, vol. 347, no. 6220, p. 1260419, 2015.

[125] G. H. Ha, J. L. Kim, and E. K. Breuer, "Transforming acidic coiled-coil proteins (taccs) in human cancer," *Cancer Lett*, vol. 336, no. 1, pp. 24–33, 2013.

[126] M. Yun, J. Rong, Z. R. Lin, Y. L. He, J. X. Zhang, Z. W. Peng, L. Q. Tang, M. S. Zeng, Q. Zhong, and S. Ye, "High expression of transforming acidic coiled coil-containing protein 3 strongly correlates with aggressive characteristics and poor prognosis of gastric cancer," *Oncol Rep*, vol. 34, no. 3, pp. 1397–405, 2015.

[127] Z. L. Huang, Z. R. Lin, Y. R. Xiao, X. Cao, L. C. Zhu, M. S. Zeng, Q. Zhong, and Z. S. Wen, "High expression of tacc3 in esophageal squamous cell carcinoma correlates with poor prognosis," *Oncotarget*, vol. 6, no. 9, pp. 6850–61, 2015.

[128] G. H. Ha, J. S. Park, and E. K. Breuer, "Tacc3 promotes epithelial-mesenchymal transition (emt) through the activation of pi3k/akt and erk signaling pathways," *Cancer Lett*, vol. 332, no. 1, pp. 63–73, 2013.

[129] S. V. Williams, C. D. Hurst, and M. A. Knowles, "Oncogenic fgfr3 gene fusions in bladder cancer," *Hum Mol Genet*, vol. 22, no. 4, pp. 795–803, 2013.

[130] I. J. Majewski, L. Mittempergher, N. M. Davidson, A. Bosma, S. M. Willems, H. M. Horlings, I. de Rink, L. Greger, G. K. Hooijer, D. Peters, P. M. Nederlof, I. Hofland, J. de Jong, J. Wesseling, R. J. Kluin, W. Brugman, R. Kerkhoven, F. Nieboer, P. Roepman, A. Broeks, T. R. Muley, J. Jassem, J. Niklinski, N. van Zandwijk, A. Brazma, A. Oshlack, M. van den Heuvel, and R. Bernards, "Identification of recurrent fgfr3 fusion genes in lung cancer through kinome-centred rna sequencing," *J Pathol*, vol. 230, no. 3, pp. 270–6, 2013.

[131] B. A. Carneiro, J. A. Elvin, S. D. Kamath, S. M. Ali, A. S. Paintal, A. Restrepo, E. Berry, F. J. Giles, and M. L. Johnson, "Fgfr3-tacc3: A novel gene fusion in cervical cancer," *Gynecol Oncol Rep*, vol. 13, pp. 53–6, 2015.

[132] R. Yao, Y. Natsume, Y. Saiki, H. Shioya, K. Takeuchi, T. Yamori, H. Toki, I. Aoki, T. Saga, and T. Noda, "Disruption of tacc3 function leads to in vivo tumor regression," *Oncogene*, vol. 31, no. 2, pp. 135–48, 2012.

[133] N. Ohoka, K. Nagai, T. Hattori, K. Okuhira, N. Shibata, N. Cho, and M. Naito, "Cancer cell death induced by novel small molecules degrading the tacc3 protein via the ubiquitin-proteasome pathway," *Cell Death Dis*, vol. 5, p. e1513, 2014.

[134] L. Altucci and H. Gronemeyer, "The promise of retinoids to fight against cancer," *Nat Rev Cancer*, vol. 1, no. 3, pp. 181–93, 2001.

[135] H. Asano, M. Aonuma, T. Sanosaka, J. Kohyama, M. Namihira, and K. Nakashima, "Astrocyte differentiation of neural precursor cells is enhanced by retinoic acid through a change in epigenetic modification," *Stem Cells*, vol. 27, no. 11, pp. 2744–52, 2009.

[136] A. M. Jimenez-Lara, N. Clarke, L. Altucci, and H. Gronemeyer, "Retinoic-acid-induced apoptosis in leukemia cells," *Trends Mol Med*, vol. 10, no. 10, pp. 508–15, 2004.

[137] B. Campos, F. S. Centner, J. L. Bermejo, R. Ali, K. Dorsch, F. Wan, J. Felsberg, R. Ahmadi, N. Grabe, G. Reifenberger, A. Unterberg, J. Burhenne, and C. Herold-Mende, "Aberrant expression of retinoic acid signaling molecules influences patient survival in astrocytic gliomas," *Am J Pathol*, vol. 178, no. 5, pp. 1953–64, 2011.

[138] C. S. Niu, M. W. Li, Y. F. Ni, J. M. Chen, J. M. Mei, J. Li, and X. M. Fu, "Effect of all-trans retinoic acid on the proliferation and differentiation of brain tumor stem cells," *J Exp Clin Cancer Res*, vol. 29, p. 113, 2010.

[139] W. K. Yung, A. P. Kyritsis, M. J. Gleason, and V. A. Levin, "Treatment of recurrent malignant gliomas with high-dose 13-cis-retinoic acid," *Clin Cancer Res*, vol. 2, no. 12, pp. 1931–5, 1996.

[140] F. Le Doze, D. Debruyne, F. Albessard, L. Barre, and G. L. Defer, "Pharmacokinetics of all-trans retinoic acid, 13-cis retinoic acid, and fenretinide in plasma and brain of rat," *Drug Metab Dispos*, vol. 28, no. 2, pp. 205–8, 2000.

[141] E. Kelly and S. J. Russell, "History of oncolytic viruses: genesis to genetic engineering," *Mol Ther*, vol. 15, no. 4, pp. 651–9, 2007.

[142] Z. S. Guo, S. H. Thorne, and D. L. Bartlett, "Oncolytic virotherapy: molecular targets in tumor-selective replication and carrier cell-mediated delivery of oncolytic viruses," *Biochim Biophys Acta*, vol. 1785, no. 2, pp. 217–31, 2008.

[143] P. K. Singh, J. Doley, G. R. Kumar, A. P. Sahoo, and A. K. Tiwari, "Oncolytic viruses and their specific targeting to tumour cells," *Indian J Med Res*, vol. 136, no. 4, pp. 571–84, 2012.

[144] C. A. Koks, S. De Vleeschouwer, N. Graf, and S. W. Van Gool, "Immune suppression during oncolytic virotherapy for high-grade glioma; yes or no?," *J Cancer*, vol. 6, no. 3, pp. 203–17, 2015.

[145] M. E. Wilcox, W. Yang, D. Senger, N. B. Rewcastle, D. G. Morris, P. M. Brasher, Z. Q. Shi, R. N. Johnston, S. Nishikawa, P. W. Lee, and P. A. Forsyth, "Reovirus as an oncolytic agent against experimental human malignant gliomas," *J Natl Cancer Inst*, vol. 93, no. 12, pp. 903–12, 2001.

[146] H. Uchida, M. Marzulli, K. Nakano, W. F. Goins, J. Chan, C. S. Hong, L. Mazzacurati, J. Y. Yoo, A. Haseley, H. Nakashima, H. Baek, H. Kwon, I. Kumagai, M. Kuroki, B. Kaur, E. A. Chiocca, P. Grandi, J. B. Cohen, and J. C. Glorioso, "Effective treatment of an orthotopic xenograft model of human glioblastoma using an egfr-retargeted oncolytic herpes simplex virus," *Mol Ther*, vol. 21, no. 3, pp. 561–9, 2013.

[147] P. Bach, T. Abel, C. Hoffmann, Z. Gal, G. Braun, I. Voelker, C. R. Ball, I. C. Johnston, U. M. Lauer, C. Herold-Mende, M. D. Muhlebach, H. Glimm, and C. J. Buchholz, "Specific elimination of cd133+ tumor cells with targeted oncolytic measles virus," *Cancer Res*, vol. 73, no. 2, pp. 865–74, 2013.

[148] X. Lun, J. Chan, H. Zhou, B. Sun, J. J. Kelly, O. O. Stechishin, J. C. Bell, K. Parato, K. Hu, D. Vaillant, J. Wang, T. C. Liu, C. Breitbach, D. Kirn, D. L. Senger, and P. A. Forsyth, "Efficacy and safety/toxicity study of recombinant vaccinia virus jx-594 in two immunocompetent animal models of glioma," *Mol Ther*, vol. 18, no. 11, pp. 1927–36, 2010.

[149] K. Tamura, H. Wakimoto, A. S. Agarwal, S. D. Rabkin, D. Bhere, R. L. Martuza, T. Kuroda, R. Kasmieh, and K. Shah, "Multimechanistic tumor targeted oncolytic virus overcomes resistance in brain tumors," *Mol Ther*, vol. 21, no. 1, pp. 68–77, 2013.

[150] Y. Kim, D. R. Clements, A. M. Sterea, H. W. Jang, S. A. Gujar, and P. W. Lee, "Dendritic cells in oncolytic virus-based anti-cancer therapy," *Viruses*, vol. 7, no. 12, pp. 6506–25, 2015.

[151] S. A. Gujar and P. W. Lee, "Oncolytic virus-mediated reversal of impaired tumor antigen presentation," *Front Oncol*, vol. 4, p. 77, 2014.

[152] R. J. Prestwich, F. Errington, E. J. Ilett, R. S. Morgan, K. J. Scott, T. Kottke, J. Thompson, E. E. Morrison, K. J. Harrington, H. S. Pandha, P. J. Selby, R. G. Vile, and A. A. Melcher, "Tumor infection by oncolytic reovirus primes adaptive antitumor immunity," *Clin Cancer Res*, vol. 14, no. 22, pp. 7358–66, 2008.

[153] N. Lapteva, M. Aldrich, L. Rollins, W. Ren, T. Goltsova, S. Y. Chen, and X. F. Huang, "Attraction and activation of dendritic cells at the site of tumor elicits potent antitumor immunity," *Mol Ther*, vol. 17, no. 9, pp. 1626–36, 2009.

[154] F. Benencia, M. C. Courreges, J. R. Conejo-Garcia, A. Mohamed-Hadley, L. Zhang, R. J. Buckanovich, R. Carroll, N. Fraser, and G. Coukos, "Hsv oncolytic therapy upregulates interferon-inducible chemokines and recruits immune effector cells in ovarian cancer," *Mol Ther*, vol. 12, no. 5, pp. 789–802, 2005.

[155] S. Miyamoto, H. Inoue, T. Nakamura, M. Yamada, C. Sakamoto, Y. Urata, T. Okazaki, T. Marumoto, A. Takahashi, K. Takayama, Y. Nakanishi, H. Shimizu, and K. Tani, "Coxsackievirus b3 is an oncolytic virus with immunostimulatory properties that is active against lung adenocarcinoma," *Cancer Res*, vol. 72, no. 10, pp. 2609–21, 2012.

[156] C. A. Koks, A. D. Garg, M. Ehrhardt, M. Riva, L. Vandenberk, L. Boon, S. De Vleeschouwer, P. Agostinis, N. Graf, and S. W. Van Gool, "Newcastle disease virotherapy induces long-term survival and tumor-specific immune memory in orthotopic glioma through the induction of immunogenic cell death," *Int J Cancer*, vol. 136, no. 5, pp. E313–25, 2015.

[157] L. Deng, J. Fan, M. Guo, and B. Huang, "Oncolytic and immunologic cancer therapy with gm-csf-armed vaccinia virus of tian tan strain guang9," *Cancer Lett*, vol. 372, no. 2, pp. 251–7, 2016.

[158] V. Cerullo, S. Pesonen, I. Diaconu, S. Escutenaire, P. T. Arstila, M. Ugolini, P. Nokisalmi, M. Raki, L. Laasonen, M. Sarkioja, M. Rajecki, L. Kangasniemi, K. Guse, A. Helminen, L. Ahtiainen, A. Ristimaki, A. Raisanen-Sokolowski, E. Haavisto, M. Oksanen, E. Karli, A. Karioja-Kallio, S. L. Holm, M. Kouri, T. Joensuu, A. Kanerva, and A. Hemminki, "Oncolytic adenovirus coding for granulocyte macrophage colony-stimulating factor induces antitumoral immunity in cancer patients," *Cancer Res*, vol. 70, no. 11, pp. 4297–309, 2010.

[159] H. L. Kaufman, D. W. Kim, G. DeRaffele, J. Mitcham, R. S. Coffin, and S. Kim-Schulze, "Local and distant immunity induced by intralesional vaccination with an oncolytic herpes virus encoding gm-csf in patients with stage iiic and iv melanoma," *Ann Surg Oncol*, vol. 17, no. 3, pp. 718–30, 2010.

[160] C. G. Lemay, J. L. Rintoul, A. Kus, J. M. Paterson, V. Garcia, T. J. Falls, L. Ferreira, B. W. Bridle, D. P. Conrad, V. A. Tang, J. S. Diallo, R. Arulanandam, F. Le Boeuf, K. Garson, B. C. Vanderhyden, D. F. Stojdl, B. D. Lichty, H. L. Atkins, K. A. Parato, J. C. Bell, and R. C. Auer, "Harnessing oncolytic virus-mediated antitumor immunity in an infected cell vaccine," *Mol Ther*, vol. 20, no. 9, pp. 1791–9, 2012.

[161] D. L. Bartlett, Z. Liu, M. Sathaiah, R. Ravindranathan, Z. Guo, Y. He, and Z. S. Guo, "Oncolytic viruses as therapeutic cancer vaccines," *Mol Cancer*, vol. 12, no. 1, p. 103, 2013.

[162] H. L. Kaufman, F. J. Kohlhapp, and A. Zloza, "Oncolytic viruses: a new class of immunotherapy drugs," *Nat Rev Drug Discov*, vol. 14, no. 9, pp. 642–62, 2015.

[163] D. R. Shafren, G. G. Au, T. Nguyen, N. G. Newcombe, E. S. Haley, L. Beagley, E. S. Johansson, P. Hersey, and R. D. Barry, "Systemic therapy of malignant human melanoma tumors by a common cold-producing enterovirus, coxsackievirus a21," *Clin Cancer Res*, vol. 10, no. 1 Pt 1, pp. 53–60, 2004.

[164] N. G. Newcombe, L. G. Beagley, D. Christiansen, B. E. Loveland, E. S. Johansson, K. W. Beagley, R. D. Barry, and D. R. Shafren, "Novel role for decay-accelerating factor in coxsackievirus a21-mediated cell infectivity," *J Virol*, vol. 78, no. 22, pp. 12677–82, 2004.

[165] G. G. Au, L. F. Lincz, A. Enno, and D. R. Shafren, "Oncolytic coxsackievirus a21 as a novel therapy for multiple myeloma," *Br J Haematol*, vol. 137, no. 2, pp. 133–41, 2007.

[166] L. J. Berry, G. G. Au, R. D. Barry, and D. R. Shafren, "Potent oncolytic activity of human enteroviruses against human prostate cancer," *Prostate*, vol. 68, no. 6, pp. 577–87, 2008.

[167] E. Chan, G. Au, D. R. Shafren, and A. Guha, "Coxsackievirus a21 as an oncolytic virotherapy agent against malignant glioma." 2010. Available from: http://www.viralytics.com/wp-content/uploads/2014/04/1009-Coxsackievirus-A21-as-an-oncolytic-virotherapy-agent-against-malignant-glioma-POSTER.pdf.

[168] D. E. Staunton, S. D. Marlin, C. Stratowa, M. L. Dustin, and T. A. Springer, "Primary structure of icam-1 demonstrates interaction between members of the immunoglobulin and integrin supergene families," *Cell*, vol. 52, no. 6, pp. 925–33, 1988.

[169] M. L. Dustin, R. Rothlein, A. K. Bhan, C. A. Dinarello, and T. A. Springer, "Induction by il 1 and interferon-gamma: tissue distribution, biochemistry, and function of a natural adherence molecule (icam-1)," *J Immunol*, vol. 137, no. 1, pp. 245–54, 1986.

[170] A. W. Boyd, S. O. Wawryk, G. F. Burns, and J. V. Fecondo, "Intercellular adhesion molecule 1 (icam-1) has a central role in cell-cell contact-mediated immune mechanisms," *Proc Natl Acad Sci U S A*, vol. 85, no. 9, pp. 3095–9, 1988.

[171] S. O. Wawryk, J. R. Novotny, I. P. Wicks, D. Wilkinson, D. Maher, E. Salvaris, K. Welch, J. Fecondo, and A. W. Boyd, "The role of the lfa-1/icam-1 interaction in human leukocyte homing and adhesion," *Immunol Rev*, vol. 108, pp. 135–61, 1989.

[172] A. Grakoui, S. K. Bromley, C. Sumen, M. M. Davis, A. S. Shaw, P. M. Allen, and M. L. Dustin, "The immunological synapse: a molecular machine controlling t cell activation," *Science*, vol. 285, no. 5425, pp. 221–7, 1999.

[173] A. K. Hubbard and R. Rothlein, "Intercellular adhesion molecule-1 (icam-1) expression and cell signaling cascades," *Free Radic Biol Med*, vol. 28, no. 9, pp. 1379–86, 2000.

[174] K. A. Roebuck and A. Finnegan, "Regulation of intercellular adhesion molecule-1 (cd54) gene expression," *J Leukoc Biol*, vol. 66, no. 6, pp. 876–88, 1999.

[175] J. Roy, M. Audette, and M. J. Tremblay, "Intercellular adhesion molecule-1 (icam-1) gene expression in human t cells is regulated by phosphotyrosyl phosphatase activity. involvement of nf-kappab, ets, and palindromic interferon-gamma-responsive element-binding sites," *J Biol Chem*, vol. 276, no. 18, pp. 14553–61, 2001.

[176] Y. de Launoit, M. Audette, H. Pelczar, S. Plaza, and J. L. Baert, "The transcription of the intercellular adhesion molecule-1 is regulated by ets transcription factors," *Oncogene*, vol. 16, no. 16, pp. 2065–73, 1998.

[177] J. Hou, V. Baichwal, and Z. Cao, "Regulatory elements and transcription factors controlling basal and cytokine-induced expression of the gene encoding intercellular adhesion molecule 1," *Proc Natl Acad Sci U S A*, vol. 91, no. 24, pp. 11641–5, 1994.

[178] K. Degitz, L. J. Li, and S. W. Caughman, "Cloning and characterization of the 5'-transcriptional regulatory region of the human intercellular adhesion molecule 1 gene," *J Biol Chem*, vol. 266, no. 21, pp. 14024–30, 1991.

[179] D. C. Look, M. R. Pelletier, and M. J. Holtzman, "Selective interaction of a subset of interferon-gamma response element-binding proteins with the intercellular adhesion molecule-1 (icam-1) gene promoter controls the pattern of expression on epithelial cells," *J Biol Chem*, vol. 269, no. 12, pp. 8952–8, 1994.

[180] S. M. Naik, N. Shibagaki, L. J. Li, K. L. Quinlan, L. L. Paxton, and S. W. Caughman, "Interferon gamma-dependent induction of human intercellular adhesion molecule-1 gene expression involves activation of a distinct stat protein complex," *J Biol Chem*, vol. 272, no. 2, pp. 1283–90, 1997.

[181] K. Pazdrak, X. Z. Shi, and S. K. Sarna, "Tnfalpha suppresses human colonic circular smooth muscle cell contractility by sp1- and nf-kappab-mediated induction of icam-1," *Gastroenterology*, vol. 127, no. 4, pp. 1096–109, 2004.

[182] N. Hadad, L. Tuval, V. Elgazar-Carmom, R. Levy, and R. Levy, "Endothelial icam-1 protein induction is regulated by cytosolic phospholipase a2alpha via both nf-kappab and creb transcription factors," *J Immunol*, vol. 186, no. 3, pp. 1816–27, 2011.

[183] C. Stratowa and M. Audette, "Transcriptional regulation of the human intercellular adhesion molecule-1 gene: a short overview," *Immunobiology*, vol. 193, no. 2-4, pp. 293–304, 1995.

[184] L. Cilenti, E. Toniato, P. Ruggiero, C. Fusco, A. R. Farina, A. Tiberio, A. C. Hayday, A. Gulino, L. Frati, and S. Martinotti, "Transcriptional modulation of the human intercellular adhesion molecule gene i (icam-1) by retinoic acid in melanoma cells," *Exp Cell Res*, vol. 218, no. 1, pp. 263–70, 1995.

[185] C. C. Chadwick, L. J. Shaw, and R. C. Winneker, "Tnf-alpha and 9-cis-retinoic acid synergistically induce icam-1 expression: evidence for interaction of retinoid receptors with nf-kappab," *Exp Cell Res*, vol. 239, no. 2, pp. 423–9, 1998.

[186] M. Bouillon, P. Tessier, R. Boulianne, R. Destrempe, and M. Audette, "Regulation by retinoic acid of icam-1 expression on human tumor cell lines," *Biochim Biophys Acta*, vol. 1097, no. 2, pp. 95–102, 1991.

[187] V. Bassi, M. Vitale, A. Feliciello, S. De Riu, G. Rossi, and G. Fenzi, "Retinoic acid induces intercellular adhesion molecule-1 hyperexpression in human thyroid carcinoma cell lines," *J Clin Endocrinol Metab*, vol. 80, no. 4, pp. 1129–35, 1995.

[188] C. L. Alexander, M. Edward, and R. M. MacKie, "The role of human melanoma cell icam-1 expression on lymphokine activated killer cell-mediated lysis, and the effect of retinoic acid," *Br J Cancer*, vol. 80, no. 10, pp. 1494–500, 1999.

[189] G. Baj, A. Arnulfo, S. Deaglio, E. Tibaldi, N. Surico, and F. Malavasi, "All-trans retinoic acid inhibits the growth of breast cancer cells by up-regulating icam-1 expression," *J Biol Regul Homeost Agents*, vol. 13, no. 2, pp. 115–22, 1999.

[190] M. E. Hegi, A. C. Diserens, T. Gorlia, M. F. Hamou, N. de Tribolet, M. Weller, J. M. Kros, J. A. Hainfellner, W. Mason, L. Mariani, J. E. Bromberg, P. Hau, R. O. Mirimanoff, J. G. Cairncross, R. C. Janzer, and R. Stupp, "Mgmt gene silencing and benefit from temozolomide in glioblastoma," *N Engl J Med*, vol. 352, no. 10, pp. 997–1003, 2005.

[191] I. Crespo, A. L. Vital, A. B. Nieto, O. Rebelo, H. Tao, M. C. Lopes, C. R. Oliveira, P. J. French, A. Orfao, and M. D. Tabernero, "Detailed characterization of alterations of chromosomes 7, 9, and 10 in glioblastomas as assessed by single-nucleotide polymorphism arrays," *J Mol Diagn*, vol. 13, no. 6, pp. 634–47, 2011.

[192] T. Scholzen and J. Gerdes, "The ki-67 protein: from the known and the unknown," *J Cell Physiol*, vol. 182, no. 3, pp. 311–22, 2000.

[193] J. Cidado, H. Y. Wong, D. M. Rosen, A. Cimino-Mathews, J. P. Garay, A. G. Fessler, Z. A. Rasheed, J. Hicks, R. L. Cochran, S. Croessmann, D. J. Zabransky, M. Mohseni, J. A. Beaver, D. Chu, K. Cravero, E. S. Christenson, A. Medford, A. Mattox, A. M. De Marzo, P. Argani, A. Chawla, P. J. Hurley, J. Lauring, and B. H. Park, "Ki-67 is required for maintenance of cancer stem cells but not cell proliferation," *Oncotarget*, vol. 7, no. 5, pp. 6281–93, 2016.

[194] K. Liu, Q. Tang, C. Fu, J. Peng, H. Yang, Y. Li, and H. Hong, "Influence of glucose starvation on the pathway of death in insect cell line sl: apoptosis follows autophagy," *Cytotechnology*, vol. 54, no. 2, pp. 97–105, 2007.

[195] J. Wu, Y. Dang, W. Su, C. Liu, H. Ma, Y. Shan, Y. Pei, B. Wan, J. Guo, and L. Yu, "Molecular cloning and characterization of rat lc3a and lc3b–two novel markers of autophagosome," *Biochem Biophys Res Commun*, vol. 339, no. 1, pp. 437–42, 2006.

[196] H. Aoki, Y. Kondo, K. Aldape, A. Yamamoto, E. Iwado, T. Yokoyama, E. F. Hollingsworth, R. Kobayashi, K. Hess, N. Shinojima, T. Shingu, Y. Tamada, L. Zhang, C. Conrad, O. Bogler, G. Mills, R. Sawaya, and S. Kondo, "Monitoring autophagy in glioblastoma with antibody against isoform b of human microtubule-associated protein 1 light chain 3," *Autophagy*, vol. 4, no. 4, pp. 467–75, 2008.

[197] N. Mizushima, "Autophagy: process and function," *Genes Dev*, vol. 21, no. 22, pp. 2861–73, 2007.

[198] S. W. Ryter, K. Mizumura, and A. M. Choi, "The impact of autophagy on cell death modalities," *Int J Cell Biol*, vol. 2014, p. 502676, 2014.

[199] L. Zhang, H. Wang, K. Ding, and J. Xu, "Fty720 induces autophagy-related apoptosis and necroptosis in human glioblastoma cells," *Toxicol Lett*, vol. 236, no. 1, pp. 43–59, 2015.

[200] S. Shen, Y. Zhang, Z. Wang, R. Liu, and X. Gong, "Bufalin induces the interplay between apoptosis and autophagy in glioma cells through endoplasmic reticulum stress," *Int J Biol Sci*, vol. 10, no. 2, pp. 212–24, 2014.

[201] R. Bertrand, E. Solary, P. O'Connor, K. W. Kohn, and Y. Pommier, "Induction of a common pathway of apoptosis by staurosporine," *Exp Cell Res*, vol. 211, no. 2, pp. 314–21, 1994.

[202] N. Mizushima and B. Levine, "Autophagy in mammalian development and differentiation," *Nat Cell Biol*, vol. 12, no. 9, pp. 823–30, 2010.

[203] U. Lendahl, L. B. Zimmerman, and R. D. McKay, "Cns stem cells express a new class of intermediate filament protein," *Cell*, vol. 60, no. 4, pp. 585–95, 1990.

[204] X. Jin, X. Jin, J. E. Jung, S. Beck, and H. Kim, "Cell surface nestin is a biomarker for glioma stem cells," *Biochem Biophys Res Commun*, vol. 433, no. 4, pp. 496–501, 2013.

[205] C. Y. Brazel, T. L. Limke, J. K. Osborne, T. Miura, J. Cai, L. Pevny, and M. S. Rao, "Sox2 expression defines a heterogeneous population of neurosphere-forming cells in the adult murine brain," *Aging Cell*, vol. 4, no. 4, pp. 197–207, 2005.

[206] V. Bramanti, D. Tomassoni, M. Avitabile, F. Amenta, and R. Avola, "Biomarkers of glial cell proliferation and differentiation in culture," *Front Biosci (Schol Ed)*, vol. 2, pp. 558–70, 2010.

[207] S. P. Memberg and A. K. Hall, "Dividing neuron precursors express neuron-specific tubulin," *J Neurobiol*, vol. 27, no. 1, pp. 26–43, 1995.

[208] Q. Xie, S. Mittal, and M. E. Berens, "Targeting adaptive glioblastoma: an overview of proliferation and invasion," *Neuro Oncol*, vol. 16, no. 12, pp. 1575–84, 2014.

[209] E. C. Holland, "Glioblastoma multiforme: the terminator," *Proc Natl Acad Sci U S A*, vol. 97, no. 12, pp. 6242–4, 2000.

[210] J. Munoz-Sanchez and M. E. Chanez-Cardenas, "A review on hemeoxygenase-2: focus on cellular protection and oxygen response," *Oxid Med Cell Longev*, vol. 2014, p. 604981, 2014.

[211] I. Nalvarte, A. E. Damdimopoulos, and G. Spyrou, "Human mitochondrial thioredoxin reductase reduces cytochrome c and confers resistance to complex iii inhibition," *Free Radic Biol Med*, vol. 36, no. 10, pp. 1270–8, 2004.

[212] J. M. Berg, J. L. Tymoczko, and L. Stryer, *The Glycolytic Pathway Is Tightly Controlled*. New York. Biochemistry, Section 16.2.: W H Freeman, 2002. Available from: http://www.ncbi.nlm.nih.gov/books/NBK22395/.

[213] X. Li, Y. Jiang, J. Meisenhelder, W. Yang, D. H. Hawke, Y. Zheng, Y. Xia, K. Aldape, J. He, T. Hunter, L. Wang, and Z. Lu, "Mitochondria-translocated pgk1 functions as a protein kinase to coordinate glycolysis and the tca cycle in tumorigenesis," *Mol Cell*, vol. 61, no. 5, pp. 705–19, 2016.

[214] C. E. Eyler, Q. Wu, K. Yan, J. M. MacSwords, D. Chandler-Militello, K. L. Misuraca, J. D. Lathia, M. T. Forrester, J. Lee, J. S. Stamler, S. A. Goldman, M. Bredel, R. E. McLendon, A. E. Sloan, A. B. Hjelmeland, and J. N. Rich, "Glioma stem cell proliferation and tumor growth are promoted by nitric oxide synthase-2," *Cell*, vol. 146, no. 1, pp. 53–66, 2011.

[215] C. H. Chan, J. K. Morrow, C. F. Li, Y. Gao, G. Jin, A. Moten, L. J. Stagg, J. E. Ladbury, Z. Cai, D. Xu, C. J. Logothetis, M. C. Hung, S. Zhang, and H. K. Lin, "Pharmacological inactivation of skp2 scf ubiquitin ligase restricts cancer stem cell traits and cancer progression," *Cell*, vol. 154, no. 3, pp. 556–68, 2013.

[216] A. Kumar, V. Rajendran, R. Sethumadhavan, and R. Purohit, "Akt kinase pathway: a leading target in cancer research," *ScientificWorldJournal*, vol. 2013, p. 756134, 2013.

[217] M. Salazar, M. Lorente, E. Garcia-Taboada, E. Perez Gomez, D. Davila, P. Zuniga-Garcia, J. Maria Flores, A. Rodriguez, Z. Hegedus, D. Mosen-Ansorena, A. M. Aransay, S. Hernandez-Tiedra, I. Lopez-Valero, M. Quintanilla, C. Sanchez, J. L. Iovanna, N. Dusetti, M. Guzman, S. E. Francis, A. Carracedo, E. Kiss-Toth, and G. Velasco, "Loss of tribbles pseudokinase-3 promotes akt-driven tumorigenesis via foxo inactivation," *Cell Death Differ*, vol. 22, no. 1, pp. 131–44, 2015.

[218] B. Wang, J. Li, Z. Ye, Z. Li, and X. Wu, "N-myc downstream regulated gene 1 acts as a tumor suppressor in ovarian cancer," *Oncol Rep*, vol. 31, no. 5, pp. 2279–85, 2014.

[219] N. Inohara, L. Ding, S. Chen, and G. Nunez, "harakiri, a novel regulator of cell death, encodes a protein that activates apoptosis and interacts selectively with survival-promoting proteins bcl-2 and bcl-x(l)," *EMBO J*, vol. 16, no. 7, pp. 1686–94, 1997.

[220] F. Z. Chakrama, S. Seguin-Py, J. N. Le Grand, A. Fraichard, R. Delage-Mourroux, G. Despouy, V. Perez, M. Jouvenot, and M. Boyer-Guittaut, "Gabarapl1 (gec1) associates with autophagic vesicles," *Autophagy*, vol. 6, no. 4, pp. 495–505, 2010.

[221] J. Zhang and P. A. Ney, "Role of bnip3 and nix in cell death, autophagy, and mitophagy," *Cell Death Differ*, vol. 16, no. 7, pp. 939–46, 2009.

[222] D. A. Ferrick, A. Neilson, and C. Beeson, "Advances in measuring cellular bioenergetics using extracellular flux," *Drug Discov Today*, vol. 13, no. 5-6, pp. 268–74, 2008.

[223] M. M. Mrugala, "Advances and challenges in the treatment of glioblastoma: a clinician's perspective," *Discov Med*, vol. 15, no. 83, pp. 221–30, 2013.

[224] L. Schneider, F. Essmann, A. Kletke, P. Rio, H. Hanenberg, W. Wetzel, K. Schulze-Osthoff, B. Nurnberg, and R. P. Piekorz, "The transforming acidic coiled coil 3 protein is essential for spindle-dependent chromosome alignment and mitotic survival," *J Biol Chem*, vol. 282, no. 40, pp. 29273–83, 2007.

[225] S. Korur, R. M. Huber, B. Sivasankaran, M. Petrich, J. Morin, P., B. A. Hemmings, A. Merlo, and M. M. Lino, "Gsk3beta regulates differentiation and growth arrest in glioblastoma," *PLoS One*, vol. 4, no. 10, p. e7443, 2009.

[226] S. E. Thompson, J. Cavitt, and K. L. Audus, "Leucine enkephalin effects on paracellular and transcellular permeation pathways across brain microvessel endothelial cell monolayers," *J Cardiovasc Pharmacol*, vol. 24, no. 5, pp. 818–25, 1994.

[227] D. J. Klionsky, K. Abdelmohsen, A. Abe, M. J. Abedin, H. Abeliovich, A. Acevedo Arozena, H. Adachi, C. M. Adams, P. D. Adams, K. Adeli, P. J. Adhihetty, S. G. Adler, G. Agam, R. Agarwal, M. K. Aghi, M. Agnello, P. Agostinis, P. V. Aguilar, J. Aguirre-Ghiso, E. M. Airoldi, S. Ait-Si-Ali, T. Akematsu, E. T. Akporiaye, M. Al-Rubeai, G. M. Albaiceta, C. Albanese, D. Albani, M. L. Albert, J. Aldudo, H. Algul, M. Alirezaei, I. Alloza, A. Almasan, M. Almonte-Beceril, E. S. Alnemri, C. Alonso, N. Altan-Bonnet, D. C. Altieri, S. Alvarez, L. Alvarez-Erviti, S. Alves, G. Amadoro, A. Amano, C. Amantini, S. Ambrosio, I. Amelio, A. O. Amer, M. Amessou, A. Amon, Z. An, F. A. Anania, S. U. Andersen, U. P. Andley, C. K. Andreadi, N. Andrieu-Abadie, A. Anel, D. K. Ann, S. Anoopkumar-Dukie, M. Antonioli, H. Aoki, N. Apostolova, S. Aquila, K. Aquilano, K. Araki, E. Arama, A. Aranda, J. Araya, A. Arcaro, E. Arias, H. Arimoto, A. R. Ariosa, J. L. Armstrong, T. Arnould, I. Arsov, K. Asanuma, V. Askanas, E. Asselin, R. Atarashi, S. S. Atherton, J. D. Atkin, L. D. Attardi, P. Auberger, G. Auburger, L. Aurelian, R. Autelli, L. Avagliano, M. L. Avantaggiati, L. Avrahami, S. Awale, N. Azad, T. Bachetti, J. M. Backer, D. H. Bae, J. S. Bae, O. N. Bae, S. H. Bae, E. H. Baehrecke, S. H. Baek, S. Baghdiguian, A. Bagniewska-Zadworna, *et al.*, "Guidelines for the use and interpretation of assays for monitoring autophagy (3rd edition)," *Autophagy*, vol. 12, no. 1, pp. 1–222, 2016.

[228] N. Mizushima, T. Yoshimori, and B. Levine, "Methods in mammalian autophagy research," *Cell*, vol. 140, no. 3, pp. 313–26, 2010.

[229] D. Glick, S. Barth, and K. F. Macleod, "Autophagy: cellular and molecular mechanisms," *J Pathol*, vol. 221, no. 1, pp. 3–12, 2010.

[230] P. Codogno and A. J. Meijer, "Autophagy and signaling: their role in cell survival and cell death," *Cell Death Differ*, vol. 12 Suppl 2, pp. 1509–18, 2005.

[231] Y. Tsujimoto and S. Shimizu, "Another way to die: autophagic programmed cell death," *Cell Death Differ*, vol. 12 Suppl 2, pp. 1528–34, 2005.

[232] A. L. Di Stefano, A. Fucci, V. Frattini, M. Labussiere, K. Mokhtari, P. Zoppoli, Y. Marie, A. Bruno, B. Boisselier, M. Giry, J. Savatovsky, M. Touat, H. Belaid, A. Kamoun, A. Idbaih, C. Houillier, F. R. Luo, J. C. Soria, J. Tabernero, M. Eoli, R. Paterra, S. Yip, K. Petrecca, J. A. Chan, G. Finocchiaro, A. Lasorella, M. Sanson, and A. Iavarone, "Detection, characterization, and inhibition of fgfr-tacc fusions in idh wild-type glioma," *Clin Cancer Res*, vol. 21, no. 14, pp. 3307–17, 2015.

[233] J. Lamb, E. D. Crawford, D. Peck, J. W. Modell, I. C. Blat, M. J. Wrobel, J. Lerner, J. P. Brunet, A. Subramanian, K. N. Ross, M. Reich, H. Hieronymus, G. Wei, S. A. Armstrong, S. J. Haggarty, P. A. Clemons, R. Wei, S. A. Carr, E. S. Lander, and T. R. Golub, "The connectivity map: using gene-expression signatures to connect small molecules, genes, and disease," *Science*, vol. 313, no. 5795, pp. 1929–35, 2006.

[234] D. Hanahan and R. A. Weinberg, "Hallmarks of cancer: the next generation," *Cell*, vol. 144, no. 5, pp. 646–74, 2011.

[235] T. TeSlaa and M. A. Teitell, "Techniques to monitor glycolysis," *Methods Enzymol*, vol. 542, pp. 91–114, 2014.

[236] S. P. Mathupala, Y. H. Ko, and P. L. Pedersen, "Hexokinase ii: cancer's double-edged sword acting as both facilitator and gatekeeper of malignancy when bound to mitochondria," *Oncogene*, vol. 25, no. 34, pp. 4777–86, 2006.

[237] G. L. Semenza, "Hif-1: upstream and downstream of cancer metabolism," *Curr Opin Genet Dev*, vol. 20, no. 1, pp. 51–6, 2010.

[238] S. P. Mathupala, Y. H. Ko, and P. L. Pedersen, "The pivotal roles of mitochondria in cancer: Warburg and beyond and encouraging prospects for effective therapies," *Biochim Biophys Acta*, vol. 1797, no. 6-7, pp. 1225–30, 2010.

[239] L. Galluzzi, F. Pietrocola, B. Levine, and G. Kroemer, "Metabolic control of autophagy," *Cell*, vol. 159, no. 6, pp. 1263–76, 2014.

[240] D. G. Hardie, F. A. Ross, and S. A. Hawley, "Ampk: a nutrient and energy sensor that maintains energy homeostasis," *Nat Rev Mol Cell Biol*, vol. 13, no. 4, pp. 251–62, 2012.

[241] A. Alexander, S. L. Cai, J. Kim, A. Nanez, M. Sahin, K. H. MacLean, K. Inoki, K. L. Guan, J. Shen, M. D. Person, D. Kusewitt, G. B. Mills, M. B. Kastan, and C. L. Walker, "Atm signals to tsc2 in the cytoplasm to regulate mtorc1 in response to ros," *Proc Natl Acad Sci U S A*, vol. 107, no. 9, pp. 4153–8, 2010.

[242] D. J. Roberts, V. P. Tan-Sah, E. Y. Ding, J. M. Smith, and S. Miyamoto, "Hexokinase-ii positively regulates glucose starvation-induced autophagy through torc1 inhibition," *Mol Cell*, vol. 53, no. 4, pp. 521–33, 2014.

[243] H. Zhang, M. Bosch-Marce, L. A. Shimoda, Y. S. Tan, J. H. Baek, J. B. Wesley, F. J. Gonzalez, and G. L. Semenza, "Mitochondrial autophagy is an hif-1-dependent adaptive metabolic response to hypoxia," *J Biol Chem*, vol. 283, no. 16, pp. 10892–903, 2008.

[244] M. C. Kuppner, E. van Meir, M. F. Hamou, and N. de Tribolet, "Cytokine regulation of intercellular adhesion molecule-1 (icam-1) expression on human glioblastoma cells," *Clin Exp Immunol*, vol. 81, no. 1, pp. 142–8, 1990.

[245] L. Guarini, M. Temponi, J. N. Bruce, A. P. Bollon, G. J. Duigou, T. A. Moulton, S. Ferrone, and P. B. Fisher, "Expression and modulation by cytokines of the intercellular adhesion molecule-1 (icam-1) in human central nervous system tumor cell cultures," *Int J Cancer*, vol. 46, no. 6, pp. 1041–7, 1990.

[246] Y. Usami, K. Ishida, S. Sato, M. Kishino, M. Kiryu, Y. Ogawa, M. Okura, Y. Fukuda, and S. Toyosawa, "Intercellular adhesion molecule-1 (icam-1) expression correlates with oral cancer progression and induces macrophage/cancer cell adhesion," *Int J Cancer*, vol. 133, no. 3, pp. 568–78, 2013.

[247] S. T. Tsai, P. J. Wang, N. J. Liou, P. S. Lin, C. H. Chen, and W. C. Chang, "Icam1 is a potential cancer stem cell marker of esophageal squamous cell carcinoma," *PLoS One*, vol. 10, no. 11, p. e0142834, 2015.

[248] C. L. Roland, S. P. Dineen, J. E. Toombs, J. G. Carbon, C. W. Smith, R. A. Brekken, and J. Barnett, C. C., "Tumor-derived intercellular adhesion molecule-1 mediates tumor-associated leukocyte infiltration in orthotopic pancreatic xenografts," *Exp Biol Med (Maywood)*, vol. 235, no. 2, pp. 263–70, 2010.

[249] T. N. Seyfried, M. el Abbadi, and M. L. Roy, "Ganglioside distribution in murine neural tumors," *Mol Chem Neuropathol*, vol. 17, no. 2, pp. 147–67, 1992.

[250] T. Oh, S. Fakurnejad, E. T. Sayegh, A. J. Clark, M. E. Ivan, M. Z. Sun, M. Safaee, O. Bloch, C. D. James, and A. T. Parsa, "Immunocompetent murine models for the study of glioblastoma immunotherapy," *J Transl Med*, vol. 12, p. 107, 2014.

[251] A. C. da Fonseca and B. Badie, "Microglia and macrophages in malignant gliomas: recent discoveries and implications for promising therapies," *Clin Dev Immunol*, vol. 2013, p. 264124, 2013.

[252] C. D. Mills, L. L. Lenz, and R. A. Harris, "A breakthrough: Macrophage-directed cancer immunotherapy," *Cancer Res*, vol. 76, no. 3, pp. 513–6, 2016.

[253] F. O. Martinez and S. Gordon, "The m1 and m2 paradigm of macrophage activation: time for reassessment," *F1000Prime Rep*, vol. 6, p. 13, 2014.

[254] C. A. J. Janeway, P. Travers, M. Walport, and e. al., *The major histocompatibility complex and its functions*. New York: Garland Science, 2001. Available from: http://www.ncbi.nlm.nih.gov/books/NBK27156/.

[255] C. Niehage, C. Steenblock, T. Pursche, M. Bornhauser, D. Corbeil, and B. Hoflack, "The cell surface proteome of human mesenchymal stromal cells," *PLoS One*, vol. 6, no. 5, p. e20399, 2011.

[256] R. van Horssen, T. L. Ten Hagen, and A. M. Eggermont, "Tnf-alpha in cancer treatment: molecular insights, antitumor effects, and clinical utility," *Oncologist*, vol. 11, no. 4, pp. 397–408, 2006.

[257] S. Biesmans, J. A. Bouwknecht, L. Ver Donck, X. Langlois, P. D. Acton, P. De Haes, N. Davoodi, T. F. Meert, N. Hellings, and R. Nuydens, "Peripheral administration of tumor necrosis factor-alpha induces neuroinflammation and sickness but not depressive-like behavior in mice," *Biomed Res Int*, vol. 2015, p. 716920, 2015.

[258] M. Li, X. Wang, M. K. Meintzer, T. Laessig, M. J. Birnbaum, and K. A. Heidenreich, "Cyclic amp promotes neuronal survival by phosphorylation of glycogen synthase kinase 3beta," *Mol Cell Biol*, vol. 20, no. 24, pp. 9356–63, 2000.

[259] F. S. Lin, C. C. Lin, C. S. Chien, S. F. Luo, and C. M. Yang, "Involvement of p42/p44 mapk, jnk, and nf-kappab in il-1beta-induced icam-1 expression in human pulmonary epithelial cells," *J Cell Physiol*, vol. 202, no. 2, pp. 464–73, 2005.

[260] M. Dziembowska, M. Danilkiewicz, A. Wesolowska, A. Zupanska, S. Chouaib, and B. Kaminska, "Cross-talk between smad and p38 mapk signalling in transforming growth factor beta signal transduction in human glioblastoma cells," *Biochem Biophys Res Commun*, vol. 354, no. 4, pp. 1101–6, 2007.

[261] G. D. Stewart, J. Nanda, D. J. Brown, A. C. Riddick, J. A. Ross, and F. K. Habib, "No-sulindac inhibits the hypoxia response of pc-3 prostate cancer cells via the akt signalling pathway," *Int J Cancer*, vol. 124, no. 1, pp. 223–32, 2009.

[262] C. J. Loveridge, A. D. MacDonald, H. C. Thoms, M. G. Dunlop, and L. A. Stark, "The proapoptotic effects of sulindac, sulindac sulfone and indomethacin are mediated by nucleolar translocation of the rela(p65) subunit of nf-kappab," *Oncogene*, vol. 27, no. 18, pp. 2648–55, 2008.

[263] S. P. Barrera, V. Castrejon-Tellez, M. Trinidad, E. Robles-Escajeda, J. Vargas-Medrano, A. Varela-Ramirez, and M. Miranda, "Pkc-dependent glyt1 ubiquitination occurs independent of phosphorylation: Inespecificity in lysine selection for ubiquitination," *PLoS One*, vol. 10, no. 9, p. e0138897, 2015.

[264] S. Muller, C. Kammerbauer, U. Simons, N. Shibagaki, L. J. Li, S. W. Caughman, and K. Degitz, "Transcriptional regulation of intercellular adhesion molecule-1: Pma-induction is mediated by nf kappa b," *J Invest Dermatol*, vol. 104, no. 6, pp. 970–5, 1995.

[265] T. Sawada, K. Kimura, T. Nishihara, N. Onoda, H. Teraoka, Y. Yamashita, N. Yamada, M. Yashiro, M. Ohira, and K. Hirakawa, "Tgf-beta1 down-regulates icam-1 expression and enhances liver metastasis of pancreatic cancer," *Adv Med Sci*, vol. 51, pp. 60–5, 2006.

[266] A. M. Madec, R. Cassel, S. Dubois, S. Ducreux, G. Vial, M. A. Chauvin, A. Mesnier, K. Chikh, D. Bosco, J. Rieusset, F. Van Coppenolle, and C. Thivolet, "Losartan, an angiotensin ii type 1 receptor blocker, protects human islets from glucotoxicity through the phospholipase c pathway," *FASEB J*, vol. 27, no. 12, pp. 5122–30, 2013.

[267] G. Bar-Klein, L. P. Cacheaux, L. Kamintsky, O. Prager, I. Weissberg, K. Schoknecht, P. Cheng, S. Y. Kim, L. Wood, U. Heinemann, D. Kaufer, and A. Friedman, "Losartan prevents acquired epilepsy via tgf-beta signaling suppression," *Ann Neurol*, vol. 75, no. 6, pp. 864–75, 2014.

[268] G. Liu, S. M. Vogel, X. Gao, K. Javaid, G. Hu, S. M. Danilov, A. B. Malik, and R. D. Minshall, "Src phosphorylation of endothelial cell surface intercellular adhesion molecule-1 mediates neutrophil adhesion and contributes to the mechanism of lung inflammation," *Arterioscler Thromb Vasc Biol*, vol. 31, no. 6, pp. 1342–50, 2011.

[269] M. Warmuth, N. Simon, O. Mitina, R. Mathes, D. Fabbro, P. W. Manley, E. Buchdunger, K. Forster, I. Moarefi, and M. Hallek, "Dual-specific src and abl kinase inhibitors, pp1 and cgp76030, inhibit growth and survival of cells expressing imatinib mesylate-resistant bcr-abl kinases," *Blood*, vol. 101, no. 2, pp. 664–72, 2003.

[270] C. H. Jung, W. J. Lee, J. Y. Hwang, S. M. Seol, Y. M. Kim, Y. L. Lee, J. H. Ahn, and J. Y. Park, "The role of rho/rho-kinase pathway in the expression of icam-1 by linoleic acid in human aortic endothelial cells," *Inflammation*, vol. 35, no. 3, pp. 1041–8, 2012.

[271] L. Clement, H. Poirier, I. Niot, V. Bocher, M. Guerre-Millo, S. Krief, B. Staels, and P. Besnard, "Dietary trans-10,cis-12 conjugated linoleic acid induces hyperinsulinemia and fatty liver in the mouse," *J Lipid Res*, vol. 43, no. 9, pp. 1400–9, 2002.

[272] L. Wang, L. Xue, H. Yan, J. Li, and Y. Lu, "Effects of rock inhibitor, y-27632, on adhesion and mobility in esophageal squamous cell cancer cells," *Mol Biol Rep*, vol. 37, no. 4, pp. 1971–7, 2010.

[273] P. Zhang, C. Goodrich, C. Fu, and C. Dong, "Melanoma upregulates icam-1 expression on endothelial cells through engagement of tumor cd44 with endothelial e-selectin and activation of a pkcalpha-p38-sp-1 pathway," *FASEB J*, vol. 28, no. 11, pp. 4591–609, 2014.

[274] J. Heikkila and K. E. Akerman, "(-)-indolactam v activates protein kinase c and induces changes in muscarinic receptor functions in sh-sy5y human neuroblastoma cells," *Biochem Biophys Res Commun*, vol. 162, no. 3, pp. 1207–13, 1989.

[275] Y. C. Shen, C. Hsu, J. Y. Chen, and A. L. Cheng, "Lack of efficacy of troglitazone at clinically achievable concentrations, with or without 9-cis retinoic acid or cytotoxic agents, for hepatocellular carcinoma cell lines," *Br J Cancer*, vol. 91, no. 8, pp. 1561–5, 2004.

[276] O. Afonja, B. M. Raaka, A. Huang, S. Das, X. Zhao, E. Helmer, D. Juste, and H. H. Samuels, "Rar agonists stimulate sox9 gene expression in breast cancer cell lines: evidence for a role in retinoid-mediated growth inhibition," *Oncogene*, vol. 21, no. 51, pp. 7850–60, 2002.

[277] M. J. Sanz, F. Albertos, E. Otero, M. Juez, E. J. Morcillo, and L. Piqueras, "Retinoid x receptor agonists impair arterial mononuclear cell recruitment through peroxisome proliferator-activated receptor-gamma activation," *J Immunol*, vol. 189, no. 1, pp. 411–24, 2012.

[278] W. Cui, Z. Zhang, W. Li, S. Mak, S. Hu, H. Zhang, S. Yuan, J. Rong, T. C. Choi, S. M. Lee, and Y. Han, "Unexpected neuronal protection of su5416 against 1-methyl-4-phenylpyridinium ion-induced toxicity via inhibiting neuronal nitric oxide synthase," *PLoS One*, vol. 7, no. 9, p. e46253, 2012.

[279] T. Lahusen, A. De Siervi, C. Kunick, and A. M. Senderowicz, "Alsterpaullone, a novel cyclin-dependent kinase inhibitor, induces apoptosis by activation of caspase-9 due to perturbation in mitochondrial membrane potential," *Mol Carcinog*, vol. 36, no. 4, pp. 183–94, 2003.

[280] M. L. Selenica, H. S. Jensen, A. K. Larsen, M. L. Pedersen, L. Helboe, M. Leist, and J. Lotharius, "Efficacy of small-molecule glycogen synthase kinase-3 inhibitors in the postnatal rat model of tau hyperphosphorylation," *Br J Pharmacol*, vol. 152, no. 6, pp. 959–79, 2007.

[281] R. J. Riley, C. Lambert, N. R. Kitteringham, and B. K. Park, "A stereochemical investigation of the cytotoxicity of mianserin metabolites in vitro," *Br J Clin Pharmacol*, vol. 27, no. 6, pp. 823–30, 1989.

[282] A. C. Altamura, F. De Novellis, M. C. Mauri, and R. Gomeni, "Plasma and brain pharmacokinetics of mianserin after single and multiple dosing in mice," *Prog Neuropsychopharmacol Biol Psychiatry*, vol. 11, no. 1, pp. 23–33, 1987.

[283] H. A. Hamed, S. Tavallai, S. Grant, A. Poklepovic, and P. Dent, "Sorafenib/regorafenib and lapatinib interact to kill cns tumor cells," *J Cell Physiol*, vol. 230, no. 1, pp. 131–9, 2015.

[284] S. Gori, G. Lunardi, A. Inno, J. Foglietta, B. Cardinali, L. Del Mastro, and L. Crino, "Lapatinib concentration in cerebrospinal fluid in two patients with her2-positive metastatic breast cancer and brain metastases," *Ann Oncol*, vol. 25, no. 4, pp. 912–3, 2014.

[285] N. Hirakawa, R. Okauchi, Y. Miura, and K. Yagasaki, "Anti-invasive activity of niacin and trigonelline against cancer cells," *Biosci Biotechnol Biochem*, vol. 69, no. 3, pp. 653–8, 2005.

[286] L. V. Hankes, H. H. Coenen, E. Rota, K. J. Langen, H. Herzog, W. Wutz, G. Stoecklin, and L. E. Feinendegen, "Effect of huntington's and alzheimer's diseases on the transport of nicotinic acid or nicotinamide across the human blood-brain barrier," *Adv Exp Med Biol*, vol. 294, pp. 675–8, 1991.

[287] J. A. Phan, A. M. Landau, D. F. Wong, S. Jakobsen, A. Nahimi, D. J. Doudet, and A. Gjedde, "Quantification of [(11)c]yohimbine binding to alpha2 adrenoceptors in rat brain in vivo," *J Cereb Blood Flow Metab*, vol. 35, no. 3, pp. 501–11, 2015.

[288] M. J. Polanco, L. F. Alguacil, and C. Gonzalez-Martin, "Pro-apoptotic properties of morphine in neuroblastoma x glioma ng108-15 hybrid cells: modulation by yohimbine," *J Appl Toxicol*, vol. 34, no. 1, pp. 19–24, 2014.

[289] A. Paolini, F. Pasi, A. Facoetti, G. Mazzini, F. Corbella, R. Di Liberto, and R. Nano, "Cell death forms and hsp70 expression in u87 cells after ionizing radiation and/or chemotherapy," *Anticancer Res*, vol. 31, no. 11, pp. 3727–31, 2011.

[290] M. L. de Groote, H. G. Kazemier, C. Huisman, B. T. van der Gun, M. M. Faas, and M. G. Rots, "Upregulation of endogenous icam-1 reduces ovarian cancer cell growth in the absence of immune cells," *Int J Cancer*, vol. 134, no. 2, pp. 280–90, 2014.

[291] J. M. Arnold, M. Cummings, D. Purdie, and G. Chenevix-Trench, "Reduced expression of intercellular adhesion molecule-1 in ovarian adenocarcinomas," *Br J Cancer*, vol. 85, no. 9, pp. 1351–8, 2001.

[292] Q. Wu, Y. Q. Chen, Z. M. Chen, F. Chen, and W. J. Su, "Effects of retinoic acid on metastasis and its related proteins in gastric cancer cells in vivo and in vitro," *Acta Pharmacol Sin*, vol. 23, no. 9, pp. 835–41, 2002.

[293] R. Harning, E. Mainolfi, J. C. Bystryn, M. Henn, V. J. Merluzzi, and R. Rothlein, "Serum levels of circulating intercellular adhesion molecule 1 in human malignant melanoma," *Cancer Res*, vol. 51, no. 18, pp. 5003–5, 1991.

[294] C. Rosette, R. B. Roth, P. Oeth, A. Braun, S. Kammerer, J. Ekblom, and M. F. Denissenko, "Role of icam1 in invasion of human breast cancer cells," *Carcinogenesis*, vol. 26, no. 5, pp. 943–50, 2005.

[295] P. P. Zhu, S. G. Yuan, Y. Liao, L. L. Qin, and W. J. Liao, "High level of intercellular adhesion molecule-1 affects prognosis of patients with hepatocellular carcinoma," *World J Gastroenterol*, vol. 21, no. 23, pp. 7254–63, 2015.

[296] W. Zhou and S. Bao, "Reciprocal supportive interplay between glioblastoma and tumor-associated macrophages," *Cancers (Basel)*, vol. 6, no. 2, pp. 723–40, 2014.

[297] M. Yang, J. Liu, C. Piao, J. Shao, and J. Du, "Icam-1 suppresses tumor metastasis by inhibiting macrophage m2 polarization through blockade of efferocytosis," *Cell Death Dis*, vol. 6, p. e1780, 2015.

[298] M. H. Barros, F. Hauck, J. H. Dreyer, B. Kempkes, and G. Niedobitek, "Macrophage polarisation: an immunohistochemical approach for identifying m1 and m2 macrophages," *PLoS One*, vol. 8, no. 11, p. e80908, 2013.

[299] H. Y. Lee, Y. A. Suh, M. J. Robinson, J. L. Clifford, W. K. Hong, J. R. Woodgett, M. H. Cobb, D. J. Mangelsdorf, and J. M. Kurie, "Stress pathway activation induces phosphorylation of retinoid x receptor," *J Biol Chem*, vol. 275, no. 41, pp. 32193–9, 2000.

[300] G. Zund, S. Uezono, G. L. Stahl, A. L. Dzus, F. X. McGowan, P. R. Hickey, and S. P. Colgan, "Hypoxia enhances induction of endothelial icam-1: role for metabolic acidosis and proteasomes," *Am J Physiol*, vol. 273, no. 5 Pt 1, pp. C1571–80, 1997.

[301] S. Koizume, S. Ito, Y. Nakamura, M. Yoshihara, M. Furuya, R. Yamada, E. Miyagi, F. Hirahara, Y. Takano, and Y. Miyagi, "Lipid starvation and hypoxia synergistically activate icam1 and multiple genes in an sp1-dependent manner to promote the growth of ovarian cancer," *Mol Cancer*, vol. 14, p. 77, 2015.

[302] A. Budnik, M. Grewe, K. Gyufko, and J. Krutmann, "Analysis of the production of soluble icam-1 molecules by human cells," *Exp Hematol*, vol. 24, no. 2, pp. 352–9, 1996.

[303] L. Yang, C. Lin, L. Wang, H. Guo, and X. Wang, "Hypoxia and hypoxia-inducible factors in glioblastoma multiforme progression and therapeutic implications," *Exp Cell Res*, vol. 318, no. 19, pp. 2417–26, 2012.

[304] J. Martinez-Quintanilla, D. He, H. Wakimoto, R. Alemany, and K. Shah, "Encapsulated stem cells loaded with hyaluronidase-expressing oncolytic virus for brain tumor therapy," *Mol Ther*, vol. 23, no. 1, pp. 108–18, 2015.

[305] H. Wakimoto, G. Fulci, E. Tyminski, and E. A. Chiocca, "Altered expression of antiviral cytokine mrnas associated with cyclophosphamide's enhancement of viral oncolysis," *Gene Ther*, vol. 11, no. 2, pp. 214–23, 2004.

[306] C. Hai, Y. M. Jin, W. B. Jin, Z. Z. Han, M. N. Cui, X. Z. Piao, X. H. Shen, S. N. Zhang, and H. H. Sun, "Application of mesenchymal stem cells as a vehicle to deliver replication-competent adenovirus for treating malignant glioma," *Chin J Cancer*, vol. 31, no. 5, pp. 233–40, 2012.

[307] A. U. Ahmed, B. Thaci, N. G. Alexiades, Y. Han, S. Qian, F. Liu, I. V. Balyasnikova, I. Y. Ulasov, K. S. Aboody, and M. S. Lesniak, "Neural stem cell-based cell carriers enhance therapeutic efficacy of an oncolytic adenovirus in an orthotopic mouse model of human glioblastoma," *Mol Ther*, vol. 19, no. 9, pp. 1714–26, 2011.

[308] C. Holohan, S. Van Schaeybroeck, D. B. Longley, and P. G. Johnston, "Cancer drug resistance: an evolving paradigm," *Nat Rev Cancer*, vol. 13, no. 10, pp. 714–726, 2013.

[309] N. M. Walton, B. M. Sutter, H. X. Chen, L. J. Chang, S. N. Roper, B. Scheffler, and D. A. Steindler, "Derivation and large-scale expansion of multipotent astroglial neural progenitors from adult human brain," *Development*, vol. 133, no. 18, pp. 3671–81, 2006.

[310] M. Spitzer, J. Wildenhain, J. Rappsilber, and M. Tyers, "Boxplotr: a web tool for generation of box plots," *Nat Methods*, vol. 11, no. 2, pp. 121–2, 2014.

[311] O. Troyanskaya, M. Cantor, G. Sherlock, P. Brown, T. Hastie, R. Tibshirani, D. Botstein, and R. B. Altman, "Missing value estimation methods for dna microarrays," *Bioinformatics*, vol. 17, no. 6, pp. 520–5, 2001.

[312] F. Buettner, K. N. Natarajan, F. P. Casale, V. Proserpio, A. Scialdone, F. J. Theis, S. A. Teichmann, J. C. Marioni, and O. Stegle, "Computational analysis of cell-to-cell heterogeneity in single-cell rna-sequencing data reveals hidden subpopulations of cells," *Nat Biotechnol*, vol. 33, no. 2, pp. 155–60, 2015.